Development of Analysis and Design Procedures for Spread Footings

by

George Mylonakis, George Gazetas, Sissy Nikolaou and Andre Chauncey

City University of New York
Department of Civil Engineering
Steinman Hall, Convent Avenue at 138th Street
New York, New York
and
University at Buffalo, State University of New York
Department of Civil, Structural and Environmental Engineering
Ketter Hall
Buffalo, New York 14260

NOTICE

Development of Analysis and Design
Procedures for Spread Footings

by

George Mylonakis[1], George Gazetas[2], Sissy Nikolaou[3] and Andre Chauncey[4]

1 Associate Professor, Dept. of Civil Engineering, City University of New York; former Research Assistant, University at Buffalo, State University of New York
2 Professor, Dept. of Civil Engineering, National Technical University, Athens, Greece and Research Professor, Dept. of Civil Engineering, University at Buffalo, State University of New York
3 Senior Geotechnical Engineer, Mueser Rutledge Consulting Engineers, New York; former Graduate Student, University at Buffalo, State University of New York
4 AMP Research Assistant, Dept. of Civil Engineering, City University of New York

Preface

The Multidisciplinary Center for Earthquake Engineering Research (MCEER) is a national center of excellence in advanced technology applications that is dedicated to the reduction of earthquake losses nationwide. Headquartered at the University at Buffalo, State University of New York, the Center was originally established by the National Science Foundation in 1986, as the National Center for Earthquake Engineering Research (NCEER).

Comprising a consortium of researchers from numerous disciplines and institutions throughout the United States, the Center's mission is to reduce earthquake losses through research and the application of advanced technologies that improve engineering, pre-earthquake planning and post-earthquake recovery strategies. Toward this end, the Center coordinates a nationwide program of multidisciplinary team research, education and outreach activities.

MCEER's research is conducted under the sponsorship of two major federal agencies, the National Science Foundation (NSF) and the Federal Highway Administration (FHWA), and the State of New York. Significant support is also derived from the Federal Emergency Management Agency (FEMA), other state governments, academic institutions, foreign governments and private industry.

The Center's FHWA-sponsored Highway Project develops retrofit and evaluation methodologies for existing bridges and other highway structures (including tunnels, retaining structures, slopes, culverts, and pavements), and improved seismic design criteria and procedures for bridges and other highway structures. Specifically, tasks are being conducted to:
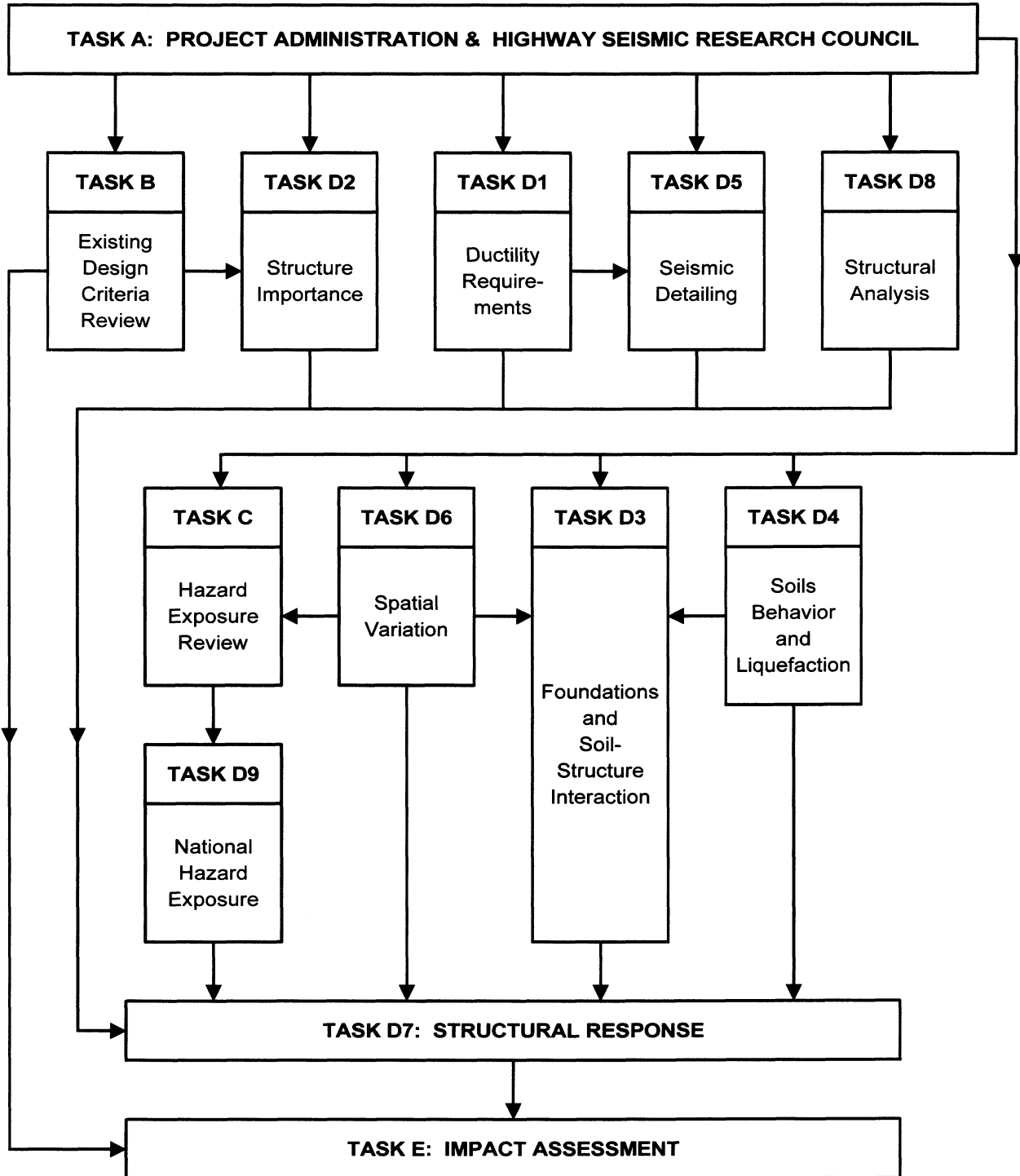- assess the vulnerability of highway systems, structures and components;
- develop concepts for retrofitting vulnerable highway structures and components;
- develop improved design and analysis methodologies for bridges, tunnels, and retaining structures, which include consideration of soil-structure interaction mechanisms and their influence on structural response;
- review and recommend improved seismic design and performance criteria for new highway structures.

Highway Project research focuses on two distinct areas: the development of improved design criteria and philosophies for new or future highway construction, and the development of improved analysis and retrofitting methodologies for existing highway systems and structures. The research discussed in this report is a result of work conducted under the new highway structures project, and was performed within Task 112-D-3.7, "Development of Analysis and Design Procedures for Spread Footings" of that project as shown in the flowchart on the following page.

This report describes a series of numerical analyses that address spread footings under dynamic and seismic loading. These analyses were conducted for a typical idealized pier with a single-column bent founded on a footing on the surface of, or embedded in, a layered soil profile. The report includes

iii

charts and tables for computing footing impedances for a variety of soil conditions and vibration modes. The decomposition of seismic response into kinematic and inertial parts is discussed, as are the effects of soil material nonlinearity on the response. A parameter study of the response of bridge piers (without uplift) showed the effect of increased period due to soil-structure interaction on seismic response and the influence of radiation damping. Finally, footing bearing capacity failure, development of pore water pressure, and uplift under seismic conditions are discussed.

SEISMIC VULNERABILITY OF NEW HIGHWAY CONSTRUCTION
FHWA Contract DTFH61-92-C-00112

TASK A: PROJECT ADMINISTRATION & HIGHWAY SEISMIC RESEARCH COUNCIL

TASK B — Existing Design Criteria Review

TASK D2 — Structure Importance

TASK D1 — Ductility Requirements

TASK D5 — Seismic Detailing

TASK D8 — Structural Analysis

TASK C — Hazard Exposure Review

TASK D6 — Spatial Variation

TASK D3 — Foundations and Soil-Structure Interaction

TASK D4 — Soils Behavior and Liquefaction

TASK D9 — National Hazard Exposure

TASK D7: STRUCTURAL RESPONSE

TASK E: IMPACT ASSESSMENT

ABSTRACT

An extensive set of graphs and tables is provided for computing the stiffness and damping of spread footings under dynamic and seismic loading. All modes of vibration (swaying, rocking, torsion) as well as various soil conditions and foundation geometries are addressed. Simplified expressions for computing the kinematic response of footings (both in translation and rotation) are provided. Special issues such as footings on a soil layer over elastic or rigid rock, and inelastic effects are discussed.

In the second part of the report, results from two parameter studies are presented for the seismic response of bridge bents on embedded footings in layered soil. The seismic excitation, in the form of vertically propagating S waves, is described through real and artificial accelerograms applied at the base of the deposit. Both *kinematic* and *inertial* interaction are taken into account. Results are presented (in both frequency and time domains) for accelerations and displacements of the bridge and the footing. Potential errors from the frequently employed simplifications of ignoring: (i) the radiation damping produced by the oscillating foundation and by the elastic bedrock and (ii) the stiffness and damping produced by the footing sidewalls, are discussed.

Additional issues such as (1) footing bearing capacity, (2) development of soil pore water pressure beneath footings, (3) footing uplift, under strong seismic excitation are addressed in the final part of the report.

KEYWORDS: Foundation; Spread footings; Dynamic analysis; Bridges; Bents; Radiation damping; Rocking motion; Soil-structure interaction; Impedance Functions

ACKNOWLEDGMENTS

TABLE OF CONTENTS

LIST OF ILLUSTRATIONS

LIST OF ILLUSTRATIONS (continued)

LIST OF ILLUSTRATIONS (continued)

LIST OF ILLUSTRATIONS (continued)

LIST OF TABLES

SECTION 1

SUMMARY AND TASK OBJECTIVES

The overall objectives of this task are to provide information relating to some of the major issues facing bridge designers, such as: (1) when should foundation stiffness be incorporated in the dynamic analyses; (2) how significant is the proper modeling of the effect of embedment on the dynamic stiffnesses ("springs" and "dashpots") of the foundation; (3) how important is the role of radiation damping and of kinematic interaction in structural response; (4) under what conditions will uplifting become significant and what is the best way to model it in design/analysis; (5) are localized soil nonlinearities under a foundation significant and how could they be taken into account in the analysis?

To this end, analytical studies are conducted for the seismic response of a typical idealized bridge pier. Sketched in Fig. 1-1, the pier is a single-column bent founded on a footing on the surface of, or embedded in, a layered soil profile.

A variety of realistic pier-bridge-deck support connections, some of which are sketched in Fig. 1-2, are studied. They range from a top free to rotate (when, for example, bridge column and beams are connected through a hinge) to a top fixed against rotation (appropriate for relatively-stiff beams fixed to the column top). Supports through elastomeric bearings can also be studied with the method. The results presented in this report are for the "fixed" and the "free" support only.

The soil-foundation-pier system is subjected to seismic excitation consisting of vertical S-waves. The excitation is described through a horizontal "rock" outcrop motion. In addition to harmonic steady-state analyses, two different motions are used in this project, both characterized by a peak ground acceleration (pga) of 0.40g: (a) artificial ("synthetic") accelerograms fitted to the AASHTO pga = 0.40g S1-soil spectrum, and (b) the Pacoima-downstream accelerogram recorded in the 1994 Northridge earthquake. Since its pga value is 0.42 g , no scaling was considered necessary for this motion. The two time histories and the corresponding response spectra are presented in Section 3.

1

In Section 2, charts and tables are provided for computing footing impedances for a variety of soil conditions and vibration modes. The decomposition of seismic response into a kinematic and an inertial part is discussed. Effects of soil material nonlinearity on the response are presented.

In Section 3, results from an extensive parameter study of the response of bridge piers (without uplift) are presented. The effect of increased period due to soil-structure interaction on seismic response and the influence of radiation damping are highlighted.

Footing bearing capacity failure, development of pore water pressure, and uplift under seismic conditions are briefly discussed in Section 4.

FIGURE 1-2 Typical column-deck support conditions
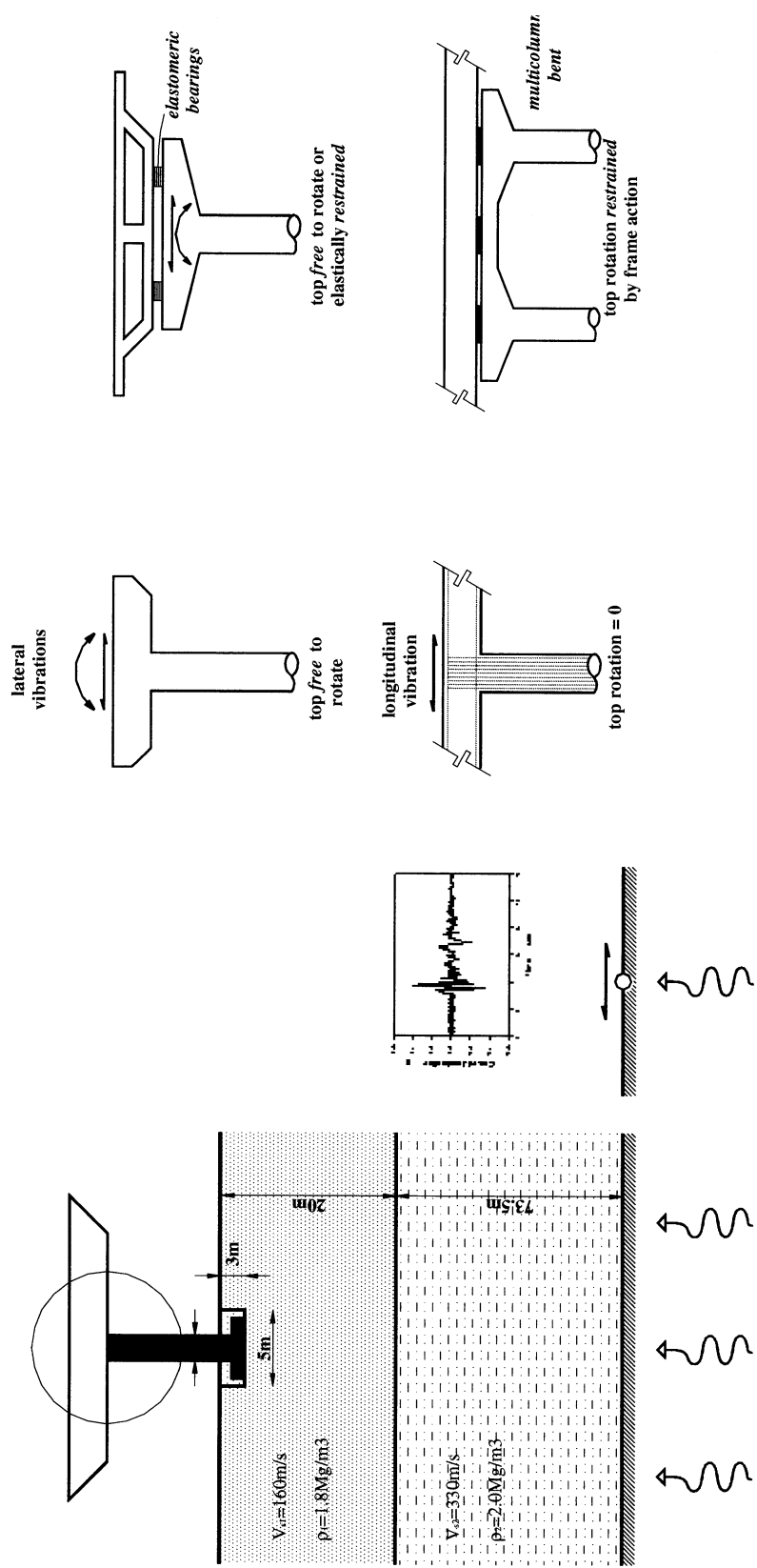
FIGURE 1-1 The pier on footing studied in this report

3

SECTION 2

ANALYSIS OF SOIL--FOOTING--BRIDGE RESPONSE:
METHODS AND RESULTS

2.1 Statement of the problem: kinematic and inertial response

During earthquake shaking, the soil deforms under the influence of the incident seismic wave and "carries" dynamically with it the foundation and the supported structure. In turn, the induced motion of the superstructure generates inertial forces which result in dynamic stresses in the base that are transmitted into the supporting soil. Thus, superstructure-induced deformations develop in the soil while additional waves emanate from the soil-foundation interface. In response, foundation and superstructure undergo further dynamic displacements, which generate further inertia forces, and so on.

The above phenomena occur simultaneously. However, it is convenient (both conceptually and computationally) to separate them into two successive phenomena, referred to as "kinematic interaction" and "inertial interaction", and obtain the response of the soil-foundation-structure system shown in Fig 2-1 as a superposition of these two interaction effects:

(a) "Kinematic Interaction" (K.I.) refers to the effects of the incident seismic waves to the system shown in Fig. 2-1b, which consists essentially of the foundation and the supporting soil, differing from the complete system of Fig. 2-1a in that the mass of the superstructure is set equal to zero. The main consequence of kinematic interaction is that it leads to a "Foundation Input Motion" (F.I.M.) which is different (usually smaller) than the motion of the free-field soil and, in addition, contains a rotational component. As will be show later on, this difference is potentially significant for embedded foundations.

(b) "Inertial Interaction" (I.I.) refers to the response of the complete structure-foundation-soil system to the excitation by D'Alembert forces associated with the acceleration of the superstructure due to the kinematic interaction (Fig. 2-1b).

5
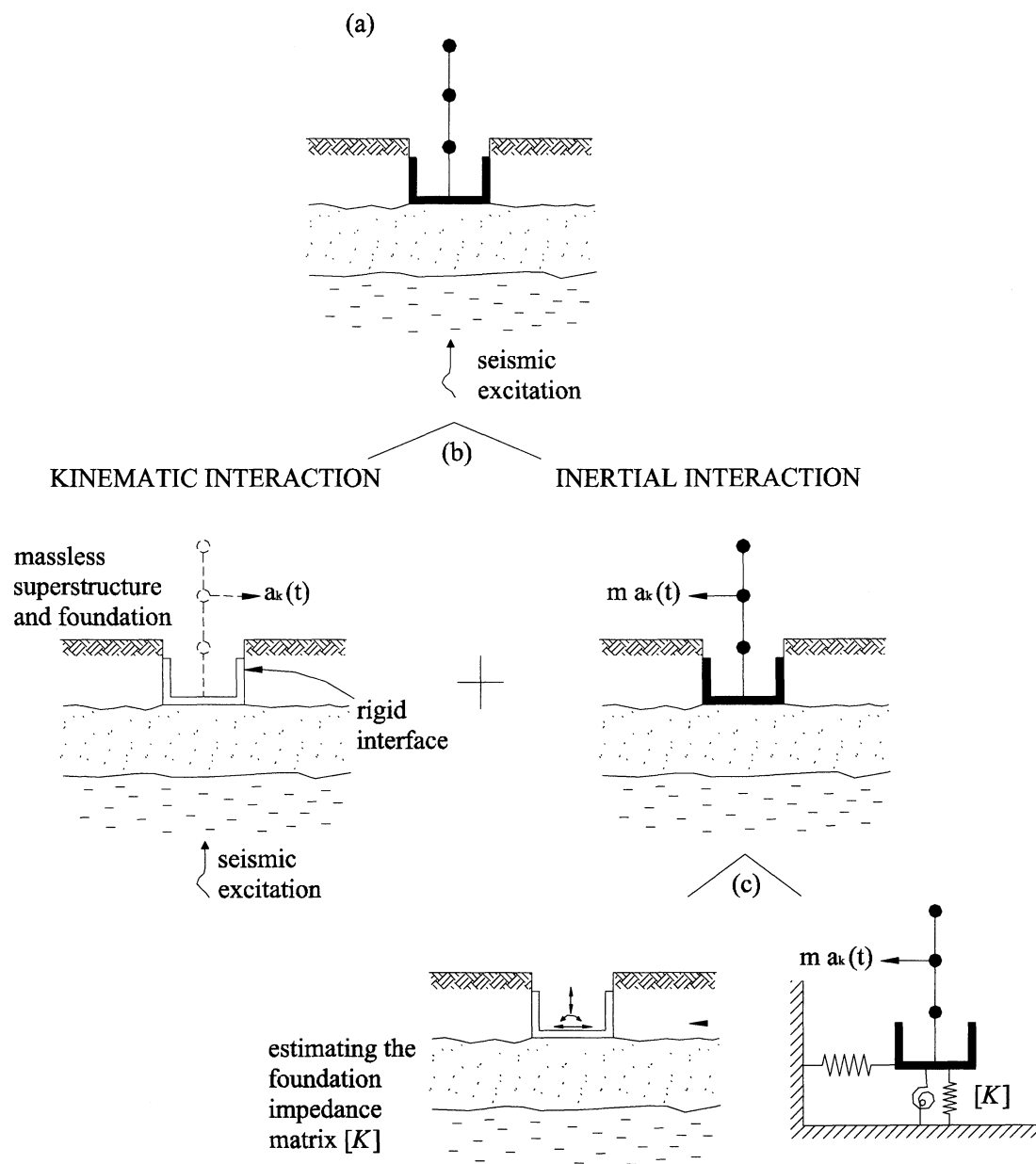
FIGURE 2-1. (a) The geometry of soil-structure interaction problem; (b) decomposition into kinematic and inertial response; (c) two-step analysis of inertial interaction.

Furthermore, for a surface or embedded foundation, "inertial interaction" (I.I.) analysis is also conveniently performed in two steps, as shown in Fig. 2-1c (after Kausel & Roesset 1974): Compute first the foundation dynamic "impedances" ("springs" and "dashpots") associated with each mode of vibration, and then determine the seismic response of the structure and foundation supported on these "springs" and "dashpots", and subjected to the "kinematic" accelerations $a_k(t)$ of the base. This Section presents methods and results for each of these three analysis steps for the seismic response.

2.2 Assessing the effects of "Kinematic Interaction" (K.I.)

The first step of the K.I. analysis is to determine the "free-field" response of the site, that is, the spatial and temporal variation of the motion before building the structure. This task requires that:

(a) The *design motion* be known at a specific ("*control*") point, which is usually taken to be at the ground surface or at the rock-outcrop surface, as sketched in Fig. 2-2. Most frequently the design motion is given in the form of a *design response spectrum* in the horizontal direction and sometimes also a second one in the vertical direction.

(b) The type of seismic waves that produce the above motion at the "control" point may be either estimated from a pertinent seismological study or simply assumed in a reasonable manner. In most cases the assumption is that the horizontal component of motion is due solely to vertically-propagating shear (S) waves and vertical dilatational (P) waves. In critical projects extreme cases of wave patterns (oblique body waves, surface waves) have to be considered.

Having established (a) and (b), wave-propagation analyses are performed to estimate the free-field motion on the line of the soil-foundation interface. The computer code SHAKE (Schnabel et al 1973) is one a well established tool for performing such analyses, and can be used with any possible location of the control point (at the ground surface, at the rock outcrop surface, or the base of the soil deposit). Other codes, performing truly non-linear response analyses (DESRA, DYNAFLOW, CHARSOIL, STEALTH, ANDRES, etc.) require that the base motion be first estimated and used as input. In these techniques, the "control" point should not be selected within the soil at a specific depth.

incident seismic waves
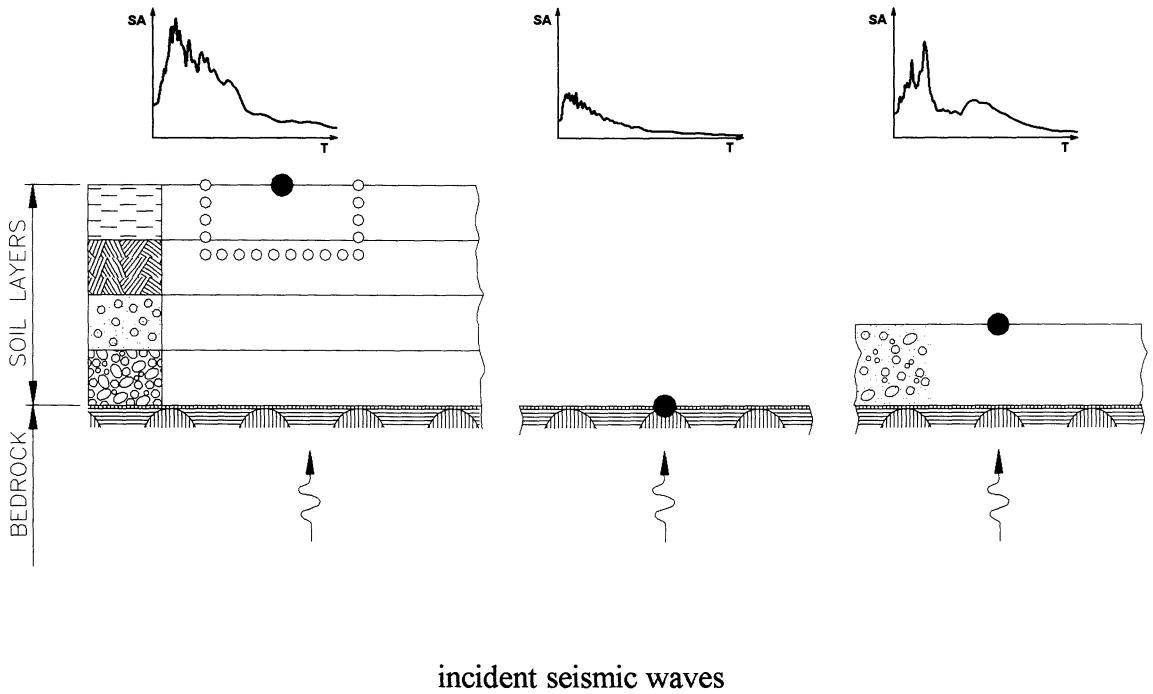
FIGURE 2-2. Selection of the "control" point where the seismic excitation is specified.

2.2.1 Simplified site response analysis

For the case of SH or SV harmonic waves propagating vertically through the soil with frequency ω, the variation of motion with depth in the free-field of a horizontally stratified deposit will be given by one-dimensional amplification theory. For a homogeneous soil layer, the amplitude of the motion at any depth z relates to the motion at the ground surface as follows:

$$A \equiv \frac{U_B}{U_A} = \cos\left(k\, z\right) \tag{2-1}$$

where k = a complex "wavenumber" in view of the presence of material damping in the soil

$$k = \frac{\omega}{V_s\,(1+2\,i\beta)^{1/2}} \tag{2-2}$$

where ω = excitation frequency, V_s = propagation velocity of shear waves in the soil, $i = \sqrt{-1}$, β = linear hysteretic damping factor of the soil material.

If material damping is ignored, function A simplifies to:

$$A = \cos\left(\frac{\omega\,z}{V_s}\right) \tag{2-3}$$

for any specific depth $z = D$ (where the structure will be founded), this "transfer" function becomes zero whenever $\omega = (2n+1)\,(\pi/2)\,(V_s\,/\,D)$, which are the natural frequencies in shear vibrations of a stratum of thickness D. This implies that these frequencies would be entirely filtered out from the seismic motion at the foundation depth D.

Since the transfer function of Eqn (2-1) is equal to or less than 1 over the whole frequency range, the amplitudes of the motion will always be de-amplified with depth. This is no longer true when there is some amount of internal damping in the soil, but for moderate values of damping the transfer function will still show some important variations with frequency and the motion at the depth D will still be less than at the surface.

It is also possible in the free field to define a pseudo-rotation (Fig. 2-3):

$$\Phi = \frac{U_A - U_B}{D} \tag{2-4}$$

For the case of the homogeneous stratum and no internal damping, the pseudo-rotation becomes

$$\Phi = \frac{U_A}{D}\left[1 - \cos\left(\frac{\omega D}{V_s}\right)\right] = 2\frac{U_A}{D}\sin^2\left(\frac{\omega D}{V_s}\right) \tag{2-5}$$

2.2.2 Simplified Kinematic Interaction analysis --- "Foundation Input Motion"

The displacement and pseudo-rotation of Eqns (2-1) and (2-5) are for depth D in the free field and constitute the "driving" motion for the kinematic response of the embedded foundations. The presence of a more-or-less rigid embedded foundation *diffracts* the 1-D seismic waves, since its rigid body motion is generally incompatible with the free-field motion. The wave field now becomes much more complicated and the resulting motion of the foundation differs from the free-field motion, and includes translational and rotational components. Since, according to Fig. 2-1, this foundation motion is used as the *excitation* in the Inertial Interaction (I.I.) step of the whole seismic response analysis, it is termed *Foundation Input Motion* (FIM).

The following simple expressions [based on results by Luco (1969), Elsabee et al (1977), Tassoulas et al (1984), Harada et (1981), and O'Rourke et al (1984)] can be used for estimating the translational and rotational components of the FIM in some characteristic cases. Specifically:

(a) For a surface foundation subjected to vertical S waves:

$$U_B \approx U_A \tag{2-6}$$

$$\Phi_B \approx 0 \tag{2-7}$$

which implies that there is no kinematic effect, and the FIM includes only a translation equal to the free-field ground surface motion.

Massless Foundation:
Kinematic Interaction   Free Field
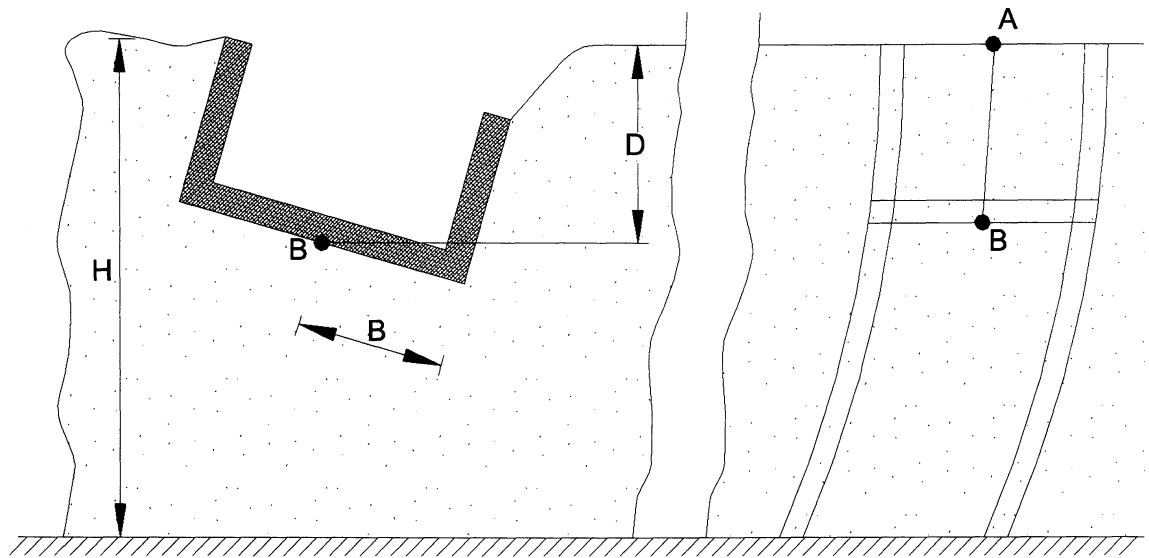
FIGURE 2-3. Definition of U_A, U_B and Φ_B for a massless foundation (kinematic interaction problem) and the associated points in the free field (from Elsabee et al, 1977).

(b) For a surface foundation subjected to oblique S or surface (Rayleigh or Love) waves, one must first determine the apparent propagation velocity V_a along the horizontal x axis (Fig. 2-4). Calling ψ the angle of incidence of an S wave:

$$V_a = \frac{V_s}{\sin \psi} \tag{2-8}$$

Different choices for the value of the angle ψ can be made and the one leading to the largest structural response be selected. For surface waves V_a will be determined from the dispersion relation of the soil deposit for each particular frequency ω. For Rayleigh waves in a practically homogeneous and deep soil deposit, V_a turns out to be only slightly less than V_s. For a deposit consisting of a multi-layer soil stratum of thickness H, having an average S-wave velocity V_r, V_a varies between V_s (lower limit) and V_r (upper limit) as follows:

$$V_a = \begin{cases} 0.90\,V_r & , f \leq f_H & (2-9a) \\[2mm] V_s & , f \geq 2f_H & (2-9b) \\[2mm] 0.90\,V_r - (0.90\,V_r - V_s)\,(f/f_H - 1) & , f_H < f \leq 2f_H & (2-9c) \end{cases}$$

where $f_H = V_s / 4H$ is the fundamental natural frequency of the soil deposit.

Finally, for a deposit with stiffnesses increasing more-or-less continuously with depth, V_α is only slightly less than the S-wave velocity $V_s(z_c)$ at a depth

$$z_c \approx \frac{1}{3}\,\lambda_R \tag{2-10}$$

where λ_R is the wave length of the Rayleigh wave $= V_\alpha / f$

Once the apparent velocity V_α along the horizontal x axis has been estimated, the components of the FIM can be determined from the following relations:

12
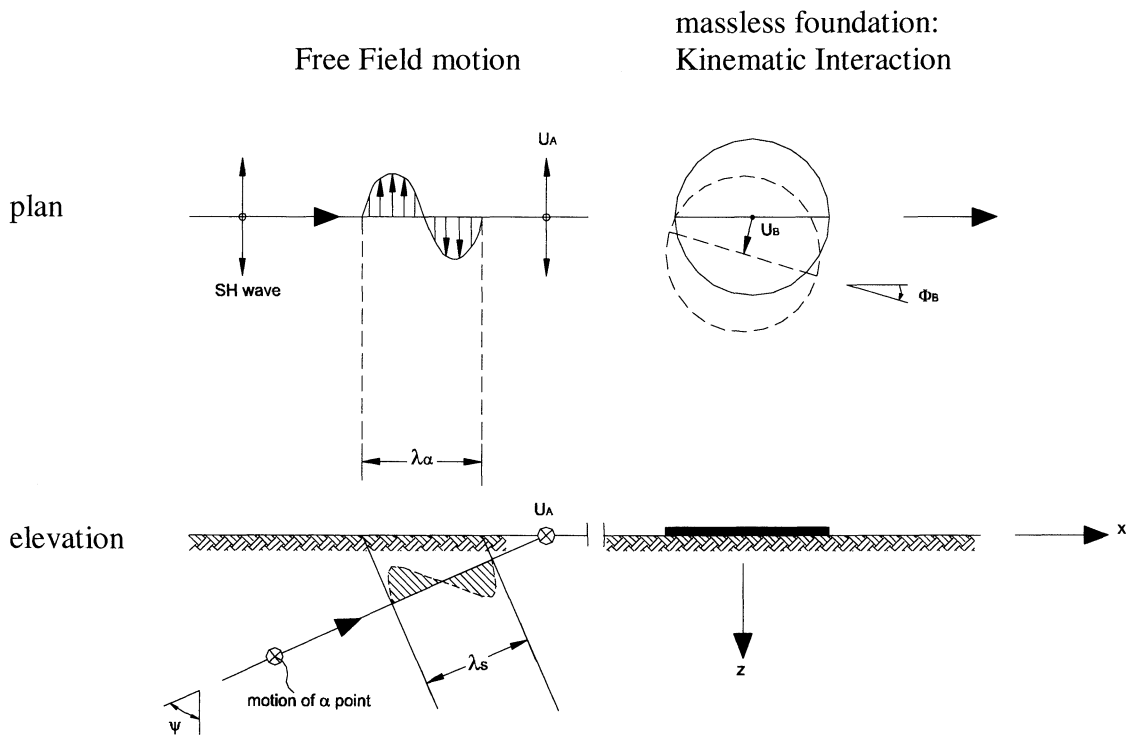
FIGURE 2-4. Inclined SH wave, apparent wave length ($\lambda_\alpha = \lambda_s / \sin\psi$), free-field surface motion (U_A), and foundation effective input motion (U_B, Φ_B).

◆ horizontal translation:

$$U_B = U_A \, I_U(\omega) \tag{2-11a}$$

$$I_U(\omega) = \begin{cases} \dfrac{\sin(\omega B / V_a)}{\omega B / V_a} & , \quad \dfrac{\omega B}{V_a} \leq \dfrac{\pi}{2} \qquad\qquad (2-11b) \\[2em] \dfrac{2}{\pi} & , \quad \dfrac{\omega B}{V_a} > \dfrac{\pi}{2} \qquad\qquad (2-11c) \end{cases}$$

◆ rotation:

$$\Phi_B = \dfrac{U_A}{B} \, I_\Phi(\omega) \tag{2-12a}$$

where:

$$I_\Phi = \begin{cases} 0.30\left[1 - \cos\left(\dfrac{\omega B}{V_a}\right)\right] & , \quad \dfrac{\omega B}{V_a} \leq \dfrac{\pi}{2} \qquad\qquad (2-12b) \\[2em] 0.30 & , \quad \dfrac{\omega B}{V_a} > \dfrac{\pi}{2} \qquad\qquad (2-12c) \end{cases}$$

in which R = the foundation halfwidth or "equivalent" radius in the direction examined; ω = the cyclic frequency of the harmonic seismic waves; Φ_B denotes rotation about the "out of plane" horizontal axis, through the center of the foundation base.

(c) For a foundation *embedded* at depth D, with or without sidewalls, and subjected to vertical and oblique SH waves, the horizontal and rotational component of FIM are:

$$U_B = U_A \, I_U(\omega) \tag{2-13a}$$

$$I_U(\omega) = \begin{cases} \cos\left(\dfrac{\pi}{2} \dfrac{f}{f_D}\right) & , \quad f \leq \dfrac{2}{3} f_D \qquad\qquad (2-13b) \\[2em] 0.50 & , \quad f \geq \dfrac{2}{3} f_D \qquad\qquad (2-13c) \end{cases}$$

14

$$\Phi_B = \frac{U_A}{B} \, I_\Phi(\omega) \tag{2-14a}$$

$$I_\Phi(\omega) = \begin{cases} 0.20 \left[1 - \cos\left(\frac{\pi}{2} \frac{f}{f_D}\right) \right] & , \; f \le f_D \tag{2-14b} \\[2ex] 0.20 & , \; f \ge f_D \tag{2-14c} \end{cases}$$

in which $f = \omega / 2\pi$ = the frequency in Hz of the harmonic seismic wave; $f_D = V_s / 4\,D$ = the frequency in shearing oscillations of a (hypothetical) soil stratum of thickness D.

Notice that the rotation is an integral and important part of the base motion for the massless foundation. Ignoring it, while de-amplifying the translational component, through the transfer function I_U (ω), may lead to errors on the unsafe side. These errors are perhaps negligible for determining the response of short squatty structures --- especially very heavy ones, but they may be substantial (i.e., of the order of 50%) for the top of tall slender structures. On the other hand, ignoring both the de-amplification of the horizontal component ($I_U = 1$) and the existence of the rotational component usually leads to slightly conservative results; this is a simplification frequently followed in practice for non-critical structures (Gazetas 1983).

2.2.3 Use of K.I. transfer functions

Equations (2-6) to (2-14) are transfer functions, relating to the free-field horizontal ground surface motion the effective foundation input motion (FIM) in the frequency domain. The mathematically correct (but still approximate) way of using the functions is as follows:

- obtain the Fourier Amplitude Spectrum $F(U_A)$ of the Design Motion at the free-field ground surface

- multiply $F(U_A)$ by I_U (ω) and by I_Φ (ω) / B to obtain the Fourier Amplitude Spectra functions (U_B and Φ_B) of the components of the FIM.

- use these functions directly as excitation in the inertial interaction analysis, if the latter is done

in the frequency domain, or obtain, through an inverse Fourier Transformation, the corresponding time histories to be used as excitation in a time domain inertial response analysis.

In practice, the most frequently used method involves a further simplification. It makes use of *Response Spectra* rather than Fourier Spectra, and is therefore particularly attractive whenever the design motion is specified in the form of a Design Response Spectrum SA(ω) at the ground surface, which is the most usual case in design codes. The response spectrum of the *effective horizontal FIM* is approximated as the product of SA(ω) × I_U (ω) for the acceleration to be applied at the foundation mass, and as the product SA(ω) × [I_U (ω) + $I_Φ$ (ω) H_c /B] for the acceleration to be applied at a structural mass located a distance H_c from the base.

2.3 Inertial interaction: Assessment of foundation "springs" and "dashpots"

As explained in paragraph 2-1, the first step in Inertial Interaction (I.I.) analysis is to determine the foundation impedances (i.e., the "springs" and "dashpots") corresponding to each mode of vibration. For the usual case of a practically-rigid foundation, there are six modes of vibration, one for each degree of freedom: three translational (dynamic displacements along the axes x, y and z) and three rotational (dynamic rotations around the same axes)

For each mode, the soil can be replaced for the dynamic analysis by a dynamic "spring" of stiffness K and by a "dashpot" of modulus C. Their values will be discussed later on. Figure 2-5 illustrates the vertical spring and dashpot ($\overline{K}_z$ and C_z) of an embedded foundation. Subjected to harmonic vertical force $P_z(t) = P_z$ cos (ω t + a) with amplitude P_z and frequency ω , this foundation experiences a harmonic steady-state displacement $u_z(t)$ which has the same frequency ω but is out-of-phase with $P_z(t)$. Thus, $u_z(t)$ can be expressed in the following two equivalent ways:

$$u_z(t) = u_z \cos(\omega t + a + \varphi) = u_1 \cos(\omega t + a) + u_2 \sin(\omega t + a) \tag{2-15}$$
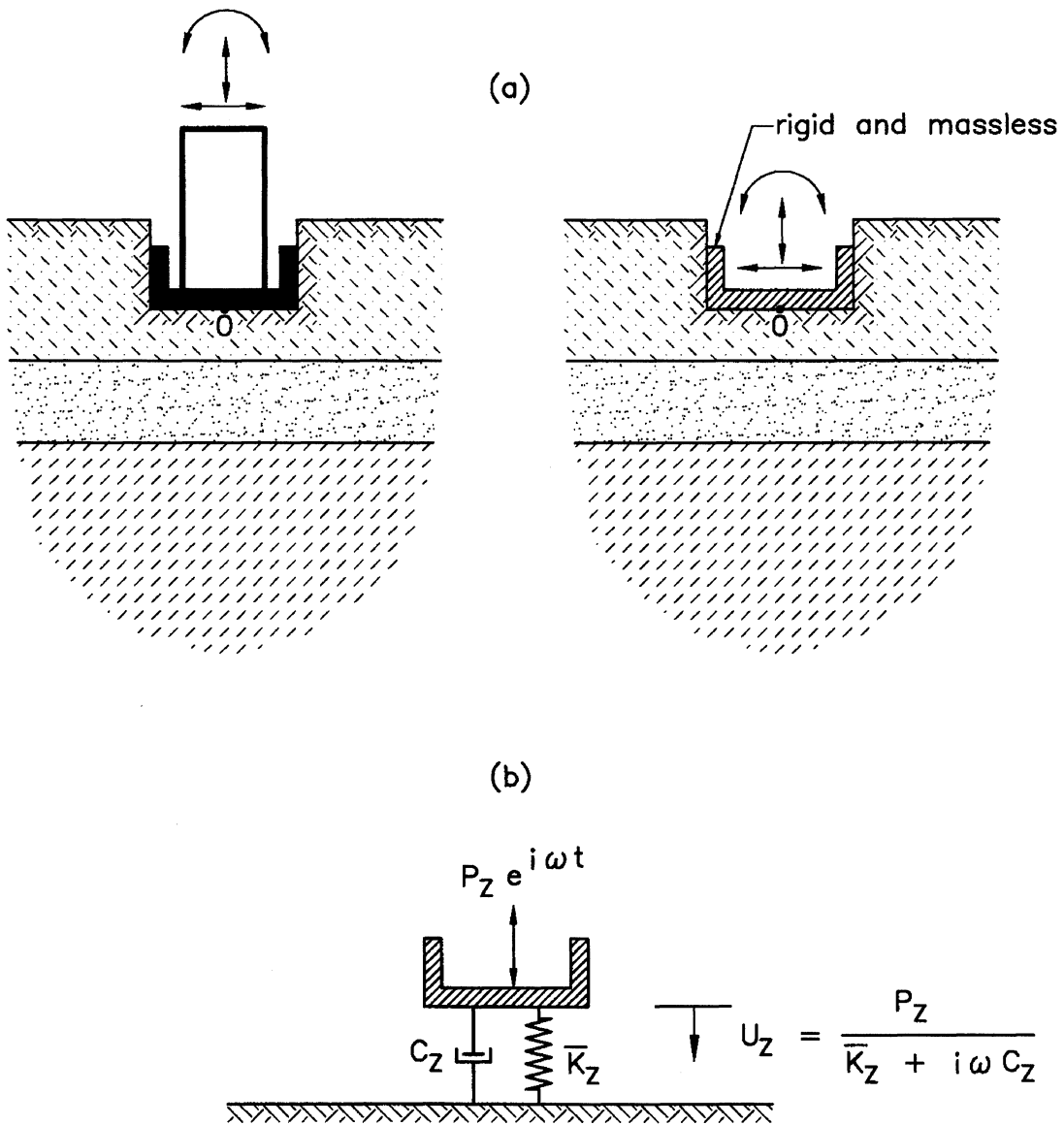
FIGURE 2-5. Physical interpretation of the dynamic "spring" and "dashpot" in the vertical mode of vibration.

where the amplitude u_z and phase angle ϕ are related to the in-phase, u_1 and the 90°-out-of-phase, u_2 , components according to:

$$u_z = \sqrt{(u_1^2 + u_2^2)} \qquad (2\text{-}16a)$$

$$\tan \phi = \frac{u_2}{u_1} \qquad (2\text{-}16b)$$

We can rewrite the foregoing expressions in an equivalent and computationally beneficial way using complex number notation:

$$P_z(t) = \overline{P}_z \exp(i \omega t) \qquad (2\text{-}17a)$$

$$u_z(t) = \overline{u}_z \exp(i \omega t) \qquad (2\text{-}17b)$$

where now $\overline{P}_z$ and $\overline{u}_z$ are complex quantities (i $= \sqrt{-1}$)

$$\overline{P}_z = P_{z1} + i P_{z2} \qquad (2\text{-}18a)$$

$$\overline{u}_z = u_{z1} + i u_{z2} \qquad (2\text{-}18b)$$

Eqns (2-17) and (2-18) are equivalent to Eqns (2-15) , (2-16) with the following relations being valid for the amplitudes:

$$P_z = \left| \overline{P}_z \right| = \sqrt{(P_{z1}^2 + P_{z2}^2)} \qquad (2\text{-}19a)$$

$$u_z = |\overline{u}_z| = \sqrt{(u_{z1}^2 + u_{z2}^2)} \qquad (2\text{-}19b)$$

while the two phase angles, α and ϕ , are included in the complex forms.

With P_z and u_z being out of phase or, alternatively, with $\overline{P}_z$ and $\overline{u}_z$ being complex numbers, the dynamic vertical impedance (force-displacement ratio) becomes:.

$$\mathcal{K}_z = \frac{\bar{P_z}}{\bar{u}_z} = \bar{K}_z + i\,\omega\,C_z \qquad\qquad (2\text{-}20)$$

in which both $\bar{K}_z$ and C_z are, in general, functions of the frequency ω. The spring constant $\bar{K}_z$ termed *dynamic stiffness*, reflects the stiffness and inertia of the supporting soil; its dependence on frequency is attributed solely to the influence which frequency exerts on inertia, since soil material properties are to a good approximation frequency-independent. The *dashpot coefficient* C_z reflects the two types of damping (radiation and material) generated in the system; the former due to energy carried by the waves spreading away from the foundation, and the latter due to energy dissipated in the soil through hysteretic action. As evident from Eqn (2-15), damping is responsible for the phase difference between the excitation P_z and the response u_z.

The above definition (Eqn 2-20) is also applicable to each of the other five modes of vibration. Thus, we define as lateral (swaying) impedance $\mathcal{K}_y$ the ratio of the horizontal harmonic force over the resulting harmonic displacement $u_y(t)$ in the same direction:

$$\mathcal{K}_y = \frac{\bar{P}_y}{\bar{u}_y} = \bar{K}_y + i\,\omega\,C_y \qquad\qquad (2\text{-}21)$$

Similarly,

- $\mathcal{K}_y$ = the longitudinal (swaying) impedance (force-displacement ratio), for horizontal motion in the long direction

- $\mathcal{K}_{rx}$ = the rocking impedance (moment-rotation ratio), for rotational motion about the long axis of the foundation basemat

- $\mathcal{K}_{ry}$ = the rocking impedance (moment-rotation ratio), for rotational motion about the short axis of the foundation

- $\mathcal{K}_t$ = the torsional impedance (moment-rotation ratio), for rotational oscillation about the vertical axis

Moreover, in embedded foundations and piles, horizontal forces along principal axes induce rotational in addition to translational oscillations; hence, a *cross-coupling* horizontal-rocking

impedance also exists: $\mathscr{K}'_{\text{x-ry}}$ and $\mathscr{K}'_{\text{y-rx}}$. The coupling impedances are usually negligibly small in shallow foundations, but their effects may become appreciable for greater depths of embedment, owing to the moments about the base axes produced by horizontal soil reactions against the sidewalls.

2.3.1 Use of impedances: Lateral seismic response of block foundation supporting a 1-DOF structure

We refer to Figure (2-6) for an example on how to use the foundation "springs" and "dashpots" to determine the response of a complete structure to harmonic earthquake-type excitation. The foundation and structure possess two orthogonal axes of symmetry, x and y, and coupled horizontal (swaying) and rotational (rocking) oscillations take place. Of interest are the foundation horizontal displacement $U_o \exp(i\omega t)$ along the x axis, foundation rotation $\Phi_o \exp(i\omega t)$ about the y axis, and the structure relative displacement $U_1 \exp(i\omega t)$. The seismic excitation is given by the free-field surface displacement $U_A \exp(i\omega t)$ of amplitude U_A and frequency ω.

As a first step, we determine the Foundation Input Motion (FIM), from the kinematic interaction analysis. Using the information of Section 2.2,

$$U_B = U_A I_U(\omega) \qquad \text{and} \qquad \Phi_B = U_A I_\Phi(\omega) / B$$

where I_U and I_Φ are the appropriate kinematic interaction factors for each frequency ω.

The governing D'Alembert equations for dynamic equilibrium of the foundation block and the structure are (Richart et al 1970):

$$\mathscr{K}'_x (U_o - U_B) + \mathscr{K}'_{\text{x-ry}} (\Phi_o - \Phi_B) = \omega^2 [m_o U_o + m_1 (U_o + H \Phi_o + U_1)] \qquad (2\text{-}22a)$$
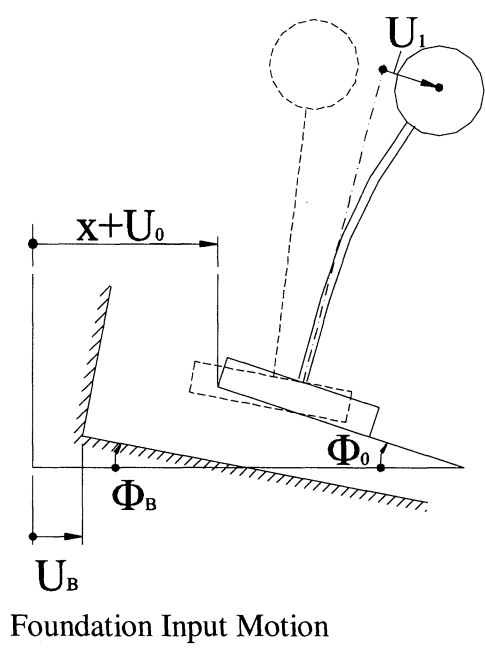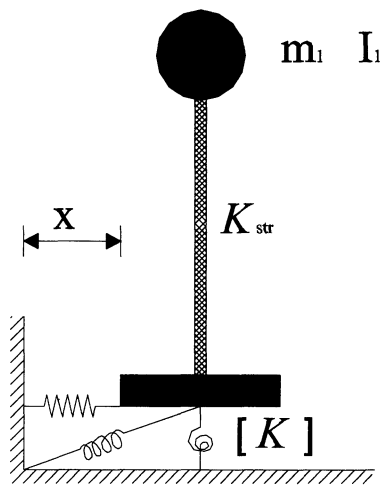
FIGURE 2-6. Seismic displacements and rotation of a foundation block supporting a 1-DOF super-structure. The seismic excitation is described through the free-field ground-surface displacement U_A, assumed to be produced by a certain type of body or surface waves.

$$\mathscr{K}'_{x\text{-}ry}\,(U_O - U_B) + \mathscr{K}'_{ry}\,(\Phi_O - \Phi_B) \;=\; \omega^2\,[I_o\,\Phi_o + I_1\,\Phi_o + m_1\,H\,(U_o + H\,\Phi_o + U_1)] \qquad (2\text{-}22b)$$

$$-m_1\,\omega^2\,(U_o + H\,\Phi_o + U_1) + K_{str}\,U_1 = 0 \qquad (2\text{-}22c)$$

in which m_o and I_o are the mass and mass moment of inertia of the foundation, m_1 and I_1 are the mass and mass moment of inertia of the superstructure and $K_{str} = K_{str} + i\,\omega\,C_{str}$ the structural impedance (stiffness and damping) of the superstructure.

The above equations are a simple algebraic system of 3 equations in 3 unknowns, despite the fact that the quantities involved are complex numbers. The solution, in matrix form, for the foundation motion is:

$$\left\{ \begin{array}{c} U_o \\ \Phi_o \end{array} \right\} = \frac{K}{K - \omega^2\,(M_o - M_b)} \left\{ \begin{array}{c} U_B \\ \Phi_B \end{array} \right\} \qquad (2\text{-}23a)$$

where:

$$K = \left[\begin{array}{cc} K_x & K_{x\text{-}ry} \\ K_{x\text{-}ry} & K_{ry} \end{array} \right] \qquad (2\text{-}23b)$$

$$[M_o] = \left[\begin{array}{cc} m_o & 0 \\ 0 & I_o \end{array} \right] \qquad (2\text{-}23c)$$

$$[M_b] = [M] + m_1 A \left[\begin{array}{cc} 1 & H \\ H & H^2 \end{array} \right] \qquad (2\text{-}23d)$$

$$[M] = \left[\begin{array}{cc} m_1 & m_1 H \\ m_1 H & m_1 H^2 + I_1 \end{array} \right] \qquad (2\text{-}23e)$$

for the superstructure:

$$U_1 = \frac{m_1\omega^2}{K_{srt} + i\omega^2 C_{str} - m_1\omega^2}\,(U_O + h\,\Phi_O) \qquad\qquad (2\text{-}24)$$

Equations (2-23) and (2-24) provide the solution in closed form. The computations, however, may be somewhat tedious if performed by hand, since K matrix involves complex numbers. On the other hand, it is noted that if a real-number notation (with amplitudes and phase angles) had been adopted (as in Eqn 2-15), Eqns (2-23) would become 6 equations with 6 unknowns – a less desirable procedure. A simple computer code could readily perform the operations of Eqns (2-23) and (2-24).

2.4 Computing dynamic impedances: Tables and Charts for dynamic "springs" and "dashpots"

The most important material and geometric factors which affect the dynamic impedances of foundations are:

(1) the shape of the foundation (circular, strip, rectangular, arbitrary)

(2) the type of soil profile (deep uniform deposit, deep multi-layer deposit, shallow stratum on rock)

(3) the amount of embedment (surface foundation, embedded foundation, piled foundation)

For a major project of critical significance a case-specific analysis must be performed, using the most suitable numerical computer program. In most practical cases, however, foundation impedances can be estimated from approximate expressions and charts. For the usual case of a practically rigid foundation, a number of analytical formulae and charts for such stiffnesses have been published (e.g., Luco 1974, Kausel & Roesset 1975, Gazetas 1983, Wong & Luco 1985, Dobry & Gazetas 1986, Guzina & Pak 1998, Vrettos 1999) and are presented in this section.

2.4.1 Surface foundation on homogeneous halfspace

For an arbitrarily-shaped foundation mat, the engineer must first determine an "equivalent" circumscribed rectangle 2B by 2L (L>B) using common sense, as sketched in Fig 2-7. Then,
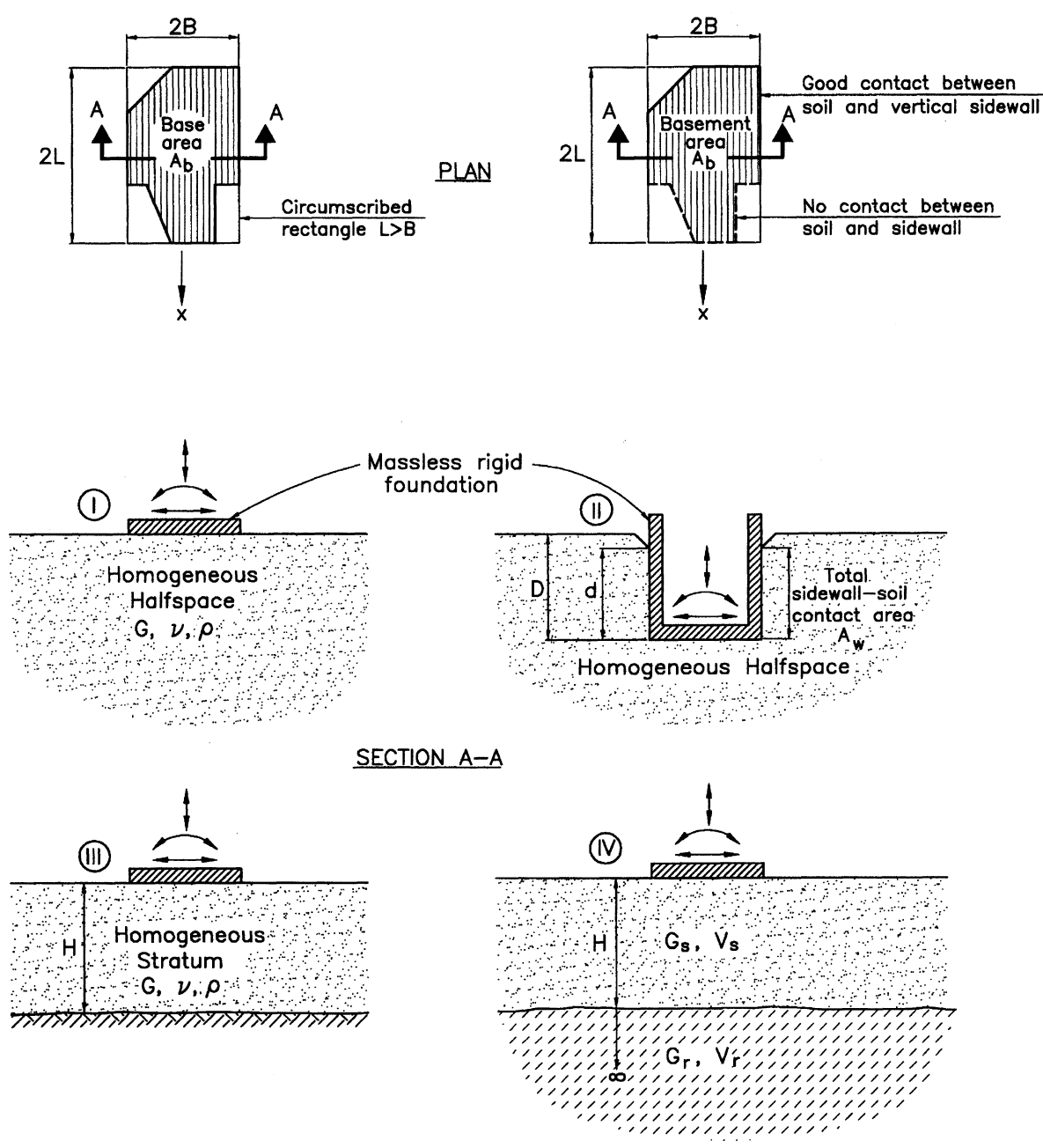
FIGURE 2-7. The four foundation-soil systems whose impedances are given in tabular/graphical form in this section. Numbers I to IV refer the corresponding tables and the associated graphs.

Table 2-I. Dynamic stiffness and dashpot coefficients for arbitrary shaped foundations on homogeneous halfspace surface.

Vibration Mode	Dynamic Stiffness $\mathcal{K} = K\,k(\omega)$		Dynamic Stiffness Coefficient k (General Shape; $0 \leq a_0 \leq 2$)‡	Radiation Dashpot Coefficient C (General Shapes)
	Static Stiffness K			
	General Shape (foundation-soil contact surface area $= A_b$ with equivalent rectangle 2Lx2B; L>B)†	Square $L = B$		
Vertical, z	$K_z = \dfrac{2GL}{1-\nu}(0.73 + 1.54\,\chi^{0.75})$ with $\chi = \dfrac{A_b}{4L^2}$	$K_z = \dfrac{4.54\,GB}{1-\nu}$	$k_z = k_z\left(\dfrac{L}{B},\,\nu,\,a_0\right)$ plotted in Graph a	$C_z = (\rho\,V_{La}\,A_b)\,\bar{c}_z$ $\bar{c}_z = \bar{c}_z\left(\dfrac{L}{B},\,a_0\right)$ plotted in Graph c
Horizontal, y (lateral direction)	$K_y = \dfrac{2GL}{2-\nu}(2 + 2.5\,\chi^{0.85})$	$K_y = \dfrac{9\,GB}{2-\nu}$	$k_y = k_y\left(\dfrac{L}{B},\,a_0\right)$ plotted in Graph b	$C_y = (\rho\,V_s\,A_b)\,\bar{c}_y$ $\bar{c}_y = \bar{c}_y\left(\dfrac{L}{B},\,a_0\right)$ plotted in Graph d
Horizontal, x (longitudinal direction)	$K_x = K_y - \dfrac{0.2}{0.75-\nu}\,GL\left(1 - \dfrac{B}{L}\right)$	$K_x = K_y$	$k_x \simeq 1$	$C_x \simeq \rho\,V_s\,A_b$
Rocking, rx (around x axis)	$K_{rx} = \dfrac{G}{1-\nu}\,I_{bx}^{.75}\left(\dfrac{L}{B}\right)^{0.25}\!\left(2.4 + 0.5\,\dfrac{B}{L}\right)$ with I_{bx} = area moment of inertia of foundation - soil contact surface around x axis	$K_{rx} = \dfrac{0.45\,GB^3}{1-\nu}$	$k_{rx} = 1 - 0.20\,a_0$	$C_{rx} = (\rho\,V_{La}\,I_{bx})\,\bar{c}_{rx}$ $\bar{c}_{rx} = \bar{c}_{rx}\left(\dfrac{L}{B},\,a_0\right)$ plotted in Graph e
Rocking, ry (around y axis)	$K_{ry} = \dfrac{G}{1-\nu}\,I_{by}^{.75}\left[3\left(\dfrac{L}{B}\right)^{0.15}\right]$ with I_{by} = area moment of inertia of foundation - soil contact surface around y axis	$K_{ry} = K_{rx}$	$\nu < 0.45:$ $k_{ry} \simeq 1 - 0.30\,a_0$ $\nu \simeq 0.5:$ $k_{ry} \simeq 1 - 0.25\,a_0\left(\dfrac{L}{B}\right)^{0.30}$	$C_{ry} = (\rho\,V_{La}\,I_{by})\,\bar{c}_{ry}$ $\bar{c}_{ry} = \bar{c}_{ry}\left(\dfrac{L}{B},\,a_0\right)$ plotted in Graph f
Torsional	$K_t = G\,J_t^{0.75}\left[4 + 11\left(1 - \dfrac{B}{L}\right)^{10}\right]$ with $J_t = I_{bx} + I_{by}$ = polar moment of inertia of foundation - soil contact surface	$K_t = 8.3\,GB^3$	$k_t \simeq 1 - 0.14\,a_0$	$C_t = (\rho\,V_s\,J_t)\,\bar{c}_t$ $\bar{c}_t = \bar{c}_t\left(\dfrac{L}{B},\,a_0\right)$ plotted in Graph g

† Note that as $L/B \to \infty$ (strip footing) the theoretical values of K_z and $K_y \to 0$; values computed from the two given formulas correspond to footing of $L/B \approx 20$

‡ $a_0 = \omega B / V_s$

(Graphs accompanying Table 2-I)

26
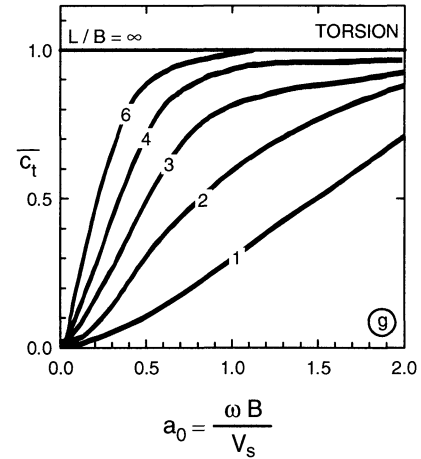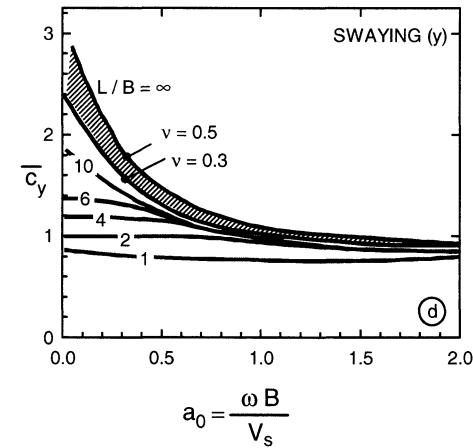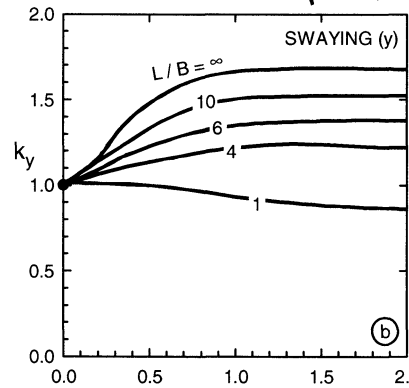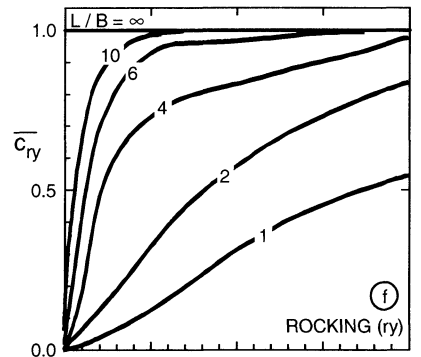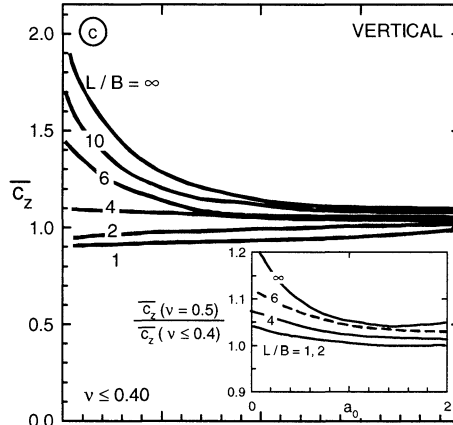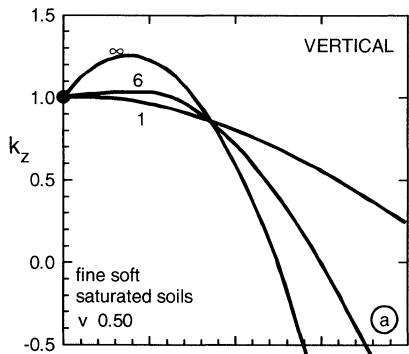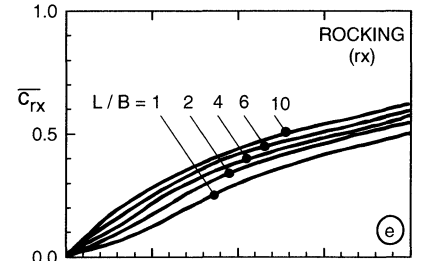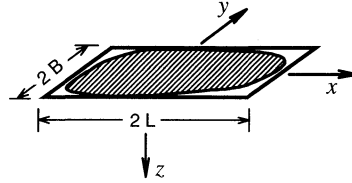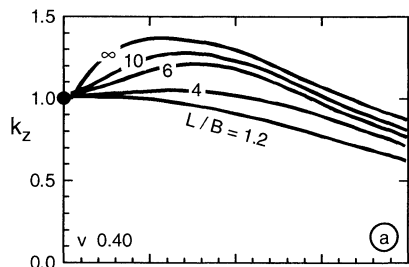
to compute the impedances in the 6 modes of vibration, from Table 2-I, (from Gazetas 1991a) all the engineer needs is the values of:

- A_b , I_{bx} , I_{by} , I_b = area, moments of inertia about x , y, and polar moment of inertia about z, of the actual soil foundation contact surface; if loss of contact under part of the foundation (e.g. along the edges of a rocking foundation) is likely, engineering judgment may be used to discount the contribution of this part

- B and L = semi-width and semi length of the circumscribed rectangle

- G, ν, V_s and V_{la} , the shear modulus, Poisson's ratio, shear wave velocity, and "Lysmer's analog" wave velocity; the latter is the apparent propagation velocity of compression-extension waves under a foundation and is related to V_s according to

$$V_{La} = \frac{3.4}{\pi\,(1-\nu)}\,V_s \tag{2-25}$$

- ω = cyclic frequency (in radians / second) of interest

This Table as well as all other Tables in this chapter gives:

- the dynamic stiffness ("springs"), $\overline{K} = \overline{K}(\omega)$ as a product of the static stiffness, K , times the dynamic stiffness coefficient k = k(ω) :

$$\overline{K}(\omega) = K \times k(\omega) \tag{2-26}$$

- the radiation damping ("dashpot") coefficient C = C(ω) . These coefficients do not include the soil hysteretic damping, β; to incorporate such damping, simply add to the foregoing C value the corresponding material dashpot coefficient $2\overline{K}\beta/\omega$:

$$\text{total C = radiation C} + \frac{2\overline{K}\beta}{\omega} \tag{2-27}$$

2.4.2 Partially and fully-embedded foundations

For a foundation embedded in a deep and relatively homogeneous soil deposit that can be modeled as a homogeneous halfspace, "springs" and "dashpots" are obtained from the formulae and charts of Table 2-II (from Gazetas 1991a). The foundation basemat can again be of arbitrary (solid) shape (Fig. 2-7). The engineer must determine the following additional parameters using the Table:

- D = the depth below the ground surface of the foundation basemat

- A_w or d = the total area of the actual sidewall-soil contact surface, or the (average) height of the sidewall that is in good contact with the surrounding soil. A_w should, in general, be smaller that the nominal area of contact to account for such phenomena as slippage and separation that may occur near the ground surface. The engineer should refer to published results of large and small scale experiments for a guidance in selecting a suitable value for A_w or d (e.g., Stokoe & Richart 1974; Novak 1985, Dobry et al 1986, Gazetas & Stokoe 1991). Note that A_w or d will not necessarily attain a single value for all modes of vibration.

- A_{ws} and A_{wce} which refer to horizontal oscillations and represent the sum of the projections of all the sidewall area in directions parallel (A_{ws}) and perpendicular (A_{wce}) to loading. Again A_{ws} and A_{wce} should be smaller than the nominal areas in shearing and compression, to account for slippage and/or separation. h = the distance of the (effective) sidewall centroid from the ground surface

- Note that most of the formulae of Table 2-II are valid for symmetric and non-symmetric contact along the perimeter of the vertical sidewalls and the surrounding soil. Note also that

28

TABLE 2-II. Dynamic stiffnesses and dashpot coefficients for arbitrary shaped foundations partially or fully embedded in a homogeneous halfspace.

Vibration Mode	Dynamic Stiffness $\mathcal{K}_{emb} = K_{emb}\, k_{emb}(\omega)$		Radiation Dashpot Coefficient $C_{emb}(\omega)$	
	Static Stiffness K_{emb} *(foundation with arbitrarily-shaped basemat A_b with equivalent rectangle $2L \times 2B$; total sidewall-soil contact area A_w (or constant wall-soil contact height d)*	Dynamic Stiffness Coefficient $k_{emb}(\omega)$ $(0 \le a_0 \le 2)$	General Foundation Shape	Rectangular Foundation $2L \times 2B \times d$
Vertical z	$K_{z,\,surf}$ obtained from Table 2-I A_w = actual sidewall-soil contact area; for constant effective contact height d along the perimeter: $A_w = d \times Perimeter$ $\chi = A_b / 4\,L^2$ $K_{z,\,emb} = K_{z,\,surf}\left[1 + \frac{1}{21}\frac{D}{B}(1+1.3\,\chi)\right]$ $\times \left[1 + 0.2\left(\frac{A_w}{A_b}\right)^{2/3}\right]$	**$\nu \le 0.4$** *Fully embedded*: $K_{z,\,emb} = K_{z,\,surf}\left[1 - 0.09\left(\frac{D}{B}\right)^{3/4} a_0{}^2\right]$ *In a trench*: $K_{z,\,tre} = K_{z,\,surf}\left[1 + 0.09\left(\frac{D}{B}\right)^{3/4} a_0{}^2\right]$ *Partially embedded*: interpolate between the two **$\nu = 0.5$** *Fully embedded, $L/B = 1-2$* $K_{z,\,emb} \simeq 1 - 0.09\left(\frac{D}{B}\right)^{3/4} a_0{}^2$ *Fully embedded, $L/B > 3$* $K_{z,\,emb} \simeq 1 - 0.35\left(\frac{D}{B}\right)^{1/2} a_0{}^{3.5}$	$C_{z,\,emb} = C_{z,\,surf} + \rho\, V_s\, A_w$ $C_{z,\,surf}$: see Table 2-I	$C_{z,\,emb} = 4\,\rho\, V_{La}\, B\, L\, \bar{c}_z$ $+ 4\,\rho\, V_s\,(B + L)\, d$ $\bar{c}_z$ according to Table 2-I
Horizontal y or x	$K_{y,\,emb} = K_{y,\,surf}\left(1 + 0.15\sqrt{\frac{D}{B}}\right)$ $\times \left[1 + 0.52\left(\frac{h}{B}\frac{A_w}{L^2}\right)^{0.4}\right]$ $K_{y,\,surf}$ obtained from Table 2-I $K_{x,\,emb}$ and $C_{x,\,emb}$ are computed similarly from $K_{x,\,surf}$ and $C_{y,\,surf}$	$K_{y,\,emb}$ and $K_{x,\,emb}$ can be estimated in terms of L/D, D/B, and d/B for each a_0 from the graphs accompanying this Table	$C_{y,\,emb} = C_{y,\,surf} +$ $+ \rho\, V_s\, A_{ws} + \rho\, V_{La}\, A_{wce}$ $A_{ws} = \sum(A_{wi} \sin\vartheta_i) =$ = total effective sidewall area shearing the soil $A_{wce} = \sum(A_{wi} \cos\vartheta_i) =$ = total effective sidewall area compressing the soil ϑ = inclination angle of surface A_{wi} from loading direction $C_{y,\,sur}$ according to Table 2-I	$C_{y,\,emb} = 4\,\rho\, V_s\, B\, L\, \bar{c}_y +$ $+ 4\,\rho\, V_s\, B\, d + 4\,\rho\, V_{La}\, L\, d$ $\bar{c}_y$ according to Table 2-I

29

TABLE 2-II (cont'd).

Vibration Mode	Dynamic Stiffness $\mathcal{K}_{emb} = K_{emb}\, k_{emb}(\omega)$		Radiation Dashpot Coefficient $C_{emb}(\omega)$	
	Static Stiffness K_{emb} (see notes in previous page)	Dynamic Stiffness Coefficient $k_{emb}(\omega)$ ($0 \le a_0 \le 2$)	General Foundation Shape	Rectangular Foundation $2L \times 2B \times d$
Rocking rx (around long. axis) **Rocking ry** (around lateral axis)	Expressions valid for any basemat shape but constant effective contact height d along the perimeter $K_{rx,emb} = K_{rx,surf} \times$ $\{1 + 1.26 \frac{d}{B} [1 + \frac{d}{B} (\frac{d}{D})^{-0.2} \sqrt{\frac{B}{L}}]\}$ $K_{ry,emb} = K_{ry,surf} \times$ $\{1 + 0.92 (\frac{d}{B})^{0.6} [1.5 + (\frac{d}{D})^{1.9} (\frac{B}{L})^{-0.6}]\}$	$K_{rx,\,emb} \approx K_{rx,\,surf}$ $K_{ry,\,emb} \approx K_{ry,\,surf}$	$C_{rx,emb} = C_{rx,sur} + \rho\, V_{La}\, I_{wce}\, \bar{c}_1 + \rho\, V_s\, (J_{ws} + \sum[A_{wce}\, \Delta_i^2])\, \bar{c}_1$ $\bar{c}_1 = 0.25 + 0.65\, \sqrt{a_0}\, (\frac{d}{D})^{-a_0/2} \times (\frac{D}{B})^{-1/4}$ I_{wce} = total moment of inertia about their base axis parallel to x of all sidewall surfaces effectively compressing the soil Δ_i = distance of surface A_{wce} from x axis J_{ws} = polar moment of inertia about their base axis parallel to x of all sidewall surfaces effectively shearing the soil $C_{ry,emb}$ is similarly evaluated from $C_{ry,sur}$ with y replacing x and, in the equation for c_1, L replacing B	$C_{rx,emb} = \frac{4}{3}\, \rho\, V_{La}\, B^3\, L\, \bar{c}_{rx}$ $+ \frac{4}{3}\, \rho\, V_{La} d^3 L \bar{c}_1$ $+ \frac{4}{3}\, \rho\, V_s Bd(B^2 + d^2)\, \bar{c}_1$ $+ 4\, \rho\, V_s B^2 d L \bar{c}_1$ with $\bar{c}_1$ as in the preceding column and $\bar{c}_{rx}$ according to Table 2-I
Coupling term Swaying-rocking x, ry **Swaying-rocking y, rx**	$K_{xry,\,emb} \approx \frac{1}{3}\, d\, K_{x,\,emb}$ $K_{yrx,\,emb} \approx \frac{1}{3}\, d\, K_{y,\,emb}$	$K_{rxy,\,emb} \approx K_{yrx,\,emb} \approx$ ≈ 1	$C_{xry,\,emb} \approx \frac{1}{3}\, d\, C_{x,\,emb}$ $C_{yrx,\,emb} \approx \frac{1}{3}\, d\, C_{y,\,emb}$	as in the previous column
Torsional	$K_{t,\,emb} = K_{t,\,surf}$ $\times [1 + 1.4\, (1 + \frac{B}{L})\, (\frac{d}{b})^{0.9}]$	$K_{t,\,emb} \approx K_{t,\,surf}$	$C_{t,emb} = C_{t,sur} + \rho\, V_{La}\, J_{wce}\, \bar{c}_2 + \rho\, V_s\, \sum[A_{wi}\, \Delta_{zi}^2]\, \bar{c}_2$ $\bar{c}_2 \approx (\frac{d}{D})^{-0.5}\, a_0^2 [a_0^2 + \frac{1}{2} (L/B)^{-1.5}]^{-1}$ J_{wce} = total moment of inertia of all sidewall surfaces compressing soil about the projection of z axis onto their plane Δ_{zi} = distance of surface A_{wi} to z axis	$C_{t,emb} = \frac{4}{3}\, \rho\, V_s\, BL(B^2 + L^2)\, \bar{c}_t$ $+ \frac{4}{3}\, \rho\, V_{La}\, d(L^3 + B^3)\, \bar{c}_2$ $+ 4\, \rho\, V_s\, d\, B\, L\, (B+L)\, \bar{c}_2$ with $\bar{c}_2$ as in the preceding column and $\bar{c}_t$ according to Table 2-I

† Note that as L/B $\to \infty$ (strip footing) the theoretical values of K_z and $K_y \to 0$; values computed from the two given formulas correspond to footing of L/B ≈ 20

‡ $a_0 = \omega B / V_s$

(**Graphs accompanying Table 2-II**)

31
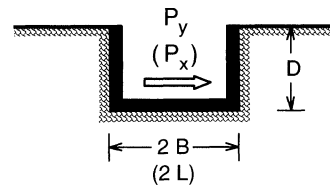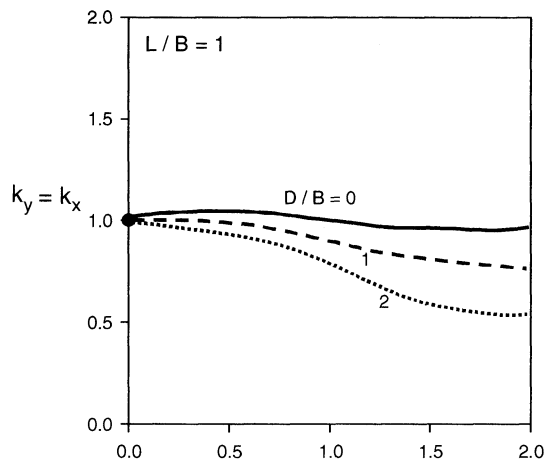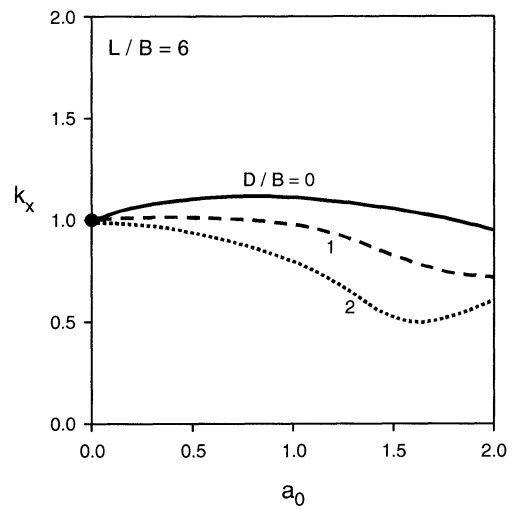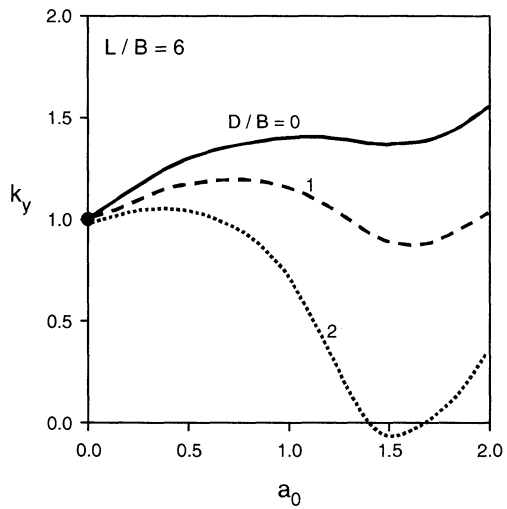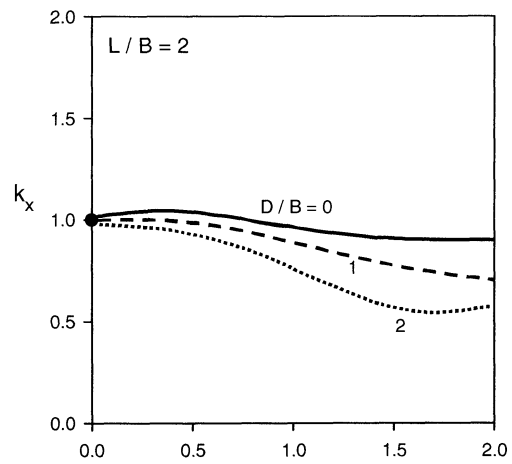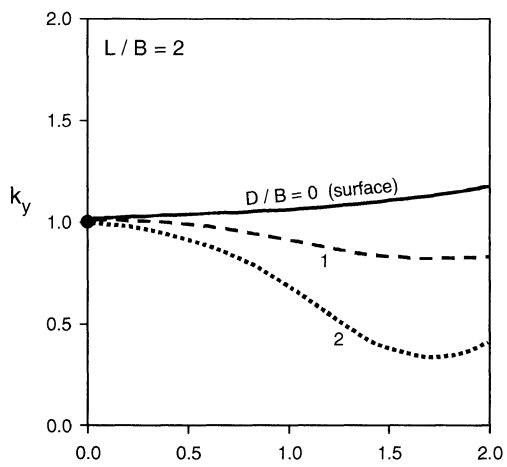
- Table 2-II compares the dynamic stiffnesses and dashpot coefficients of an embedded foundation $\overline{K}_{emb} = \overline{\overline{K}}_{emb} \times k_{emb}$ and C_{emb} with those of the corresponding surface foundation, $\overline{K}_{sur} = \overline{\overline{K}}_{sur} \times k_{sur}$ and C_{sur}.

2.4.3 The presence of bedrock at shallow depth
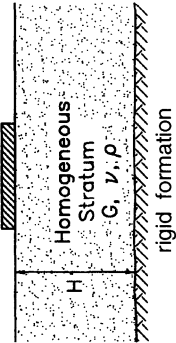
Natural soil deposits are frequently underlain by very stiff material or bedrock at a shallow depth, rather than extending to practically infinite depth as the homogenous halfspace implies. The proximity of such stiff formation to the oscillating surface modifies the static stiffness, K, and dashpot coefficients C(ω). Specifically, with reference to Table 2-III and its charts:

(a) The static stiffnesses in all modes decrease with the relative depth to bedrock H/B. This is evident from all formulae of Table 2-III, which reduce to the corresponding halfspace stiffnesses when H/R approaches infinity.

Particularly sensitive to variations in the depth to rock are the vertical stiffnesses --- the effect being far more pronounced with strip footings (factor 3.5 versus 1.3). Horizontal stiffnesses are also appreciably affected. On the other hand, for H/R > 1.5 the response to torsional loads is essentially independent of the layer thickness.

As indication of the causes of this different behavior (between circular and strip footings and, in any footing, between the different types of loading) can be obtained by comparing the depths of the "zone of influence" in each case. Circular and square foundations on a homogeneous halfspace induce vertical normal stresses σ_z along the centerline of the footing that become practically negligible at depths exceeding 5 footing radii ($z_v = 5$ R); with strip foundations vertical stresses practically vanish only below 15 footing widths ($z_v = 15$ B). The depth of influence, z_h, for the horizontal stresses τ_{zx}, due to lateral loading is about 2R and 6B for circle and strip, respectively. On the other hand, for all foundation shapes (strip, rectangle, circle), moment loading is "felt" down to a depth, z_r, of about 2B or 2R. For torsion, finally $z_t = 0.75$ R or 0.75 B.

Table 2-III. Dynamic stiffnesses and dashpot coefficients for surface foundations on homogeneous stratum over bedrock.

Homogeneous Stratum G, ν, ρ — H — rigid formation

	Foundation Shape	Circular Foundation of Radius B = R	Rectangular Foundation 2B by 2L (L > B)	Strip Foundation 2L → ∞
Static stiffness K	Vertical, z	$K_z = \frac{4GR}{1-\nu}\left(1 + 1.3\frac{R}{H}\right)$	$K_z = \frac{2GL}{1-\nu}\left[0.73 + 1.54\left(\frac{B}{L}\right)^{3/4}\right]\left(1 + \frac{B/H}{0.5+B/L}\right)$	$\frac{K_z}{2L} \approx \frac{0.73\,G}{1-\nu}\left(1 + 3.5\frac{B}{H}\right)$
	Horizontal, y	$K_y = \frac{8GR}{2-\nu}\left(1 + 0.5\frac{R}{H}\right)$	*	$\frac{K_y}{2L} \approx \frac{2G}{2-\nu}\left(1 + 2\frac{B}{H}\right)$
	Horizontal, x	$K_x = K_y$	*	—
	Rocking, rx	$K_{rx} = \frac{8GR^3}{3(1-\nu)}\left(1 + 0.17\frac{R}{H}\right)$	*	$\frac{K_{rx}}{2L} = \frac{\pi\,G\,B^2}{2(1-\nu)}\left(1 + 0.2\frac{B}{H}\right)$
	Rocking, ry	$K_{rx} = K_{ry}$	*	—
	Torsional, t	$K_t = \frac{16\,G\,R^3}{3}\left(1 + 0.10\frac{R}{H}\right)$	*	—
Dynamic stiffness coefficient $k(\omega)$	Vertical, z	$k_z = k_z(H/R, a_0)$ is obtained from Graph III-1	$k_z = k_z(H/B, L/B, a_0)$ is plotted in Graph III-2 for rectangles and strip	
	Horizontal, y or x	$k_y = k_y(H/R, a_0)$ is obtained from Graph III-1	*	$k_y = k_y(H/B, a_0)$ is obtained from Graph III-3
	Rocking, rx or ry	$k_\alpha(H/R) \approx k_\alpha(\infty)$, $\alpha = rx, ry, t$	*	$k_{rx} \approx k_{rx}(\infty)$
	Torsional, t		*	
Radiation dashpot coefficient $C(\omega)$	Vertical, z	$C_z(H/B) \approx 0$ at $f < f_c$; regardless of foundation shape. $\quad C_z(H/B) \approx 0.8\,C_z(\infty)$ at $f \geq 1.5\,f_c$. At intermediate frequencies: interpolate linearly. $\quad f_c = \frac{V_{La}}{4H}$, $\quad V_{La} = \frac{3.4\,V_s}{\pi(1-\nu)}$ $\quad$ Similarly for C_x		
	Horizontal, y or x	$C_y(H/B) \approx 0$ at $f < \frac{3}{4}f_s$; $\quad C_y(H/B) \approx C_y(\infty)$ at $f > \frac{4}{3}f_s$; $\quad f_s = \frac{V_s}{4H}$. At intermediate frequencies: interpolate linearly. $\quad$ Similarly for C_{ry}		
	Rocking, rx or ry	$C_{rx}(H/B) \approx 0$ at $f < f_c$; $\quad C_{rx}(H/B) \approx C_{rx}(\infty)$ at $f > f_c$ $\quad$ Similarly for C_{ry}		
	Torsional, t	$C_t(H/B) \approx C_t(\infty)$		

* Not available

33

III-3 STRIP

III-2 RECTANGLE

III-1 CIRCLE
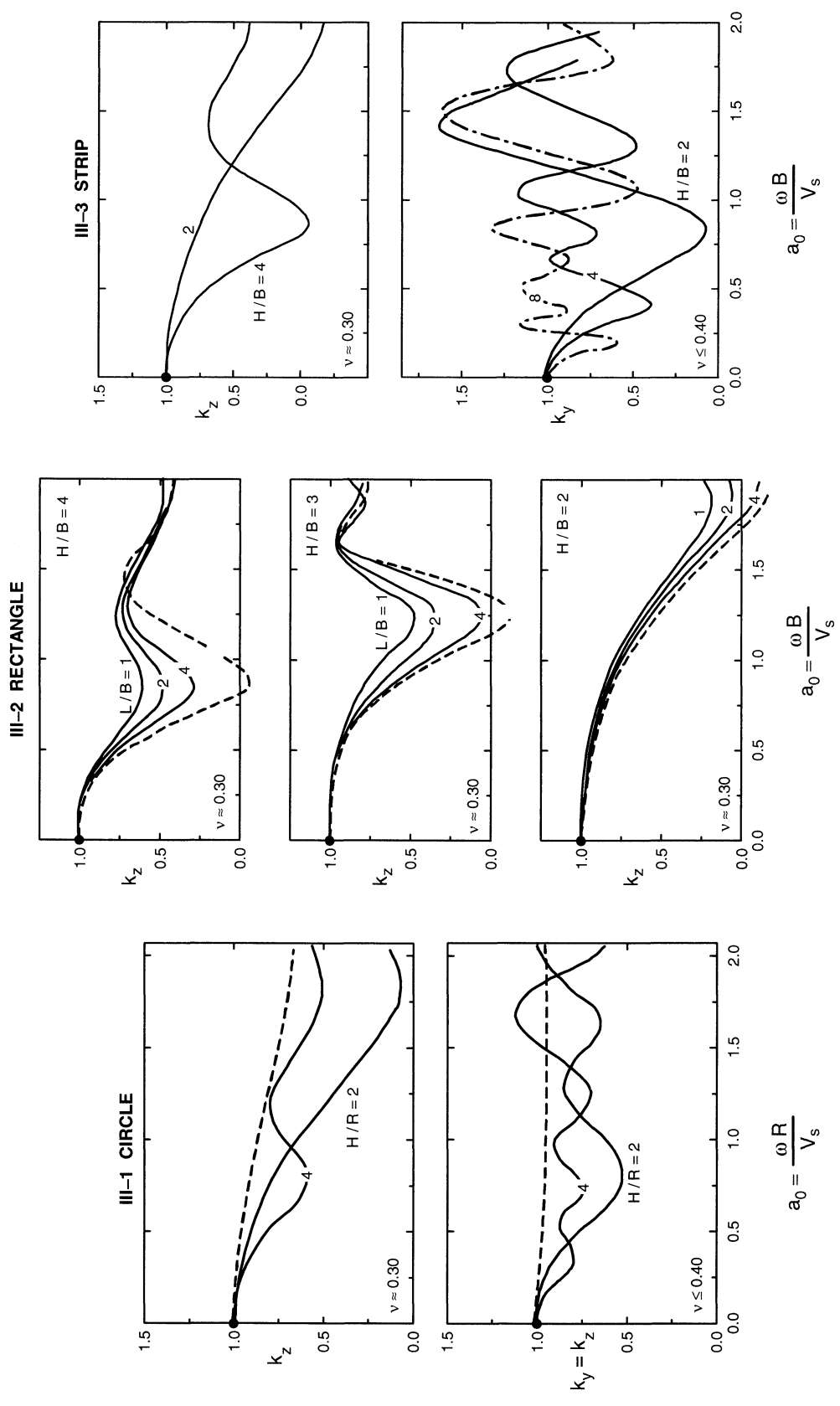
(Graphs accompanying Table 2-III)

34

Apparently when a rigid formation extends into the "zone of influence" of a particular loading mode, it eliminates the corresponding deformations and thereby increases the stiffness.

(b) The variation of the dynamic stiffness coefficients with frequency reveals an equally strong dependence on the depth to bedrock H/B. On a stratum, $k(\omega)$ is not a smooth function but exhibits undulations (peaks and valleys) associated with the natural frequencies (in shearing and compression-extension) of the stratum. In other words, the observed fluctuations are the outcome of resonance phenomena: waves emanating from the oscillating foundation reflect at the soil-bedrock interface and return back to their source at the surface. As a result, the amplitude of the foundation motion may significantly increase at frequencies near the natural frequencies of the deposit. Thus, the dynamic stiffness (being the inverse of displacements) exhibits troughs, which can be very steep when the hysteretic damping of the soil is small (in fact, in certain cases, $k(\omega)$ would be exactly zero if the soil were ideally elastic).

For the "shearing" modes of vibration (swaying and torsion) the natural fundamental frequency of the stratum which controls the behavior of $k(\omega)$ is:

$$f_s = \frac{V_s}{4H} \tag{2-28}$$

where H denotes the thickness of the layer, while for the "compressing" modes (vertical, rocking) the corresponding frequency is:

$$f_c = \frac{V_{La}}{4H} = \frac{3.4}{\pi(1-v)} f_s \tag{2-29}$$

(c) The variation of the dashpot coefficient, C , with frequency reveals a twofold effect on the presence of a rigid base at relatively shallow depth. First, $C(\omega)$ also exhibit undulations (crests and troughs) due to wave reflections at the rigid boundary. These fluctuations are more pronounced with strip than with circular foundations, but are not as significant as for the corresponding stiffnesses $k(\omega)$. Second, and far more important from a practical viewpoint, is that at low frequencies below the first resonant ("cut-off") frequency of each mode of vibration, radiation damping is zero or negligible for all shapes of footings and all modes of vibration. This is due to the fact that no surface waves can exist in a soil stratum over bedrock at such low

frequencies; and, since the bedrock also prevents waves from propagating downward, the overall radiation of wave energy from the footing is negligible or nonexistent.

Such an elimination of radiation damping may have severe consequences for heavy foundations oscillating vertically or horizontally, which would have enjoyed substantial amounts of damping in a very deep deposit (halfspace) --- recall illustrative examples for Tables 2-I and 2-II. On the other hand, since the low-frequency values of C in rocking and torsion are small even in a halfspace, operating below the cut-off frequencies may not change appreciably from the presence of bedrock.

Note that at operating frequencies f beyond f_s or f_c , as appropriate for each mode, the "stratum" damping fluctuates about the halfspace damping C (H/B = ∞). The "amplitude" of such fluctuations tends to decrease with increasing H/B. Moreover, if some wave energy penetrates into bedrock (as it does happen in real life thanks to some weathering of the upper masses of rock) the fluctuations tend to wither away --- hence the recommendation of Table 2-III .

2.4.4 Foundations on soil stratum over halfspace

The homogeneous halfspace and the stratum-on-rigid-base are two idealizations of extreme soil profiles. A more realistic soil model, the stratum over halfspace, is studied in this subsection. Besides the H/R or H/B ratio, the ratio G_s / G_r (or the wave velocity ration V_s / V_r) is needed to describe such a soil model. When G_s / G_r tends to zero the stratum-on-rigid base ("bedrock") is recovered; when it becomes equal to 1, the model reduces to a homogeneous halfspace. For intermediate situations, i.e., with 0< G_s / G_r < 1 , "springs" and "dashpots" can be estimated using the information of this subsection.

Table 2-IV presents formulas for the static stiffness of circular and strip foundations, in terms of G_s / G_r and H/R (for the circle) or H/B (for the strip). These formulas are valid for $G_s \le G_r$, i.e., a halfspace stiffer than the layer. At the lower limit, G_s / $G_r \to 0$, the expressions reduce to those of Table 2-III for a layer on rigid base. At the upper limit, G_s / $G_r \to 1$, the halfspace expressions (Table 2-I) are recovered. At intermediate values, as the rigidity of the supporting.

TABLE 2-IV. **Static stiffnesses of circular and strip foundations on soil stratum over halfspace.**

Vibration Mode	General Expression $K = K\,(G_s\,/\,G_r,\ H\,/\,B) = K\,(1,\infty)\ \times\ \dfrac{1 + m\,(B\,/\,H)}{1 + m\,(B\,/\,H)\,(G_s - G_r)}$		
	$K\,(1,\infty)$	m	
		Circle	Strip
Vertical		1.3	3.5
Horizontal	K of homogeneous halfspace	0.5	2.0
Torsional		0.17	0.2

halfspace decreases, the static stiffnesses of the foundation decrease, apparently due to increasing magnitude of strains in the halfspace. The results are intuitively obvious and need no further explanation

The dynamic stiffness and damping coefficients as functions of frequency also exhibit intermediate behavior between those for halfspace and for stratum over bedrock. Thus the observed undulations are not as sharp as the undulations on a stratum over bedrock, depending, of course, on the value of G_s / G_r.

In general, compared to a stratum over bedrock, the flexibility of the base layer (halfspace) produces a *decrease* in stiffness but an *increase* in radiation damping. The latter stems from the fact that waves emitted from the foundation-soil interface penetrate into the halfspace, rather than being fully reflected.

For the earthquake problem, this increase in radiation damping is practically most significant for the swaying dashpot at frequencies $\omega = 2 \pi f$ below the fundamental frequency of the *top* soil stratum. Recall that at such frequencies, when the halfspace is a rigid bedrock, no radiation damping can generate, and hence resonance amplifications in the seismic response may develop. In this case this is no longer true. Figure 2-8 gives a chart for estimating the swaying dashpot C_y for several values of the ratio V_s / V_r. This chart applies to circle or square foundations with $H/R \approx 3$ to 4 and for strip foundations with $H /B = 2$. The chart can only be used as a guide in other cases.

On the other hand, rotational modes of vibration generate little damping below their respective cutoff frequencies, and the significance of rock flexibility is of minor practical significance. This actually is also true for higher frequencies, since "destructive" interference of waves emitted from a rotating (in rocking or torsion) foundation limits the depth these waves can reach. Hence the flexibility or rigidity of the base layer is again of practically little significance .

Additional information on this topic can be found in Hadjian & Luco (1977), Luco (1974), Gazetas & Roesset (1976), and Gazetas (1983).
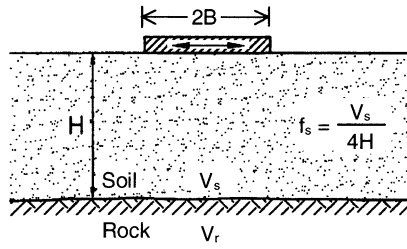
Symbol	Foundation Shape	H/B	V_s / V_r
○	Circle	3.55	0.3 - 0.6 - 0.8
□	Strip	2	0.24 - 0.5
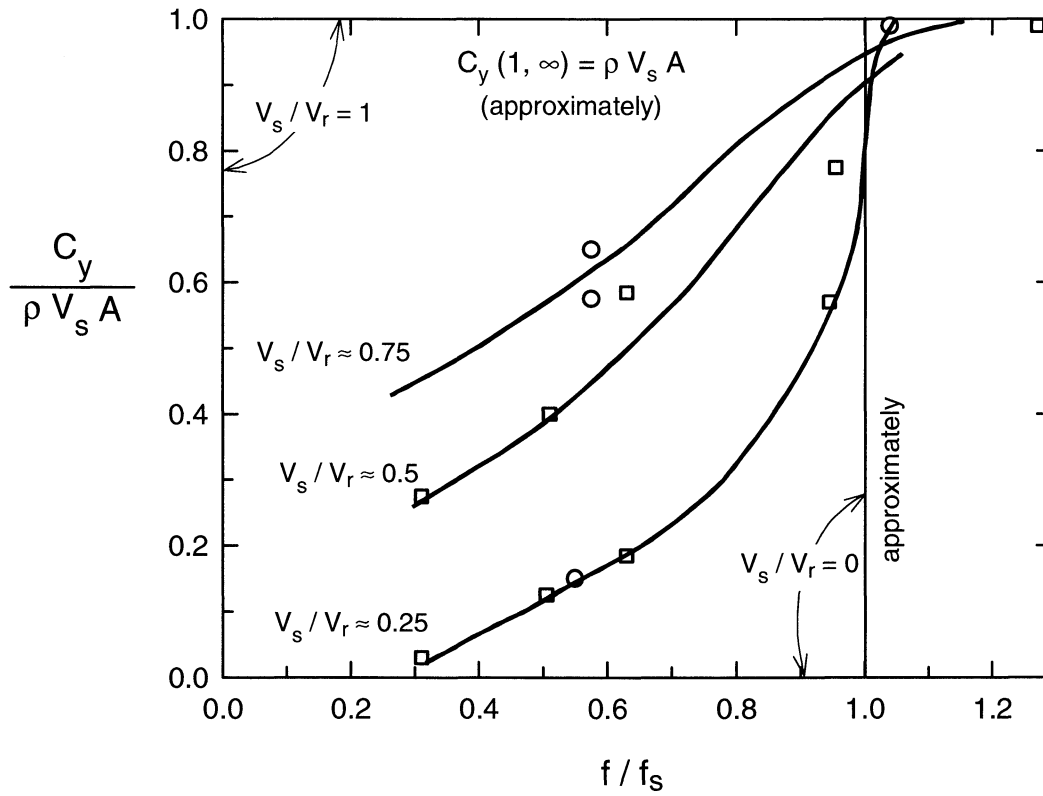
FIGURE 2-8. Horizontal radiation dashpot C_y of a foundation on a soil layer underlain by "flexible" rock, as a fraction of the homogeneous halfspace value C_y $(1, \infty)$, for various ratios V_s / V_r.

39

2.5 Effect of soil nonlinearity

In current soil-structure interaction practice, the nonlinear plastic soil behavior is usually approximated through a series of iterative linear analyses, using soil properties (moduli and damping ratios) that are consistent with the level of shearing strains resulting from the previous analysis (Lysmer et al, 1974; Kausel et al, 1976). These analyses may utilize a wealth of available experimental soil data relating the decrease in (secant) shear modulus and the increase in (effective) damping ratio with increasing amplitude of shear strain.

Nonlinearities in the free-field soil are treated routinely with programs such as SHAKE. Much less work has been reported on nonlinearities on the dynamic impedance functions of rigid strip foundation. One interesting study has been conducted by Jakub & Roesset (1977). In this, the soil is modeled as homogeneous or inhomogeneous stratum over rigid base with $H / B = 1, 2,$ and 4. A Ramber-Osgood model was used to simulate the nonlinear constitutive relations of soil and iterative linear analyses were performed. One of the two parameters of the Ramber-Osgood model, r , was kept constant equal to 2, while the second one, α , was varied so as to cover a wide range of typical soil stress-strain relations. For such a model, the variation of secant modulus and effective damping ratio with stress amplitude is given by:

$$\frac{G}{G_o} = \frac{1}{1 + a \frac{\tau}{G_o\, \gamma_y}} \qquad\qquad (2\text{-}30a)$$

$$\beta = \frac{2}{3\,\pi}\, a\, \frac{G}{G_o}\, \frac{\tau}{G_o\, \gamma_y} \qquad\qquad (2\text{-}30b)$$

in which: G_o = the initial shear modulus for low levels of strain; γ_y = a characteristic shear strain, typically ranging from 0.0001% to 0.01% ; and τ = the amplitude of the induced shear stress.

It was concluded that a reasonable approximation to the swaying and rocking impedances of a rigid strip may be obtained from the available linear viscoelastic solutions, provided that the "effective" values of G and β are estimated from Eqns. (2-30) with

$$\tau = \tau_c \qquad\qquad (2\text{-}31)$$

where τ_c is the statically induced shear stress at a depth equal to 0.50 B , immediately below the foundation edge. Note that the above depth coincides with the depth of maximum shear strain under a vertically-loaded strip footing (e.g., Tschebotarioff 1973).

For design purposes and as a first approximation, we mention here that the average shear modulus for the soil beneath a footing can be determined according the NEHRP-97 recommendations, as a function of the design seismic coefficient of the structure (Table 2-V). Alternatively, one may use approximate "cone" models to derive strain-compatible moduli (Wolf, 1994).

TABLE 2-V. Values of G/G_{max} and V/V_{max} for soil beneath foundations (NEHRP-97).

	Spectral Response Acceleration, S_{D1}			
	$\leq$ 0.10	$\leq$ 0.15	0.20	$\geq$ 0.30
G/G_{max}	0.81	0.64	0.49	0.42
V/V_{max}	0.90	0.80	0.70	0.65

2.6 Illustrative Example

An application of the methodology described in this report are given in this paragraph. The dynamic stiffnesses (springs) and damping coefficients (dashpots) for the six modes of vibration for a specific footing shape and embedment condition. Note that for non-rectangular footing basemats an equivalent circumscribed rectangle should be drawn, as shown in Figure 2-7 and Tables 2-1, 2-2, and 2-3. The impedance results are not sensitive to the exact shape and any reasonable shape with good engineering judgment can be applied. The symbols used are:

A_b = area of footing

I_{bx} , I_{by} , I_{bz} = area moments of inertia about the x , y , and z axes of the actual soil-foundation contact surface

B , L = half-width and half-length of the equivalent circumscribed rectangle ($L > B$) around a or the dimensions of a rectangular footing

G , v = soil shear modulus and Poisson's ratio

V_s = shear wave velocity

V_{La} = Lysmer's analog wave velocity = $\dfrac{3.4}{\pi(1-v)}$ V_s

$\omega = 2\ \pi f$ = circular frequency (rad/sec) of the applied force that can be one of the dominant frequencies of the seismic excitation or the frequency of operation of a vibrating machine

2.6.1 Example

The present example is taken from Gazetas (1991b)

$2B = 5$ m ; $2L = 16$ m ; $D = 6$ m ; $L/B = 3.2$; $\chi = A_b / 4\,L^2 \approx 0.26$

$V_s = $; $v = 0.40$; $\rho_s = 1.85$ Mg/m^3 ; $V_{La} \approx 459$ m/sec

$f = 20$ Hz ; $a_0 = \omega B / V_s \approx 1.23$
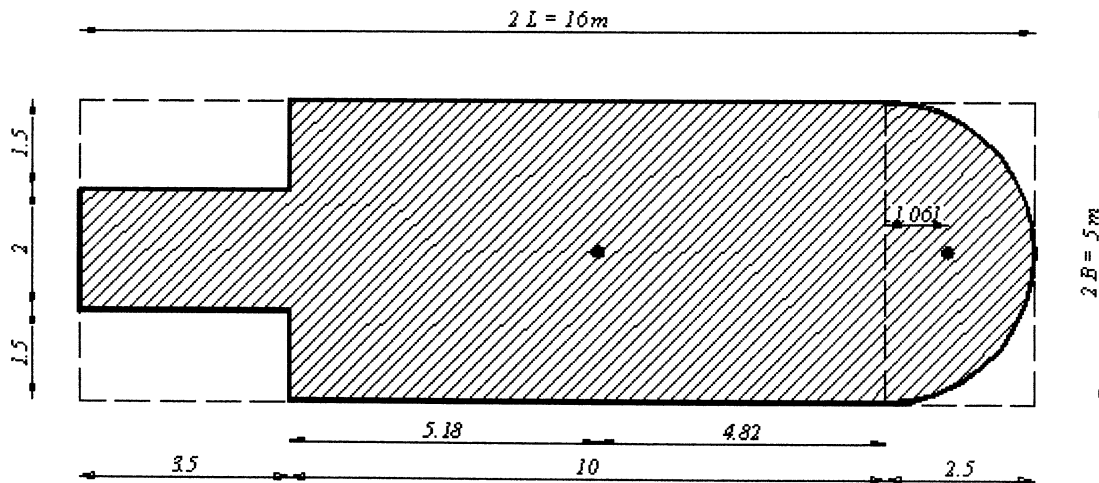
FIGURE 2-9. Example Studied

Vertical Mode

Static Stiffness (Table 2-I)

$$K_z = \frac{2\,G\,L}{1-v}\,(0.73 + 1.54\,\chi^{0.75}) = \frac{2\times 120{,}000\times 8.0}{1-0.40}\times(0.73 + 1.54\times 0.26^{0.75}) \approx$$

$$\approx 4.13 \times 10^6 \text{ kN/m}$$

Dynamic Stiffness Coefficient (Graphs accompanying Table 2-I)

$a_0 \approx 1.23; \quad k_z \approx 0.92$

$\overline{K}_z = k_z \times K_z = 0.92 \times 4.13 \times 10^6 = 3.80 \times 10^6 \, kN/m$

Radiation Damping (Table 2-I)

$a_0 \approx 1.23; \quad \overline{c}_z = 1.0$

$C_{z,rad} = (\rho \, V_{La} \, A_b) \, \overline{c}_z = (1.85 \times 460 \times 66.82) \, 1.0 = 5.66 \times 10^4 \, kNs/m$

Material Damping

$\omega = 125.7 \, rad/sec; \quad \beta = 5\%$

$C_{z,mat} = \frac{2\overline{K}_z}{\omega} \beta = \frac{2 \times 3.8 \times 10^6}{125.7} \times 0.05 \approx 3.02 \times 10^3 \, kNs/m$

Total Damping

$C_z = C_{z,rad} + C_{z,mat} = 5.66 \times 10^4 + 3.02 \times 10^3 \approx 5.96 \times 10^4 \, kNs/m$

Horizontal Modes

Static Stiffness (Table 2-I)

$K_y = \frac{2\,GL}{2-\nu} (2 + 2.5 \, \chi^{0.85}) = \frac{2 \times 120,000 \times 8.0}{2-0.40} \times (2 + 2.5 \times 0.26^{0.85}) \approx 3.35 \times 10^6 \, kN/m$

$K_x = K_y - \frac{0.2}{0.75-\nu} \, G L \, (1 - \frac{B}{L}) =$

$= 3.35 \times 10^6 - \frac{0.2}{0.75-0.40} \, 120,000 \times 8.0 \times (1 - \frac{2.5}{8}) \approx 2.98 \times 10^6 \, kN/m$

Dynamic Stiffness Coefficient (Graphs accompanying Table 2-I)

$a_0 \approx 1.23; \quad k_y \approx 1.14 \; ; \quad k_x \approx 1.14$

$\overline{K}_y = k_y \times K_y = 1.14 \times 3.35 \times 10^6 = 3.82 \times 10^6 \, kN/m$

$\overline{K}_x = k_x \times K_x = 1.14 \times 2.98 \times 10^6 = 3.39 \times 10^6 \, kN/m$

Radiation Damping (Table 2-I)

$a_0 \approx 1.23; \quad \overline{c}_y = 1.0$

$C_{y,rad} = (\rho \, V_s \, A_b) \, \overline{c}_y = (1.85 \times 255 \times 66.82) \times 1.0 = 3.14 \times 10^4 \, kNs/m$

$C_{x,rad} = (\rho \, V_s \, A_b) = (1.85 \times 255 \times 66.82) = 3.14 \times 10^4 \, kNs/m$

Material Damping

$\omega = 125.7 \, rad/sec; \quad \beta = 5\%$

$C_{y,mat} = \frac{2\overline{K}_y}{\omega} \beta = \frac{2 \times 3.82 \times 10^6}{125.7} \times 0.05 \approx 3.04 \times 10^3 \, kNs/m$

$C_{x,mat} = \frac{2\overline{K}_x}{\omega} \beta = \frac{2 \times 3.39 \times 10^6}{125.7} \times 0.05 \approx 2.70 \times 10^3 \, kNs/m$

Total Damping

$$C_y = C_{y,rad} + C_{y,mat} = 3.14 \times 10^4 + 3.04 \times 10^3 \approx 3.44 \times 10^4 \, kNs/m$$
$$C_x = C_{x,rad} + C_{x,mat} = 3.14 \times 10^4 + 2.70 \times 10^3 \approx 3.41 \times 10^4 \, kNs/m$$

Rocking Modes ry (Transverse Axis) and rx (Longitudinal Axis)

Static Stiffness (Table 2-I)

$$K_{ry} = \frac{G}{1-v} I_{by}^{0.75} \left[3 \left(\tfrac{L}{B}\right)^{0.15}\right] = \frac{120,000}{1-0.40} \times 1100^{0.75} \times \left[3 \, (3.2)^{0.15}\right] \approx 1.36 \times 10^8 \, kN \, m$$

$$K_{rx} = \frac{G}{1-v} I_{bx}^{0.75} \left(\tfrac{L}{B}\right)^{0.25} (2.4 + 0.5 \tfrac{B}{L}) = \frac{120000}{1-0.40} \times 121.1^{0.75} \times 3.2^{0.25} \times (2.4 + \tfrac{0.5}{3.2})^{0.25} \approx$$
$$\approx 2.50 \times 10^7 \, kN \, m$$

Dynamic Stiffness Coefficient (Graphs accompanying Table 2-I)

$a_0 \approx 1.23$; $k_{ry} \approx 1 - 0.3 \, a_0 = 0.631$; $k_{rx} \approx 1 - 0.2 \, a_0 = 0.754$
$\overline{K}_{ry} = k_{ry} \times K_{ry} = 0.631 \times 1.36 \times 10^8 = 8.58 \times 10^7 \, kN \, m$
$\overline{K}_{rx} = k_{rx} \times K_{rx} = 0.754 \times 2.50 \times 10^7 = 1.89 \times 10^7 \, kN \, m$

Radiation Damping (Table 2-I)

$a_0 \approx 1.23$; $\overline{c}_{ry} = 0.75$; $\overline{c}_{rx} = 0.4$
$C_{ry,rad} = (\rho \, V_{La} \, I_{by}) \, \overline{c}_{ry} = (1.85 \times 460 \times 1100) \times 0.75 = 7.02 \times 10^5 \, kNm \, s$
$C_{rx,rad} = (\rho \, V_{La} \, I_{bx}) \, \overline{c}_{rx} = (1.85 \times 460 \times 121.1) \times 0.4 = 4.12 \times 10^4 \, kN \, m \, s$

Material Damping

$\omega = 125.7$ rad/s; $\beta = 5\%$
$C_{ry,mat} = \frac{2 \overline{K}_{ry}}{\omega} \beta = \frac{2 \times 8.58 \times 10^7}{125.7} \times 0.05 \approx 6.82 \times 10^4 \, kNm \, s$
$C_{rx,mat} = \frac{2 \overline{K}_{rx}}{\omega} \beta = \frac{2 \times 1.89 \times 10^7}{125.7} \times 0.05 \approx 1.50 \times 10^4 \, kNm \, s$

Total Damping

$C_{ry} = C_{ry,rad} + C_{ry,mat} = 7.02 \times 10^5 + 6.82 \times 10^4 \approx 7.70 \times 10^5 \, kNm \, s$
$C_x = C_{x,rad} + C_{x,mat} = 4.12 \times 10^4 + 1.50 \times 10^4 \approx 5.62 \times 10^4 \, kNm \, s$

Torsional Mode

Static Stiffness (Table 2-I)

$$K_t = G \, J_{tb2}^{0.75} \left[4 + 11 \, (1 - \tfrac{B}{L})^{10}\right] = 120,000 \times 1221.1^{0.75} \times \left[4 + 11 \times (1 - \tfrac{1}{3.2})^{10}\right] \approx$$
$$\approx 4.24 \times 10^9 \, kN \, m$$

Dynamic Stiffness Coefficient (Graphs accompanying Table 2-I)

$a_0 \approx 1.23$; $k_t \approx 1 - 0.14 \, a_0 = 0.83$

$$\overline{K}_t = k_t \times K_t = 0.83 \times 4.24 \times 10^9 = 3.52 \times 10^9 \, kN \, m$$

Radiation Damping (Table 2-1)

$$a_0 \approx 1.23 \; ; \; \overline{c}_t = 0.9$$
$$C_{t,rad} = (\rho \, V_s \, J_t) \, \overline{c}_t = (1.85 \times 255 \times 1221.1) \times 0.9 = 5.18 \times 10^5 \, kNm \, s$$

Material Damping

$$\omega = 125.7 \text{ rad/s}; \quad \beta = 5\%$$
$$C_{t,mat} = \frac{2 \overline{K}_t}{\omega} \beta = \frac{2 \times 3.52 \times 10^9}{125.7} \times 0.05 \approx 2.80 \times 10^6 \, kNm \, s$$

Total Damping

$$C_t = C_{t,rad} + C_{t,mat} = 5.18 \times 10^5 + 2.80 \times 10^6 \approx 3.32 \times 10^6 \, kNm \, s$$

SECTION 3

PARAMETRIC STUDY OF THE SEISMIC RESPONSE
OF PIER ON FOOTING WITHOUT UPLIFT

To answer some of the questions raised in the task objectives, a systematic parameter study was conducted on an idealized bridge model, once the accuracy of the developed computer code had been demonstrated. One of features of this code relates to the unavoidable soil nonlinearities during strong seismic excitation. Such nonlinearities are of two types: *"primary"*, arising from the shear-wave induced deformations in the free-field soil; and *"secondary"* arising from the stresses induced by the oscillating foundation. Whereas established methods of analysis are available for handling the former type of nonlinearities (through equivalent linear or truly nonlinear algorithms), no simple realistic solution is known for the latter. The approach described in Section 2 is taken in our code and different soil moduli are used for the analysis of wave-propagation and for the computation of the dynamic stiffnesses --- consistently with the overall level of strains at characteristic points under the footing.

3.1 Fundamental study

The bridge pier sketched in Figs 1-1 and 3-11 is an lightly idealized version of an actual bridge. It involves a single column bent of height $H_c = 6$ m and diameter $d_c = 1.3$ m, founded with a 5-m-diameter (R = 2.5 m) footing placed at a depth D = 3 meters below the ground surface. The axial load carried by the system, P = 3500 kN, is typical of a two-lane highway bridge with a span of about 35 m. Considering a shear wave velocity and a mass density for the top layer of 80 m/s and 2 Mg/m³, respectively, and using the approximate relation $E_s / S_u \approx 1000$, the undrained shear strength of the top layer is calculated to be of the order of 40 kPa. Accordingly, the static factor of safety of the footing is about :

$$FS \equiv \frac{q_u}{q} = \frac{1.3 \times 5.14 \times 40 + 3 \times 20}{3500 / (\pi \times 2.5^2)} \approx 2 \tag{3-1}$$

which is a sufficient, although marginal, value for a bridge footing.

The contact area between the sidewalls and the surrounding soil, d, was considered to be either zero (no sidewall-soil contact) or d = 0.5 D (partial sidewall-soil contact).

Results were obtained for excitation by vertical S waves, described through a horizontal "rock"outcrop motion. Both harmonic steady-state and time-history analyses were performed, in the frequency and time domains, respectively. The former were applied to investigate the fundamentals (e.g., SSI period, effective damping) of the dynamic behavior of the system; the latter were performed to obtain predictions of the response to actual motions. In the time-domain analyses, two different excitation time histories were used, both having a peak horizontal acceleration (PGA) of about 0.40g:

(a) an artificial accelerogram approximately fitted to the NEHRP-94 pga = 0.4 g,

(b) the Pacoima downstream motion, recorded (on "soft rock" outcrop) during the Northridge 1994 earthquake (since the pga is 0.42 g, scaling of this motion was not considered necessary).

The two motions and their five and ten percent damped spectra are shown in Figs 3-1 and 3-2. These motions cover a range of possible "rock" outcrop excitations, necessary for checking the limitations (or showing the generality) of our conclusions. The same set of motions has been used by the authors in an earlier study of pile-supported bridge piers (Mylonakis et al 1995).

The results presented in this subsection refer to a bridge with a top (deck) free to rotate, subjected to the Pacoima 1994 motion, and rigid rock conditions. A second set of parametric results, which incorporate more general boundary conditions, are presented later on.

The harmonic steady-state and transient seismic response of this pier, obtained in a complete analysis, is displayed in Figs 3-3 and 3-4. These results should be compared with those in Figs 3-5 to 3-10, each pair of which corresponds to a particular case as follows:

(a) no soil-structure interaction (SSI), i.e. the footing is considered as rigidly supported (*Figures 3-5, 3-6*

48

(b) embedment having partial sidewall contact (d = 1.5 m) with the surrounding soil: *Figs 3-7, 3-8*

(c) no radiation damping, i.e. setting for all modes of vibration $C_{rad} = 0$: *Figs 3-8, 3-9*

The following conclusions can be drawn from these graphs:

1. Ignoring *SSI* reduces the fundamental natural period of the system (from 0.83 to 0.53s), bringing it closer to resonance with the second-mode natural period of the soil deposit (0.48s) --- see Figures 3-5 and 3-6. In addition, the effect of the soil radiation and hysteretic damping on the bridge response disappear. Naturally, therefore, the resulting no-SSI bridge transfer functions exhibit a (spurious) sharp and high peak at T = 0.53s (Fig. 3-5).

Moreover, the rock outcrop excitations are richer in the period region of 0.50s than of 0.80s, which accentuates the peak at T = 0.53s.

As a result, the no-SSI time histories of bridge-deck and footing accelerations are, both, nearly *two times larger* than those of the complete solution (with SSI). Also of interest is to notice the change in the nature of the bridge-deck response time histories: the (largest) peak in the complete solution, at *t ≈ 4 sec*, is in unison with the long-period ground (free-field) oscillations occurring after about 3 sec --- apparently produced by resonance at the fundamental period of the soil deposit. The *early part* of the free-field ground motion, with much shorter periods, is a product of "secondary" resonance between the strong short-period early part of the Pacoima-Northridge excitation and the second natural mode of the soil deposit. However, the effect of this part of the ground motion on the bridge is obviously completely insignificant.

The no-SSI response shows exactly the opposite trends, with its (largest) peak occurring at *t ≈ 2.5s*, in phase with the strong ground motion observed at that time.

It should be pointed out that the foregoing trends should not be generalized to *any* bridge-footing system. For example, had the frequency of the earthquake excitation been different (or, alternatively the thickness of the soil profile been smaller or larger), the above trends could be reversed.
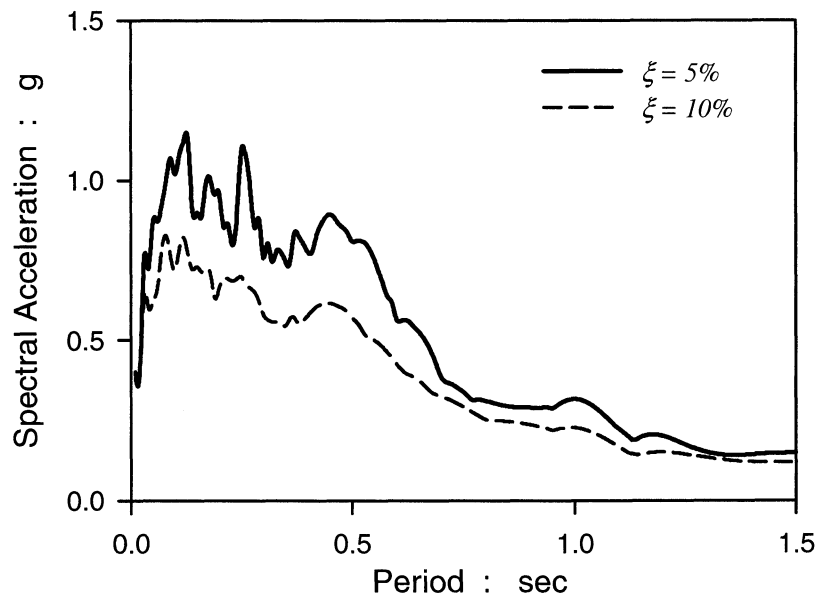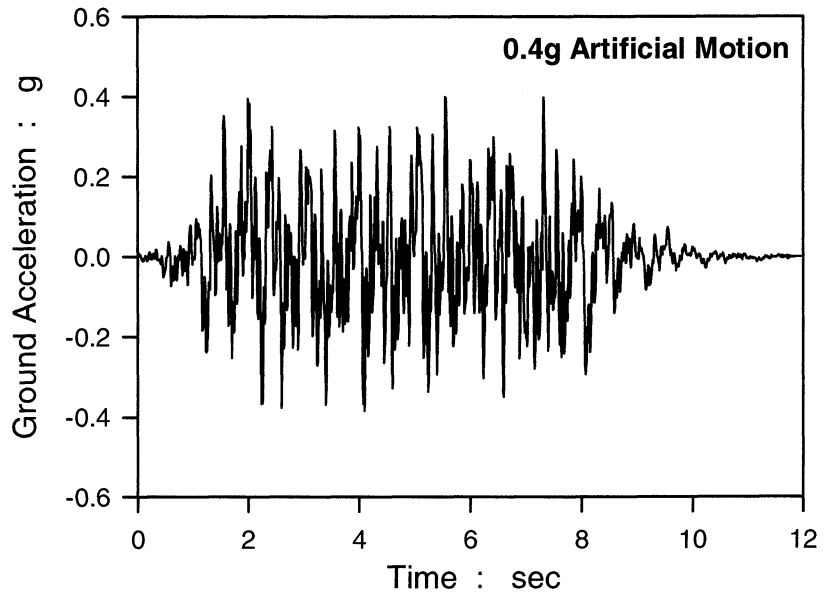
FIGURE 3-1. The artificial 0.4g motion and its corresponding response spectra for 5% and 10% damping.
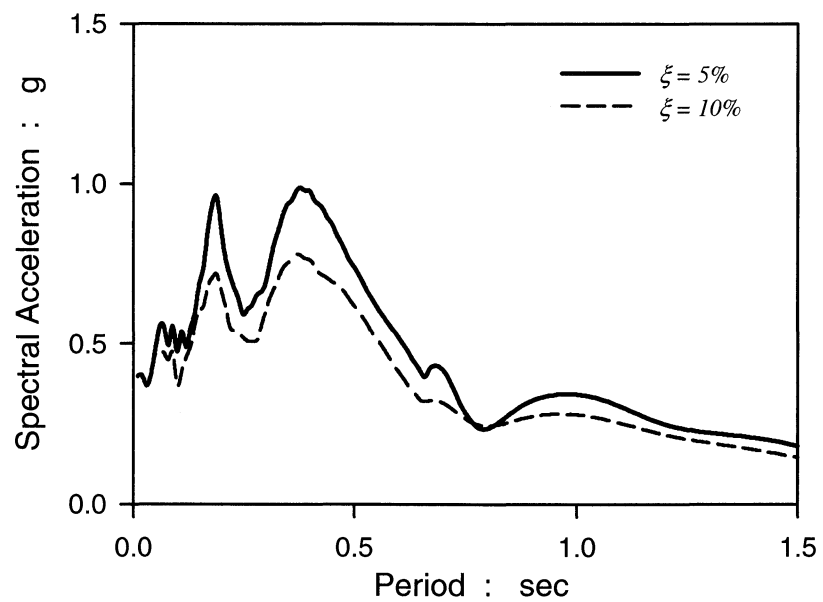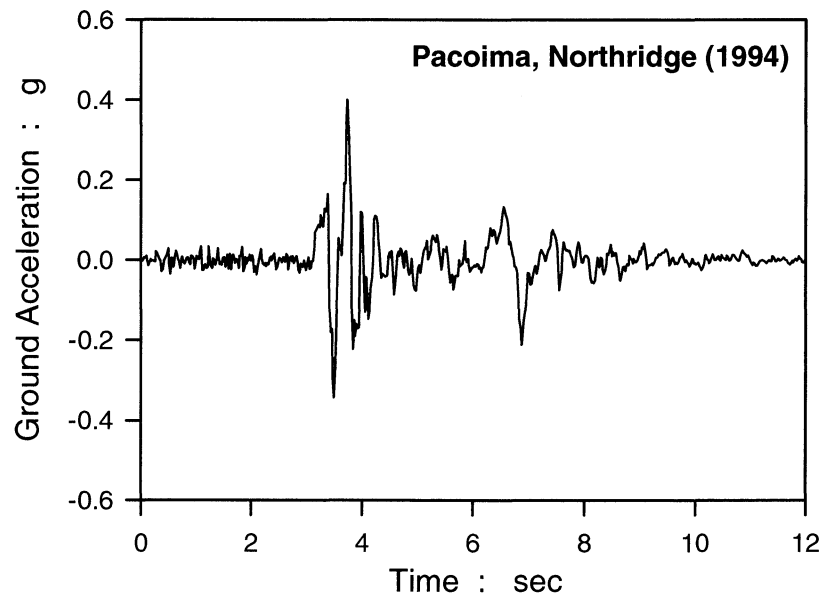
FIGURE 3-2. The Pacoima, Northridge (1994) motion and its corresponding response spectra for 5% and 10% damping.

Upper plot — y-axis: w.r.t. ROCK OUTCROP MOTION (0 to 25); x-axis: 0 to 2
Legend:
— FREE FIELD
··· FOOTING
— BRIDGE

Lower plot — y-axis: w.r.t. FREE-FIELD SURFACE MOTION (0 to 8); x-axis: PERIOD (s), 0 to 2
Legend:
··· FOOTING
— BRIDGE

SOIL PROFILE
SOFTCLAY
H = 93.5 m
Rigid Bedrock
IR = infinite

FOOTING
R = 2.5 m
d = 0.0 m
D = 3 m

COLUMN
Hc = 6 m
dc = 1.3 m
Ec = 25 GPa
$\xi = 5\%$
ms = 350 Mg
mb = 120 Mg
Column top
Free to Rotate
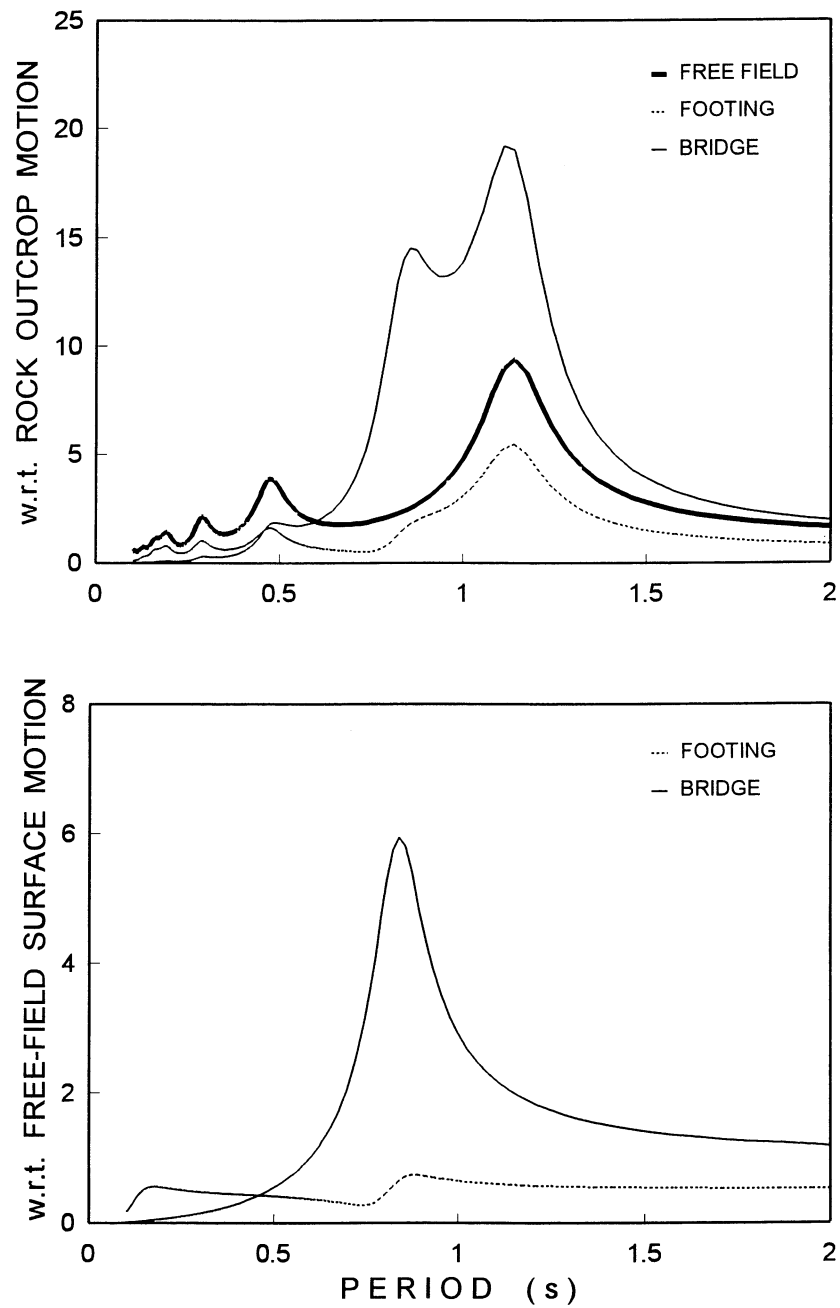
FIGURE 3-3. Complete solution : harmonic steady-state transfer functions

52
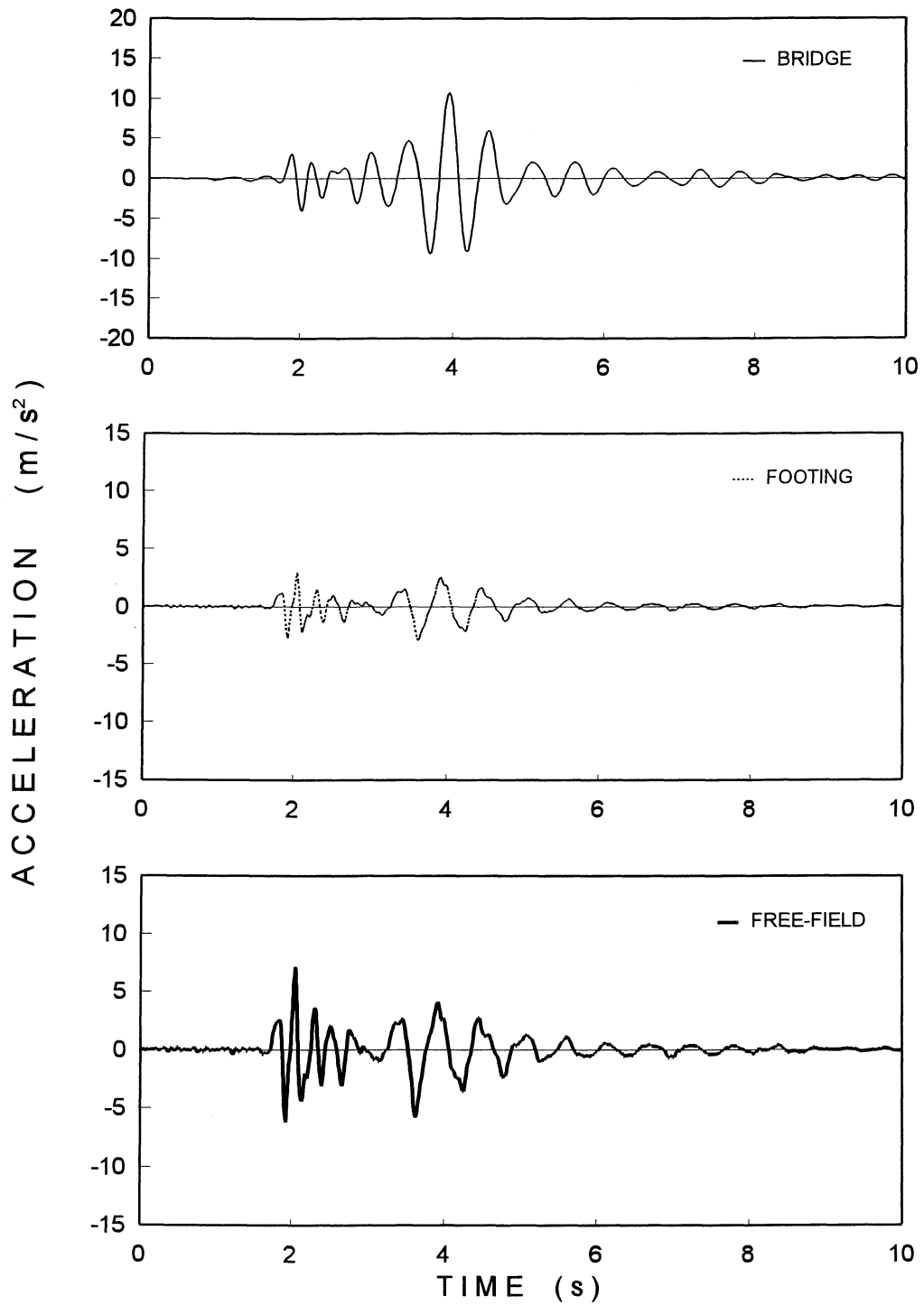
FIGURE 3-4. Complete solution: acceleration time histories for Pacoima, Northridge (1994) rock motion.
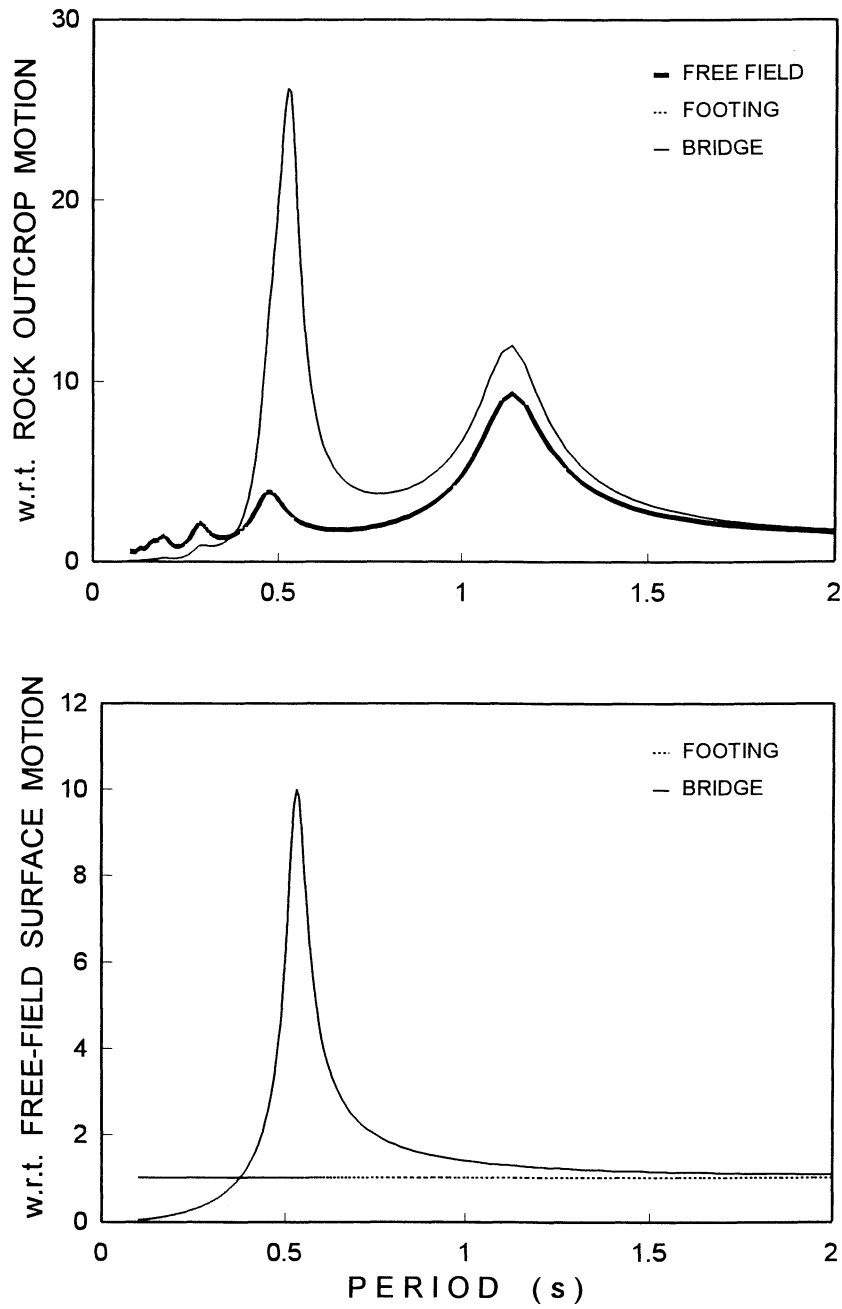
FIGURE 3-5. Solution ignoring SSI: harmonic steady-state transfer functions.

54
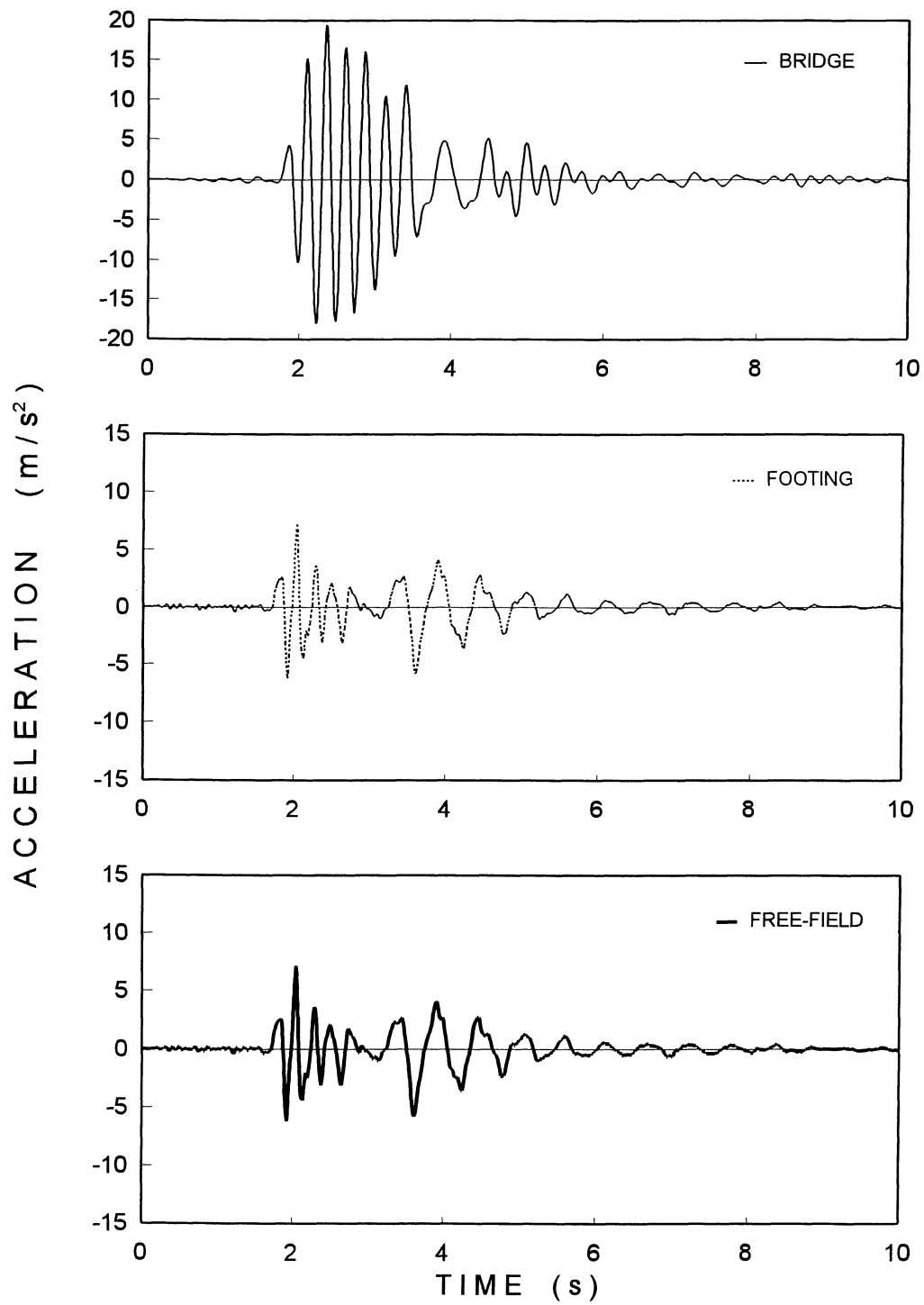
FIGURE 3-6. Solution ignoring SSI: acceleration time histories for Pacoima, Northridge (1994) rock motion.

SOIL PROFILE
SOFTCLAY
H = 93.5 m
Rigid Bedrock
IR = infinite

FOOTING
R = 2.5 m
d = 1.5 m
D = 3 m

COLUMN
Hc = 6 m
dc = 1.3 m
Ec = 25 GPa
$\xi = 5\%$
ms = 350 Mg
mb = 120 Mg
Column top
Free to Rotate
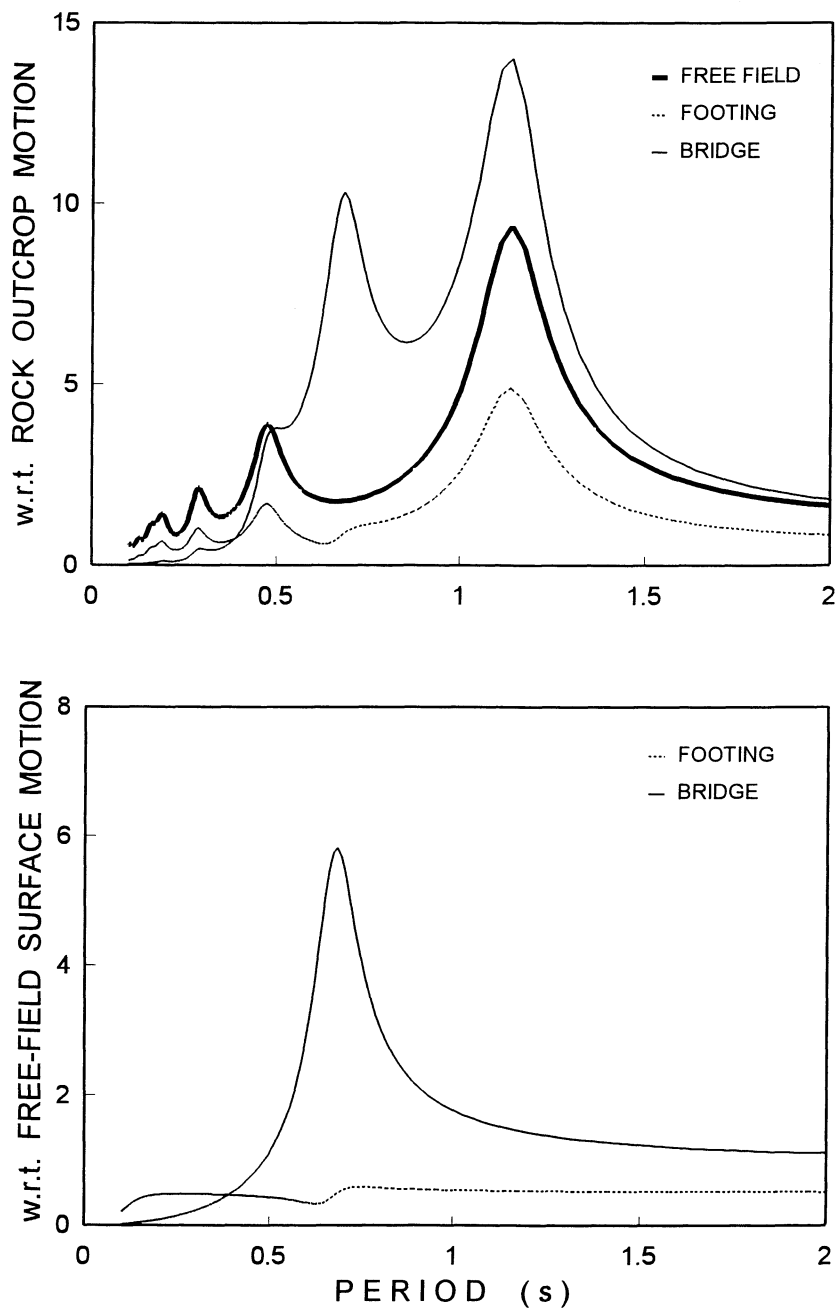
FIGURE 3-7. Solution for improved embedment: harmonic steady-state transfer functions.

56
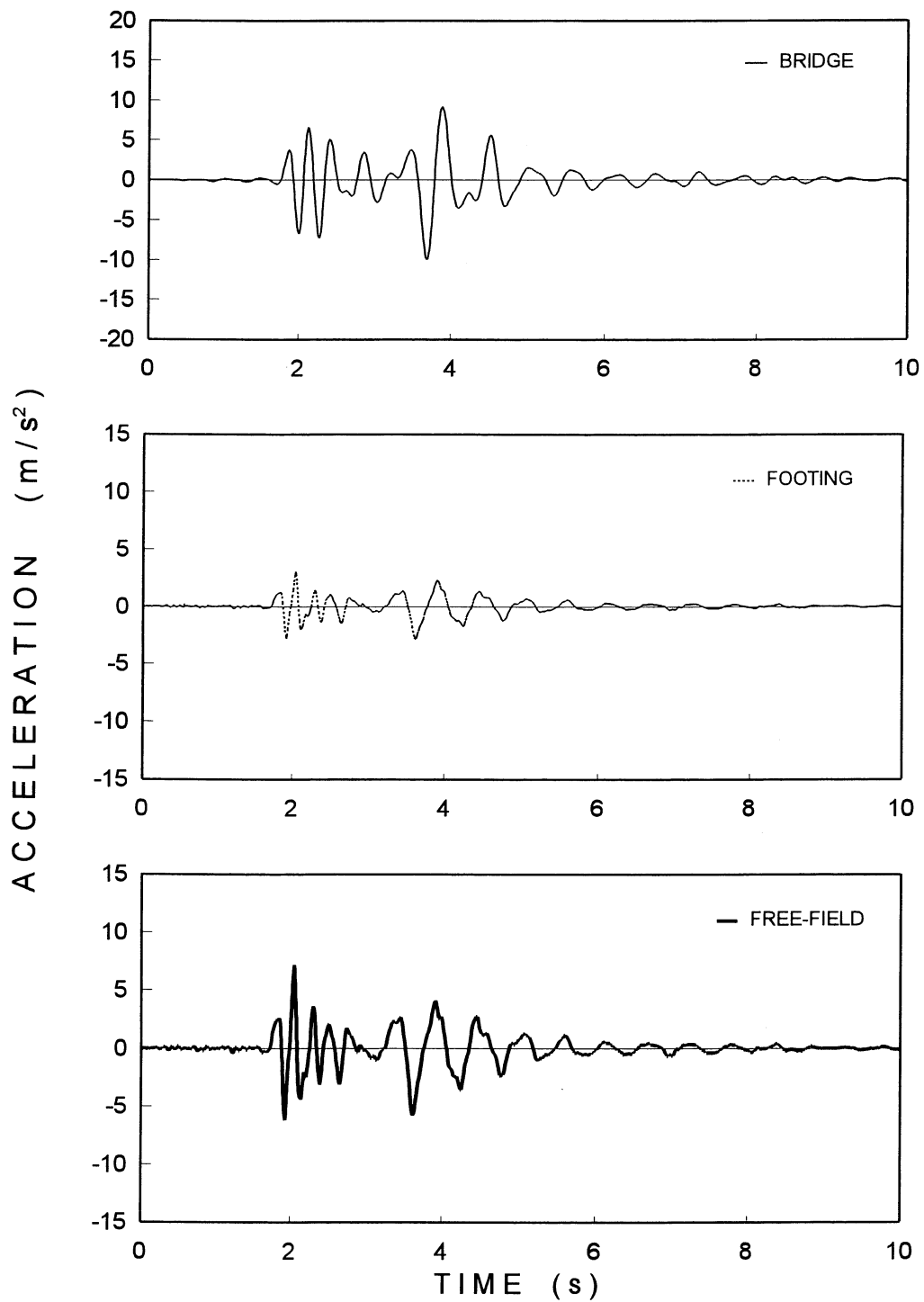
FIGURE 3-8. Solution for improved embedment: acceleration time histories for Pacoima, Northridge (1994) rock motion.

57
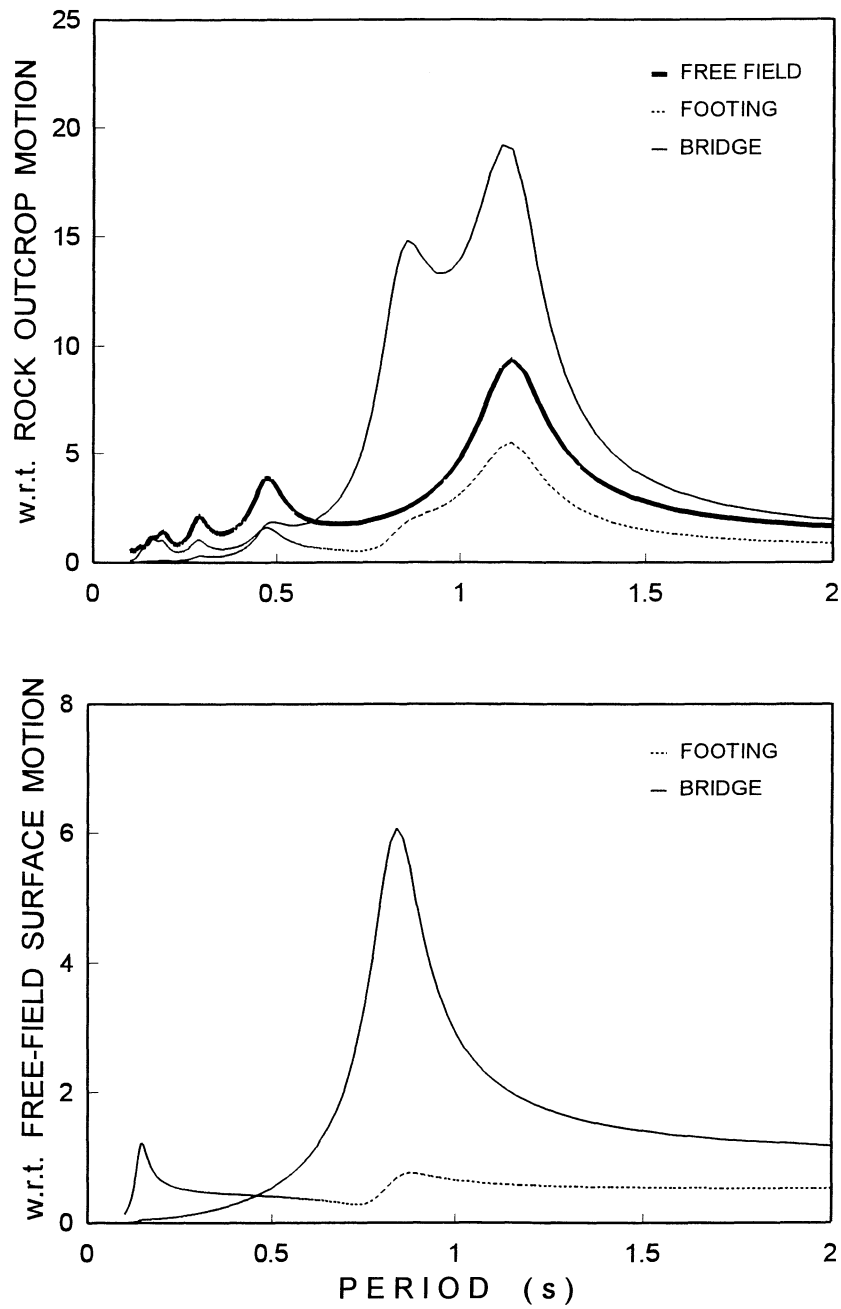
FIGURE 3-9. Solution neglecting radiation damping: harmonic steady-state transfer functions.
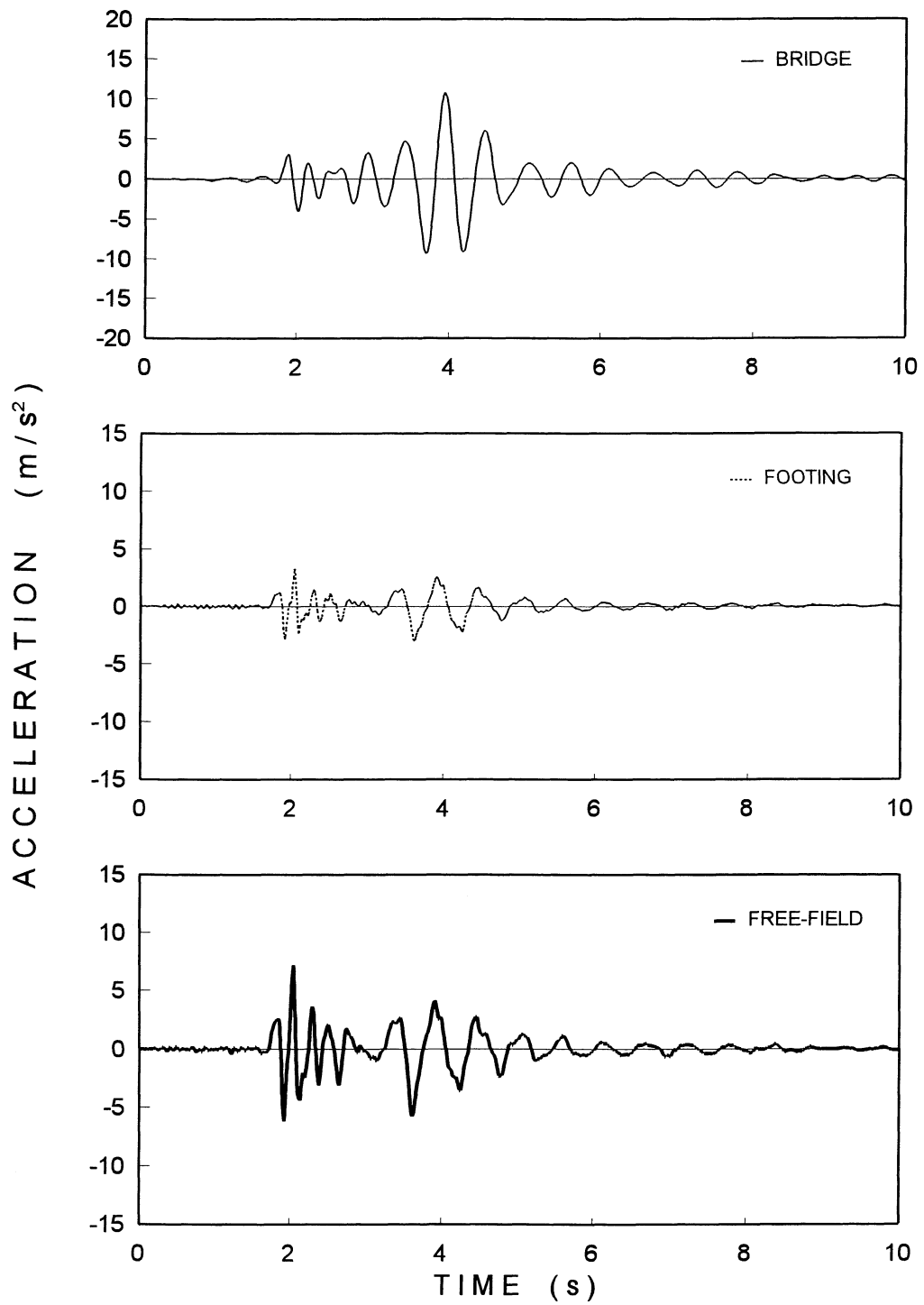
FIGURE 3-10. Solution neglecting radiation damping: acceleration time histories for Pacoima, Northridge (1994) rock motion.

59

2. Increasing the effectiveness of the embedment (by ensuring a good contact between the footing sidewall and the surrounding soil) generates additional radiation damping and reduces the fundamental natural period of the pier system. These effects are seen clearly in the steady-state transfer functions of Fig. 3-7. The behavior in the time domain (Fig. 3-8) shows characteristics partly similar to each of the two cases discussed above (SSI and no-SSI). The peak deck acceleration, however, is not significantly affected by the increase in embedment.

3. Neglecting radiation damping in this case has a minor effect both in the frequency and time domains. Two are the reasons: (a) While the fundamental period of the pier considering SSI (T $\approx$ 0.83 sec) is below the fundamental period of the whole deposit (T $\approx$ 1.15 sec), the main cutoff period (above which there is little or no radiation damping) is the second natural period corresponding to the resonance of the first (crucial) soft soil layer. Thus, radiation damping in the complete solution is small and neglecting it is of little significance at resonance. (b) In addition, the excitation is not particularly rich in 0.80-sec-period components, so even the small decrease in overall damping is of no further consequence.

3.2 Additional parameter studies

In order to get more understanding on the seismic behavior of pier-footing systems of the type shown in Fig. 1-1, additional parametric investigations were performed. Specifically, insight was sought toward the following issues: (1) the effect of the rotational restraint atop the pier; (2) the effect of radiation through the bedrock at the base of the profile, of seismic waves propagating vertically up and down through the soil; (3) the effect of the stiffness of the near-surface soil; (4) the effect of the overall thickness of the profile; (5) the effect of the size and the embedment depth of the footing, on the response of the system.

To this end, a second soil-footing-bridge model was developed, as shown in Fig 3-10. In this new idealization, the thickness of the second soil layer, H_2, was taken to be equal to 84 m (which is hereafter referred to as "Deep Profile" or "Profile A"), or 30 m (hereafter called "Shallow Profile" or "Profile B"). Two different values were used for the shear wave velocity of the top layer: V_{s1} = 80 m/s and 160 m/s which correspond to a ratio V_{s1}/V_{s2} of ¼ and ½, respectively (V_{s2} = 330
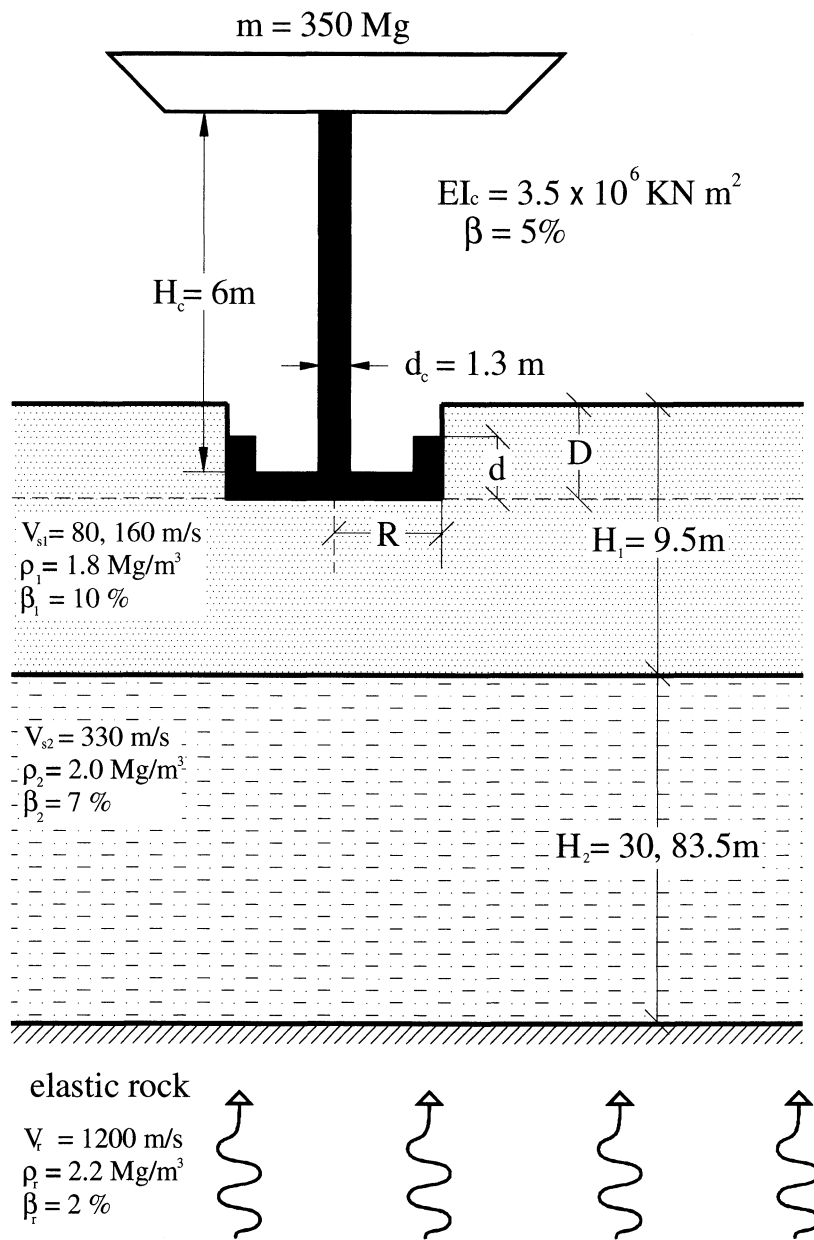
FIGURE 3-11. The bridge system studied in this section.

In the figure:

$m = 350 \text{ Mg}$

$EI_c = 3.5 \times 10^6 \text{ KN m}^2$
$\beta = 5\%$

$H_c = 6\text{m}$

$d_c = 1.3 \text{ m}$

D

d

R

$V_{s1} = 80, 160 \text{ m/s}$
$\rho_1 = 1.8 \text{ Mg/m}^3$
$\beta_1 = 10\%$

$H_1 = 9.5\text{m}$

$V_{s2} = 330 \text{ m/s}$
$\rho_2 = 2.0 \text{ Mg/m}^3$
$\beta_2 = 7\%$

$H_2 = 30, 83.5\text{m}$

elastic rock

$V_r = 1200 \text{ m/s}$
$\rho_r = 2.2 \text{ Mg/m}^3$
$\beta_r = 2\%$

m/s). Six different footing sizes were considered, expressed through the dimensionless ratio R /D ranging from 1 to 3. Finally, the embedment depth of the footing, D, was taken equal to 3m or 1.5m (a "shallow" and a "deep" footing, respectively), which corresponds to a ratio D/H_c (H_c = column height = 6 m) of ½ and ¼. In this study, full contact was considered between the footing sidewalls and the surrounding soil (i.e., d = D). The rest of the problem parameters were kept constant and are provided in Fig. 3-9. It should be noted that the case D = 1.5m, R/D = 1, corresponds to a footing radius R of only 1.5m. Whereas this extremely small footing leads to a safety factor of less that 1, the case was considered to provide insight in the elastodynamic response of bridges on very flexible foundations.

Table 3-I summarizes the parametric analyses performed for this alternative bridge system. The cases should read as follows: for example, "A421" means Profile A, V_{s1}/V_{s2} = ¼, D /H = ½, and R/D = 1. Wherever the symbol F is added (e.g., "A421F"), it implies that the pier top is free to rotate (cantilevered pier). Otherwise, the pier top is assumed to be restrained against rotation (fixed-head pier). The boundary conditions at the bottom of the profile (i.e., rigid or elastic rock) are mentioned explicitly in the corresponding graphs and tables.

As in the first parameter study, results were obtained in both the frequency and time domains for harmonic steady-state excitation and the two transient motions (Artificial and Pacoima). In total, 60 parametric cases were examined. The results are summarized in Tables 3-II to 3-VI in terms of peak response for the horizontal acceleration at the free-field soil, the footing, and the bridge deck. The full set of graphs is provided in Appendix A.

TABLE 3-I. The parametric cases studied in Section 3-2.

Profile	V_{s1}/V_{s2}	R / D (for D / H₁ = 1 / 4)			R / D (for D / H₁ = 1 / 2)		
		1	2	3	1	2	3
A	1 / 4	A441	A442	A443	A421	A422	A423
	1 / 2	A241	A242	A243	A221	A222	A223
B	1 / 4	B441	B442	B443	B421	B422	B423
	1 / 2	B241	B242	B243	B221	B222	B223

3.2.1 Discussion

The following are worthy of note based on the results of this parameter study:

(1) In the case of the *soft* surface soil layer (V_{s1} = 80 m/s) and for fixed head-conditions atop the pier, the maximum steady-state amplification of the motion of the deck (with respect to the free--field soil), is of the order of 2 to 3 (see Figs A-1 to A-6, A13 to A18). This is equivalent to an equivalent damping ratio of the SDOF pier

$$\tilde{\beta} \approx \frac{1}{2A} \approx 15\% \ \ to \ \ 25\% \tag{3-2}$$

which implies that an significant amount of energy is dissipated through the surface layer in the form of wave radiation. [To this end, recall that: (i) the material damping in the structure and the soil is less than 10% (Fig. 3-10), and (ii) full contact exists between footing sidewalls and soil.] In contrast, when the surface layer is stiffer (V_{s2} = 160 m/s) or the pier top is free to rotate, the amplification increases to approximately 5 to 6, which is equivalent to about 8 to 10% damping (Figs A-7 to A-12, A-19 to A-24, A-109 to A-114). This implies that the significance of radiation damping is much smaller and energy dissipation is more evenly balanced between the structure and the soil.

(2) The fundamental period of the deep (H_2 = 84 m) soil deposit appears to be about 1.1 s (Fig. A-1 to A-12). As it can be easily checked, the response at this period is largely dominated by the characteristics of the thick and stiff lower sandy layer (S-wave velocity 330 m/s, corresponding period $4H_2/V_{s2} \approx$ 1s). In the case of "elastic rock" conditions, the relatively small impedance contrast, I_R, between this layer and the underlain soft rock:

$$I_R \approx \frac{\rho_r V_r}{\rho_{s2} V_{s2}} = \frac{2.2 \times 1200}{2 \times 330} \approx 4 \tag{3-3}$$

generates sufficient radiation damping to reduce the soil amplification at this period to a mere 3.3. One could have expected such a low value at resonance, on the basis of Roesset's simple one-layer formula:

$$A \approx \frac{1}{(\pi/2)\beta_{s2} + (I_R)^{-1}} \approx \frac{1}{(\pi/2)0.07 + 1/4} \approx 2.8 \qquad (3\text{-}4)$$

The second natural period, T_2, of the soil deposit appears to equal almost 0.5 s (V_{s1} = 80 m/s) and the respective amplification, A_2 , is nearly 4 --- a rather substantial value for a second-mode resonance (Fig A-1). Apparently, this mode is dominated by the characteristic of the top clay layer: natural period of the top layer = 4H / V_s = 4 x 9.5 / 80 = 0.48 s . The relatively high amplification reflect the smaller radiation into the underlain stiff soil layer, due to the now larger "impedance" contrast:

$$I_R = \frac{2 \times 330}{1.5 \times 80} \approx 5.5 \qquad (3\text{-}5)$$

compared to $I_R \approx 4$ between the second layer and underlying base.

(3) For the response of the fixed-head bridge (Figs A-1 to A-24, Figs A-55 to A-78), the role of the second resonance in the soil is much more significant than the first, for two reasons: *First*, the fundamental natural period of the pier-foundation-soil system is between about 0.3 and 0.6 s --- much closer to T_2 than to T_1; hence, the amplitude increase and broadening of the bridge amplification curve (with respect to rock outcrop motion) at resonance. Second, in the time domain, the response of the spectra of both rock excitations (Figs A-25 to A-52) show that most of the incident seismic energy is carried by harmonic components with periods smaller than or about equal to 0.5 sec. This is, in fact, the usual case with "rock" motions. For periods exceeding by far 0.5 s (e.g. T = $T_1 \approx 1.1$ s , for the Deep Profile), the input motion is too weak to produce a substantial soil or structure response, despite the unquestionably amplification by a factor A $\approx$ 3.3 . As a result, the bridge acceleration histories (for fixed-head conditions) show prevailing periods of the order of 0.5 s, with hardly an evidence of a role for the fundamental natural period of the deposit. Similar observations have been reported by Mylonakis et al (1997) for a similar pile-supported bent.

(4) In the case of a free-head pier (Figs A-109 to A-114), opposite trends are observed. In this case, the natural period of the bridge-foundation system varies between about 1.1 sec (for the "small" R = 1.5 m footing --- Fig A-109), to approximately 0.6 s for the "large" R = 4.5 m footing

(Fig. A-111). In the first case, the fundamental natural period of the system coincides with that of the deep soil profile, leading to a substantial amplification of the response with respect to the rock outcrop: A ≈ 65 (Fig. A-109). This is more than 5 times the one in the corresponding fixed-head case (Fig. A-55). In contrast, with the shallow profile (Fig. A-112) the fundamental natural period of the soil, $T_1 ≈ 0.6s$, is much smaller that of the free-head pier (1.1 s) leading to a peak amplification with respect to rock outcrop of only 12. It is worth mentioning that this value is smaller than the A ≈ 13 of the (much more heavily damped) fixed-head pier (Fig. A-67).

(5) In the time domain, the effects of the superposition of the various frequency components tend to smoothen out (or even reverse) the differences observed in the steady-state peaks. For example, despite the aforementioned huge differences in bridge deck acceleration between cases A441F and B441F (Figs A-109, A-112), the peak values in the time domain (obtained from the 0.4 g artificial motion) are almost equal: 10.6 and 10.3 m/s^2 in the two cases, respectively (see Table 2-IV).

Based on the above observations, it appears difficult to determine *a priori* whether soil-structure interaction will increase or decrease the response of a bridge. In the realm of equivalent linear analysis this seems to be controlled by the following parameters:

(a) Radiation *damping*: if the fundamental period of the flexibly-supported bridge is significantly smaller than the "cutoff" frequency of the soil (such as in the case of a short pier on a deep and soft deposit), radiation damping will be significant and the response of the system at resonance will decrease. In particular, if the cutoff period of the soil is very large (such as in the case of a structure on halfspace), radiation damping will be substantial. This implies that modeling the soil as a halfspace (as done in existing seismic regulations), may lead to *unconservative* estimates of structural response.

(b) *Resonance between structure and soil.* If the modified, due to SSI, fundamental natural period of the system is close to one of the natural periods of the soil layer (especially the first or second), resonance will develop which will tend to increase the response. If the Foundation Input Motion (FIM) is rich in that period, the increase can be substantial.

(c) *Double Resonance.* If the fundamental natural period of the system coincides with *both* the natural period of the soil and the predominant period of the earthquake motion (*at rock level*), double resonance will develop (i.e., between structure, soil, and excitation). In this case the response may increase substantially.

(d) *Non-linear effects.* The development of plastic deformations in the structure and soil, including foundation uplift and development of pore water pressure, may increase the "effective"[1] natural period of the structure and the soil and, thereby, alter the response. This period shift may lead to either de-resonance (if, for instance, yielding develops as a result of resonance), or to resonance, which may lead to the so-called "progressive collapse".

In conclusion, design of critical bridges to be founded on soft soil in earthquake prone areas requires careful assessment of both soil and seismic environments. Use of design spectra and simplified / generalized soil profiles may not reveal the actual seismic risk in the structure.

---

[1] The term "effective" is used because in the nonlinear range natural period ceases to exist in the classical sense.

TABLE 3-II. Cases A441 – B223: Summary of results for 0.4g artificial motion and 0.4g harmonic steady-state motion. Absolute values are used for all entries.

Boundary Conditions: ELASTIC ROCK , NO ROTATION AT COLUMN TOP						
CASE	Free-Field Acceleration (m/s²)		Footing Acceleration (m/s²)		Bridge Acceleration (m/s²)	
	Frequency	Time	Frequency	Time	Frequency	Time
A441	15.05	6.87	12.27	3.86	43.9	12.90
A442	15.05	6.87	9.80	3.74	21.25	9.02
A443	15.05	6.87	8.98	3.56	16.62	7.38
A421	15.05	6.87	7.80	3.03	16.23	7.16
A422	15.05	6.87	7.84	2.95	13.21	5.96
A423	15.05	6.87	7.89	2.94	12.54	5.87
A241	11.25	4.53	6.12	2.52	39.98	9.49
A242	11.25	4.53	5.68	2.52	26.58	9.49
A243	11.25	4.53	5.68	2.34	27.05	8.07
A221	11.25	4.53	5.68	2.16	27.05	8.71
A222	11.25	4.53	5.64	2.14	31.12	8.72
A223	11.25	4.53	5.64	2.17	32.41	9.15
B441	21.17	9.46	15.95	5.35	47.82	17.20
B442	21.17	9.46	12.82	5.08	27.24	11.60
B443	21.17	9.46	12.11	4.85	23.95	10.20
B421	21.17	9.46	11.09	4.19	24.74	9.66
B422	21.17	9.46	11.02	4.07	18.74	8.68
B423	21.17	9.46	11.13	4.06	16.86	8.68
B241	13.21	7.76	7.68	3.90	42.34	12.80
B242	13.21	7.76	7.21	3.90	32.42	10.60
B243	13.21	7.76	7.06	3.94	31.71	10.60
B221	13.21	7.76	6.78	3.68	35.75	11.30
B222	13.21	7.76	6.78	3.77	34.57	11.10
B223	13.21	7.76	6.86	3.84	35.44	11.50

TABLE 3-III. Cases A441 – B441: Summary of results for Pacoima, Northridge (1994) and 0.4g harmonic steady-state motion. Absolute values are used for all entries.

Boundary Conditions: ELASTIC ROCK , NO ROTATION AT COLUMN TOP						
CASE	Free-Field Acceleration (m/s²)		Footing Acceleration (m/s²)		Bridge Acceleration (m/s²)	
	Frequency	Time	Frequency	Time	Frequency	Time
A441	15.05	8.21	12.27	3.60	43.90	13.20
A442	15.05	8.21	9.80	4.38	21.25	11.30
A443	15.05	8.21	8.98	4.40	16.62	9.67
B441	21.17	11.70	15.95	5.28	47.82	19.20
B442	21.17	11.70	12.82	6.27	27.24	16.50
B443	21.17	11.70	12.11	6.37	23.95	14.10

TABLE 3-IV. Cases A441 – B223: Summary of results for 0.4g artificial motion and 0.4g harmonic steady-state motion. Absolute values are used for all entries.

Boundary Conditions: RIGID ROCK , NO ROTATION AT COLUMN TOP						
CASE	Free-Field Acceleration (m/s²)		Footing Acceleration (m/s²)		Bridge Acceleration (m/s²)	
	Frequency	Time	Frequency	Time	Frequency	Time
A441	41.16	15.90	23.13	6.75	56.84	21.40
A442	41.16	15.90	21.56	6.79	30.89	16.50
A443	41.16	15.90	22.97	7.35	49.78	15.80
A421	41.16	15.90	20.93	6.64	30.14	15.40
A422	41.16	15.90	20.78	6.74	26.22	13.40
A423	41.16	15.90	20.89	6.86	24.97	12.70
A241	35.95	18.90	18.70	7.16	59.19	21.00
A242	35.95	18.90	18.23	7.02	30.03	26.60
A243	35.95	18.90	18.15	7.70	21.09	27.60
A221	35.95	18.90	18.11	7.38	35.40	29.40
A222	35.95	18.90	18.07	8.05	37.08	28.30
A223	35.95	18.90	18.11	8.50	39.16	28.40
B441	40.38	25.70	21.13	11.20	52.14	37.90
B442	40.38	25.70	24.26	12.20	43.90	31.60
B443	40.38	25.70	22.97	12.00	49.78	27.10
B421	40.38	25.70	21.13	10.80	52.14	26.60
B422	40.38	25.70	20.93	10.80	41.16	26.60
B423	40.38	25.70	21.21	10.70	36.85	20.60
B241	37.79	22.40	21.80	10.40	64.29	34.40
B242	37.79	22.40	20.50	10.80	42.34	29.40
B243	37.79	22.40	20.11	11.20	37.20	31.10
B221	37.79	22.40	19.36	10.40	39.59	33.10
B222	37.79	22.40	19.36	10.60	37.98	32.60
B223	37.79	22.40	19.52	10.70	39.04	33.00

TABLE 3-V. Cases A441 – B441: Summary of results for Pacoima, Northridge (1994) and 0.4g harmonic steady-state motion. Absolute values are used for all entries.

Boundary Conditions: RIGID ROCK , NO ROTATION AT COLUMN TOP						
CASE	Free-Field Acceleration (m/s^2)		Footing Acceleration (m/s^2)		Bridge Acceleration (m/s^2)	
	Frequency	Time	Frequency	Time	Frequency	Time
A441	41.16	9.77	23.13	4.24	56.84	15.70
A442	41.16	9.77	21.56	5.21	30.89	13.90
A443	41.16	9.77	22.97	5.29	49.78	12.00
B441	40.38	16.10	21.13	7.96	52.14	26.80
B442	40.38	16.10	24.26	8.51	43.90	23.70
B443	40.38	16.10	22.97	8.77	49.78	20.30

TABLE 3-VI. Cases A441 – B443: Summary of results for 0.4g artificial motion and 0.4g harmonic steady-state motion. Absolute values are used for all entries.

Boundary Conditions: RIGID ROCK , COLUMN TOP FREE TO ROTATE						
CASE	Free-Field Acceleration (m/s^2)		Footing Acceleration (m/s^2)		Bridge Acceleration (m/s^2)	
	Frequency	Time	Frequency	Time	Frequency	Time
A441F	41.16	15.90	18.93	7.86	245	10.60
A442F	41.16	15.90	21.68	6.65	57.23	16.90
A443F	41.16	15.90	21.40	6.77	45.47	19.40
B441F	40.38	25.70	20.50	12.60	44.69	10.30
B442F	40.38	25.70	13.72	11.00	106.62	31.90
B443F	40.38	25.70	17.37	11.00	179.14	37.70

SECTION 4

PORE PRESSURE GENERATION AND SOIL FAILURE; FOUNDATION UPLIFT

4.1 Bearing capacity

The inertia developing during an earthquake on the masses of the superstructure transmit onto the foundation an horizontal force of amplitude H_ε , an overturning moment of amplitude M_ε and, whenever vertical excitation is being considered, an additional vertical force of amplitude V_ε . The foundations must be designed to avoid, with an adequate factor of safety, bearing capacity failure under the combined action of $V = V_\varepsilon + V_{st}$, $M = M_\varepsilon + M_{st}$, $H = H_\varepsilon + H_{st}$, where the subscript "st" denotes the static components of the loads.

With the exception of soils whose strength degrades under strong cyclic loading (e.g. liquefiable soils, sensitive clays), current state of practice usually assumes that the ultimate capacity of a foundation carrying such loads is not influenced by the dynamic character of H_ε , M_ε and V_ε . Static bearing capacity theories are therefore used, such as Meyerhof's (1963) and Hansen-Brinch's (1975), which provide "correction factors" to account for the presence of the lateral loads H and M.

In recent years, theoretical (and some experimental) evidence has been published showing that the horizontal inertia forces that develop in the soil within the failure zone can have a detrimental effect on bearing capacity. With increasing acceleration levels, Richards et al (1993) found a rapid degradation of bearing capacity. Such degradation can be expressed as a decrease of the "Terzaghi" bearing capacity factors N_γ , N_q and N_c with increasing acceleration α_h in the soil. On the other hand, analytical studies by Pecker (1996) showed that soil inertia has a rather minor effect on bearing capacity.

In addition to the *limit* analyses and the Coulomb-wedges type of analyses used by Richards and his coworkers, the *kinematic* reduction in bearing capacity (i.e. the one stemming from the soil inertia, only) was investigated by the authors using an elastoplastic finite element code. The soil mass acceleration was simulated by equivalent distributed inertia forces applied statically on the

finite element mesh (pseudostatic approach). A vertical load, N , was applied on the footing, and the bearing capacity was calculated for different values of soil mass acceleration.

Moreover, a simplified analytical solution was developed for undrained loading using limit equilibrium analysis for the *kinematic* reduction of cohesion-related factor (from N_{cs} to N_{ce}). A circular failure mechanism was used and N_{cs} was expressed in terms of the soil (uniform) acceleration α (= A / g), the undrained shear strength S_u , the unit weight γ , and the width B of the strip footing.

In Figure 4-1 the computed reduction of N_c , N_q , N_γ is plotted as a function of α. The figure compares the results of finite element analyses with those by Shi & Richards (1995). For the N_c factor, for which the analytical solution (for γ B / S_u = 3) is also included, Shi & Richards predict no reduction, while a slight reduction is obtained with the finite element code and the analytical method. As the discrepancy is not significant, it could be concluded that in general the N_c factor is only slightly affected soil mass acceleration. *This means that the kinematic effect (inertia in the soil only) is not significant when estimating the bearing capacity of the frictionless soil (ϕ = 0).* A possible exception: where the acceleration is very high *and* the γ B / S_u ratio is very large (e.g., γ B / S_u > 5).

In contrast, differences between our finite element solutions and those of Shi & Richards (1995) are obvious for $N_{\gamma e}$ and N_{qe} . The values proposed by Shi & Richards are significantly smaller than those obtained here. In Fig. 4-2 the ratios $N_{\gamma e}$ / $N_{\gamma s}$ and N_{qe} / N_{qs} are plotted against the seismic acceleration. The plots include the reduction given by Meyerhof and by Brinch Hansen (solely inertial loading, in the form of inclined static load), and the factor given by Shi & Richards when both inertial and kinematic loading is applied. The contribution of kinematic loading (soil inertia) is verified by plotting Meyerhof's results multiplied by the results of finite-element analyses for kinematic loading. It is obvious that the reduction due to kinematic loading alone, is very small when compared to the reduction due to inertial loading. The soil inertia ("kinematic") effect is judged as even more insignificant when considering the differences among the various methods for
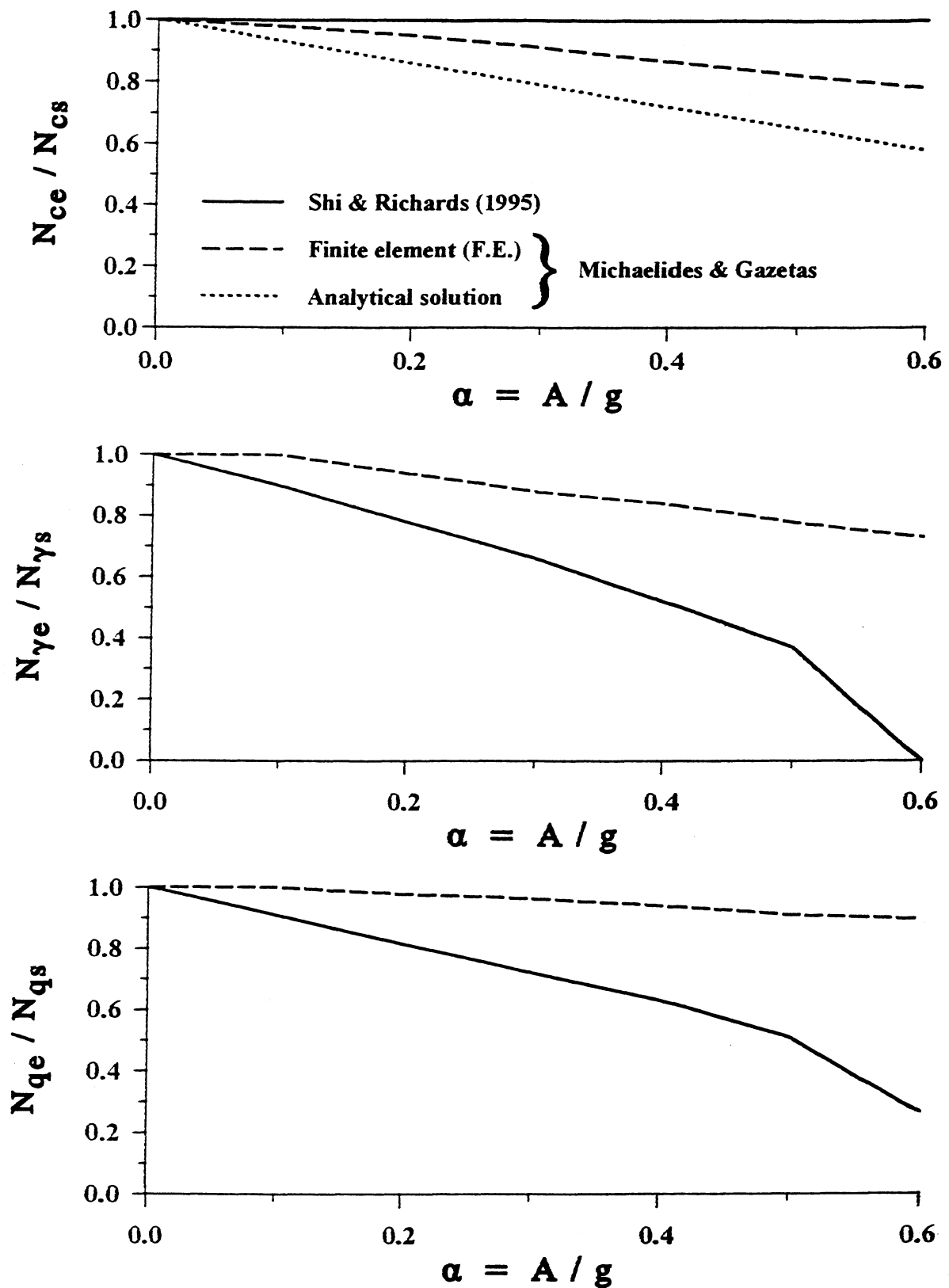
FIGURE 4-1. Ratio of seismic to static bearing capacity factors. Kinematic loading of the foundation (inertia only in the soil under the footing).
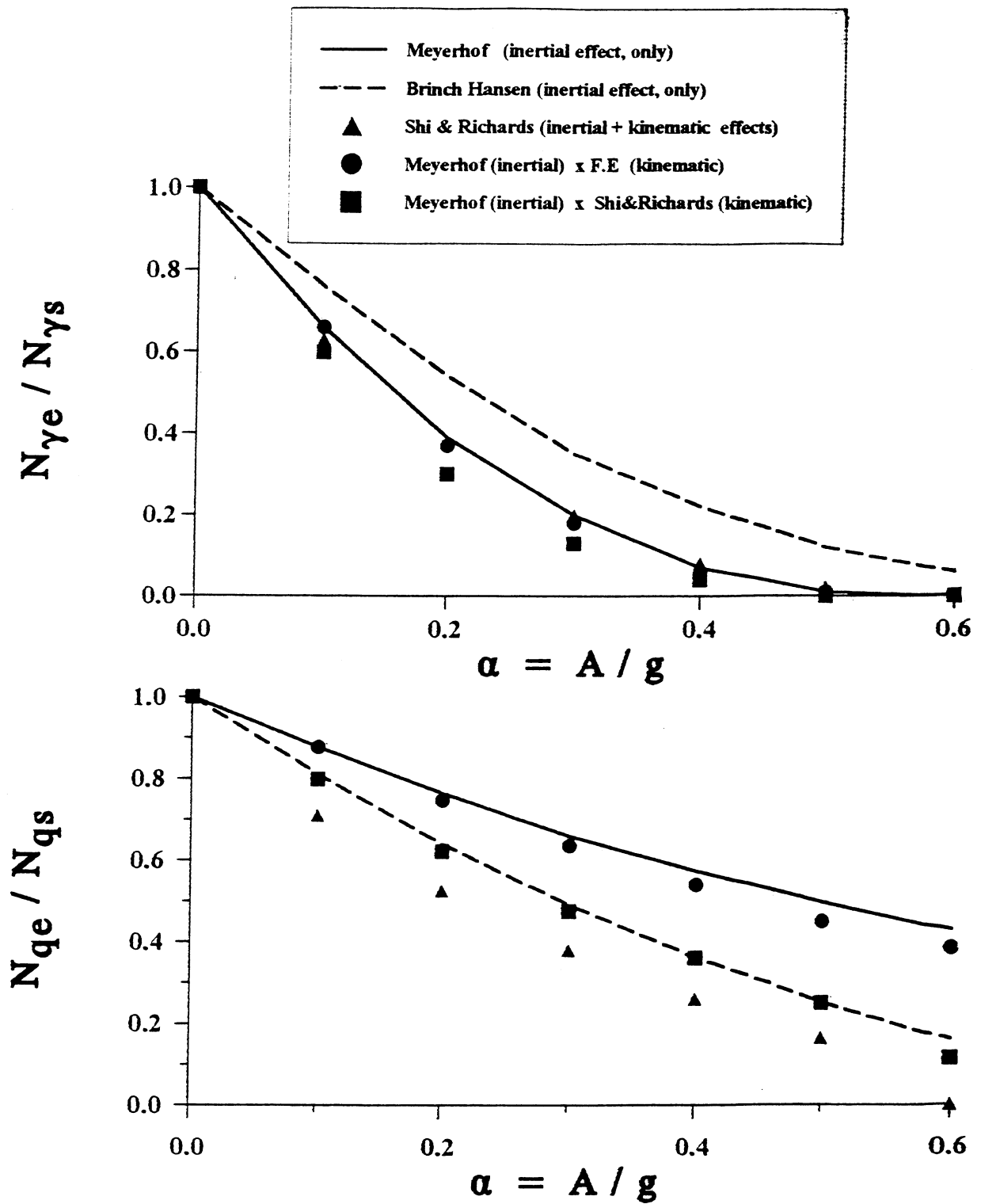
FIGURE 4-2. Combined kinematic loading (inertia of the soil) and inertial loading (inertia forces from the superstructure making the load "inclined") on the total reduction of bearing capacity factors N_γ and N_q.

the inertial effect (Meyerhof versus Brinch Hansen). For this reason, not only is the difference in kinematic reduction given by the two methods insignificant, but as a good approximation the kinematic effect could in most cases be ignored.

From all the above, it is concluded that the *kinematic* component of loading may in some cases be important, but it does not seem to be as crucial as it was initially suggested by early solutions to this problem. Its contribution to the "degradation" of the bearing capacity of a surface footing is rather negligible compared to the degradation due to the inclination and eccentricity that arise from the inertia of the superstructure, and the detrimental development of cyclic pore-water pressures.

In any case, seismic bearing capacity is quite different from static failure. Whereas a static bearing failure could lead to substantial sudden displacements, bearing capacity settlement in an earthquake takes place at the "moments" when the horizontal acceleration, α_h , exceeds a certain critical value α_c . This can only happen in an earthquake for a finite number of small time periods. Thus seismic settlement would be expected to be finite, and made up of a number of small increments.

This is analogous to the accumulation of displacement during earthquake shaking of a slope (the well known "Newmark" concept). The critical acceleration, α_c, in this case can be approximated by the pseudostatically applied acceleration that produces a factor of safety equal to 1.

For the bearing capacity problem, the critical acceleration is obtained as the acceleration that produces a bearing capacity factor of 1, under constant V, H, and M. The permanent vertical displacement, δ, when $a_h > a_c$ can then be computed from the following approximated formulas:

$$\delta \approx 2\Delta \tag{4-1}$$

where Δ is the displacement computed according to Newmark (1965) / Franklin-Chang (1977) / Richards-Elms (1979):

$$\Delta \approx 0.1 \frac{u_h^2}{a_h} \left[\frac{a_c}{a_h} \right]^{-4} \tag{4-2}$$

where u_h = the peak value of horizontal ground velocity.

4.2 The method of Pecker et al (1996)

Pecker et al (1996) proposed a simple static formula for determining the bearing capacity of footings on the surface of cohesive soil deposits. According to that method, the bearing capacity of strip footings on the surface of a homogeneous material following the Tresca criterion without tensile strength (saturated clay), is given, in terms of total stresses, by:

$$\frac{(\beta \overline{H})^2}{(a \overline{V})^a [1 - a \overline{V}]^b} + \frac{(\gamma \overline{M})^2}{(a \overline{V})^c [1 - a \overline{V}]^d} - 1 = 0 \tag{4-3a}$$

Where $\overline{V}$, $\overline{T}$, $\overline{M}$ are dimensionless factors defined as

$$\overline{V} = \frac{V}{S_u B}, \qquad \overline{T} = \frac{V}{S_u B}, \qquad \overline{M} = \frac{V}{S_u B^2}, \qquad \overline{N} = \frac{N}{S_u B} \tag{4-3b}$$

$$a = 0.7, \qquad b = \tfrac{1}{2}, \qquad c = 2.14 \qquad d = 1.81 \tag{4-3c}$$

$$a = \frac{1}{\pi + 2}, \qquad \beta = \tfrac{1}{2} \qquad \gamma = 0.36 \tag{4-3d}$$

with the conditions: $\quad 0 < a \overline{N} \leqslant 1, \quad |\overline{T}| \leqslant 1 \tag{4-3e}$

In the above equations S_u denotes the undrained shear strength of the material, and B the width of the footing. Based on results from the above equation and other analytical studies, Pecker et al (1996) and Pecker (1996b) conclude the following:

1. For foundations designed with a safety factor higher than 2 under a vertical centered load, the effect of seismic forces in the soil (soil inertia) can be neglected without loss of accuracy. In contrast, for foundations with small safety factors, soil inertia forces may reduce significantly bearing capacity.

2. In normally-consolidated clays, bearing capacity is not strongly influenced by soil anisotropy.

3. If the load eccentricity e (computed as e = M / V) is less than 0.3 times the width of the footing B no significant permanent displacements tend to develop and, accordingly, any load combination (T, V, M) is acceptable. In contrast, if e/B is larger that 0.4, the magnitude of permanent displacements is very sensitive to small variations in the magnitude of the applied loads.

The above conclusions are in accord with those of the preceding section.

4.3 Pore-water pressure and permanent displacement of foundations under seismic excitation

Seismic excitation induces several cycles of loading, unloading, reloading to the soil elements below foundations. For dry soils, the result of this cyclic loading is to accumulate permanent strains in the soil and permanent displacements in the foundation. For saturated soils, permanent strains and displacements are followed by excess pore water pressure built up, which may ultimately lead to a bearing capacity failure in the case of strong and sustained seismic shaking.

From a practical point of view, it is important to note that the above phenomena occur at relatively high levels of seismic acceleration, when the cyclic shear strain amplitude in the soil exceeds a minimum value γ_p , referred to in the literature as (plastic) threshold strain (Dobry & Ladd, 1982; Dobry et al. 1980). Although γ_p appears to depend on various factors (e.g. soil type, density, static and cyclic stress history or number of shaking cycles) experimental data show that it is of the order of 10^{-4} for sands and 4×10^{-4} for clays (Fig. 4-3).

Analytical computations of permanent foundation settlements and pore pressures require an elaborate modeling of the cyclic soil response and the foundation-soil interaction, especially when soil is at a near-failure state of stress, due to the combined static and dynamic loading. However, for well designed foundations with an adequate factor of safety against static and seismic loads, it is possible to perform simplified computations following essentially the same general methodology as in the case of static loading: the foundation is divided into horizontal layers with "uniform" soil properties; stresses, permanent vertical strain and pore pressure in each layer are computed from the results of cyclic tests or from equivalent empirical relationships.

Based upon the empirical relationships for permanent strain accumulation proposed by Bouckovalas and Gazetas (1996) and Egglezos and Bouckovalas (1998) for normally consolidated clays and sands, one may derive the following empirical equations for approximate computation of permanent vertical strains, ε_v, and residual pore pressures, $\Delta u/\sigma_{3C}$, under triaxial test conditions.

$$\varepsilon_v = C_1 \left(C_2 Q^{d1} + 1/3 \right) \gamma_c^{d2} N^{d3} \tag{4-4a}$$

$$\frac{u_r}{\overline{\sigma}_{oct}} = 1 - \exp(C_3 \gamma_c^{d2} N^{d3}) \tag{4-4b}$$

with

$$Q = \frac{q}{\sigma_{fc} M} \tag{4-4c}$$

where γ_c is the cyclic shear strain amplitude in percent; N is the number of cycles with uniform shear strain

$$\overline{\sigma}_{oct} = (\overline{\sigma}_1 + \overline{\sigma}_2 + \overline{\sigma}_3)/3 \tag{4-4d}$$

$$q = (\sigma_1 - \sigma_3)/2 \tag{4-4e}$$

$$M = 3 \sin \phi_p / \left(3 - \sin \phi_p \right) \tag{4-4f}$$

and ϕ_p is the peak friction angle.

Equations 4-4 assume that during seismic loading the soil under the foundations can deform freely in the horizontal direction, it may consequently overestimate the permanent vertical strains. Alternatively, for lower-bound computations, one may use the following empirical relationship derived for cyclic odoemeter test conditions, with no lateral strain allowed:

$$\varepsilon_v = C_1 \gamma_c^{d/2} N^{d/3} \tag{4-3}$$
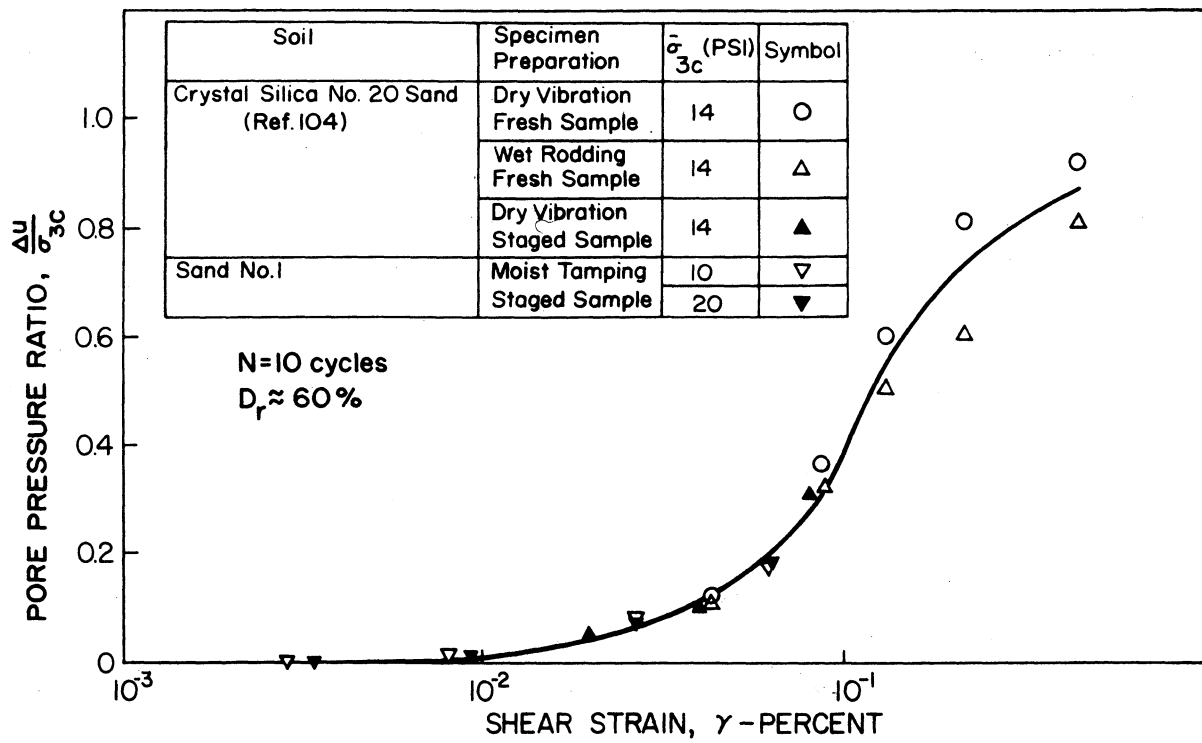
FIGURE 4-3. Effect of strain amplitude on residual pore water pressure (after Dobry and Ladd, 1980).

Typical values of the parameters C_1, C_2, C_3, d_1, d_2, d_3 of the above equations are given in the Table 4-I for fine sands of medium density and for normally consolidated clays.

Table 4-I. Values of parameters C_1, C_2, C_3, d_1, d_2, and d_3 for pore pressure computation, (from Bouckovalas, 1991).

	SANDS (D_r = 50–70%)	CLAYS (Normally Consolidated)
C_1	0.016	0.005
C_2	7.27	117
C_3	1.92	2.14
d_1	2.00	5.00
d_2	1.26	1.70
d_3	0.40	0.50

4.4 Partial footing uplift

For severe earthquakes, large overturning moments arise which may lead to tension in part of the area of contact of the basemat of the structure and of the soil, according to a calculation based on a linear theory. As tension is incompatible with the constitutive model of soil, the basemat will become partially separated from the underlying soil (uplift).

The phenomenon has been observed in many earthquakes. For example, during the Arvin-Tehachapi, California earthquake of July 1952, a number of tall, slender, petroleum-cracking towers stretched their anchor bolts and rocked back and forth on their foundation. After the Alaska earthquake of March 1964, ice was found under some oil tanks, evidence that lift-off occurred during the earthquake. Rocking of monuments and tombstones has been observed in many earthquakes; for example, during the Assam, India earthquake of June 1897, rocking was so strong that it resulted in overturning of these small structures.

A considerable amount of analytical and experimental work on the response of uplifting flexible systems has been performed [see Chopra and Yim (1985), Huckelbridge and Clough (1978), Meek (1975, 1978), Psycharis (1981, 1983), Yim and Chopra (1984a, 1984b, 1985)]. The

analytical solutions of the problem is quite complicated, because the system continuously changes between the regimes of full contact and uplift. As a result the behavior is nonlinear, although in some cases the differential equations, which govern the motion in each regime, can be linearized. Figure 4-3 illustrates the model utilized herein (following the work of Psycharis, 1983). It consists of a 1-DOF system supported on a dynamic Winkler bed of linear springs and dashpots. The footing is not bonded to the soil and, thus, downward reactions cannot be generated. In this way, the system uplifts whenever the overturning moment about O or O′ is greater than the restoring one. Also, it is assumed that friction is sufficient so that sliding does not occur.

In general, it can be said that lift-off results in a softer vibrating system which behaves non-linearly, overall, although the response is composed of a sequence of linear responses. After lift-off, the solution of the equations of motion include hyperbolic terms upon which harmonic terms are superimposed. The effect of uplift is mainly shown in the *effective fundamental period* of the system which increases with the amount of lift-off. The word "effective" is used because the uplifting system does not posses a fundamental natural period in the classical sense. This period is always larger than both the fundamental period without lift-off and the fundamental period of the fixed-base superstructure. In contrast to the first mode, the second and higher modes of the structural model are not affected by either the soil-structure interaction or the uplift. Figure 4-4 (from Psycharis, 1983) portrays the increase in effective period $\tilde{T}$ with increasing magnitude of uplift. The latter is measured through the parameter β which is equal to the ratio of the maximum angle of rotation, ϕ^c_{max}, which would occur if uplift were not allowed, over the critical angle, ϕ_{cr}, at which lift-off happens in the absence of vertical oscillations. Psycharis (1983) has suggested the following algebraic expressions for $\tilde{T} = \tilde{T}(\beta)$:

$$\tilde{T} / T_1 = (2 / \pi) \left[\arcsin(1 / \beta) + \sqrt{\beta^2 - 1} \right] \tag{4-3}$$

in which T_1 is the fundamental natural period of the interacting system when lift-off is not allowed. It is seen that the apparent fundamental period increases rapidly with the value of the normalized impulse, and for large values of β, the ratio $\tilde{T} / T_1$ is essentially proportional to β.

At the same time, the "effective" damping of the system, $\tilde{\xi}$, may decrease (fewer "dashpots" are dissipating energy during uplift). The ratio of $\tilde{\xi}$ over the ξ of the system without uplift is plotted, also as a function of β in Fig. 4-5 (Psycharis, 1983). It is seen that $\tilde{\xi}$ is a decreasing function of β except for $\beta \leq 1.2$; evidently, at such small values of β the impact of the uplifting footing overcompensates for the decreased radiation damping in the soil.

As a result of the above-mentioned phenomena (increase in $\tilde{T}$, decrease or increase in $\tilde{\xi}$), the dynamic behavior of a structure allowed to uplift may be very different from the response without lift-off. It seems that the angle of rotation increases non-linearly with the excitation, but the effect on the amplitude of the relative deflection and the resulting stresses is not clear, although the appearance of the response is greatly affected. In general, it cannot be concluded from this study whether uplift is beneficial to the structural response or not; the work done so far indicates that this depends on the parameters of the system and the characteristics of the excitation.
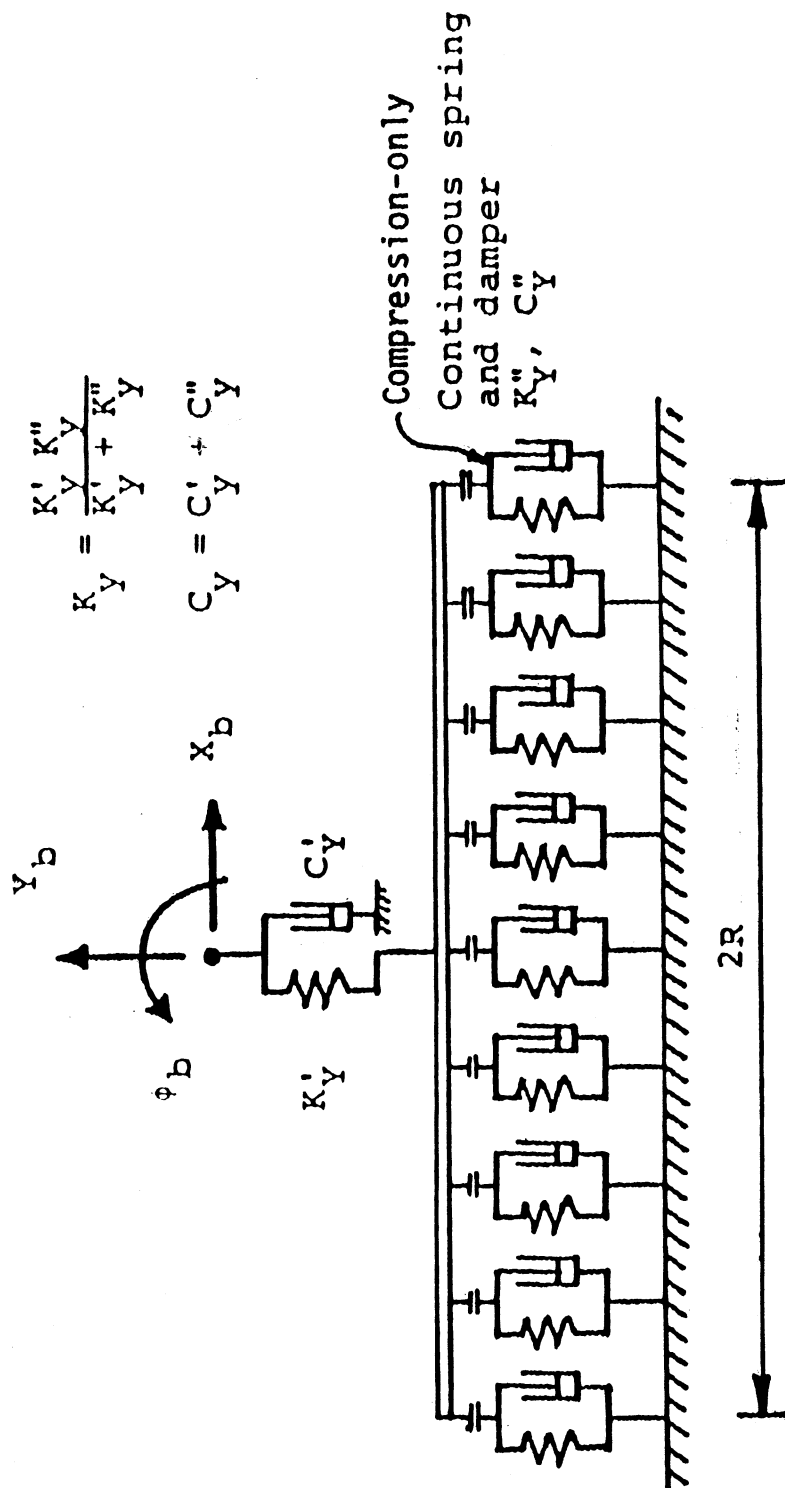
FIGURE 4-4. Model utilized in this report to incorporate footing uplift using non-linear (tensionless) springs and dashpots.
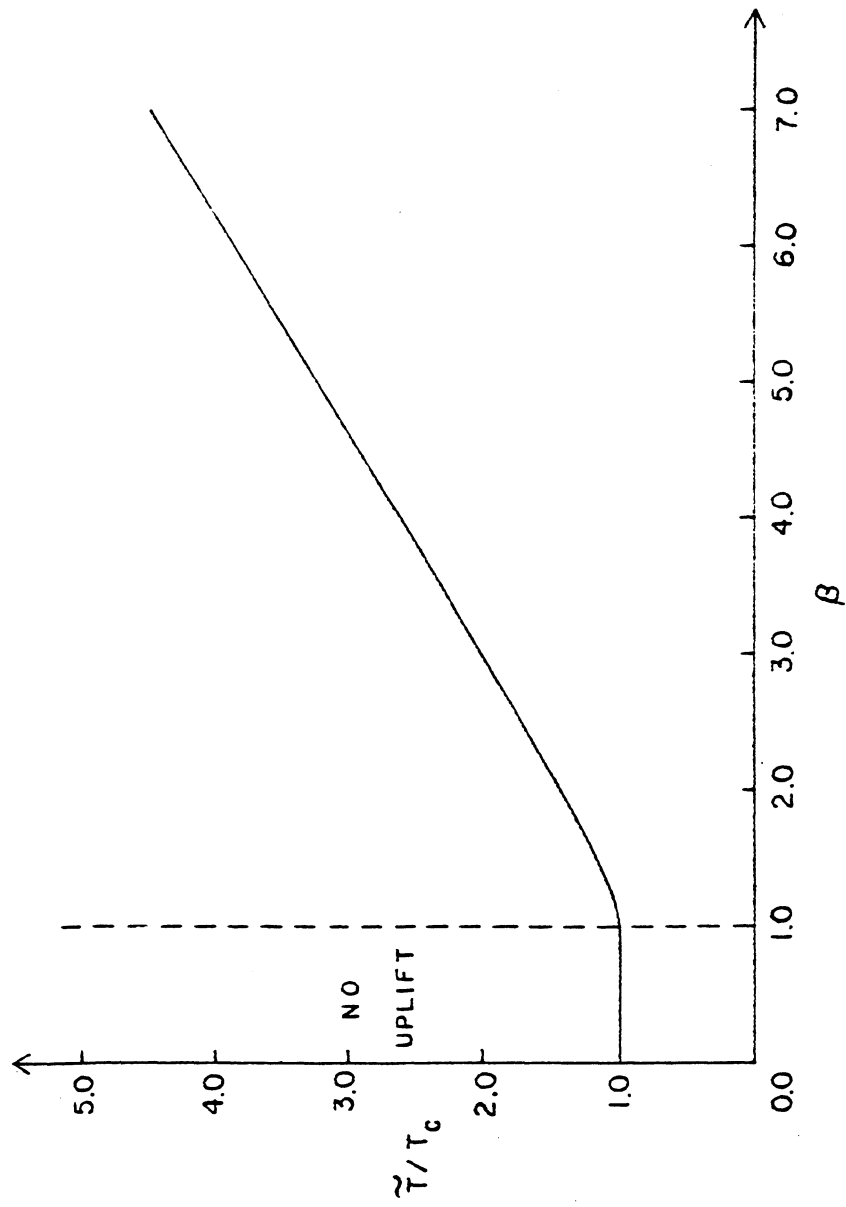
FIGURE 4-5. Increase of the effective period $\tilde{T}$ with uplift, as a function of the normalized impulse, β.
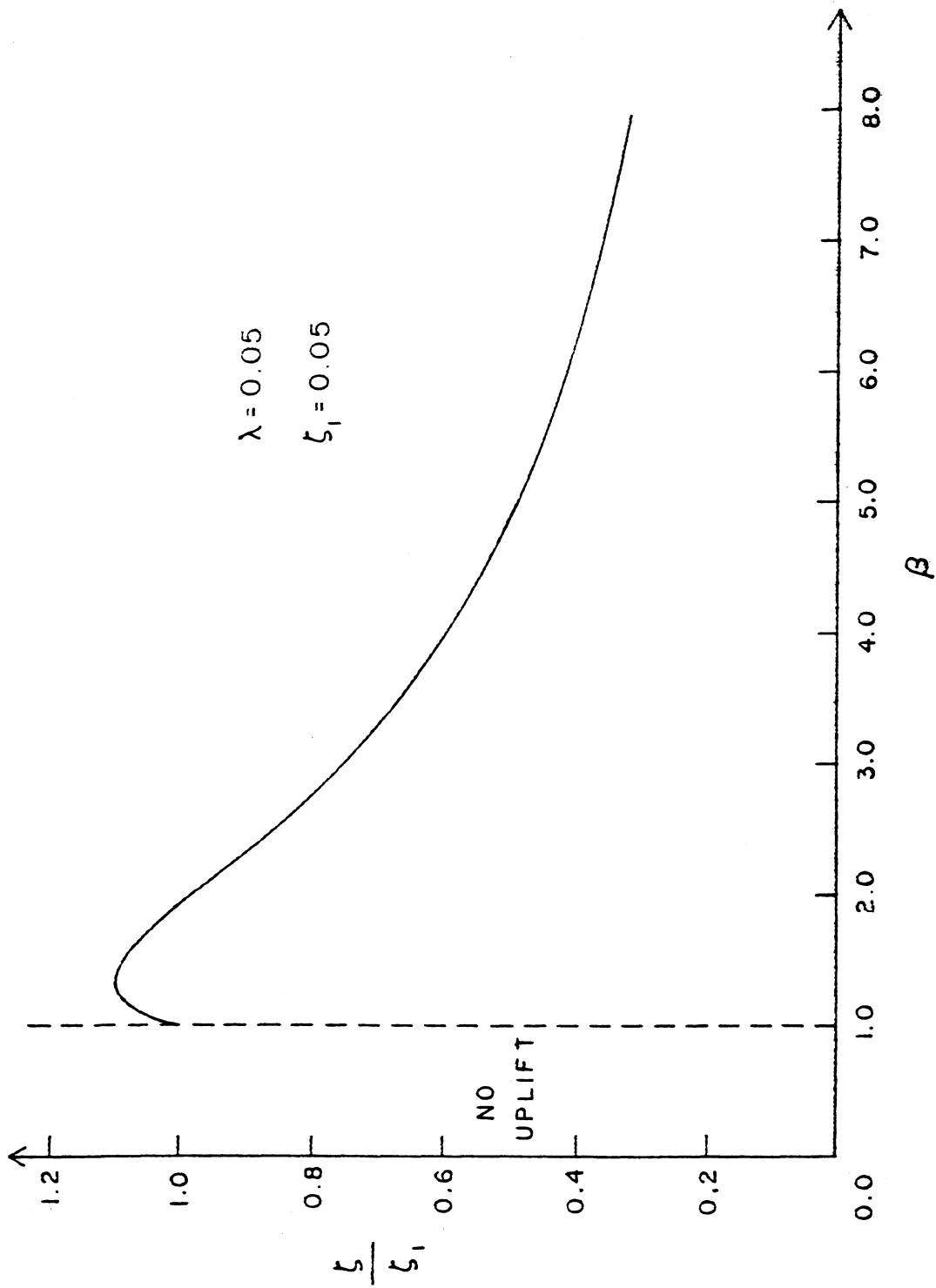
FIGURE 4-6. The ratio of $\tilde{\xi}$ over the ξ of the system without uplift as a function of β.

λ = 0.05

ζ_1 = 0.05

NO
UPLIFT

β

$\dfrac{\zeta}{\zeta_1}$

SECTION 5

CONCLUSIONS

The main conclusions drawn from this study are:

Section 2

1. The decomposition of soil-structure interaction into a kinematic and an inertial part provides a convenient way to analyze this complicated boundary-value problem. To account for the unavoidable nonlinearities in the soil during strong seismic excitation, it is reasonable (though not strictly correct) to separate soil nonlinearity into "primary", arising from the shear-wave induced deformations in the free-field soil, and "secondary", arising from the stresses induced by the oscillating foundation (which is concentrated close to the surface). Although both phenomena occur simultaneously, in the realm of equivalent linear analyses different soil moduli can be used in the two steps.

2. Kinematic Interaction leads to a "Foundation Input Motion" which is usually smaller than the motion of the free-field soil and, in addition, to a rotational component. Ignoring the rotational excitation may lead to errors in the unsafe side. These errors are small when determining the response of short squatty structures but may be large for tall slender structures.

On the other hand, neglecting kinematic interaction altogether usually leads to slight conservative results. It is therefore recommended for design of non-critical bridges.

3. In embedded foundations and piles, horizontal forces induce rotational, in addition to translational, oscillations, hence a "cross-coupling" horizontal-rocking impedance exists. Ignoring the coupling stiffness may lead to underestimation of the fundamental period of a flexibly-supported pier. On the other hand, coupling impedances are usually small in shallow foundations and can be ignored.

4. The contact between the sidewalls of an embedded footing and the surrounding soil tends to increase both the stiffness (spring constant) and damping (dashpot constant) of the footing. The actual sidewall area that is in "good" contact with the surrounding soil is usually smaller than the

nominal contact area. The actual contact area does not necessarily attain a single value for all modes of vibration.

5. If bedrock is present at shallow depths beneath a footing, the static stiffness in all modes of vibration increases. Particularly sensitive to the presence of bedrock is the vertical mode. Horizontal stiffnesses may also be appreciably affected. The torsional and rocking stiffnesses are essentially not affected.

6. The variation of the dynamic stiffness coefficients is also sensitive to the presence of bedrock. The amplitude of the foundation motion may increase significantly at frequencies near the natural frequency of the deposit. Radiation damping is insignificant at frequencies below the "cutoff" frequency of the layer. As with their static counterparts, torsional and rocking damping impedances are not particularly sensitive to the presence of bedrock.

7. The dynamic impedances of footings on a soil stratum overlying a halfspace exhibit intermediate behavior between those for halfspace and for a stratum over bedrock. The flexibility of the halfspace leads to a *decrease* in stiffness but an *increase* in radiation damping. The latter stems from the fact that waves emitted from the foundation-soil interface penetrate into the halfspace rather than being fully reflected. For the earthquake problem, the increase in radiation damping is most significant in the swaying dashpot, at frequencies below the "cutoff" frequency of the stratum.

Section 3

1. The damping characteristics of a flexibly-supported bridge depend primarily on the radiation damping in the soil and on the relative stiffness between structure and soil. In the case of a stiff superstructure (e.g., a short fixed-head pier) and soft soil, wave radiation is significant and the overall damping may exceed 20 percent. With a more flexible superstructure and stiffer soil, the influence of wave radiation decreases; the overall damping may be less than 10 percent.

2. It appears difficult to determine a priori whether soil-structure interaction will increase or decrease the response of a bridge. In the realm of equivalent linear analyses this seems to be controlled by the following main parameters: (a) *The system damping*: if the fundamental period

of the flexibly-supported bridge is significantly smaller than the "cutoff" frequency of the soil (e.g., a rigid pier on a deep and soft deposit), radiation damping will be significant and the response of the system will decrease. In particular, if the cutoff period of the soil is very large (e.g., a pier on halfspace), radiation damping may be substantial regardless of natural period of the system. This implies that modeling the soil as a halfspace, as done in existing seismic regulations (ATC-3, NEHRP-97), may lead to *unconservative* estimates of the response. (b) *Resonance between structure and soil.* If the increase in fundamental natural period due to SSI brings the period of the bridge close to a natural period (especially the first or the second) of the soil, resonance will develop which will tend to increase the response. However, if the frequency content of the excitation is not strong in that particular period, the increase may be insignificant. (c) *Double Resonance.* If the fundamental natural period of the system coincides with *both* the natural period of the soil and the predominant period of the earthquake motion (at rock level), double resonance will develop (i.e., between structure, soil, and excitation). In this case the response may increase dramatically. Whether or not this will result to damage is related to several additional parameters that are not discussed in this study. (d) *Non-linear effects.* The development of plastic deformations in the structure and soil, including development of pore water pressure and uplift, may increase the effective natural period of the structure and the soil. This shift in period may lead to either de-resonance or resonance (e.g., bringing the structure closer to the predominant period of the excitation), which, in turn, may lead to "progressive collapse". To date, such strong nonlinearities are beyond the state of the art of seismic soil-structure interaction.

In conclusion, design of critical bridges to be founded on soft soil in earthquake prone areas requires careful assessment of both soil and seismic environments. Use of design spectra and simplified / generalized soil profiles may not reveal the actual seismic risk in the structure.

The conclusions drawn from the parameter studies should not be generalized to bridge piers, soil deposits and seismic excitations with characteristics vastly different from these of the studied cases. However, the observed phenomena and the discussed interplay between the various natural periods of the system and the dominant periods of the ground excitation, can be of help in predicting qualitatively the response in other cases, or in interpreting the results of numerical studies.

Section 4

1. Soil inertia appears to be less significant for estimating the bearing capacity of footings than suggested by early solutions of the problem. For strip foundations designed with adequate safety factor against centered gravity loads (i.e., larger than 2), the effect of the inertial forces in the soil can be neglected. With smaller safety factors soil inertial effects can be important, but this is not of practical significance.

2. To limit the development of permanent displacements, strip footings on the surface of cohesive soils should be designed for eccentricities smaller than 0.3. If the eccentricity is larger than 0.4 significant displacements may develop.

3. During uplift the effective fundamental natural period of a foundation-structure system always increase, whereas damping may decrease. The higher modes of vibration are not affected by either the uplift or the soil-structure interaction. Both the increase in period and the decrease in damping can be calculated approximately through simplified expressions and graphs provided in the report.

As with SSI effects, it cannot be concluded whether uplift is beneficial to structural response. It seems that this depends on the parameters of system and the characteristics of the excitation.

SECTION 6

REFERENCES AND RELATED BIBLIOGRAPHY

1. Bouckovalas, G. and Gazetas, G. (1994) "Seismic Bearing Capacity of Shallow Foundations", Prenormative Research in support of EC8, CEC-Human Capital and Mobility, ERB CHRX-CT92-0011

2. Brinch Hansen J. (1970). "A Revised and Extended Formula for Bearing Capacity", *Bulletin No. 28, Danish Geotechnical Institute*, Copenhagen

3. Budhu M. and Al-Karni A. (1993). "Seismic Bearing Capacity of Soils", *Geotechnique*, Vol.. 43, No. 1, pp. 181-187

4. Chopra, A.K. and Yim, S. C-S. (1985). "Simplified Earthquake Analysis of Structures with Foundation Uplift", *Journal Structural Engineering Division*, ASCE, Vol.. 111, No. 4, pp. 906-930

5. Dobry, R. and Gazetas, G. (1986). "Dynamic Response of Arbitrary Shaped Foundations", *Journal Geotechnical Engineering Division*, ASCE, Vol.. 112, No. 2, pp. 109-135

6. Dobry, R. and Ladd, R.S. (1980). Discussion on "Soil Liquefaction and Cyclic Mobility Evaluation for Level Ground during Earthquakes" by Seed, H.B., and "Liquefaction Potential: Science versus Practice", by Peck, R.B., *Journal Geotechnical Engineering Division*, ASCE, Vol.. 106, No. 2, pp. 720-724

7. Dobry, R., Gazetas, G., and Stokoe, K.H., II (1986). "Dynamic Response of Arbitrarily Shaped Foundations: Experimental Verification", *Journal Geotechnical Engineering Division*, ASCE, Vol.. 112, No. 2, pp. 136-149

8. Dobry, R.., Ladd, R.S., Yokel, F.Y., Chung, R.M., and Powell, D. (1982). "Prediction of Pore Water Pressure Buildup and Liquefaction of Sands during Earthquakes by the Cyclic Strain Method", NBS Building Science Series 138, National Bureau of Standards, Gaithersburg, Maryland, 150 pp. et al 1982

9. Dobry, R. (1989). "Some Basic Aspects of Soil Liquefaction during Earthquakes", Annals of the New York Academy of Sciences, Vol.. 558

10. Egglezos, D. N., Bouckovalas, G. D. (1998). "Analytical Relationships for Earthquake Induced Pore Pressure in Sand, Clay, and Silt", Proceedings of the Eleventh European Conference on Earthquake Engineering, A.A. Balkema, Rotterdam, 1998

11. Elsabee, F., Morray, J.P. and Roesset, J.M. (1977). "Dynamic Behavior of Embedded Foundations", *Research Report R77-33, MIT*

12. Franklin, A.G. and Chang (1977). "Earthquake Resistance of Earth and Rockhill Dams, Rep. 5: Permanent Displacements of Earth Embakments by Newmark Sliding Block Analysis", *WES, S-71*

13. Gazetas, G. (1983). "Analysis of Machine Foundation Vibrations: State of the Art", Int. Jnl. of Soil Dynamics and Earthquake Engineering, Vol.. 2, pp. 2-42

14. Gazetas, G. (1991a). "Formulas and Charts for Impedances of Surface and Embedded Foundations", *Journal Geotechnical Engineering,* ASCE, Vol.. 117, No. 9, pp. 1363-1381

15. Gazetas, G. (1991b). "Foundation Vibrations", *Foundation Engineering Handbook,* 2nd Edition, Van Nostrand Reinholds, H.Y. Fang, ed., Ch. 15, pp. 553-593

16. Gazetas, G. and Roesset, J.M. (1976). "Forced Vibrations of Strip Footing in Layered Soils", *Method of Structural Analysis*, ASCE, Vol.. 1, pp. 115-131

17. Gazetas, G. and Stokoe, K.H. (1991). "Free Vibration of Embedded Foundations: Theory Versus Experiment", *Journal Geotechnical Engineering,* ASCE, Vol.. 117, No. 9, pp. 1382-1401

18. Hadjian, A.H. and Luco, J.E. (1977). "On the Importance of Layering on Impedance Functions", Proceed., *6th World Conference on Earthquake Engineering*, New Delhi

19. Brinch Hansen, J. (1970). "A revised and Extended Formula for Bearing Capacity", Bulletin No. 28, Danish Geotechnical Institute, Copenhagen

20. Harada, T., Kubo, K. and Katayama, T. (1981). "Dynamic Soil-Structure Interaction by Continuum Formulation Method", *Report No. 190, Institute of Industrial Science,* University of Tokyo

21. Huckelbridge, A.A. and Clough, R.W. (1978). "Seismic Response of Uplifting Building Frames", *Journal Structural Engineering Division,* ASCE, Vol.. 104, No. 8, pp. 1211-1229

22. Hudson, D.E. (1979). "Reading and Interpreting Strong Motion Accelerograms", *Earthquake Engineering Research Institute*, Berkeley, California

23. Jakub, M. and Roesset, J.M. (1977). "Nonlinear Stiffness of Foundations", *Research Report R77-35,* MIT

24. Kausel, E. (1974). Forced Vibrations of Circular Foundations on Layered Media, Research Report R74-11, MIT

25. Kausel, E. and Roesset, J.M. (1975). "Dynamic Stiffness of Circular Foundations", *Journal of the Engineering Mechanic Division, ASCE*, Vol.. 101, pp. 771-785

26. Kausel, E., Roesset, J.M., and Christian, J.T. (1976). "Nonlinear Behavior in Soil-structure Interaction", Journal of Geotechnical Engineering Division, ASCE, Vol.. 102, GT12, pp. 1159-1178

27. Kausel, E. and Roesset, J.M. (1977). "Dynamic Stiffness of Circular Foundations", *Journal Engineering Mechanics Division,* ASCE, Vol.. 101, pp. 771-785

28. Lam, I. & Martin G. (1986). "Seismic Design of Highway Bridge Foundation", *Report FHWA/RD-86/101 to Federal Highway Administration*

29. Luco, J.E. and Westman, R. A. (1971). "Dynamic Response of Circular Footings", Journal of Engineering Mechanic Division, ASCE, 97, EM5, 1381

30. Luco, J.E. (1974). "Impedance Functions of a Rigid Foundation on a Layered Medium", *Nuclear Engineering. and Design*, Vol.. 31, pp. 204-217

31. Lysmer et al, (1975). FLUSH-A Computer Program of Approximate 3-D Analysis of Soil-Structure Interaction Problems, Report No. EERC 75-30, University of California, Berkeley

32. Meek, J.W. (1975). "Effects of Foundation Tipping on Dynamic Response", *Journal Structural Engineering Division,* ASCE, Vol.. 101, No. 7, pp. 1297-1311

33. Meyerhof, G.G. (1963). "Some Recent Research on the Bearing Capacity of Foundations", *Canadian Geotechnical Journal*, Vol.. 1, No. 1, pp. 16-26

34. Michaelides, O. (1993). "Ultimate Load on Foundations under Lateral Static and Seismic Excitation", *Diploma Thesis*, National Technical University of Athens, Greece

35. Mylonakis, G., Nikolaou, A.& Gazetas, G. (1995). "Parametric Results for Seismic Response of Pile Supported Bridge Bents", NCEER-95-0021, National Center for Earthquake Engineering Research, State University of New York, Buffalo

36. Mylonakis, G., Nikolaou, A., and Gazetas, G. (1997): "Soil-Pile-Bridge Seismic Interaction: Kinematic and Inertial Effects. Part I : Soft Soil", *Journal of Earthquake Engineering and Structural Dynamics*, Vol.. 26, pp. 337-359

37. Mylonakis, G. and Gazetas, G. (2000). "Seismic Soil-Structure Interaction: Beneficial or Detrimental?", *Journal of Earthquake Engineering*, Vol. 4, No. 3., pp. 377-401

38. Newmark, N. (1965). "Effects of Earthquakes on Dams and Embankments", *Geotechnique*, Vol.. 15, No. 2, pp. 139-160.

39. Novak, M. (1985). "Experiments with Shallow and Deep Foundations", *Vibration Problems in Geotechnical Engineering*, ASCE, G. Gazetas and E.T. Selig, eds., pp. 1-26

40. Pecker A. et al (1996). "Seismic Bearing Capacity of Shallow Foundations on Soft Soils", Contract CI1-CT92-0069, Final Report, Geodynamic et Structure

41. Pecker, A. (1996). "Seismic Design of Shallow Foundations", Proceedings, 11th World Conference on Earthquake Engineering, Elsevier Science, Disk 4, Paper No. 2076

42. Psycharis, I.N. (1981). "Dynamic Behavior of Rocking Structures Allowed to Uplift", *Report No. EERL 81-82*, Earthquake Engineering Research Laboratory, California Institute of Technology, Pasadena, California

43. Psycharis, I.N. (1983). "Dynamics of Flexible Systems with Partial Lift-Off", *Earthquake Engineering & Structural Dynamics*, Vol.. 11, No. 4, pp. 501-521

44. Roesset, J.M. (1977). "Soil Amplification of Earthquakes", *Numerical Methods in Geotechnical Engineering*, McGraw-Hill, C.S. Desai & J.T. Christian, eds., Ch. 19, pp. 639-682

45. Richards, R. and Elms, D. (1979). "Seismic Behavior of Gravity Retaining Walls", Journal of the Geotechnical Engineering Division, ASCE, Vol.. 105, No. GT4, pp. 449-464

46. Richards, R. Jr., Elms, D.G., & Budhu, M. (1990). "Dynamic Fluidization of Soils", *Journal Geotechnical Engineering Division, ASCE*, Vol.. 116, pp. 740-759

47. Richards, R. Jr., Elms, D.G., & Budhu, M. (1993). "Seismic Bearing Capacity and Settlements of Foundations", *Journal Geotechnical Engineering Division, ASCE*, Vol.. 119, pp. 662-675

48. Sarma, S.K. and Iossifelis, I.S. (1990). "Seismic Bearing Capacity Factors of Shallow Strip Footings", *Geotechnique*, Vol.. 40, No. 2, pp. 265-273

49. Schnabel, P.B., Lysmer, J & Seed,, H. B. (1972). "SHAKE: A Computer Program for Earthquake Response Analysis of Horizontally Layered Sites", Report EERC 72-12, Berkeley: University of California

50. Shi X. and Richards R. (1995). "Seismic Bearing Capacity with Variable Shear Transfer", *Bulletin of the New Zealand National Society for Earthquake Engineering*, Vol.. 28, No. 2, June 1995

51. Stewart, J. P., Seed, R.B., and Fenves, G. L. (1999). "Seismic Soil-Structure Interaction in Buildings. II: Empirical Findings", J. Geotech. Engrg., ASCE, Vol.. 125, No. 1, pp. 38-48

52. Stokoe, K.H. and Richart, F.E. (1974). "Dynamic Response of Embedded Machine Foundations", Journal of the Geotechnical Engineering Division, ASCE, Vol. 100, No. GT-4, pp. 427-447

53. Tassoulas, J.L. (1984). "An Investigation of the Effect of Rigid Sidewalls on the Response of Embedded Circular Foundations to Obliquely-Incident SV and P Waves", *Dynamic Soil-Structure Interaction*, A.A. Balkema, pp. 55-63

54. Tschebotarioff, G. P. (1973). Foundations, Retaining and Earth Structures, 2nd ed. McGraw-Hill, New York, 642 pp.

55. Vesic A.S. (1975). "Bearing Capacity of Shallow Foundations", *Foundation Engineering Handbook,* 1st Edition, Van Nostrand Reinholds, H.Y. Fang, ed., Ch. 3

56. Wolf, J.P. (1985). Dynamic Soil-Structure Interaction, Prentice Hall Inc.

57. Wolf, J.P. (1994). "Simple Physical Models for Foundation Vibrations", Prentice Hall Inc.

58. Wong, H.L. and Luco, J.E. (1985). "Tables of Impedance Functions for Square Foundations on Layered Media", Soil Dynamics & Earthquake Engineering, Vol. 4. pp. 64-81

59. Yim, S. C-S. and Chopra, A.K. (1984a). "Earthquake Response of Structures with Partial Uplift on Winkler Foundation", *Earthquake Engineering & Structural Dynamics*, No. 12, pp. 263-281

60. Yim, S. C-S. and Chopra, A.K. (1984a). "Dynamics of Structures on Two-Spring Foundation Allowed to Uplift", *Journal Engineering Mechanics Division, ASCE*, Vol.. 110, No. 7, pp. 1124-1146

APPENDIX A

ADDITIONAL PARAMETER STUDIES

Deep Profile
H = 93 m
V_{S1} = 80 m/s
Elastic Rock
I_R = 4

Footing
D = 1.5 m
d = 1.5 m
R = 1.5 m

Column
H_c = 6 m
d_c = 1.3 m
E_c = 25 GPa.
β = 5%
m_s = 350 Mgr.
No rotation at
column top
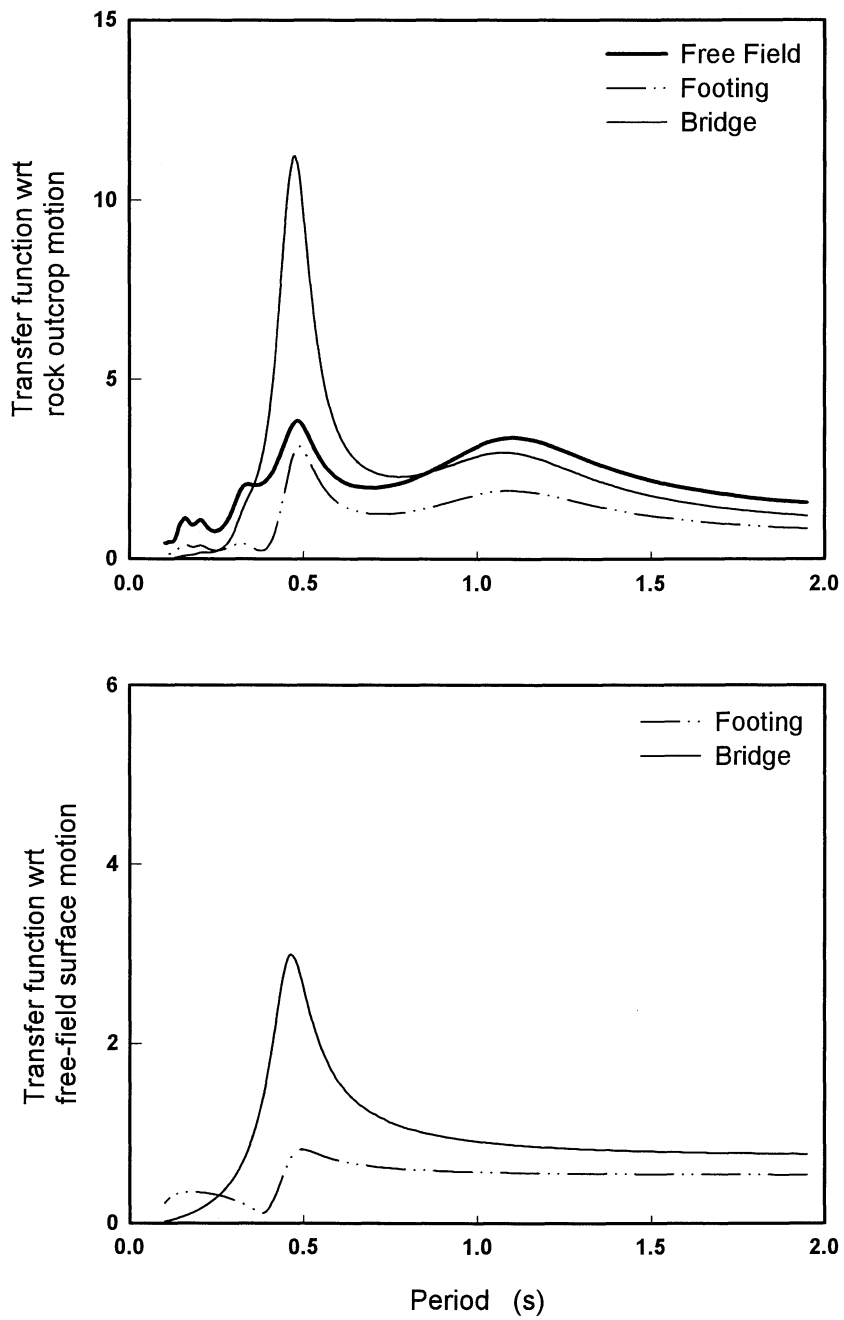
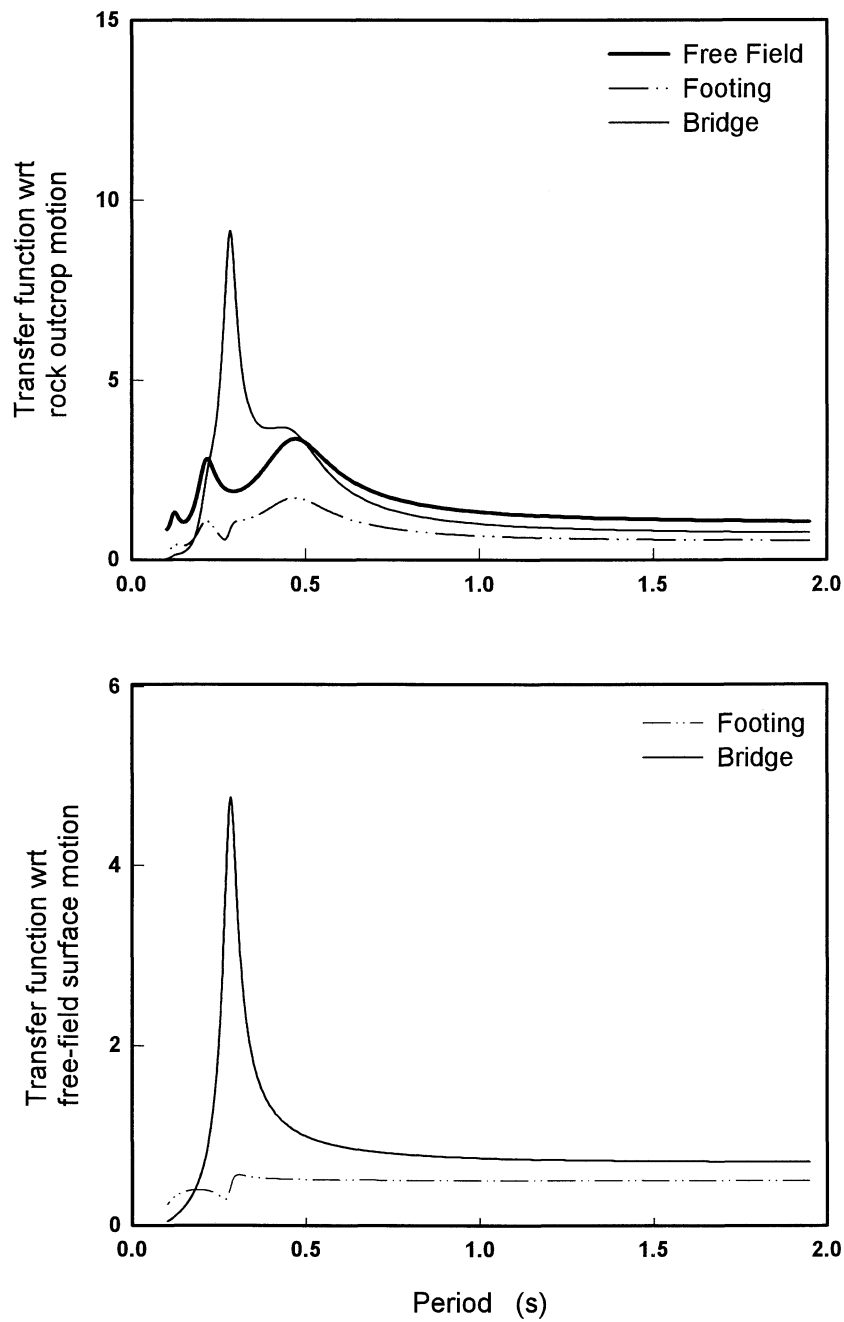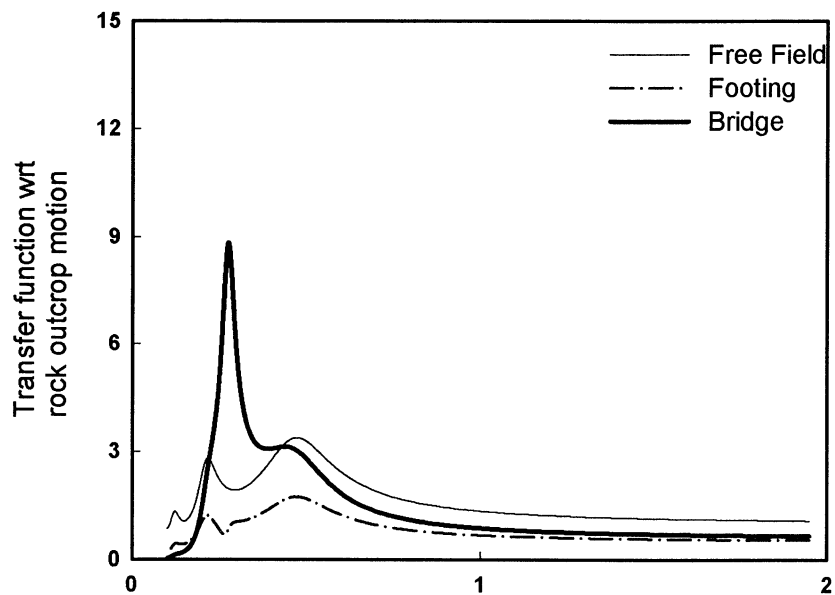**FIGURE A-1 Case A441: Harmonic Steady-State Transfer Functions**

Deep Profile
H = 93 m
V_{S1} = 80 m/s
Elastic Rock
I_R = 4

Footing
D = 1.5 m
d = 1.5 m
R = 3.0 m

Column
H_c = 6 m
d_c = 1.3 m
E_c = 25 GPa
β = 5%
m_s = 350 Mg
No rotation at column top
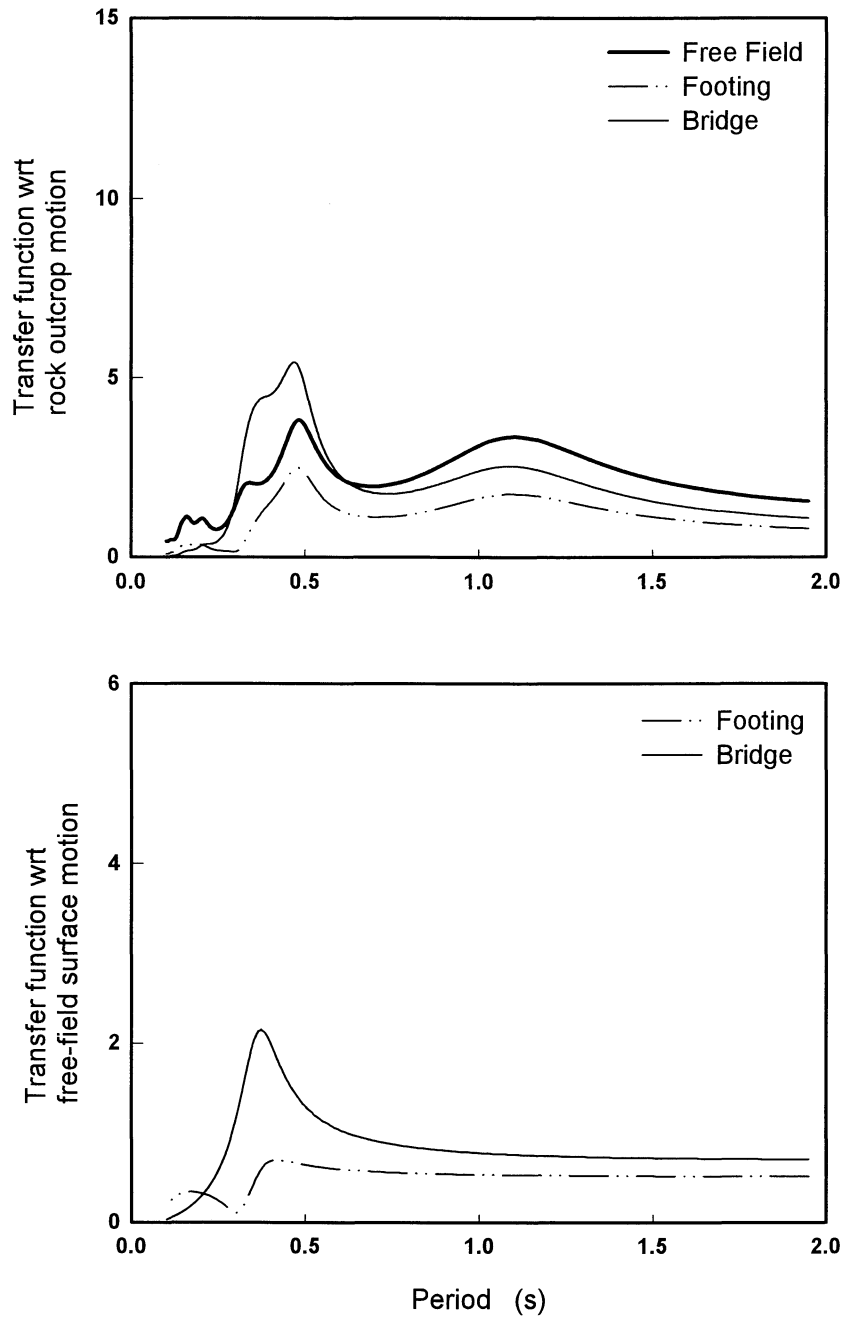
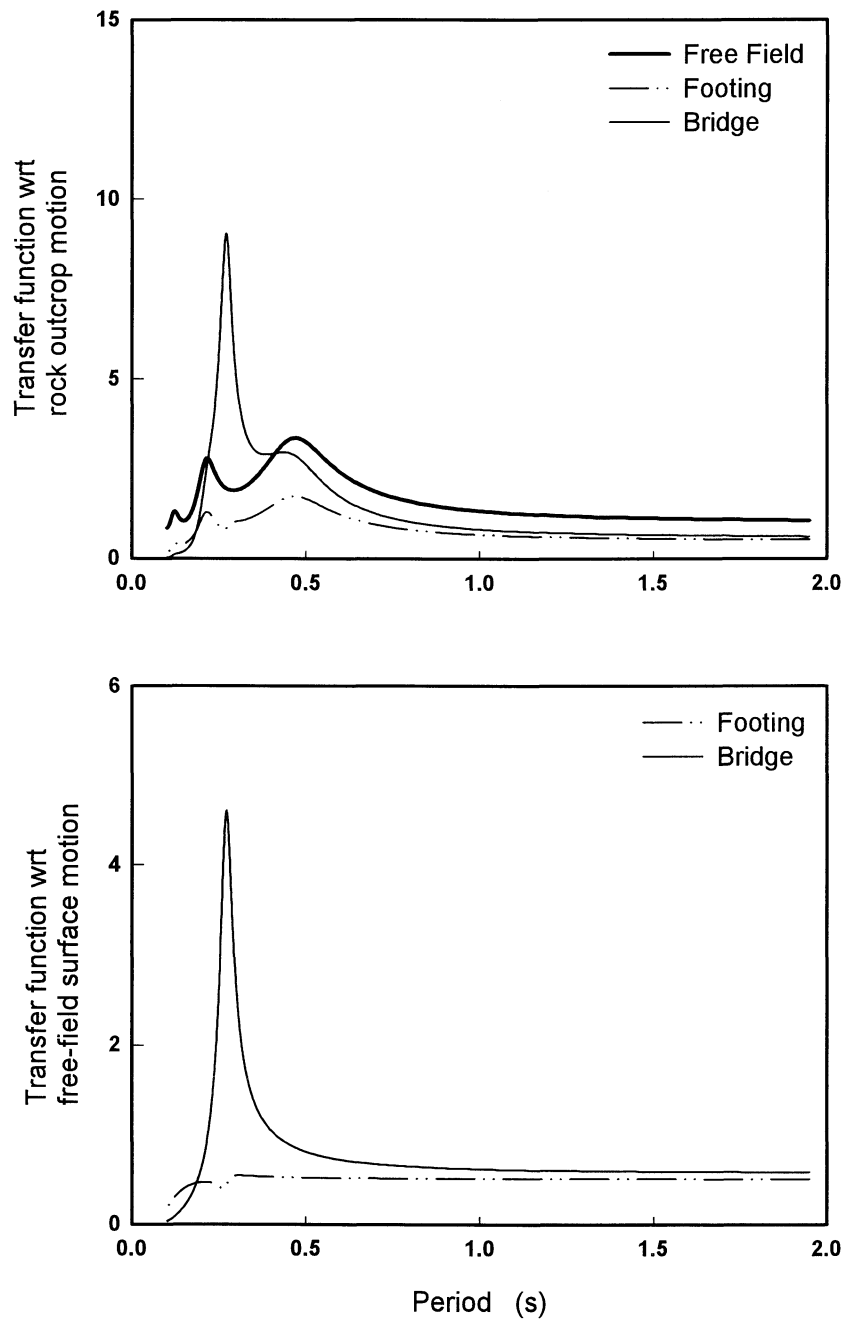**FIGURE A-2 Case A442: Harmonic Steady-State Transfer Functions**

Deep Profile
H = 93 m
V_{S1} = 80 m/s
Elastic Rock
I_R = 4

Footing
D = 1.5 m
d = 1.5 m
R = 4.5 m

Column
H_c = 6 m
d_c = 1.3 m
E_c = 25 GPa
β = 5%
m_s = 350 Mg
No rotation at
column top
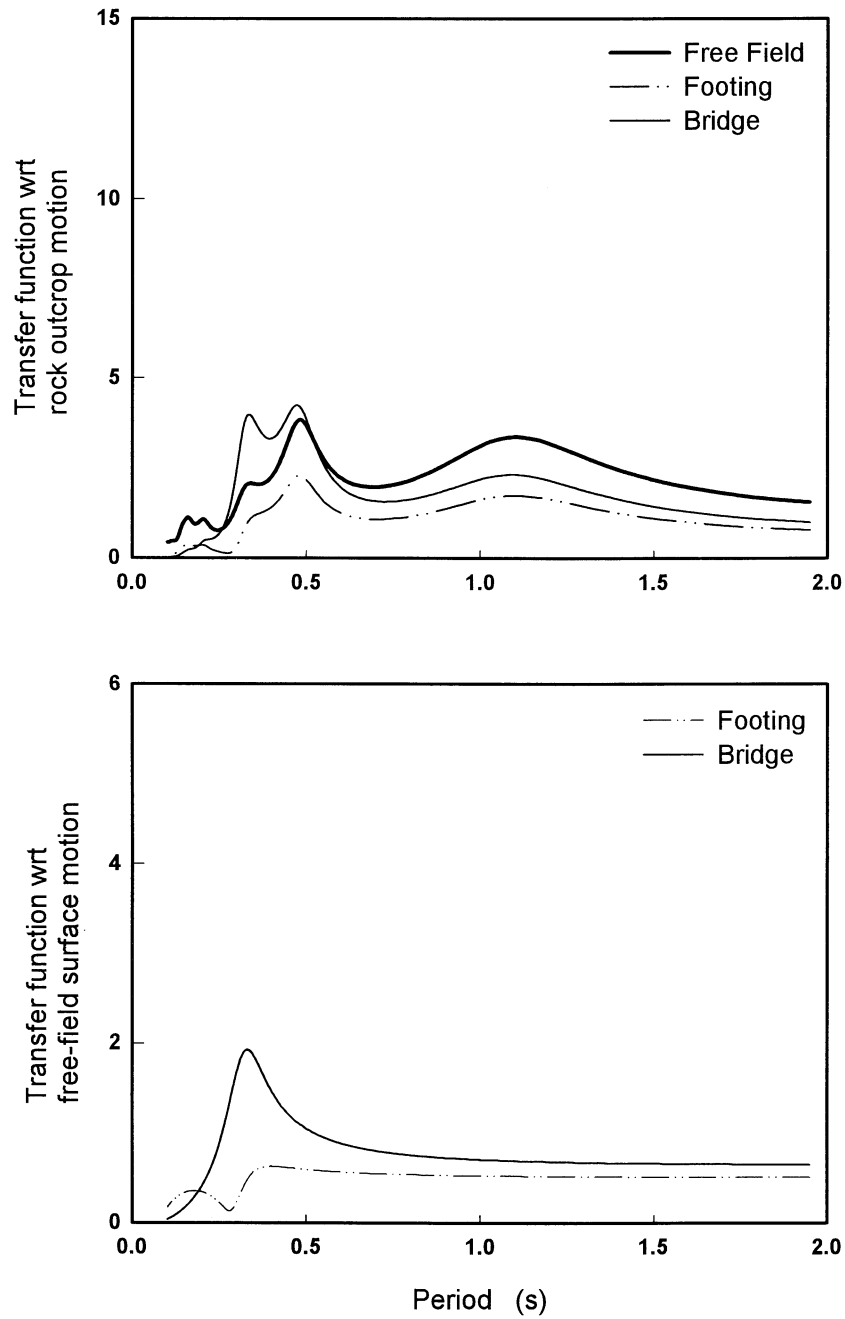
FIGURE A-3 Case A443: Harmonic Steady-State Transfer Functions
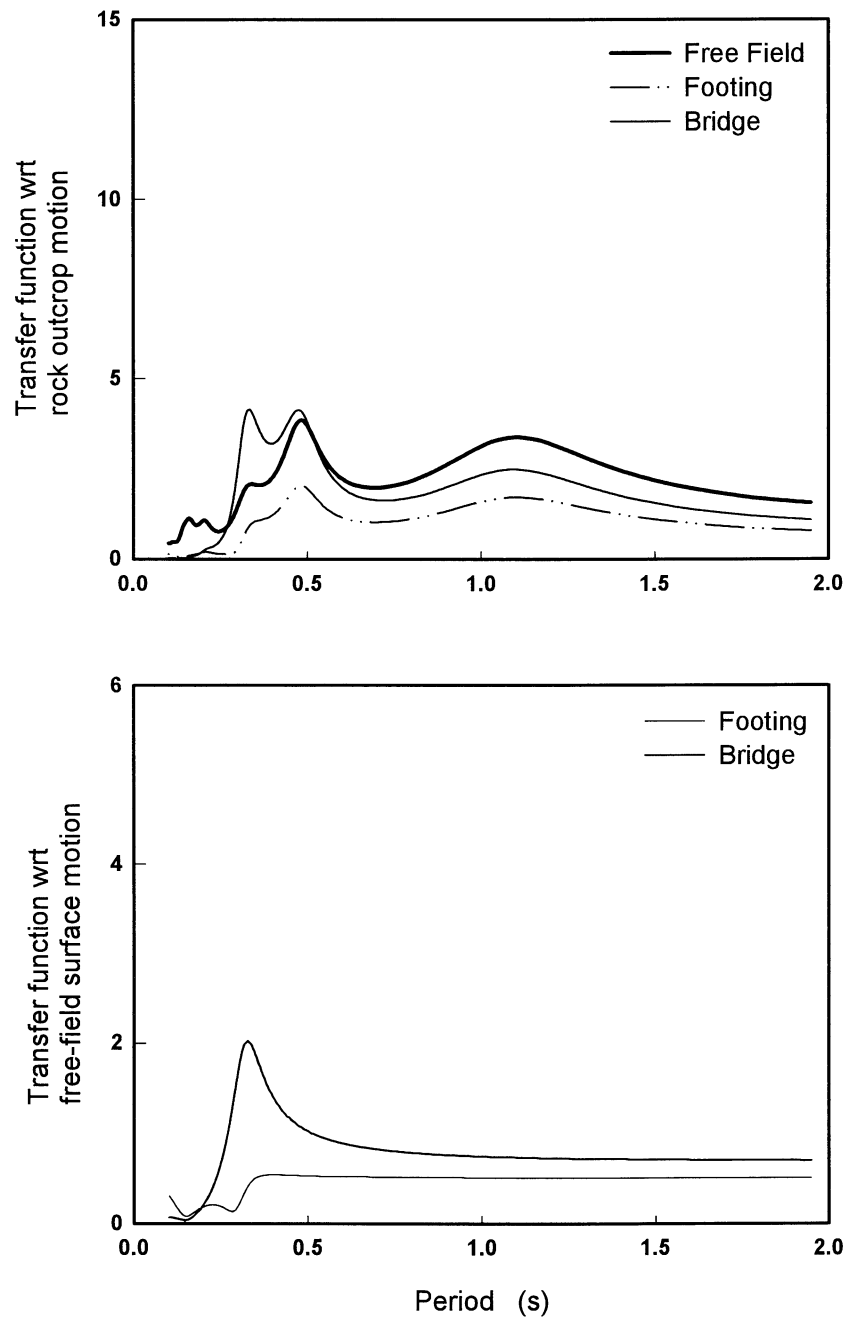
Deep Profile
H = 93 m
V_{S1} = 80 m/s
Elastic Rock
I_R = 4

Footing
D = 3.0 m
d = 3.0 m
R = 3.0 m

Column
H_c = 6 m
d_c = 1.3 m
E_c = 25 GPa
β = 5%
m_s = 350 Mg
No rotation at
column top

FIGURE A-4 Case A421: Harmonic Steady-State Transfer Functions

Deep Profile
H = 93 m
V_{S1} = 80 m/s
Elastic Rock
I_R = 4

Footing
D = 3.0 m
d = 3 m
R = 6.0 m

Column
H_c = 6 m
d_c = 1.3 m
E_c = 25 GPa
β = 5%
m_s = 350 Mg
No rotation at
column top
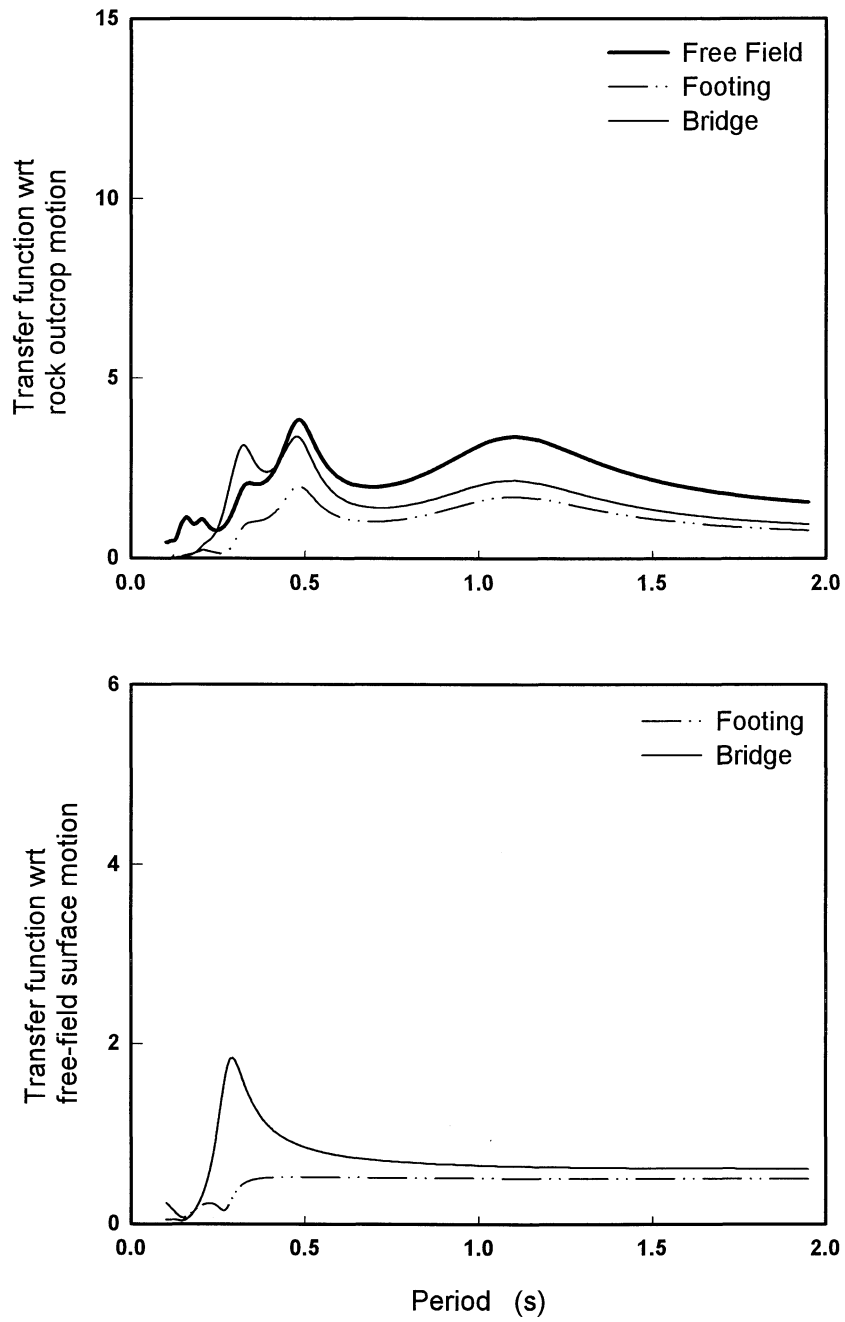
FIGURE A-5 Case A422: Harmonic Steady-State Transfer Functions
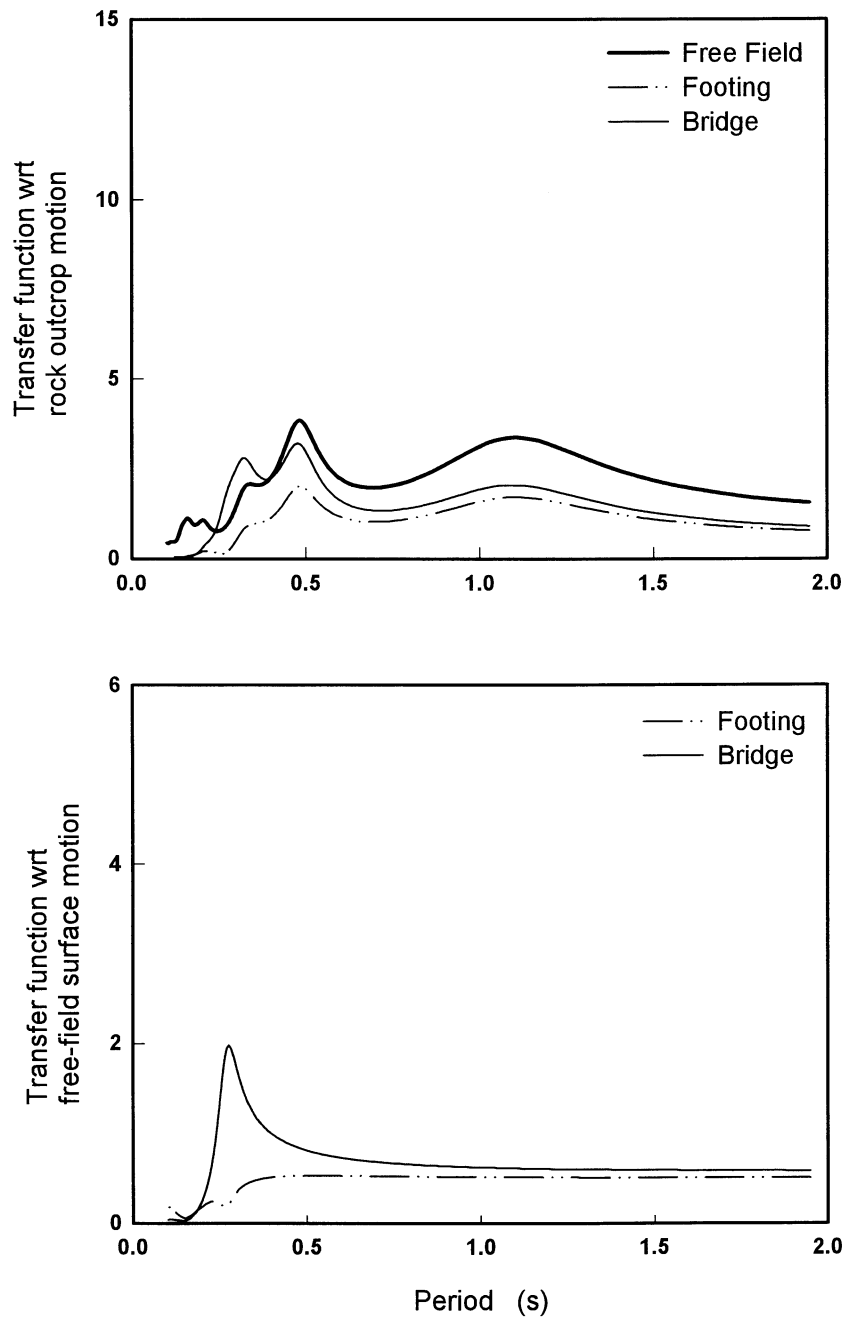
Deep Profile
H = 93 m
V_{S1} = 80 m/s
Elastic Rock
I_R = 4

Footing
D = 3.0 m
d = 3.0 m
R = 9.0 m

Column
H_c = 6 m
d_c = 1.3 m
E_c = 25 GPa
β = 5%
m_s = 350 Mg
No rotation at
column top

FIGURE A-6 Case A423: Harmonic Steady-State Transfer Functions
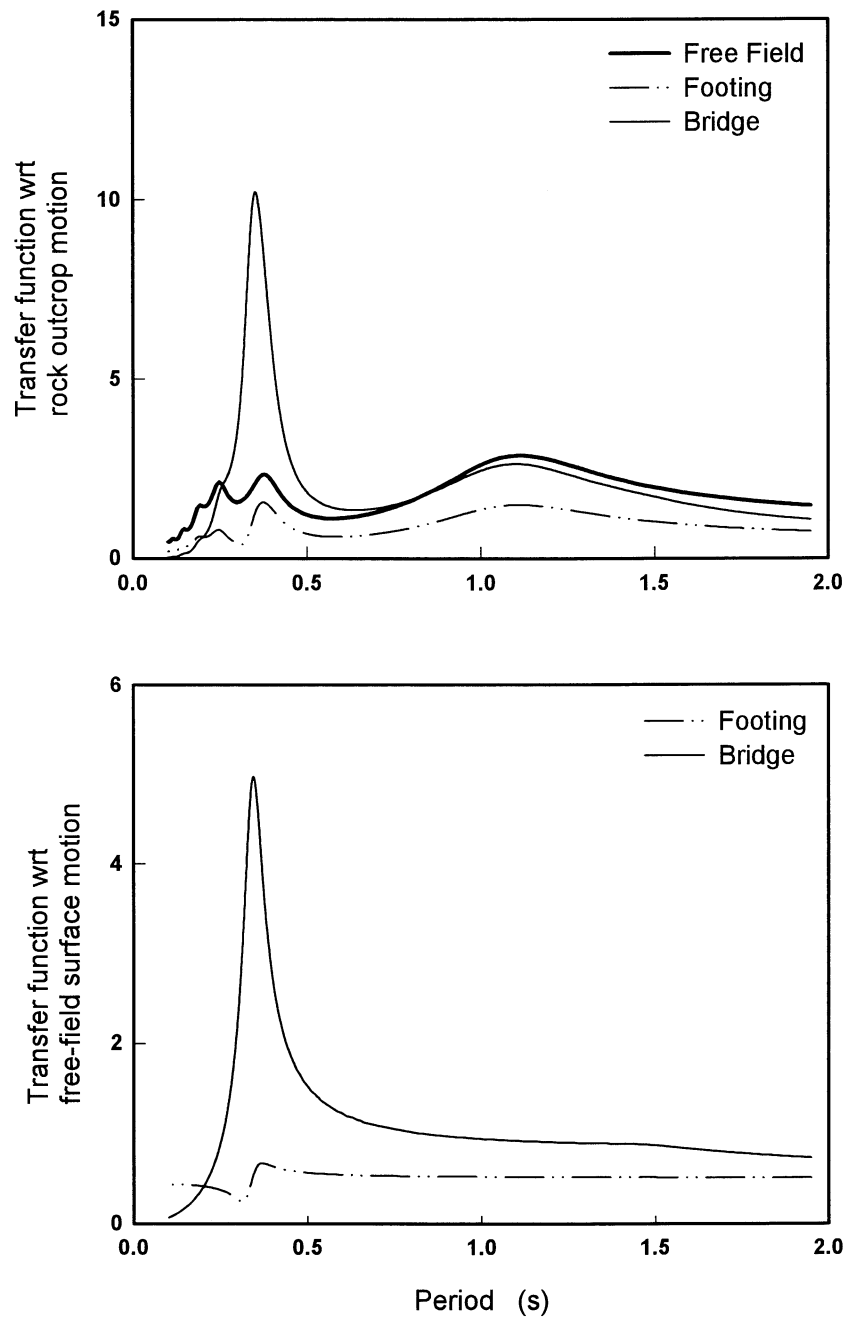
FIGURE A-7 Case A241: Harmonic Steady-State Transfer Functions

The chart shows two plots and a parameter box:

Upper plot — y-axis: "Transfer function wrt rock outcrop motion" (0 to 15), x-axis: Period (0.0 to 2.0). Legend: Free Field, Footing, Bridge.

Lower plot — y-axis: "Transfer function wrt free-field surface motion" (0 to 6), x-axis: Period (0.0 to 2.0). Legend: Footing, Bridge. x-axis label: Period (s).

Parameter box:

Deep Profile
H = 93 m
V_{S1} = 160 m/s
Elastic Rock
I_R =4

Footing
D = 1.5 m
d = 4.0 m
R = 3.0 m

Column
H_c = 6 m
d_c = 1.3 m
E_c = 25 GPa.
β = 5%
m_s = 350 Mgr.
No rotation at
column top

FIGURE A-8 Case A242: Harmonic Steady-State Transfer Functions

107

Left axis (top chart): Transfer function wrt rock outcrop motion

Legend (top chart): Free Field, Footing, Bridge

Left axis (bottom chart): Transfer function wrt free-field surface motion

Legend (bottom chart): Footing, Bridge

X-axis: Period (s)

Side box:

Deep Profile
H = 93 m
V_{S1} = 160 m/s
Elastic Rock
I_R = 4

Footing
D = 1.5 m
d = 1.5 m
R = 4.5 m

Column
H_c = 6 m
d_c = 1.3 m
E_c = 25 GPa
β = 5%
m_s = 350 Mg
No rotation at
column top
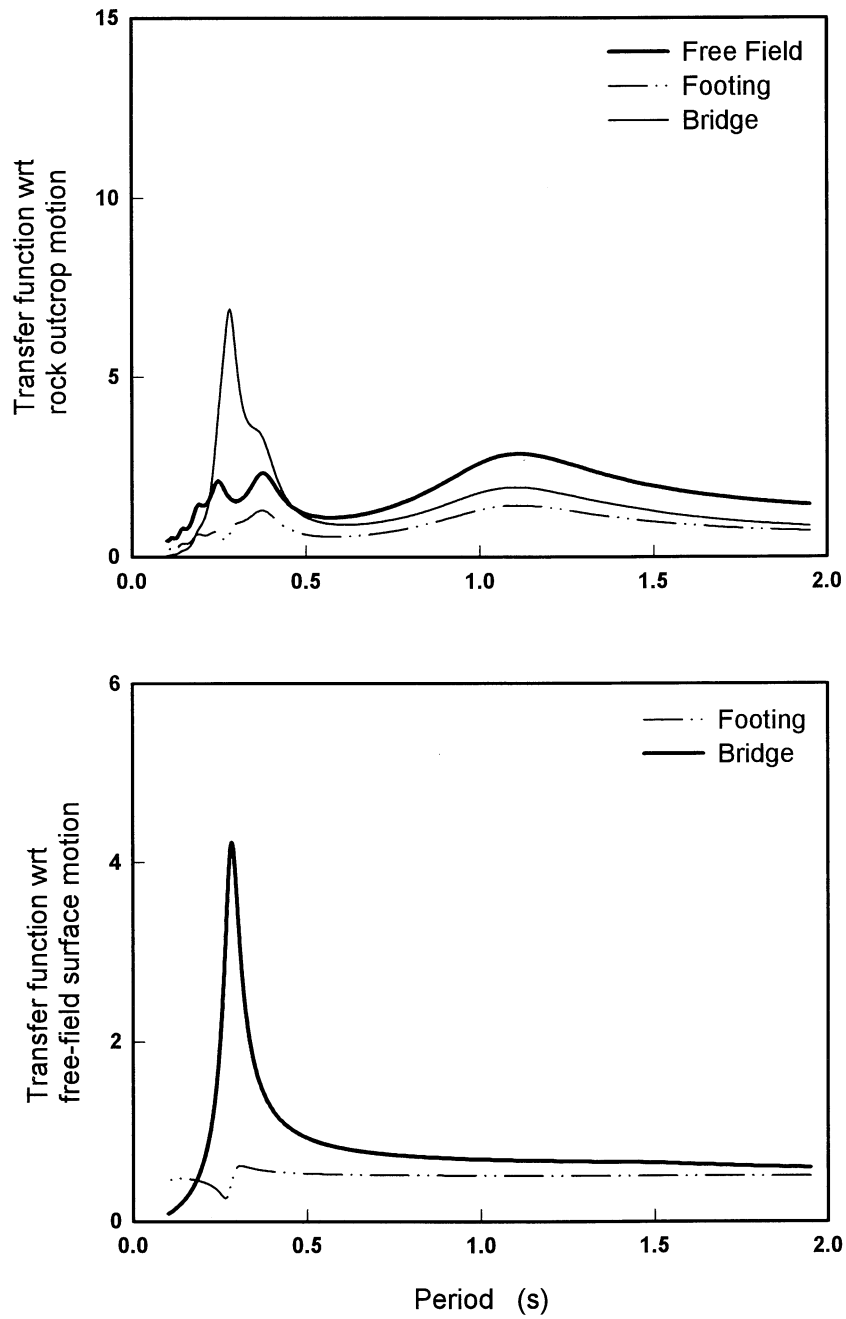
FIGURE A-9 Case A243: Harmonic Steady-State Transfer Functions

108
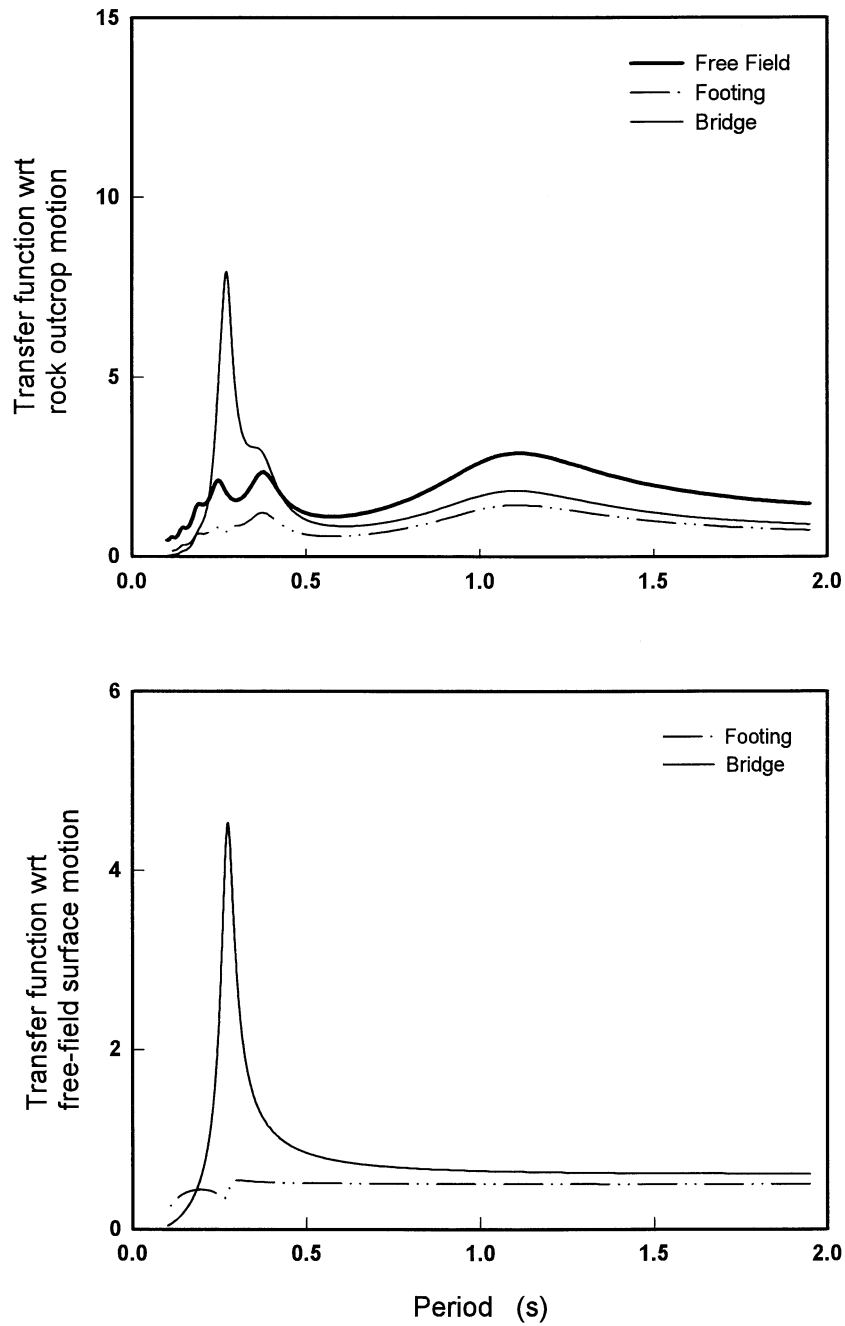
Deep Profile
H = 93 m
V_{S1} = 160 m/s
Elastic Rock
I_R = 4

Footing
D = 3 m
d = 3 m
R = 3 m

Column
H_c = 6 m
d_c = 1.3 m
E_c = 25 GPa
β = 5%
m_s = 350 Mg
No rotation at
column top

FIGURE A-10 Case A221: Harmonic Steady-State Transfer Functions

The chart shows two transfer function plots.

Top plot: Transfer function wrt rock outcrop motion (y-axis, 0 to 15) vs Period (s). Legend: Free Field, Footing, Bridge.

Bottom plot: Transfer function wrt free-field surface motion (y-axis, 0 to 6) vs Period (s), 0.0 to 2.0. Legend: Footing, Bridge.

Side box:

Deep Profile
H = 93 m
V_{S1} = 160 m/s
Elastic Rock
I_R = 4

Footing
D = 3.0 m
d = 3.0 m
R = 6.0 m

Column
H_c = 6 m
d_c = 1.3 m
E_c = 25 GPa
β = 5%
m_s = 350 Mg
No rotation at
column top

FIGURE A-11 Case A222: Harmonic Steady-State Transfer Functions
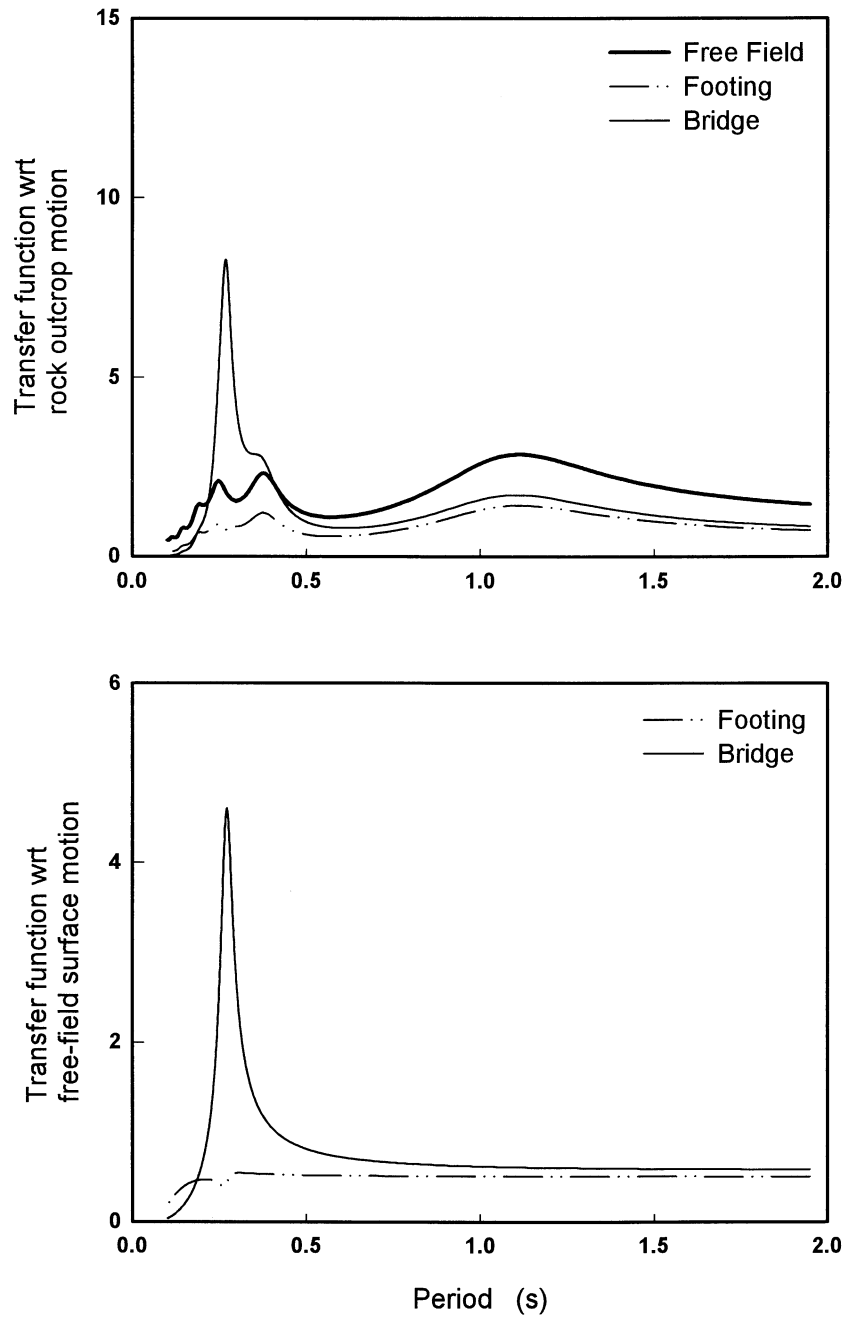
FIGURE A-12 Case A223: Harmonic Steady-State Transfer Functions
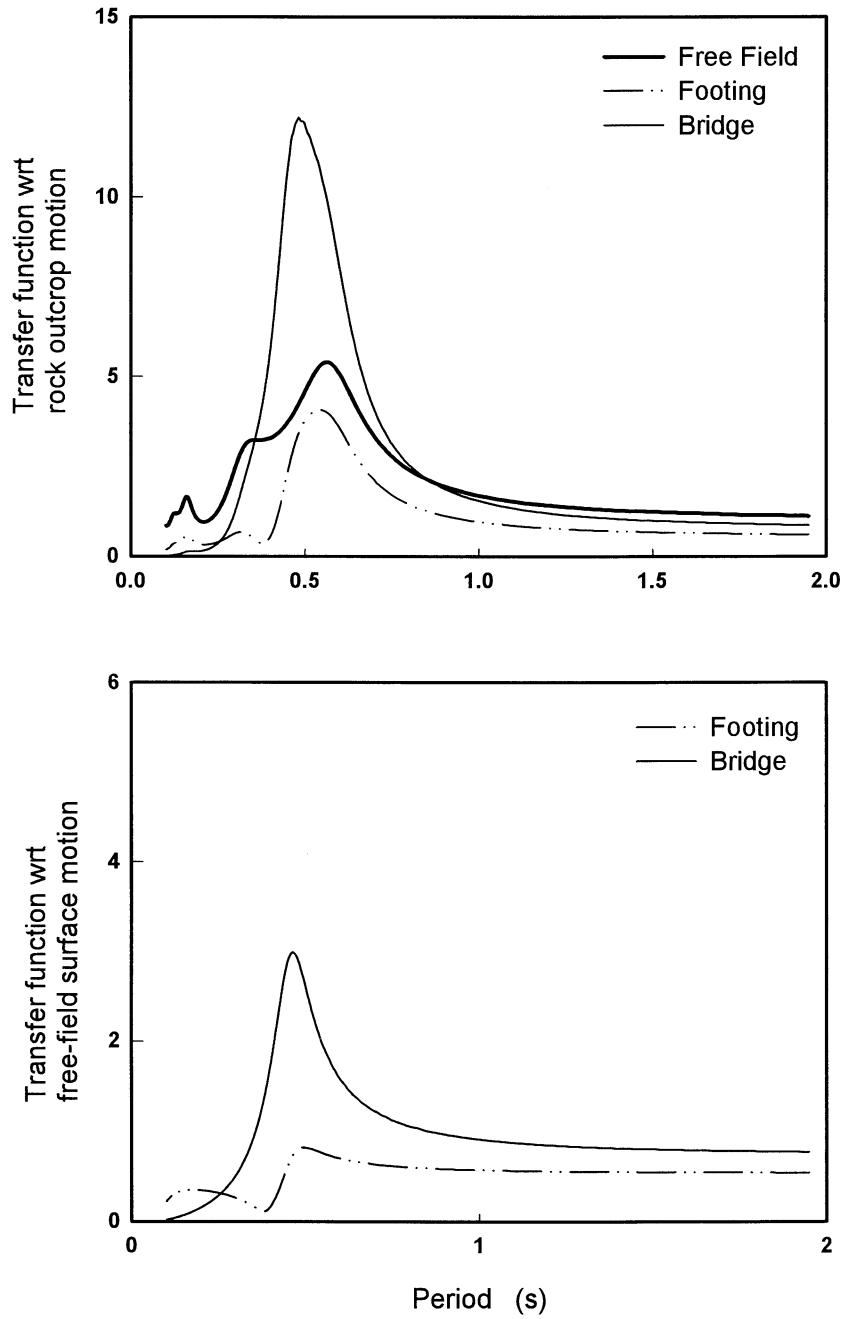
FIGURE A-13 Case B441: Harmonic Steady-State Transfer Functions

Shallow Profile
H = 39.5 m
V_{S1} = 80 m/s
Elastic Rock
I_R = 4

Footing
D = 1.5 m
d = 1.5 m
R = 3.0 m

Column
H_c = 6 m
d_c = 1.3 m
E_c = 25 GPa
β = 5%
m_s = 350 Mg
No rotation at
column top
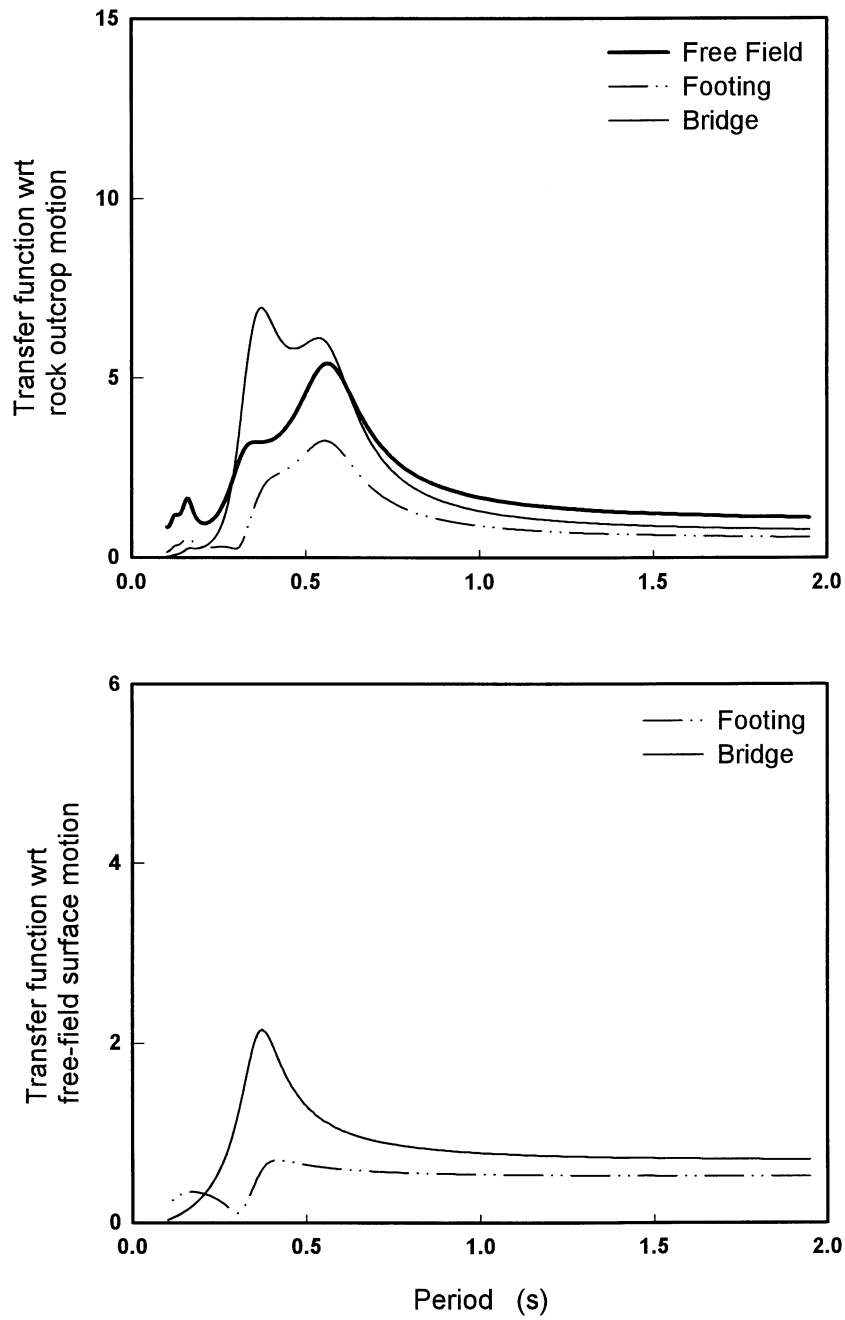
FIGURE A-14 Case B442: Harmonic Steady-State Transfer Functions
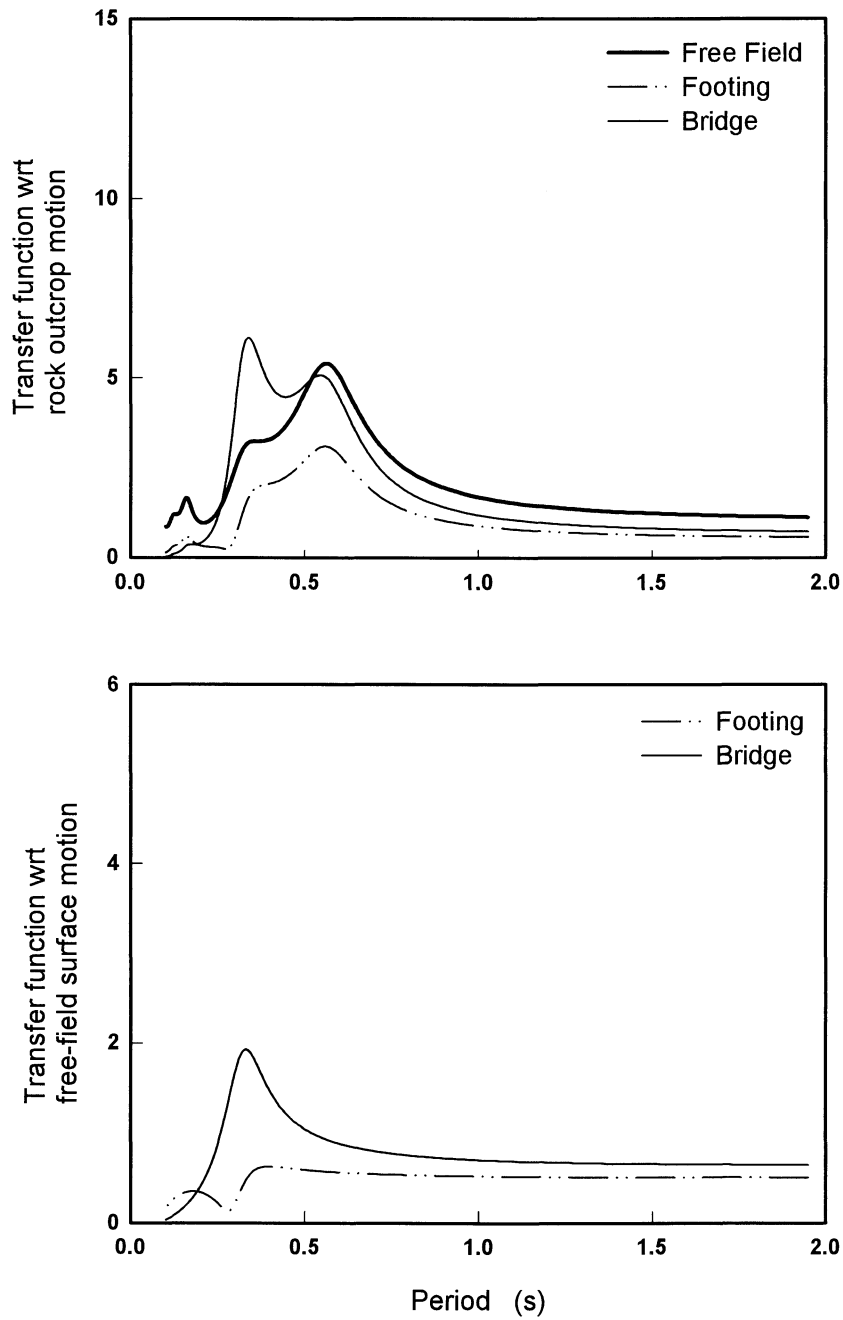
FIGURE A-15 Case B443: Harmonic Steady-State Transfer Functions

Shallow Profile
H = 39.5 m
V_{S1} = 80 m/s
Elastic Rock
I_R = 4

Footing
D = 3.0 m
d = 3.0 m
R = 3.0 m

Column
H_c = 6 m
d_c = 1.3 m
E_c = 25 GPa
β = 5%
m_s = 350 Mg
No rotation at
column top
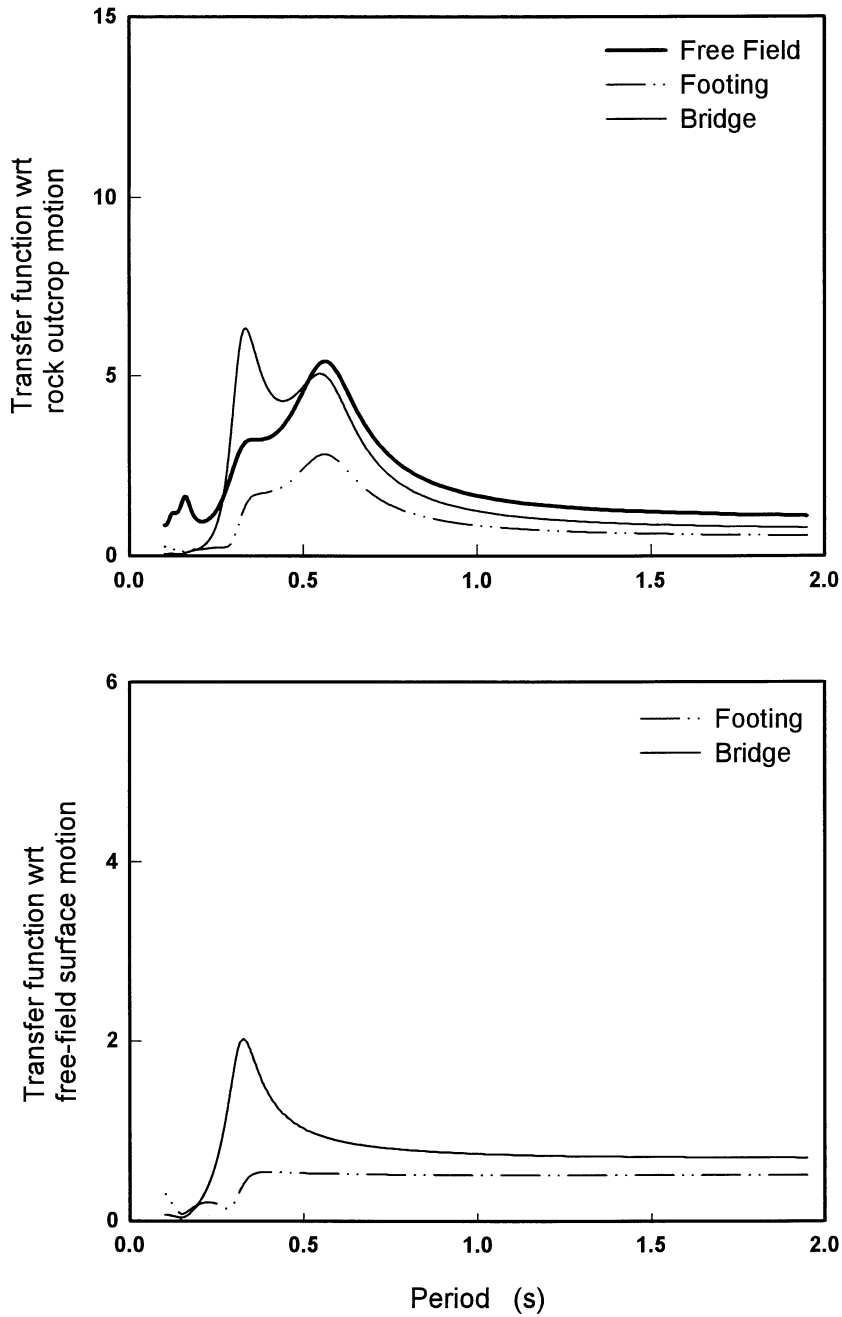
FIGURE A-16 Case B421: Harmonic Steady-State Transfer Functions

Shallow Profile
H = 39.5 m
V_{S1} = 80 m/s
Elastic Rock
I_R = 4

Footing
D = 3.0 m
d = 3.0 m
R = 6.0 m

Column
H_c = 6 m
d_c = 1.3 m
E_c = 25 GPa.
β = 5%
m_s = 350 Mgr.
No rotation at
column top
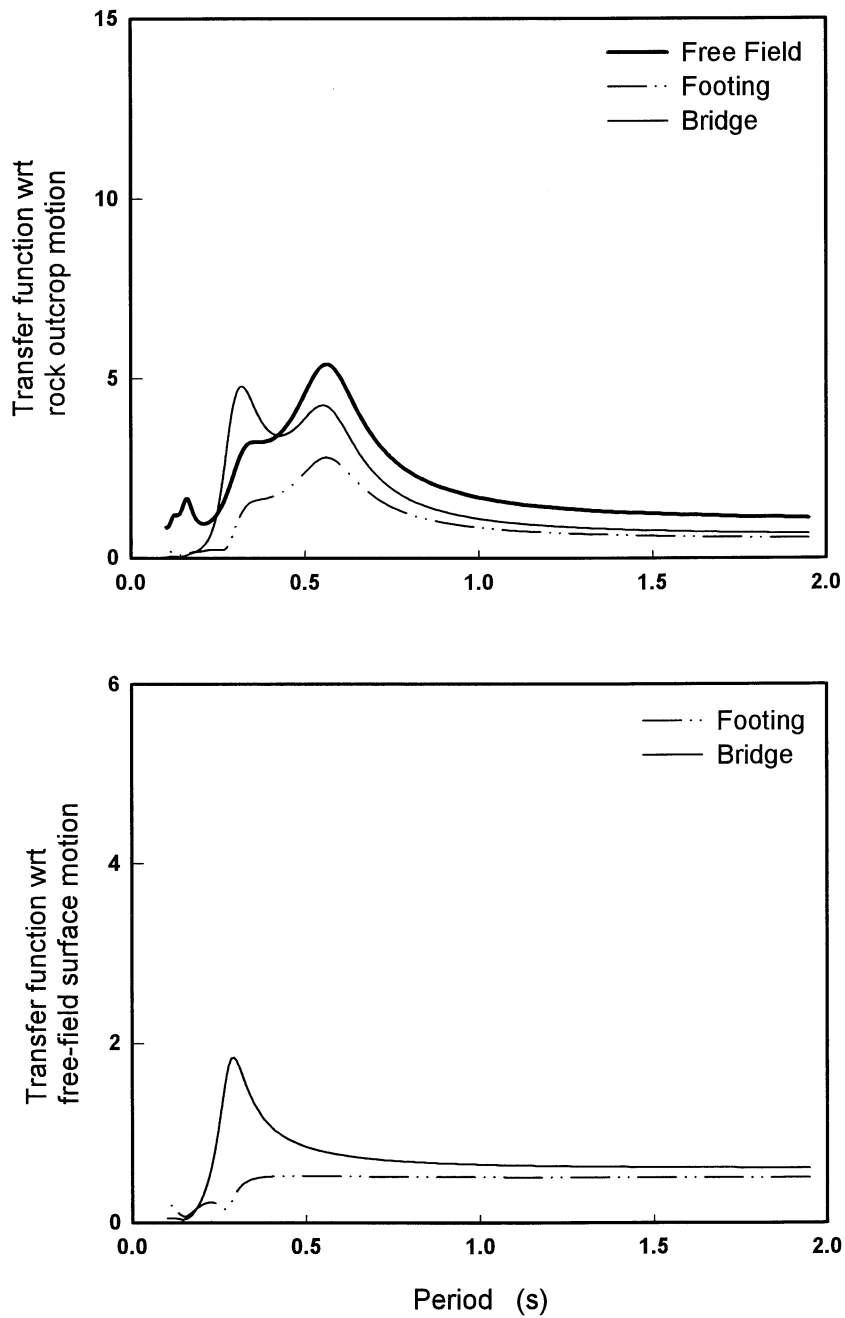
FIGURE A-17 Case B422: Harmonic Steady-State Transfer Functions
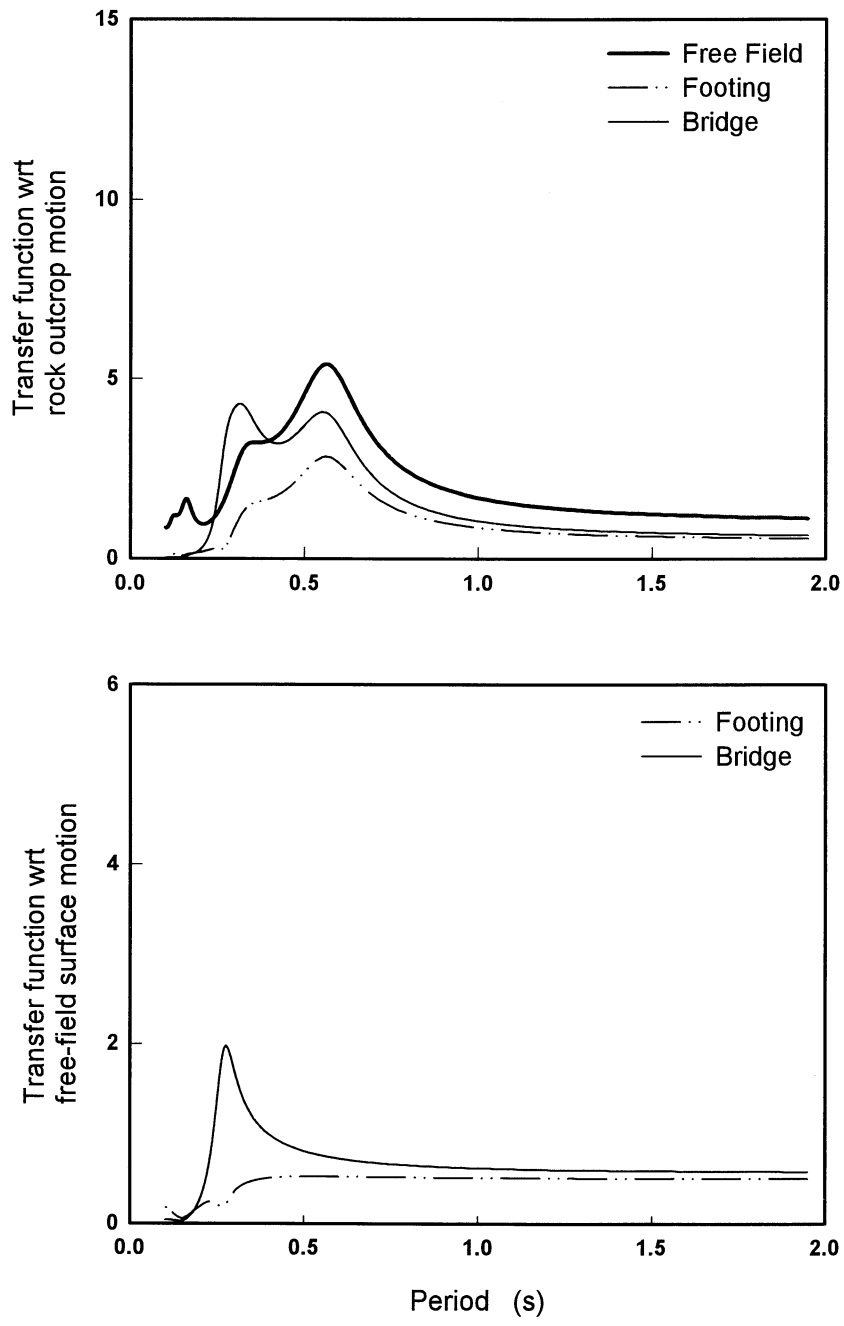
FIGURE A-18 Case B423: Harmonic Steady-State Transfer Functions

Shallow Profile
H = 39.5 m
V_{S1} = 160 m/s
Elastic Rock
I_R = 4

Footing
D = 1.5 m
d = 1.5 m
R = 1.5 m

Column
H_c = 6 m
d_c = 1.3 m
E_c = 25 GPa
β = 5%
m_s = 350 Mg
No rotation at
column top
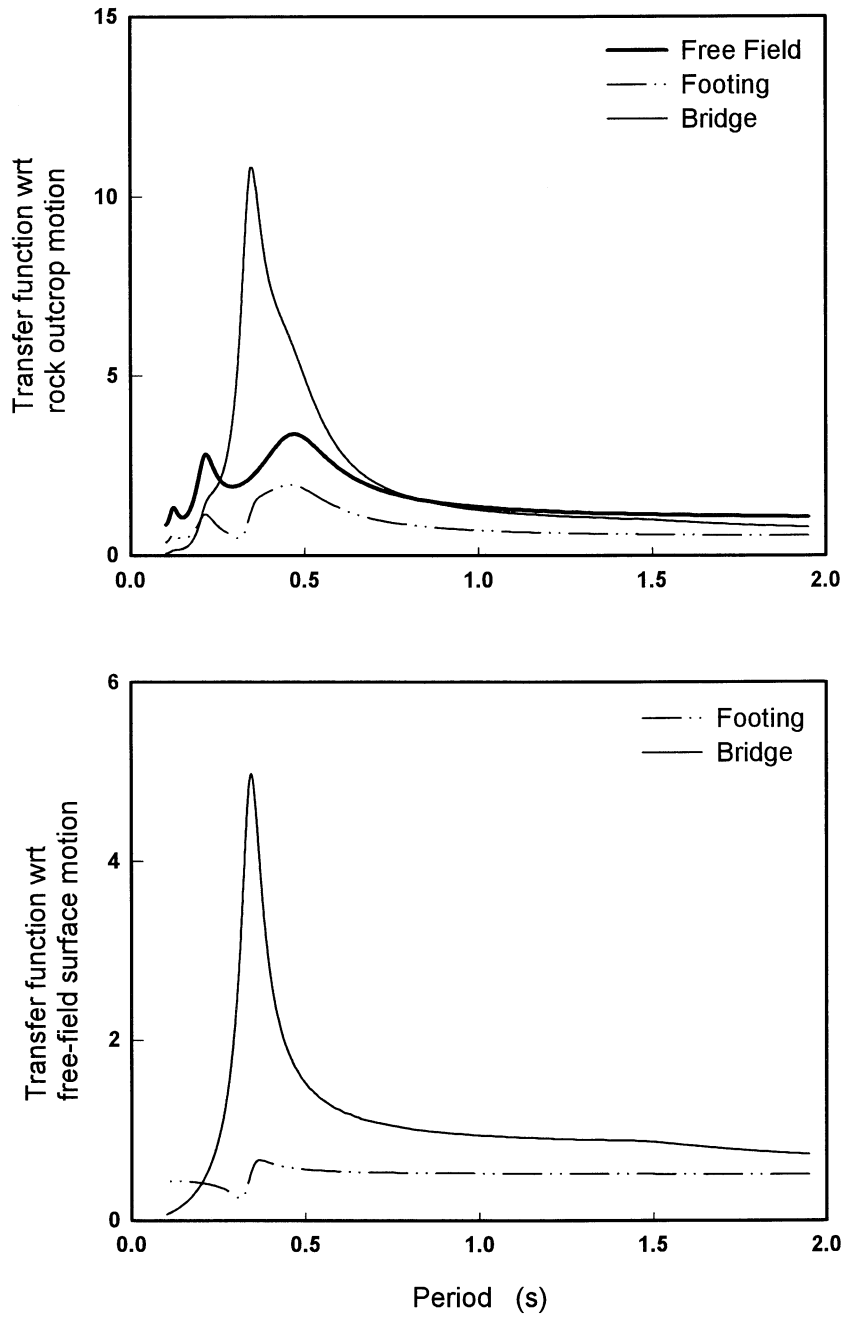
FIGURE A-19 Case B241: Harmonic Steady-State Transfer Functions
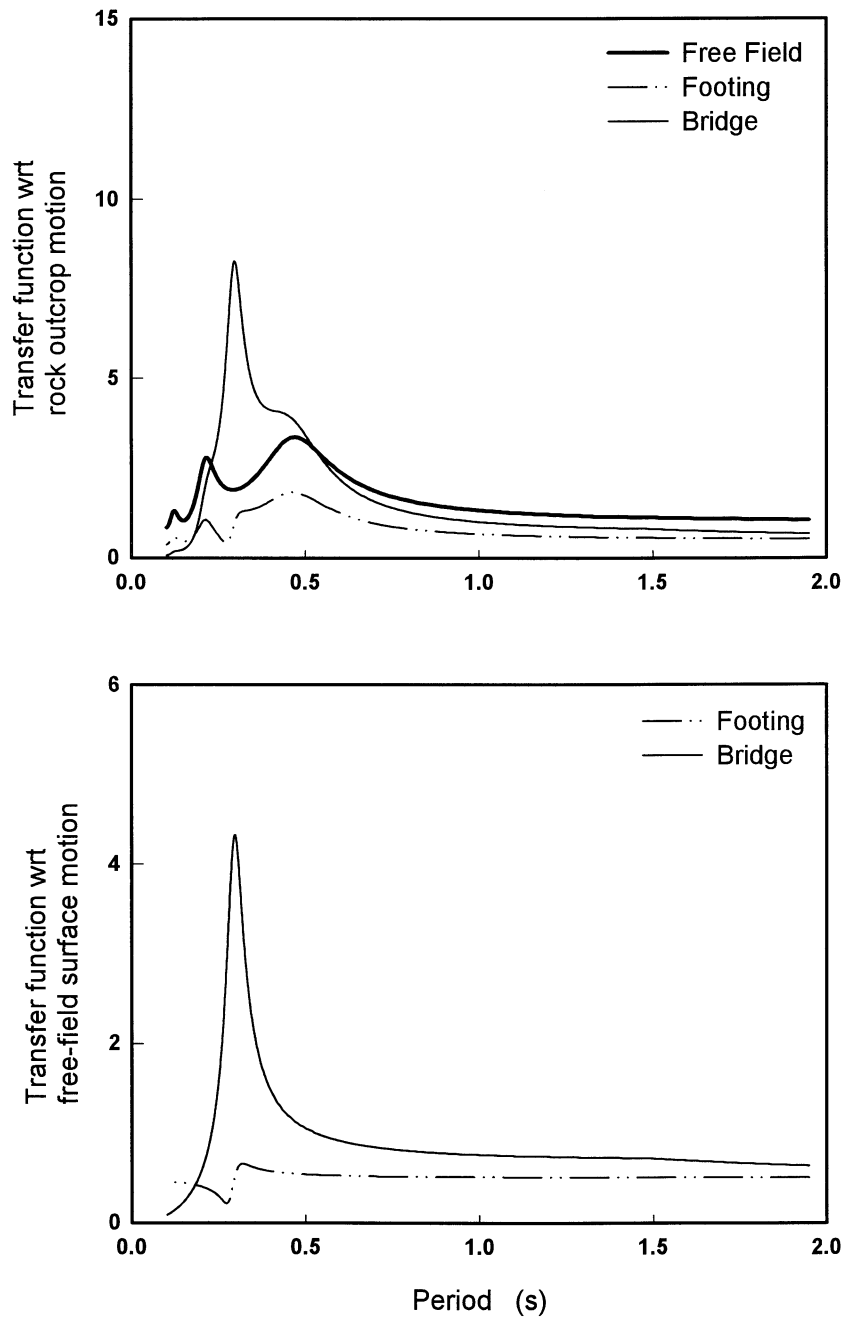
Shallow Profile
H = 39.5 m
V_{S1} = 160 m/s
Elastic Rock
I_R = 4

Footing
D = 1.5 m
d = 1.5 m
R = 3.0 m

Column
H_c = 6 m
d_c = 1.3 m
E_c = 25 GPa
β = 5%
m_s = 350 Mg
No rotation at
column top

FIGURE A-20 Case B242: Harmonic Steady-State Transfer Functions
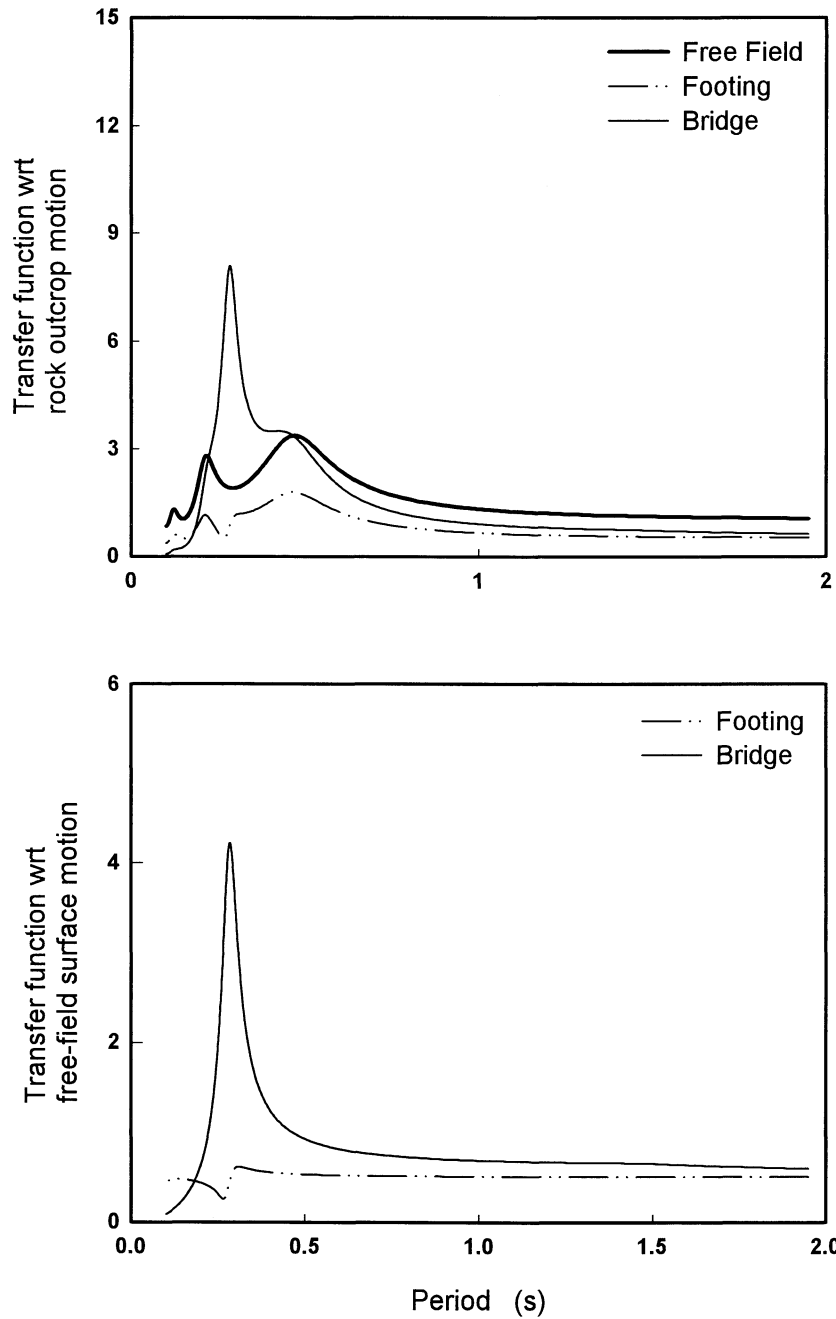
FIGURE A-21 Case B243: Harmonic Steady-State Transfer Functions

Shallow Profile
H = 39.5 m
V_{S1} = 160 m/s
Elastic Rock
I_R = 4

Footing
D = 3.0 m
d = 3.0 m
R = 3.0 m

Column
H_c = 6 m
d_c = 1.3 m
E_c = 25 GPa
β = 5%
m_s = 350 Mg
No rotation at
column top

FIGURE A-22 Case B221: Harmonic Steady-State Transfer Functions

Shallow Profile
H = 39.5 m
$V_{S1} = V_{S2}$ = 160 m/s
Elastic Rock

Footing
D = 3.0 m
R = 6.0 m

Column
H = 6 m
d = 1.3 m
E = 25 GPa.
β = 5%
m = 350 Mgr.
No rotation at
column top
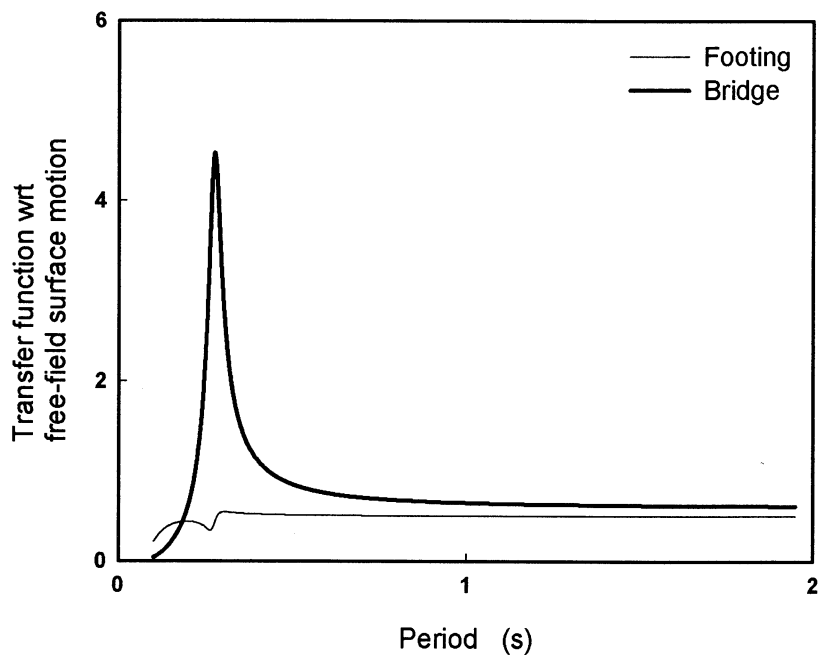
FIGURE A1-23 Case B222: Harmonic Steady-State Transfer Functions

Shallow Profile
H = 39.5 m
V_{S1} = 160 m/s
Elastic Rock
I_R = 4

Footing
D = 3.0 m
d = 3.0 m
R = 9.0 m

Column
H_c = 6 m
d_c = 1.3 m
E_c = 25 GPa
β = 5%
m_s = 350 Mg
No rotation at
column top

FIGURE A-24 Case B223: Harmonic Steady-State Transfer Functions
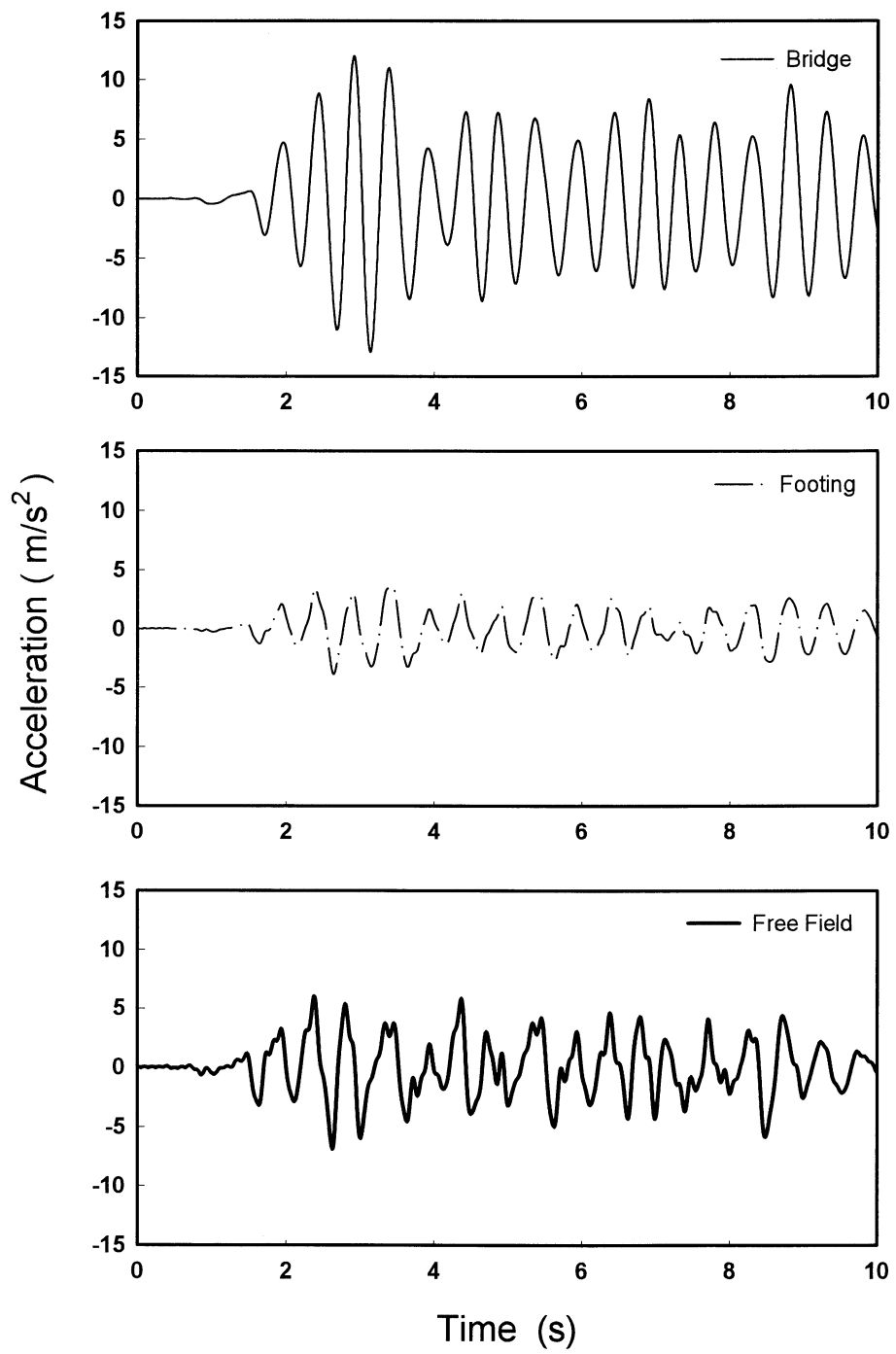
FIGURE A-25 Case A441: Acceleration histories for 0.4g artificial excitation
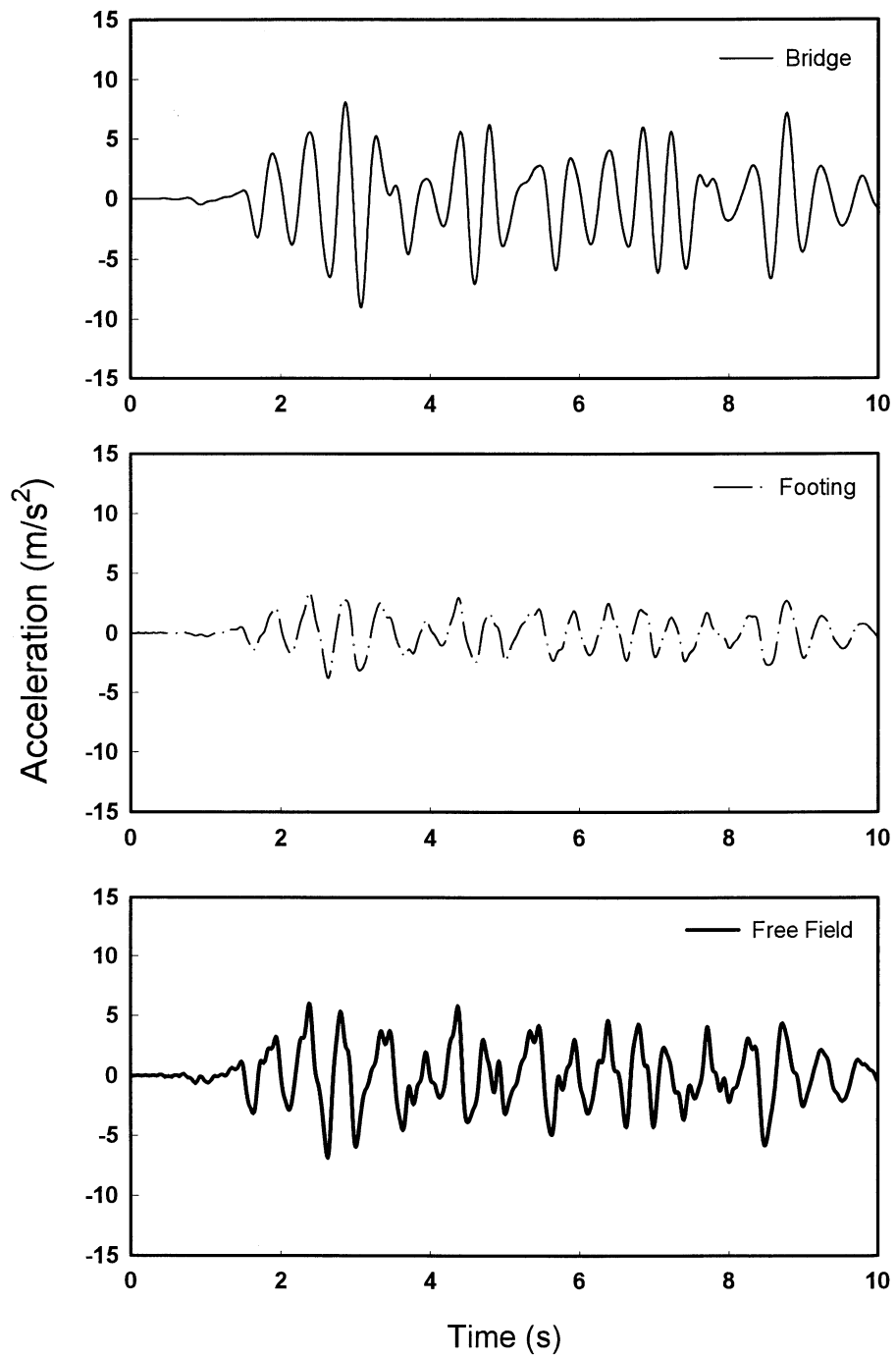
FIGURE A-26 Case A442: Acceleration histories for 0.4g artificial excitation
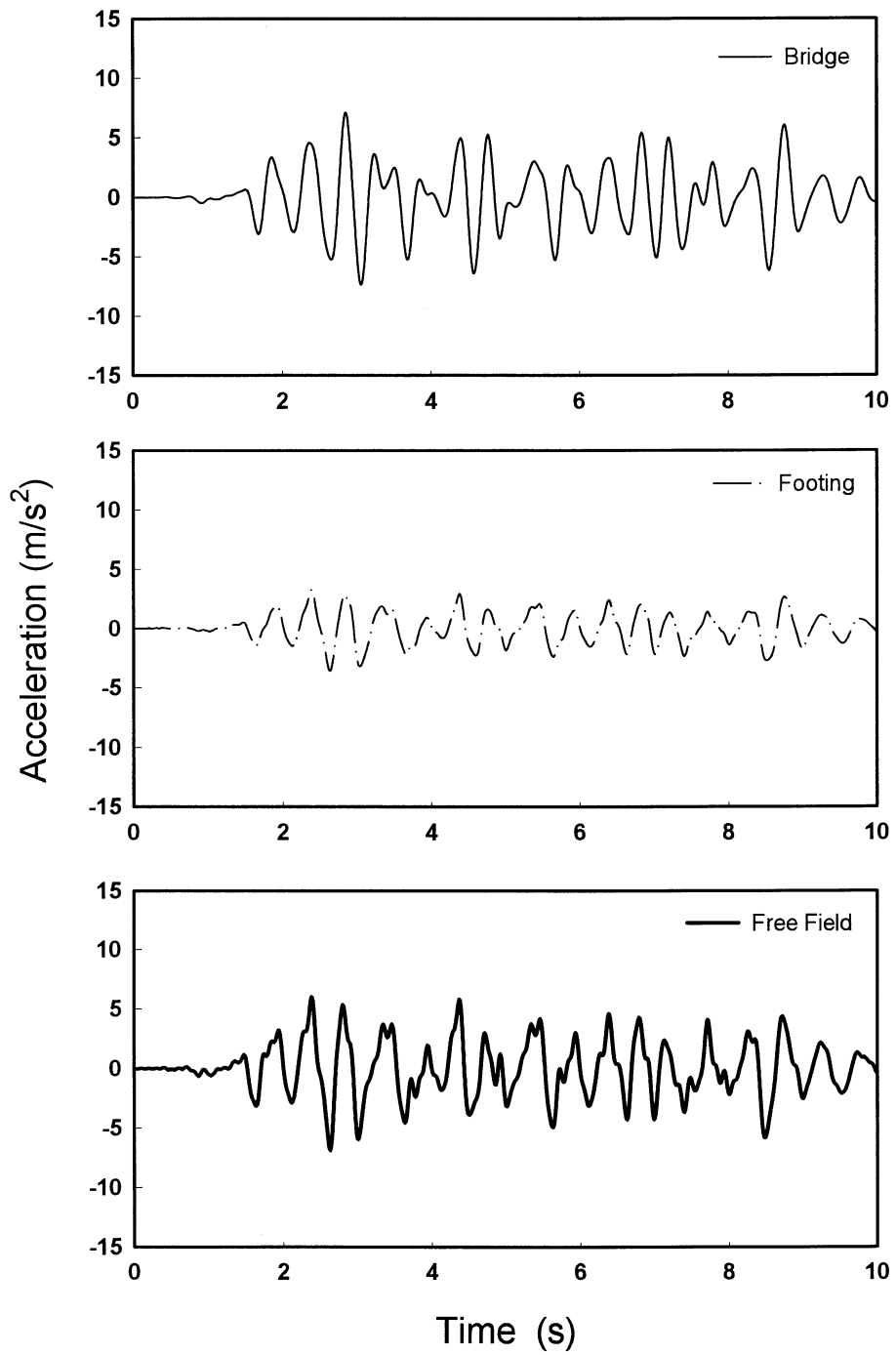
FIGURE A-27 Case A443: Acceleration histories for 0.4g artificial excitation
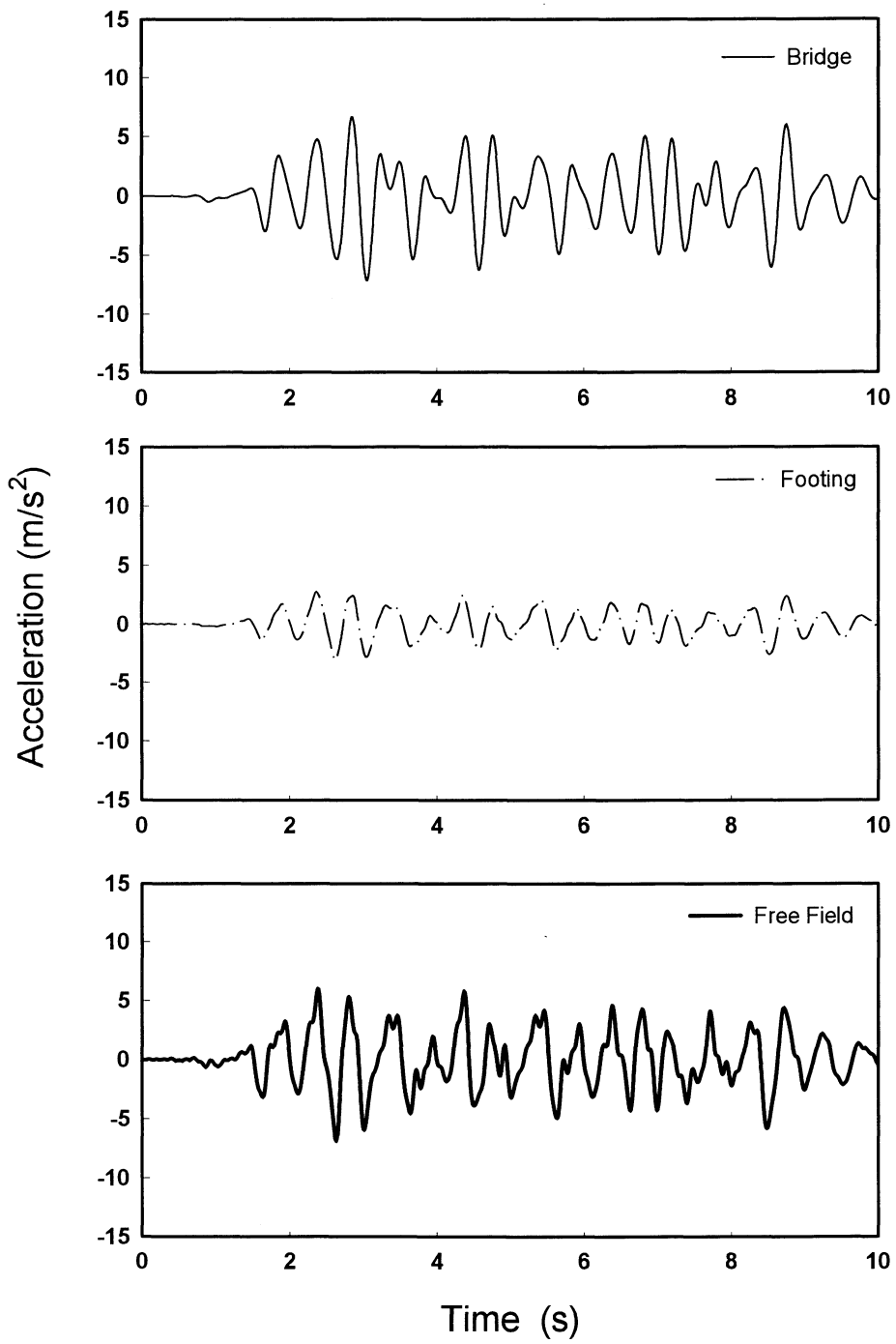
FIGURE A-28 Case A421: Acceleration histories for 0.4g artificial excitation
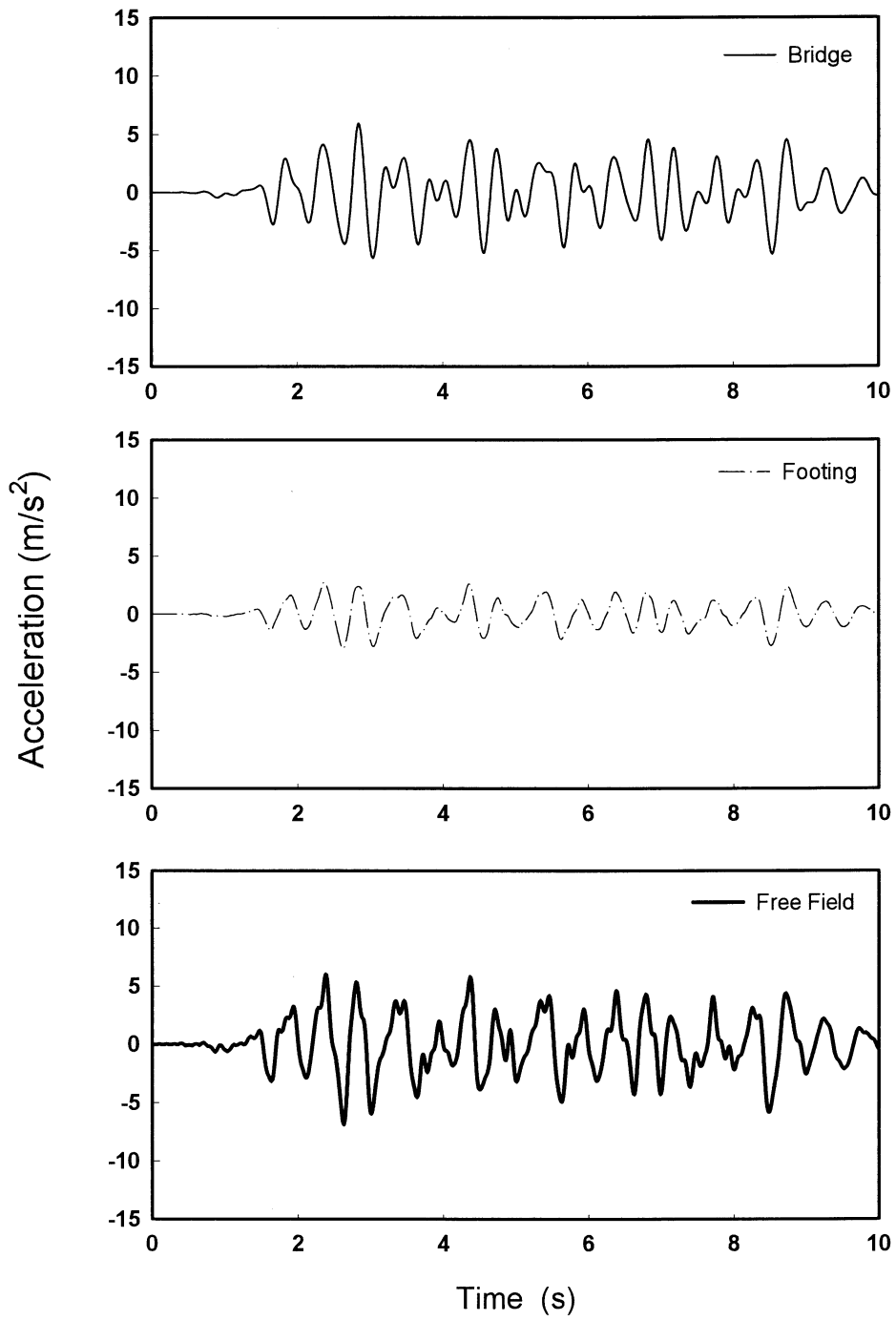
FIGURE A-29 Case A422: Acceleration histories for 0.4g artificial excitation
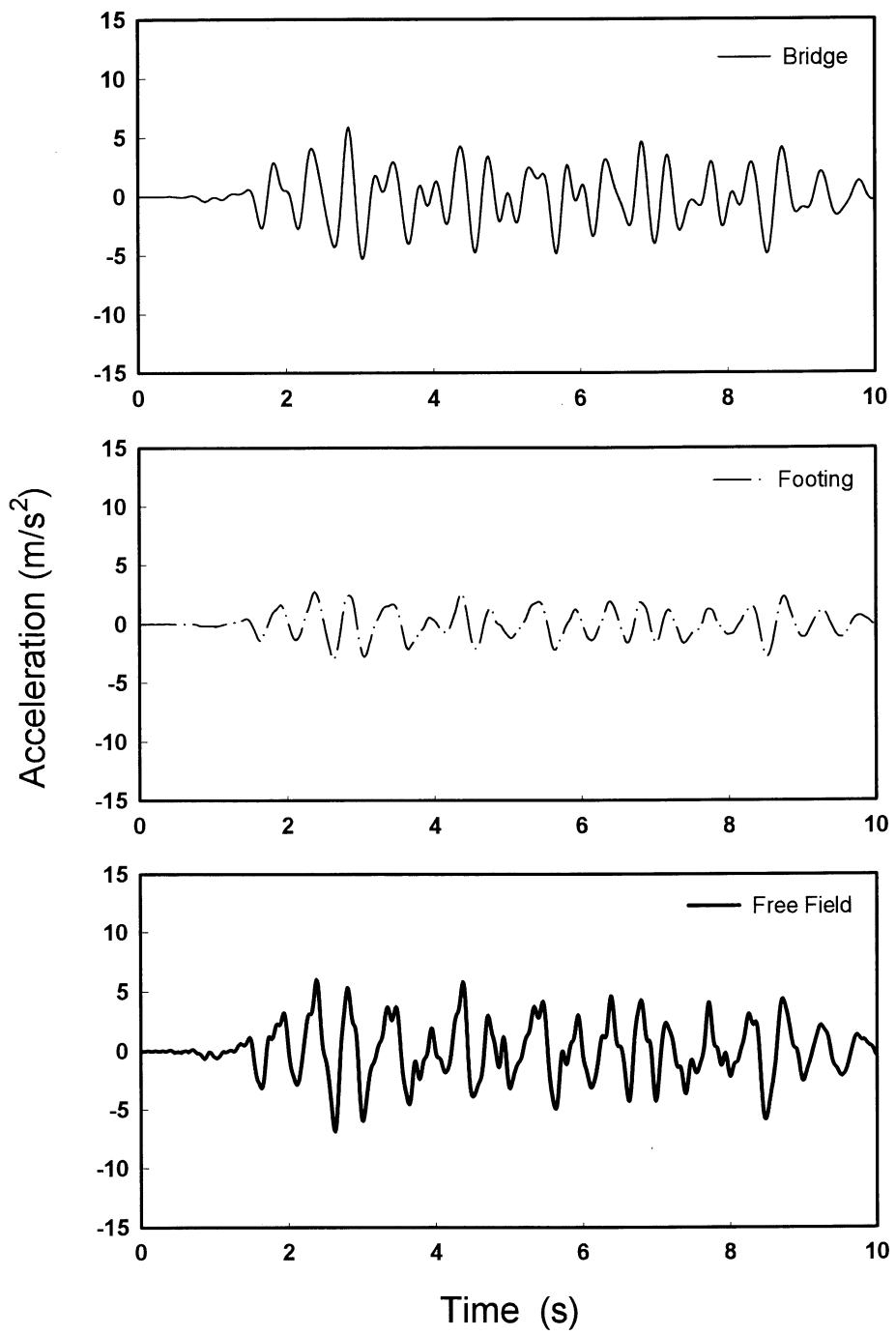
FIGURE A-30 Case A423: Acceleration histories for 0.4g artificial excitation
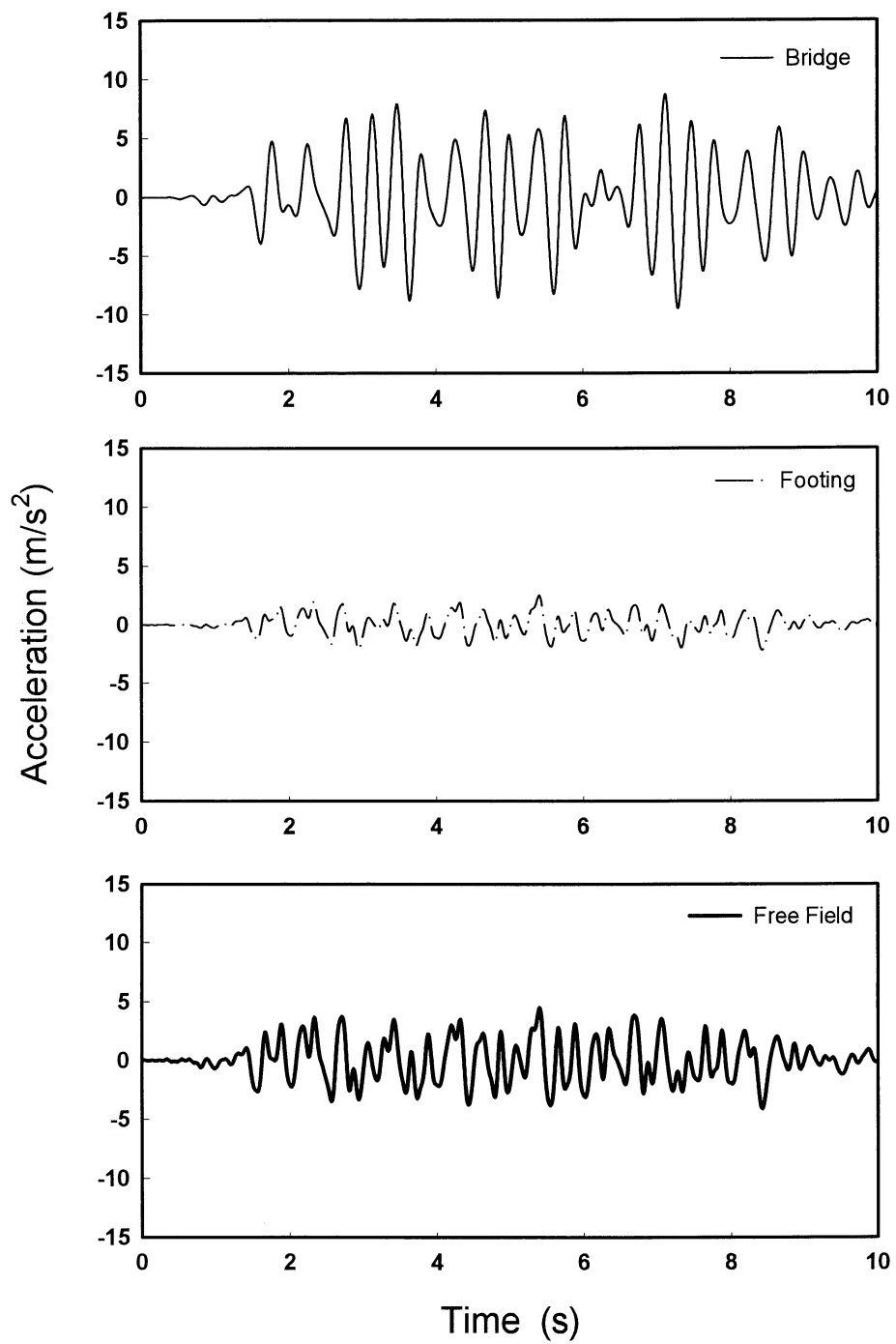
FIGURE A-31 Case A241: Acceleration histories for 0.4g artificial excitation
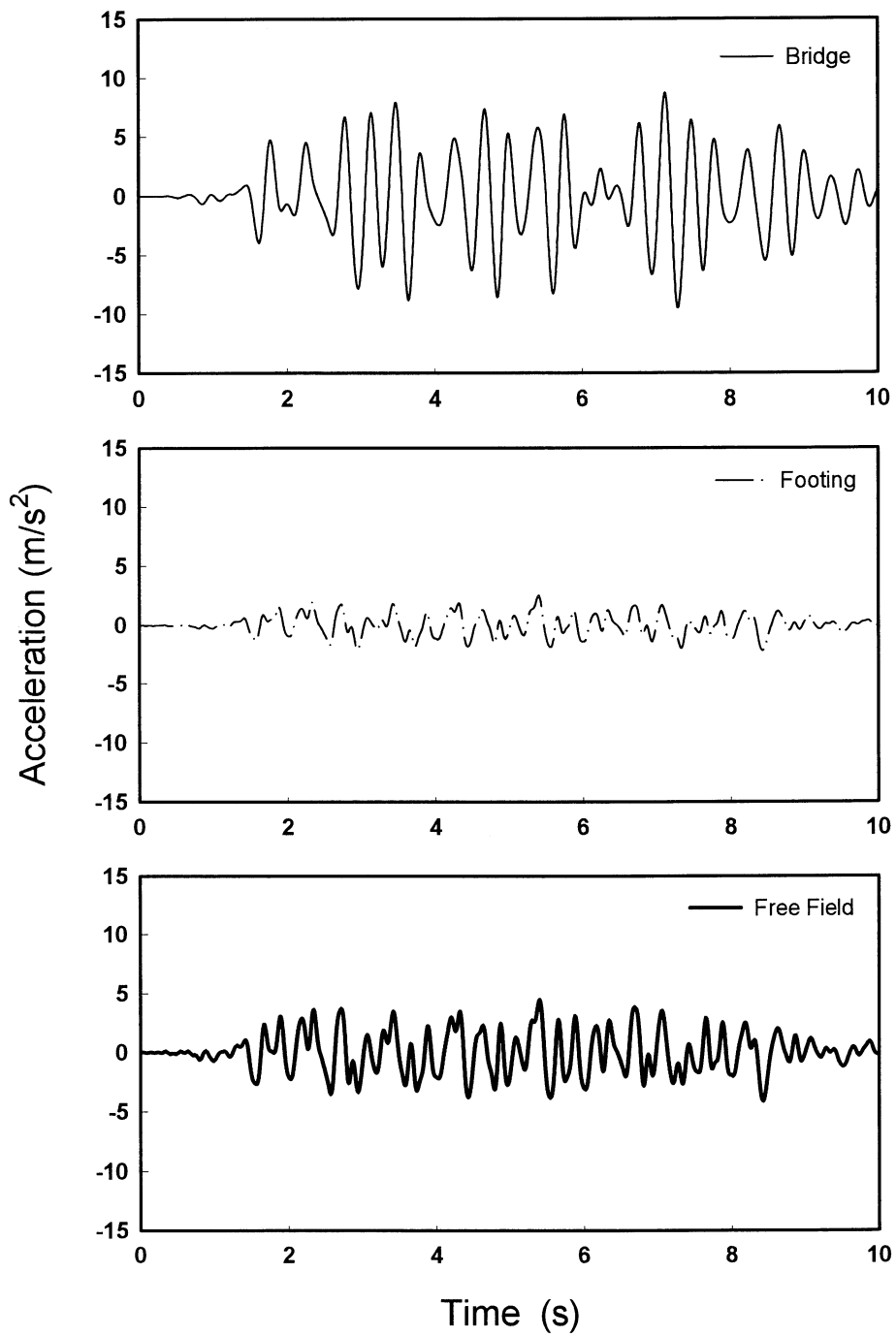
FIGURE A-32 Case A242: Acceleration histories for 0.4g artificial excitation
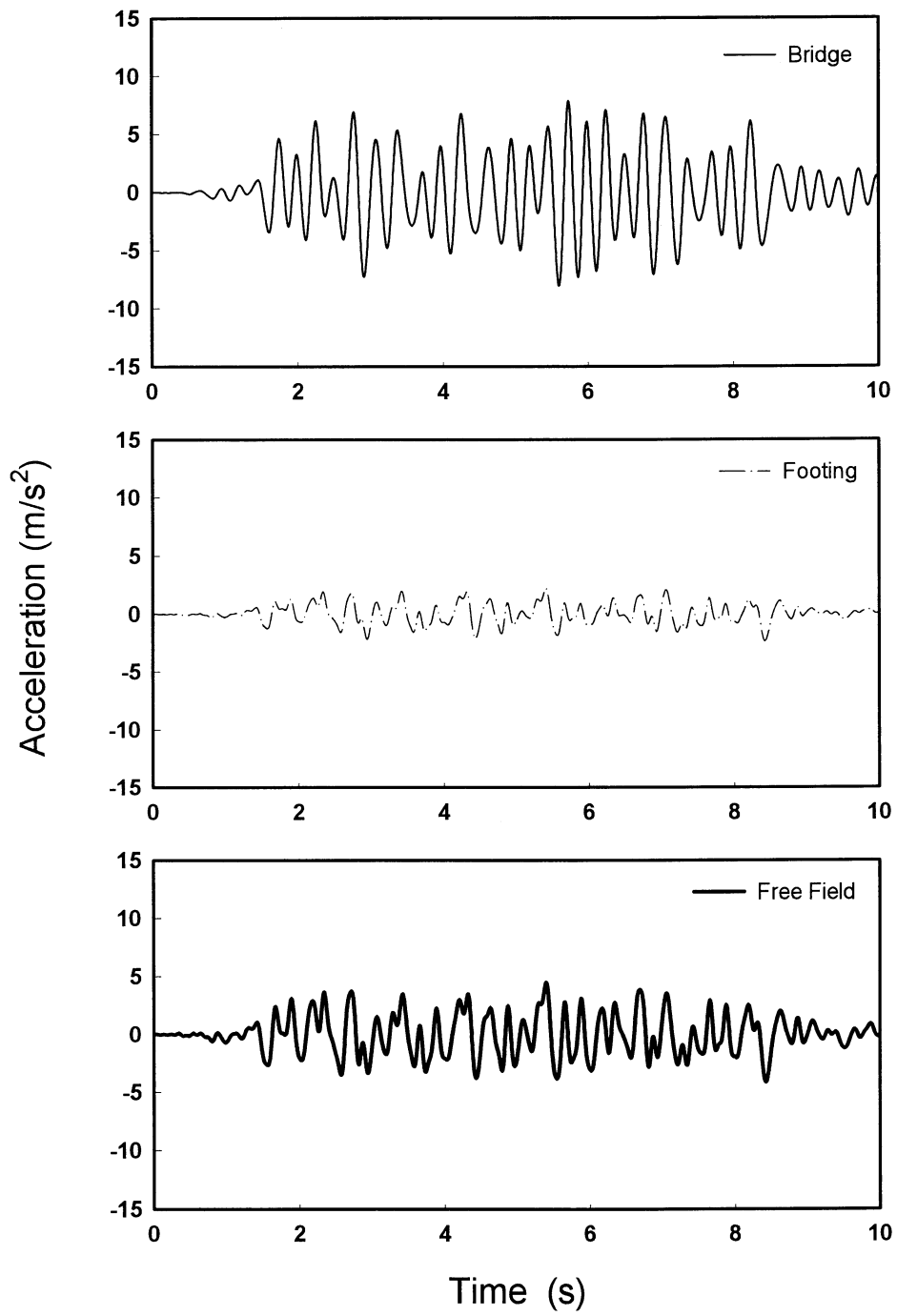
FIGURE A-33 Case A243: Acceleration histories for 0.4g artificial excitation
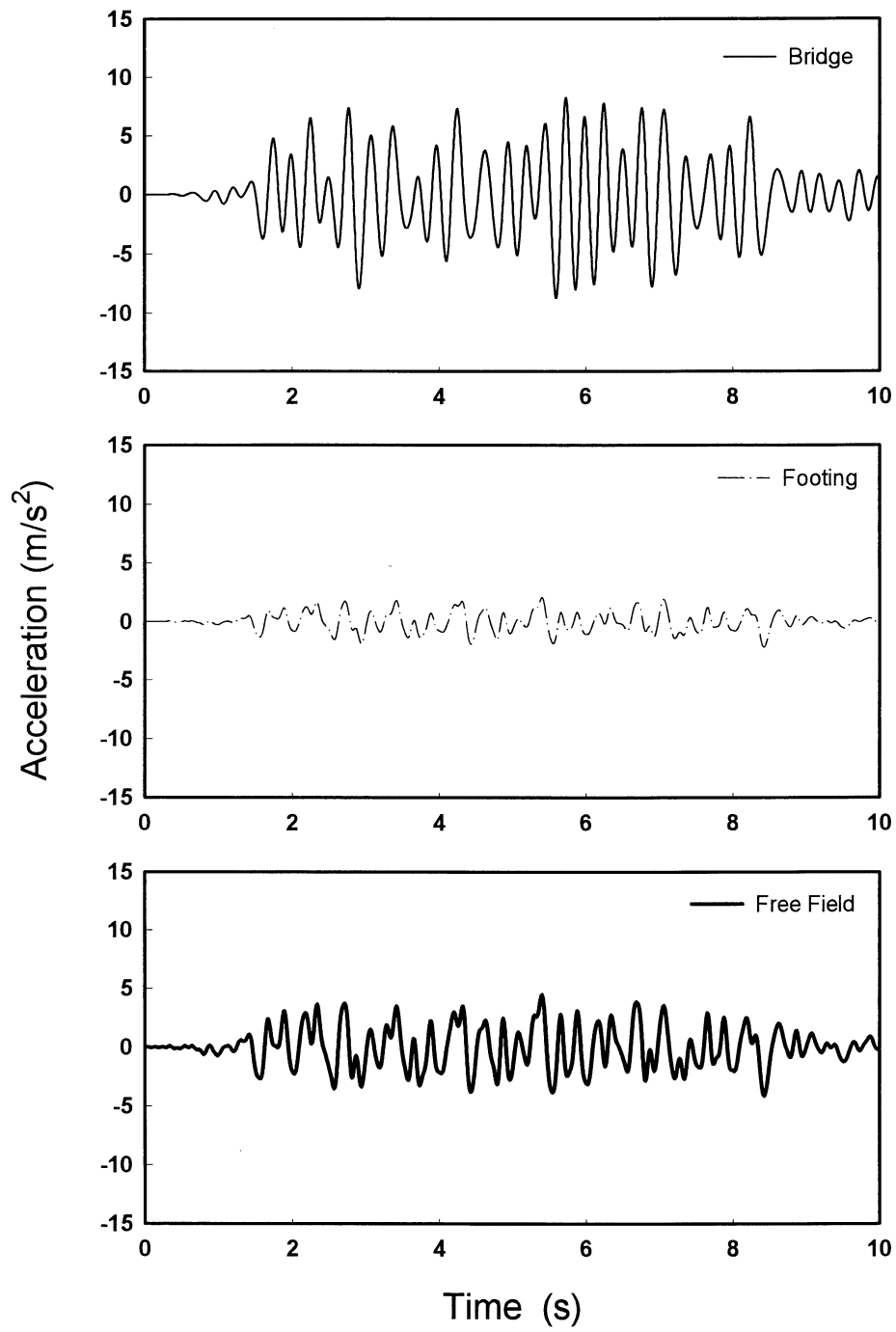
FIGURE A-34 Case A221: Acceleration histories for 0.4g artificial excitation
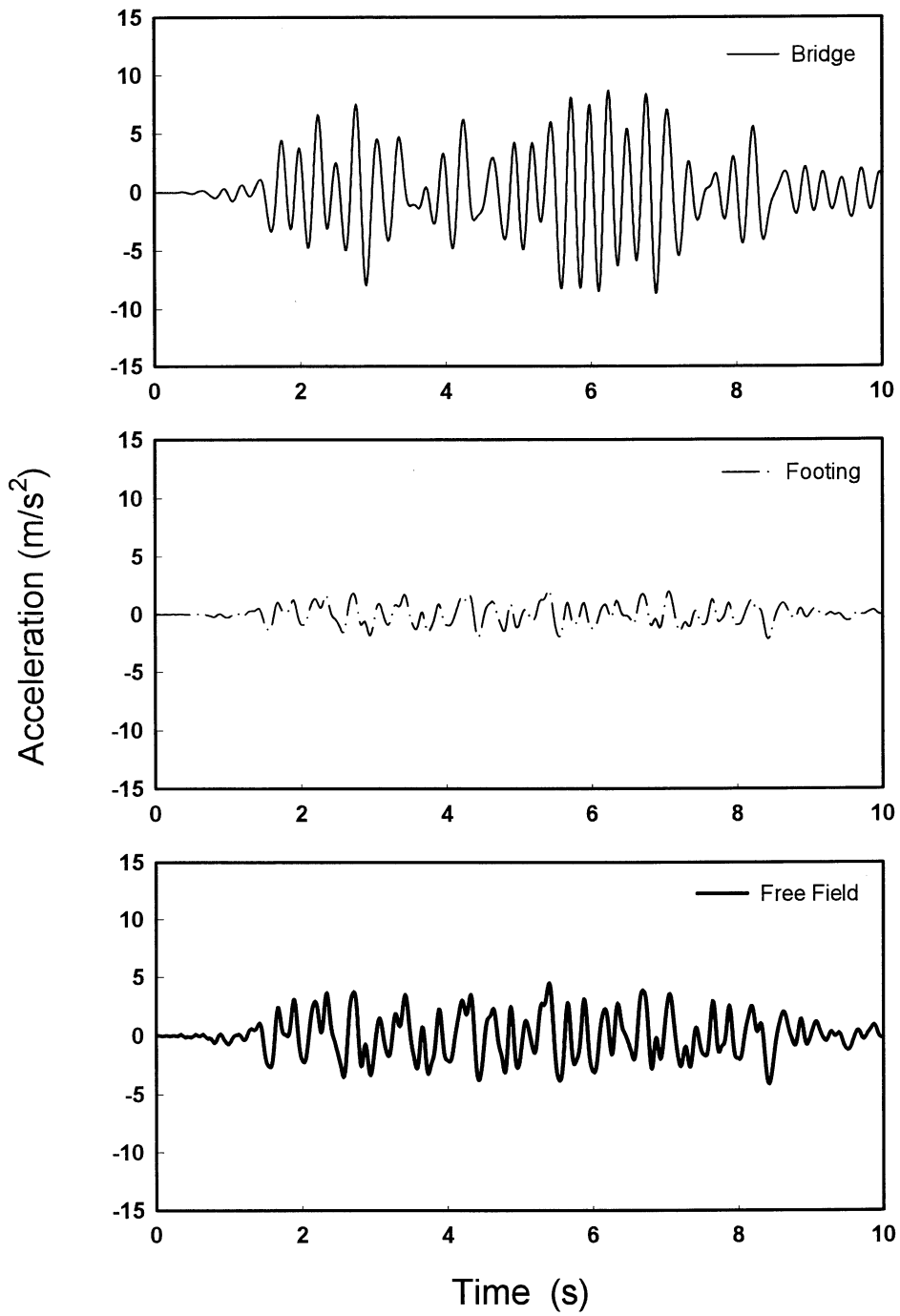
FIGURE A-35 Case A222: Acceleration histories for 0.4g artificial excitation
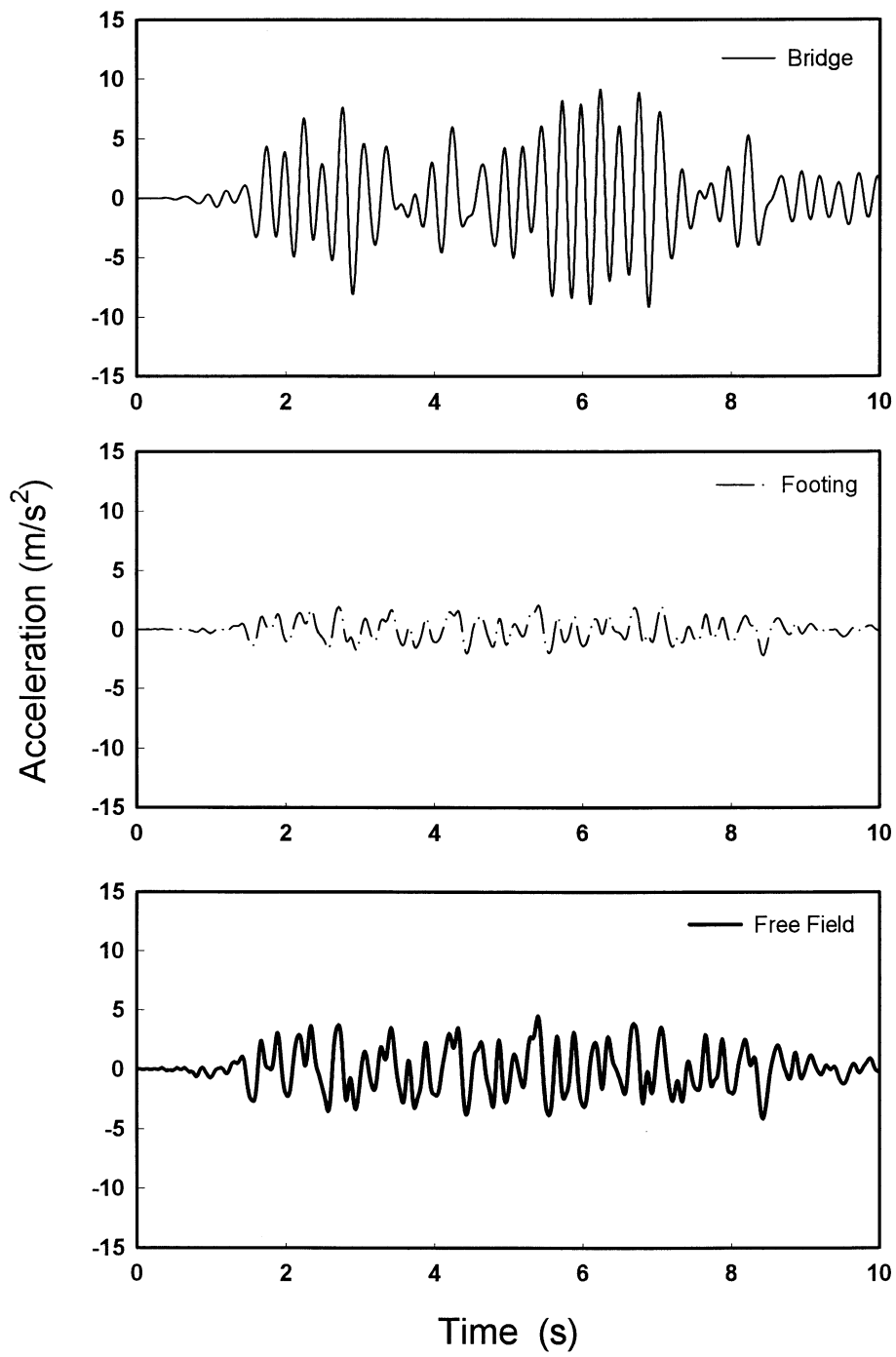
FIGURE A-36 Case A223: Acceleration histories for 0.4g artificial excitation
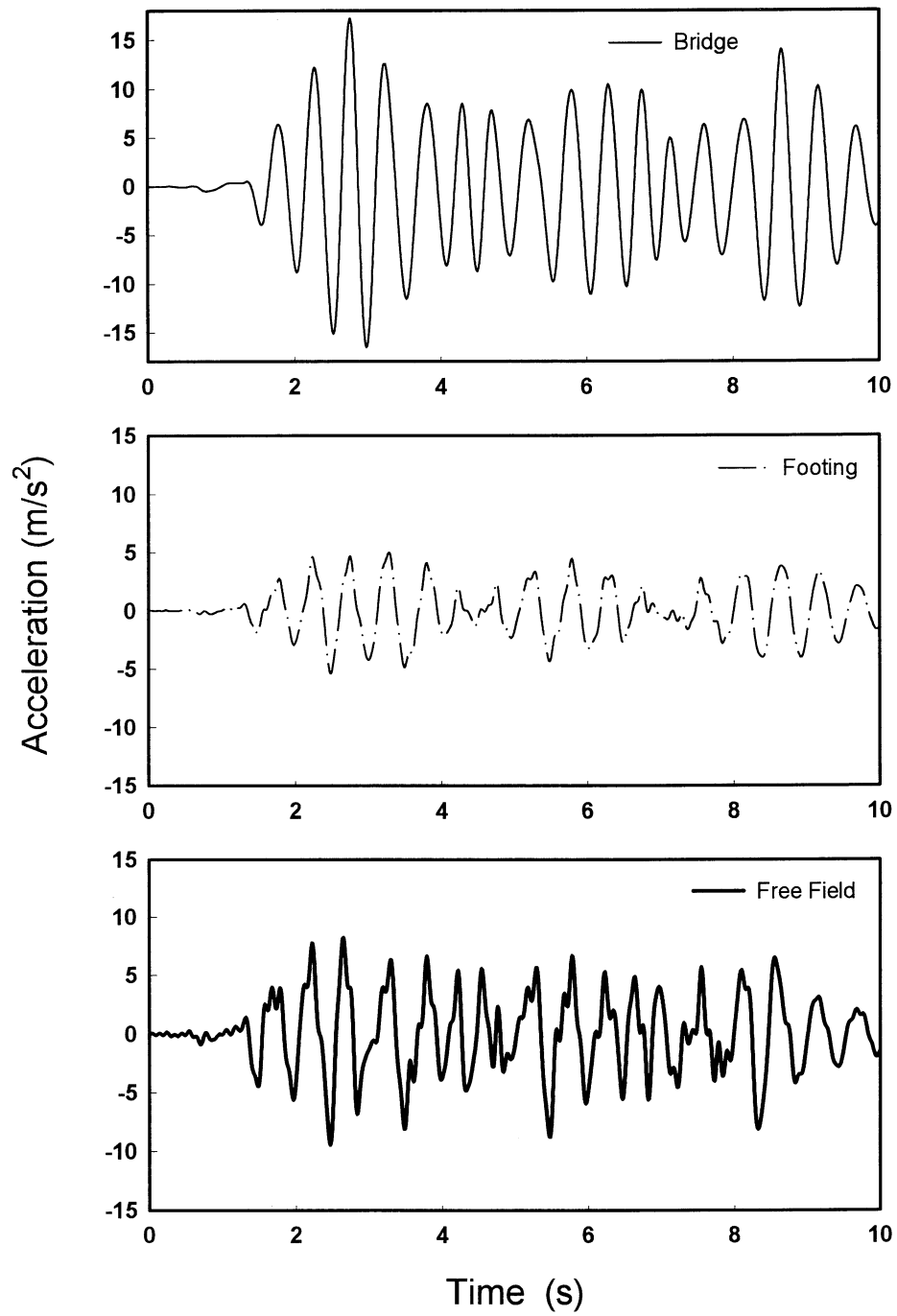
FIGURE A-37 Case B441: Acceleration histories for 0.4g artificial excitation
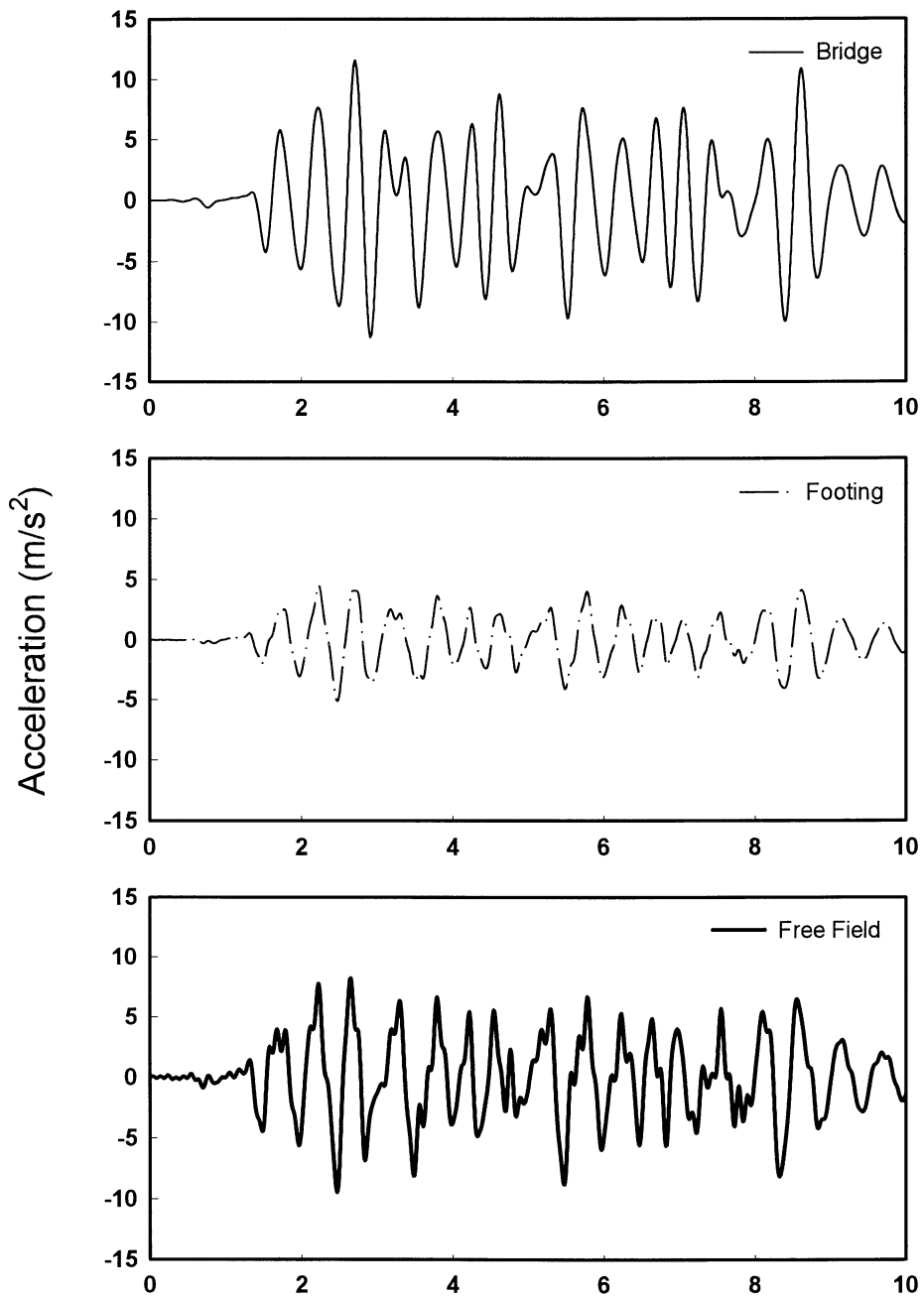
FIGURE A-38 Case B442: Acceleration histories for 0.4g artificial excitation

137
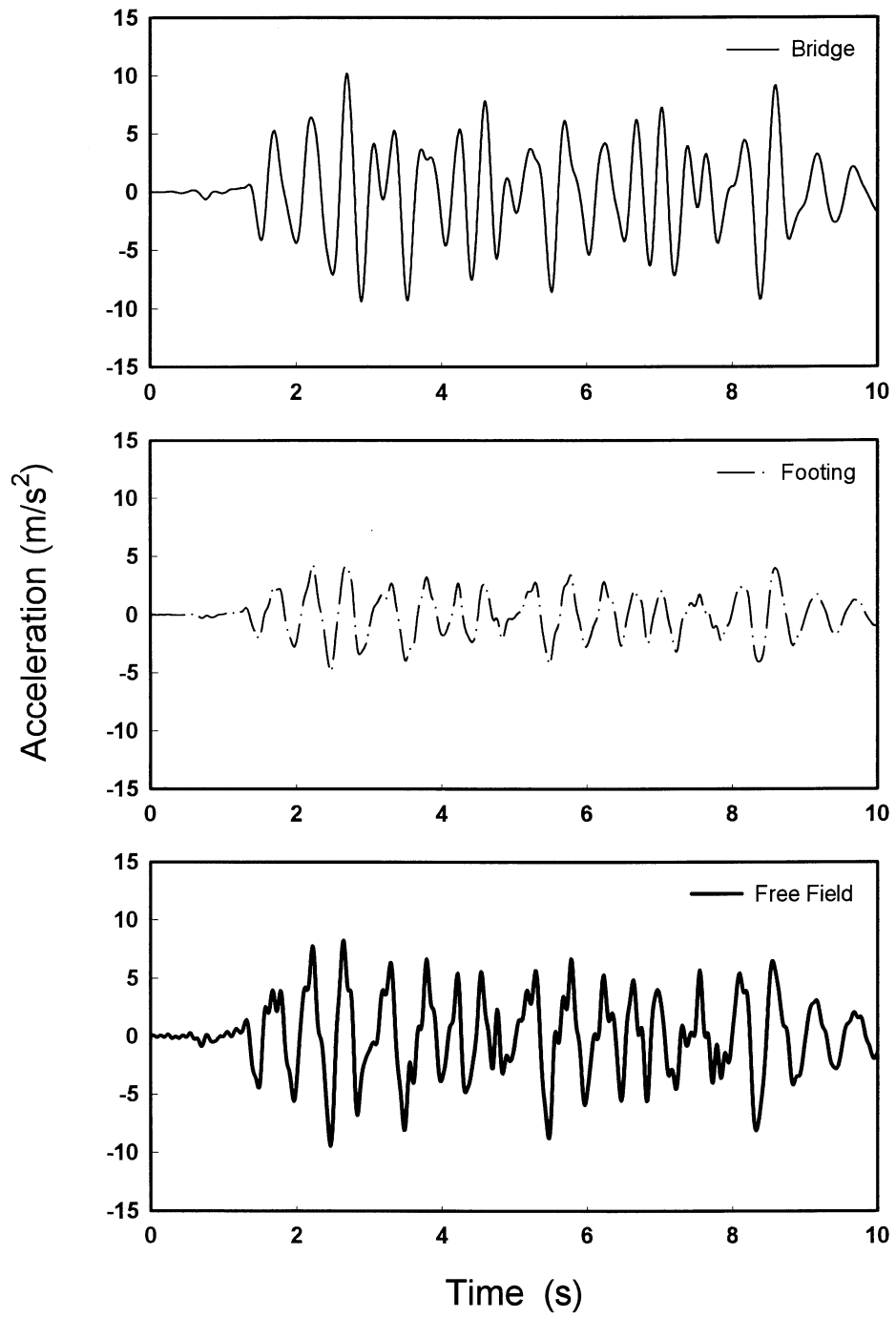
FIGURE A-39 Case B443: Acceleration histories for 0.4g artificial excitation
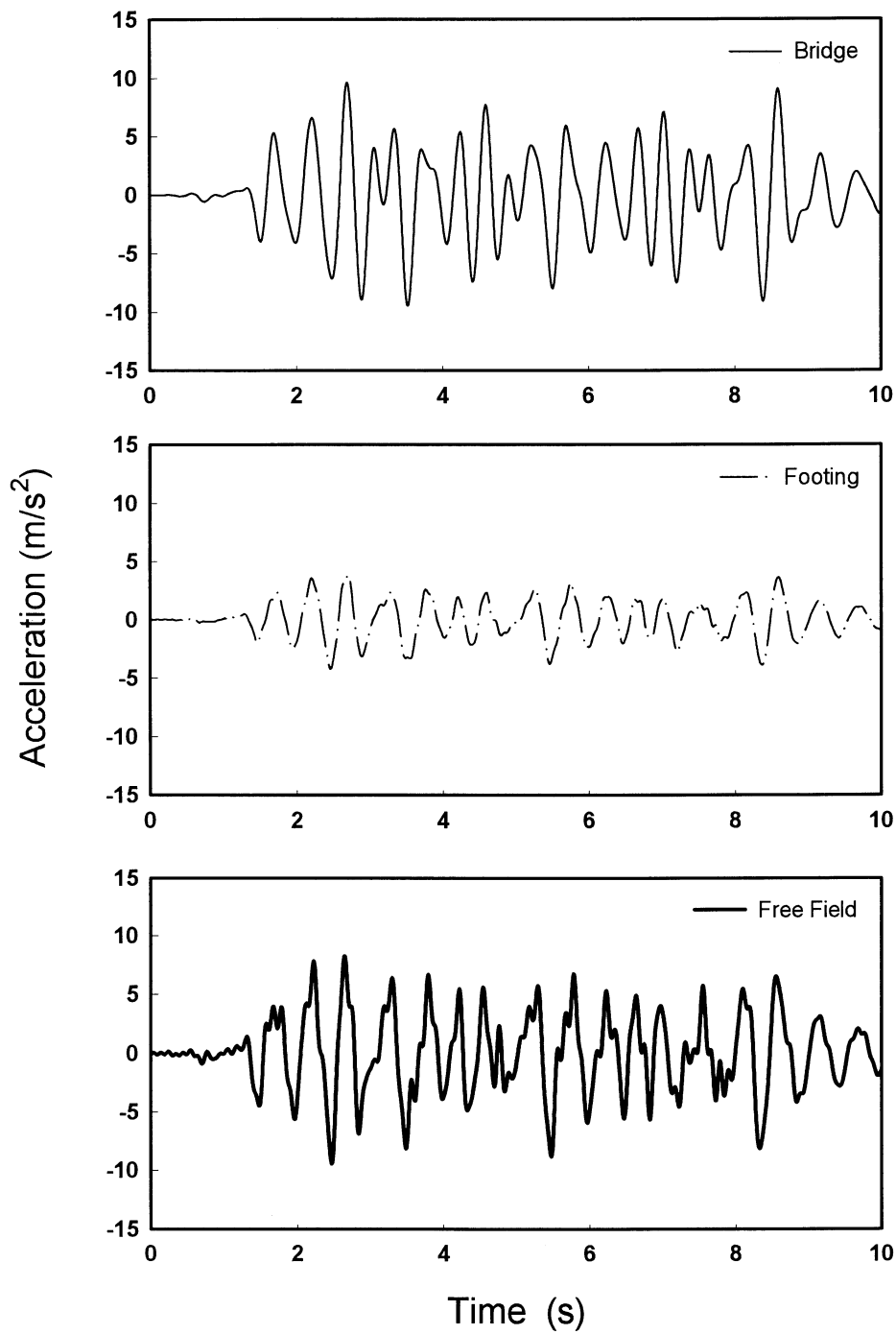
FIGURE A-40 Case B421: Acceleration histories for 0.4g artificial excitation
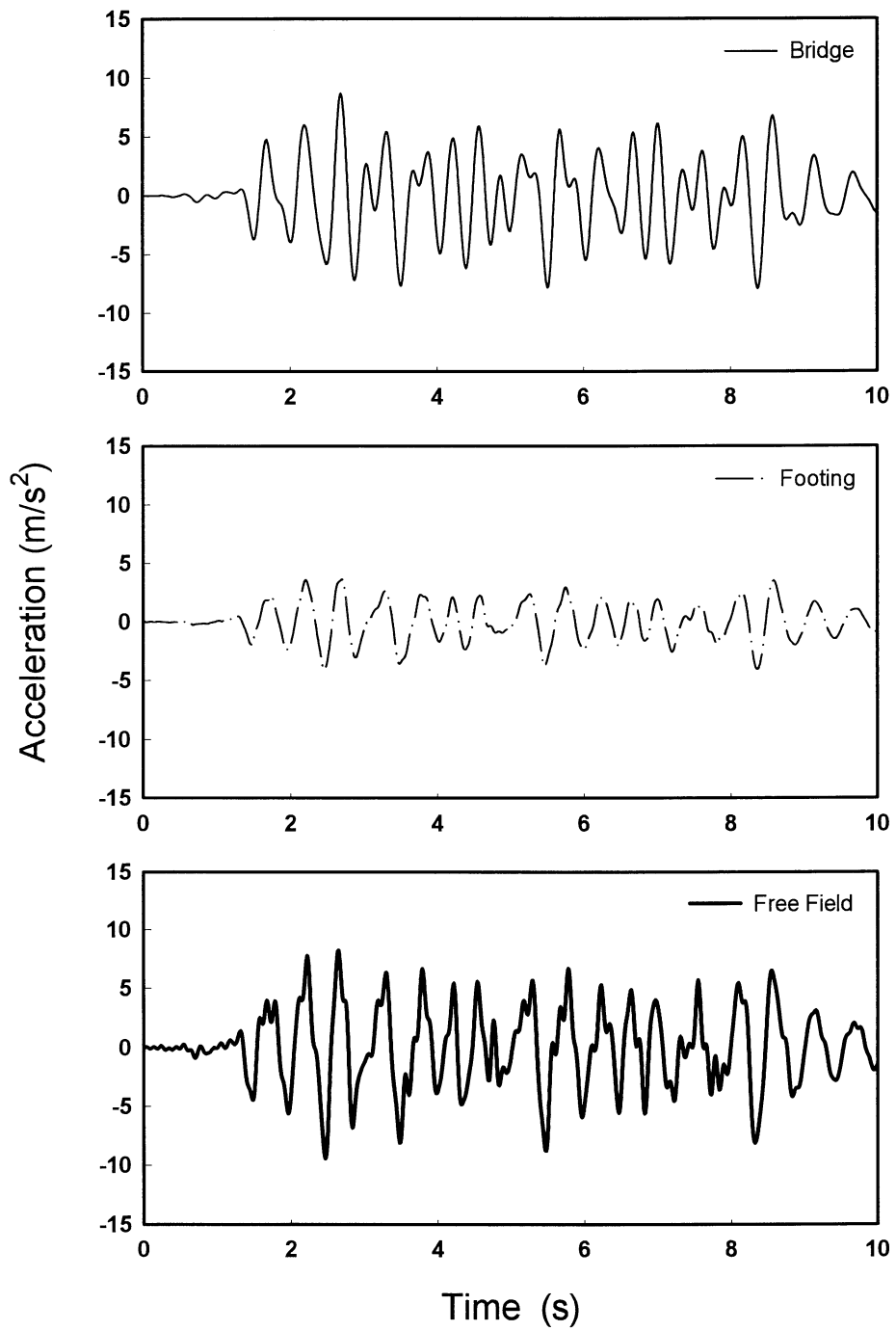
FIGURE A-41 Case B422: Acceleration histories for 0.4g artificial excitation
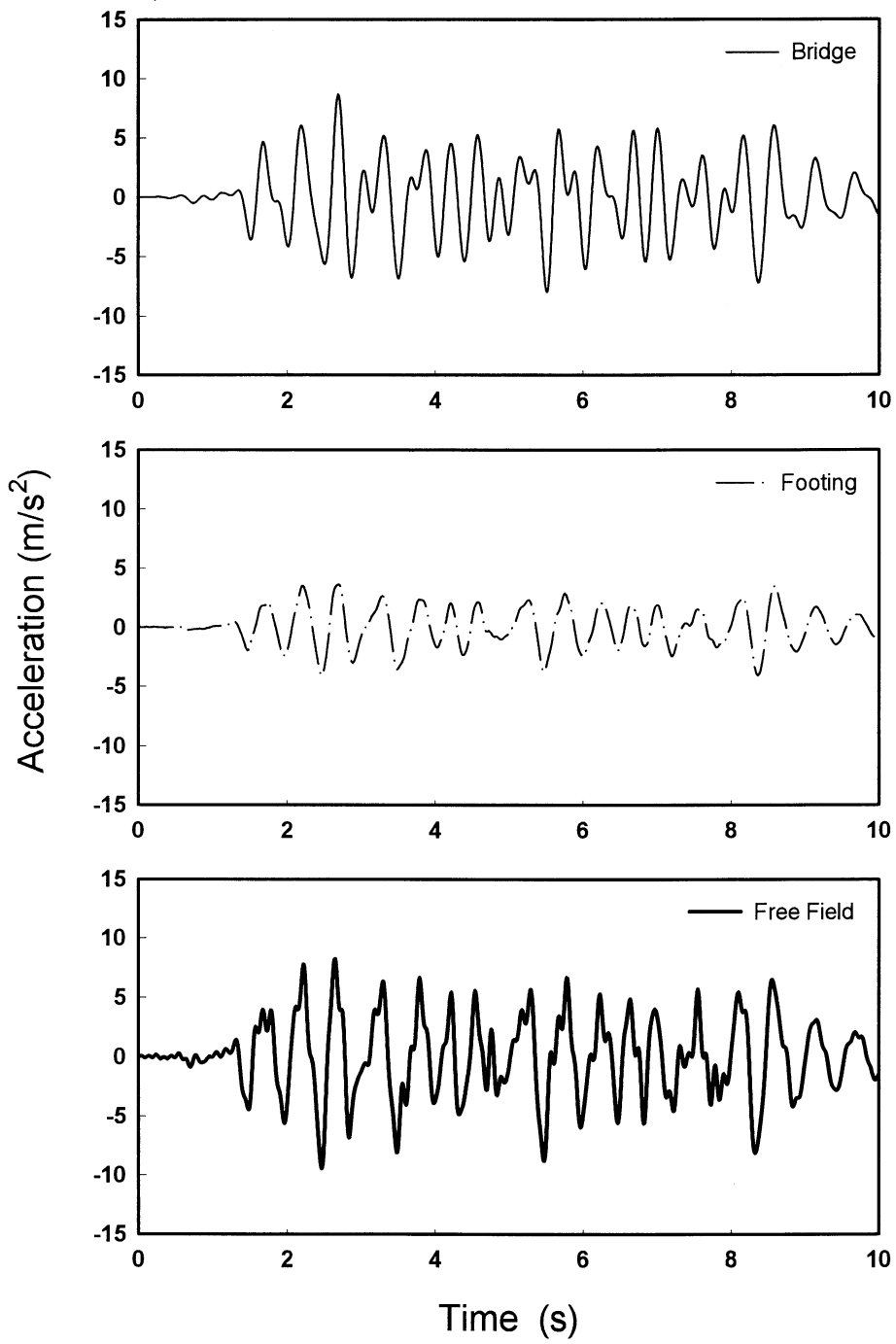
FIGURE A-42 Case B423: Acceleration histories for 0.4g artificial excitation
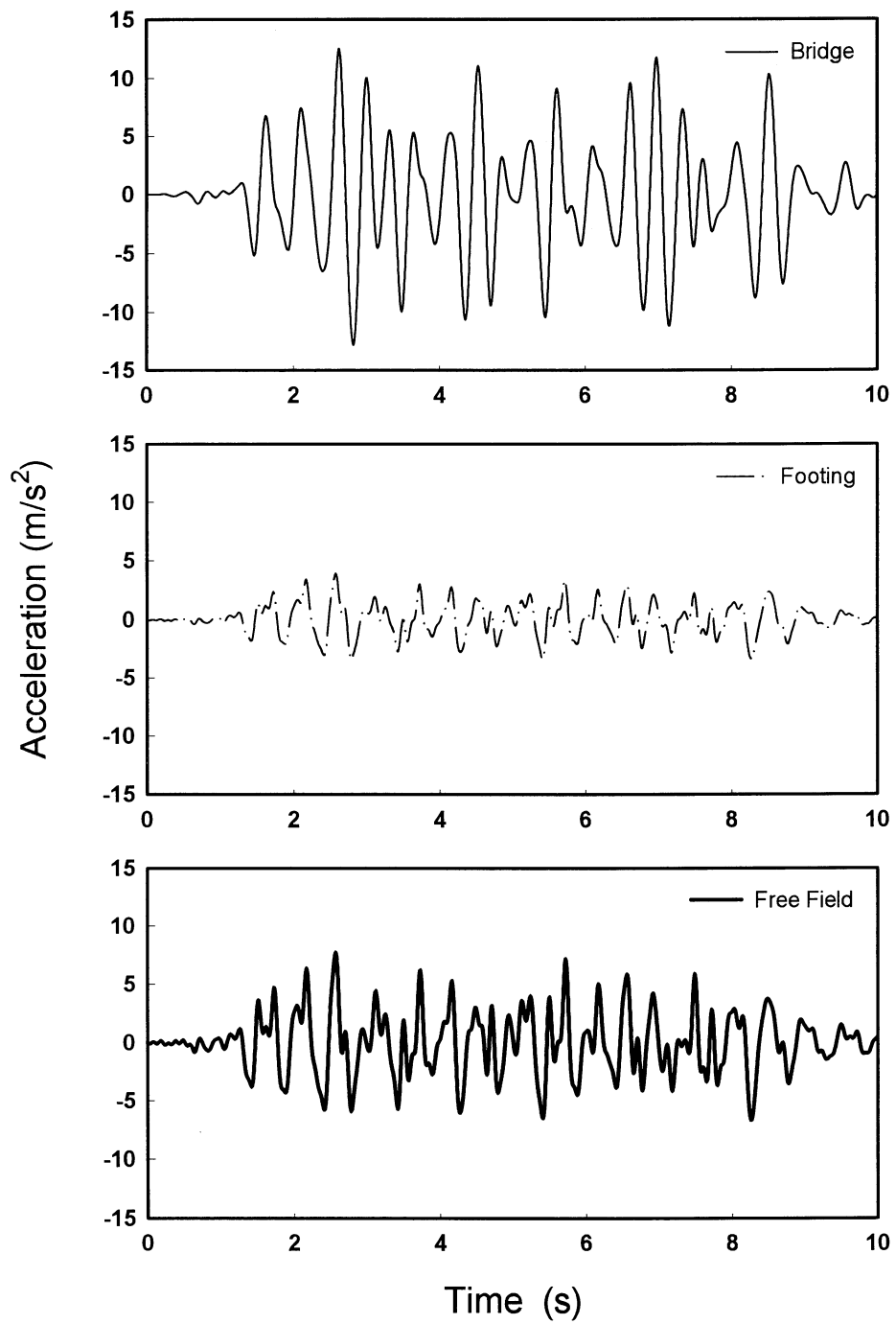
FIGURE A-43 Case B241: Acceleration histories for 0.4g artificial excitation

142
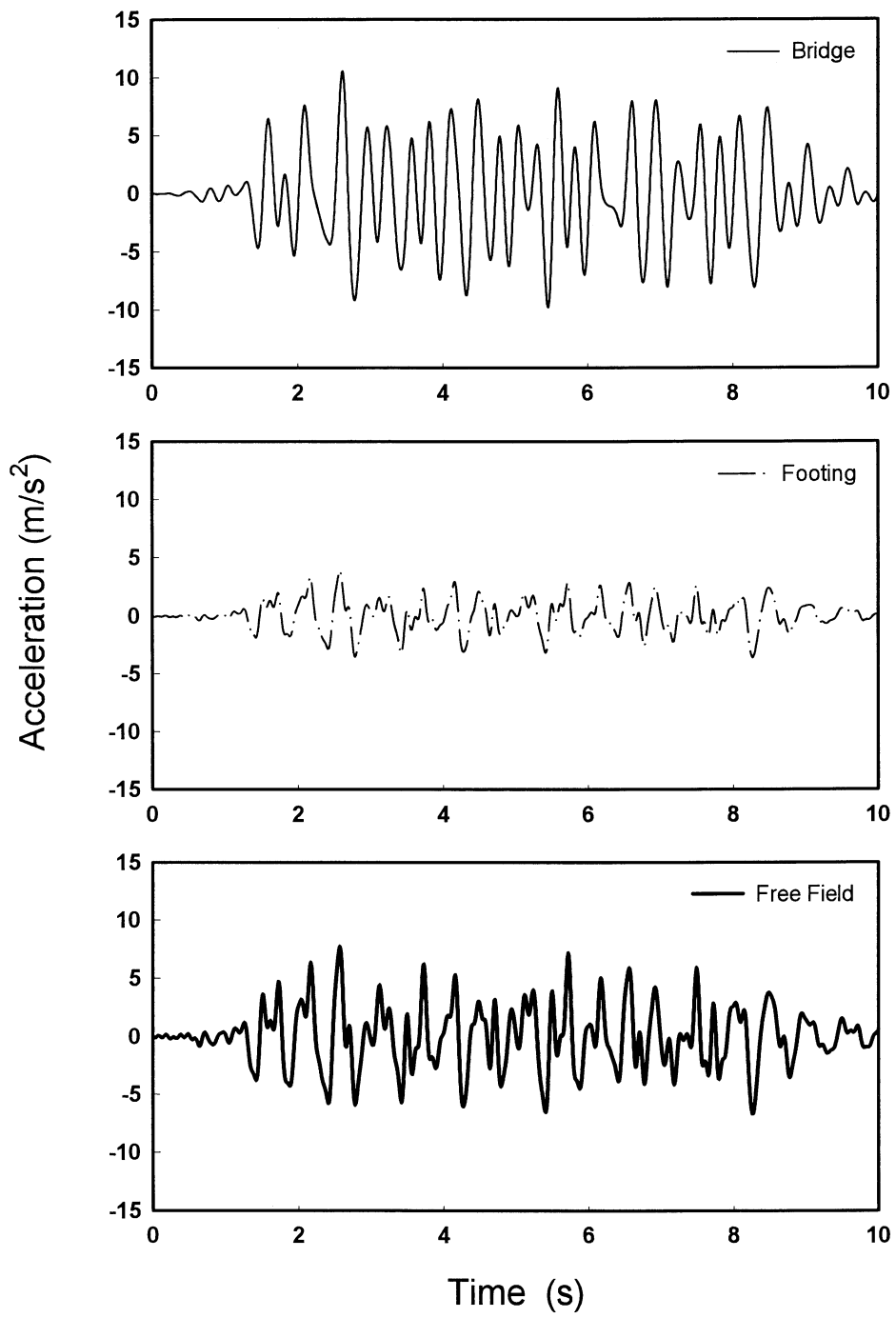
FIGURE A-44 Case B242: Acceleration histories for 0.4g artificial excitation
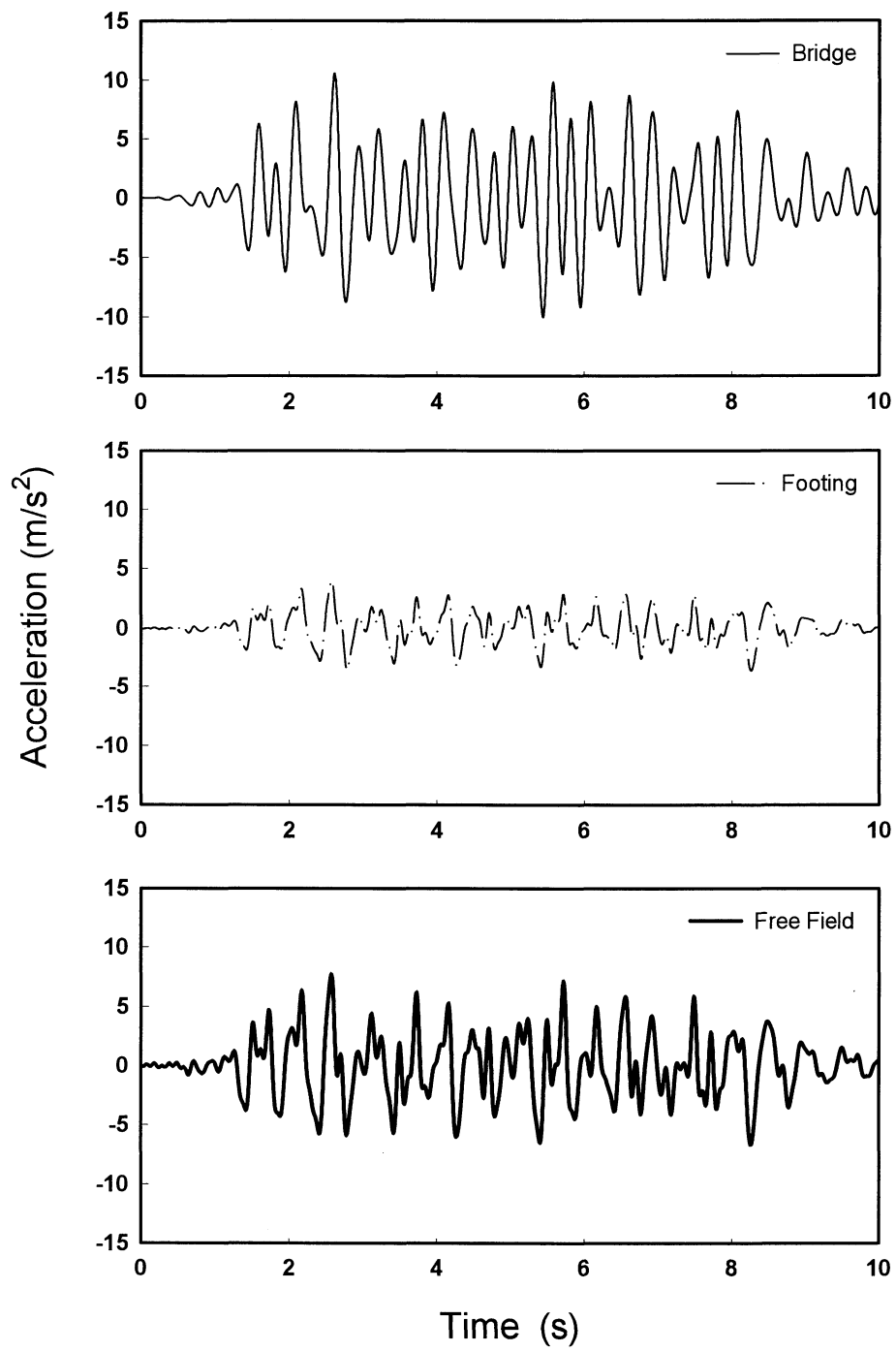
FIGURE A-45 Case B243: Acceleration histories for 0.4g artificial excitation
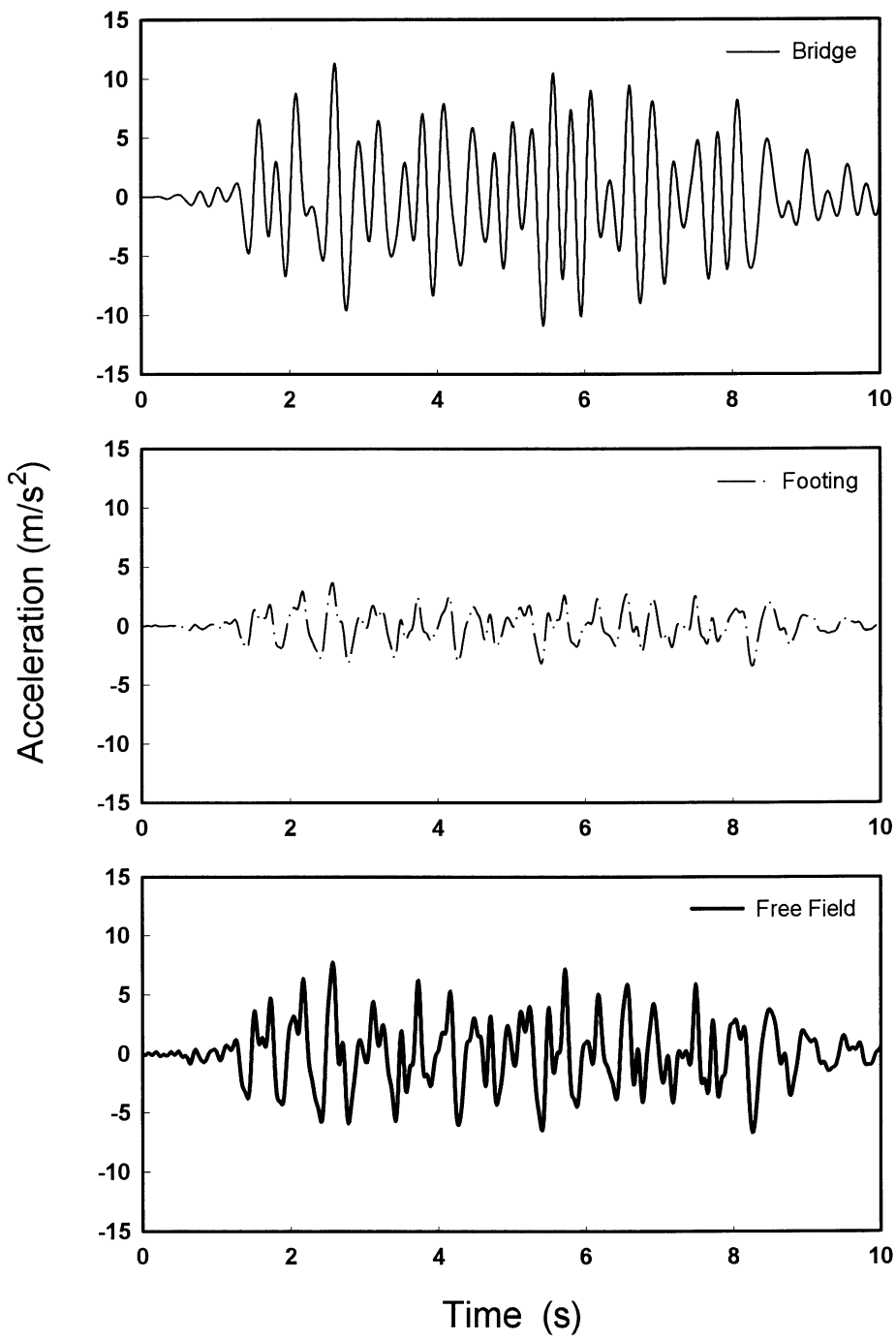
FIGURE A-46 Case B221: Acceleration histories for 0.4g artificial excitation

145
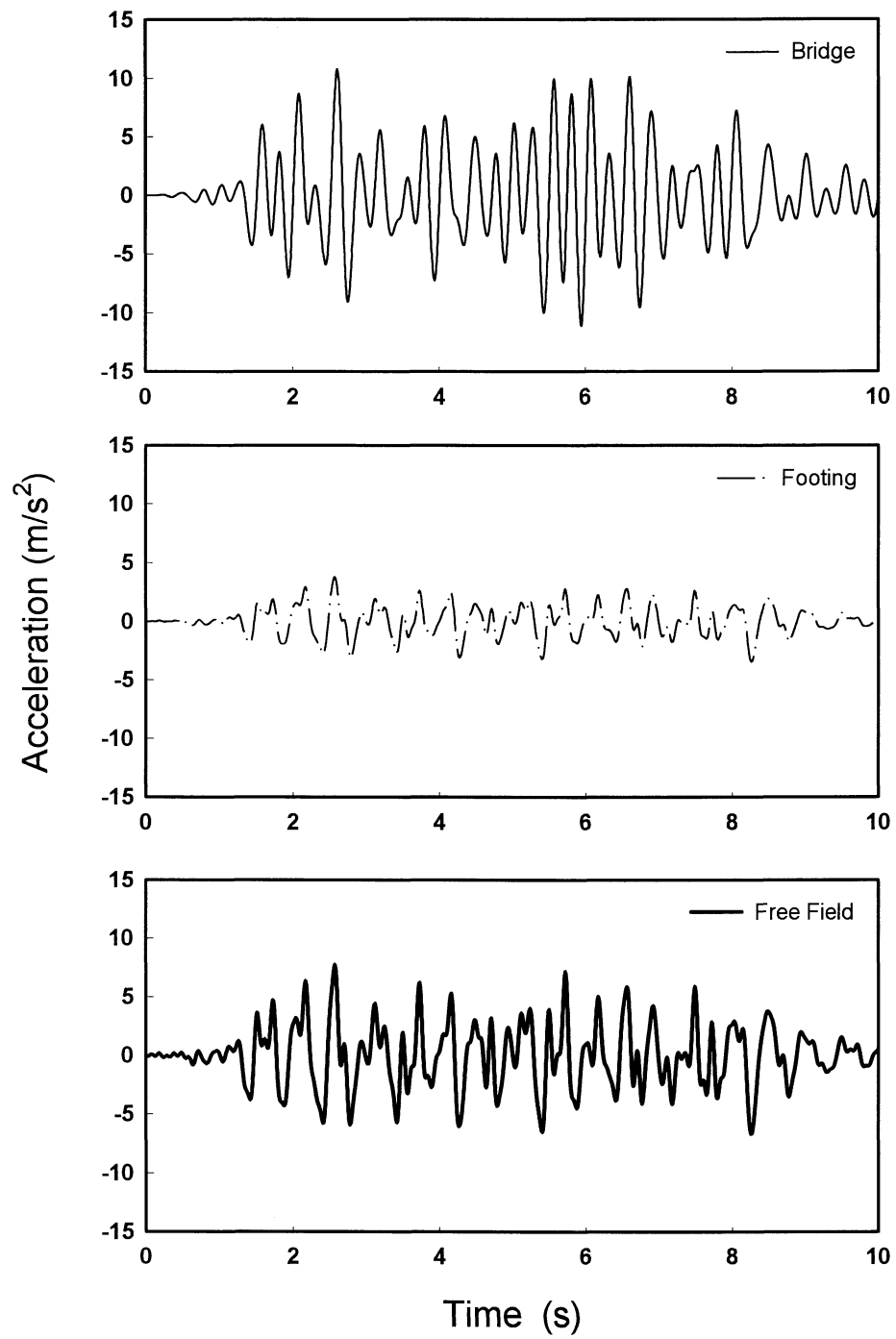
FIGURE A-47 Case B222: Acceleration histories for 0.4g artificial excitation
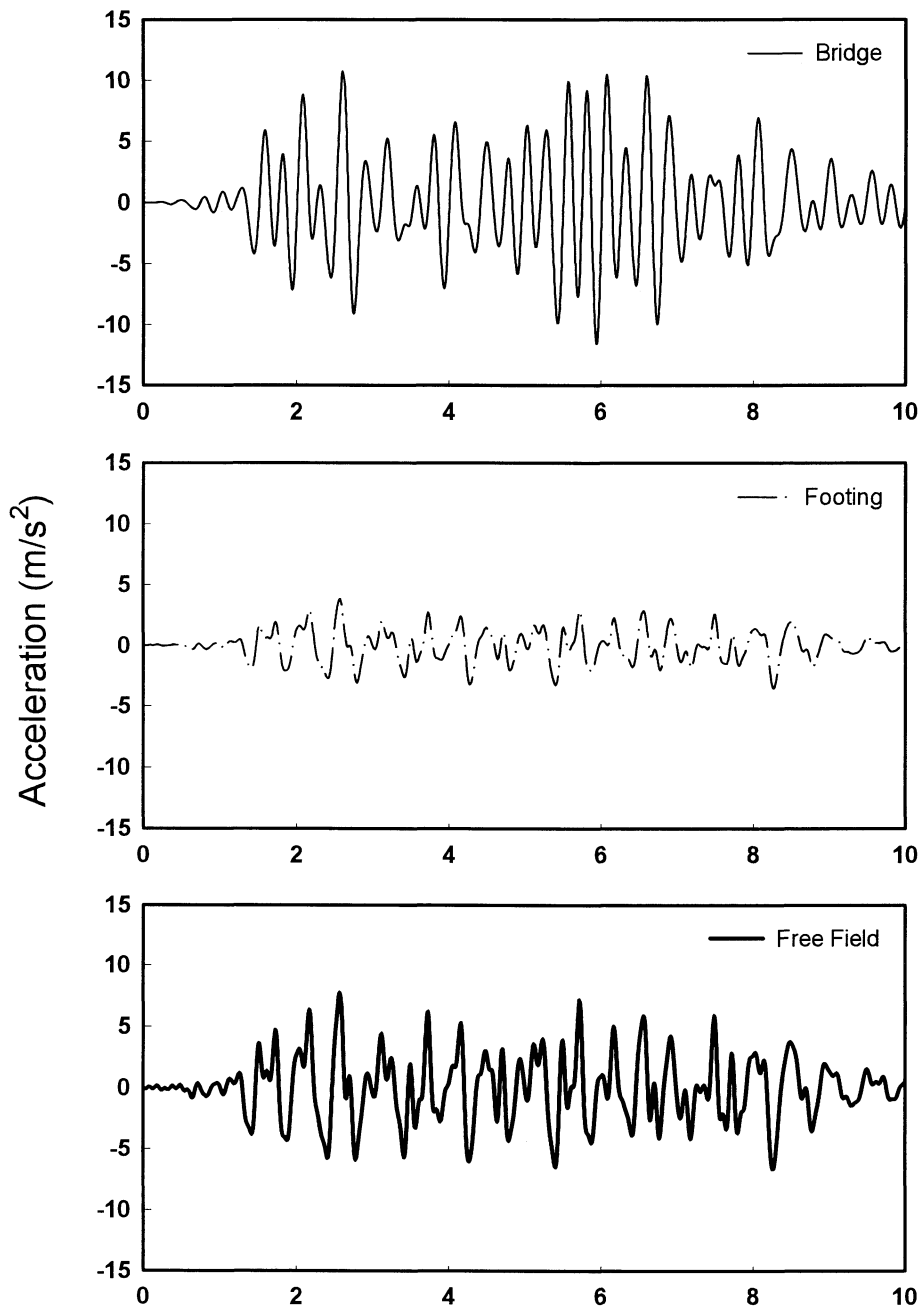
FIGURE A-48 Case B223: Acceleration histories for 0.4g artificial excitation

147
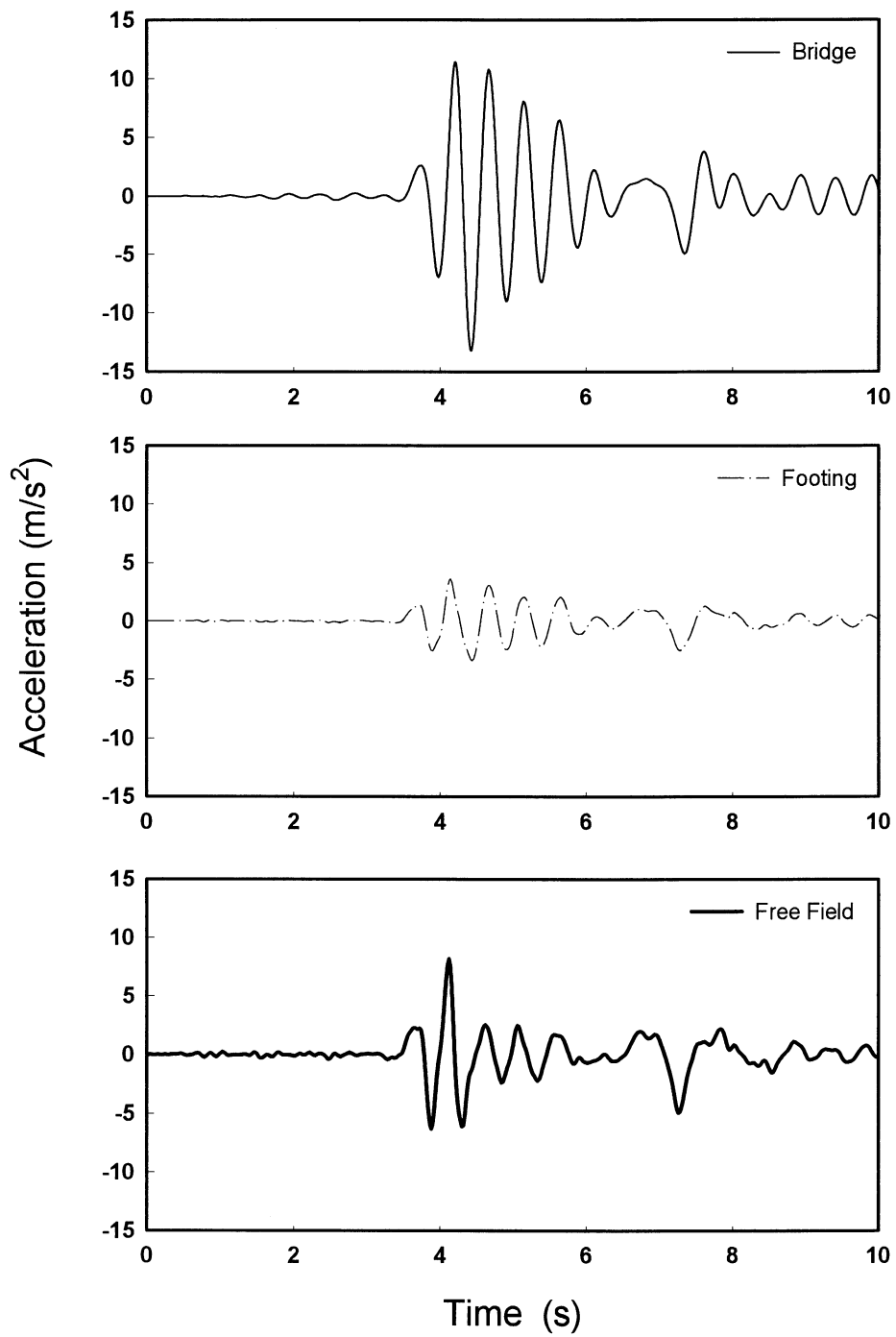
FIGURE A-49 Case A441: Acceleration histories for Pacoima, Northridge (1994) rock motion
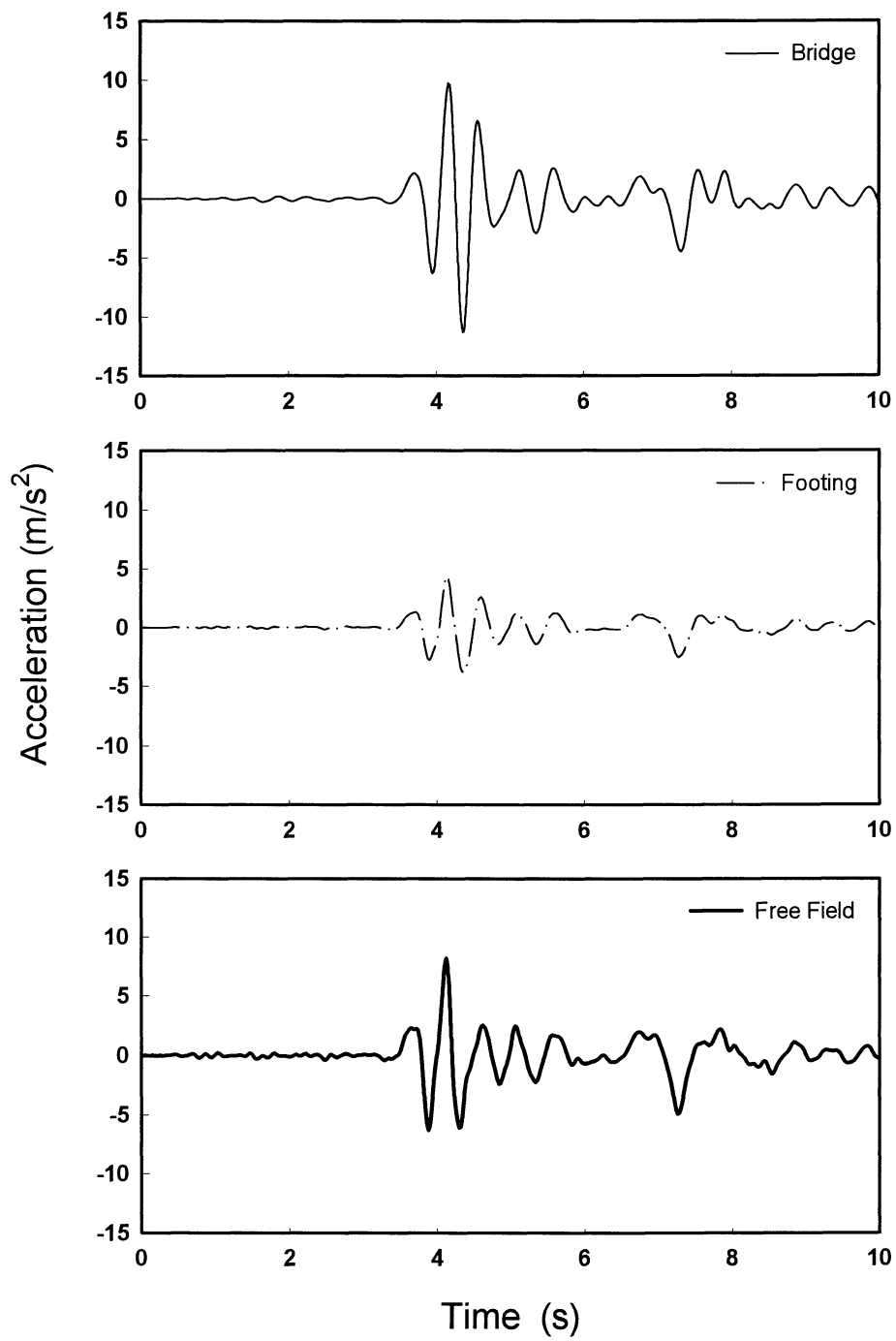
FIGURE A-50 Case A442: Acceleration histories for Pacoima, Northridge (1994) rock motion
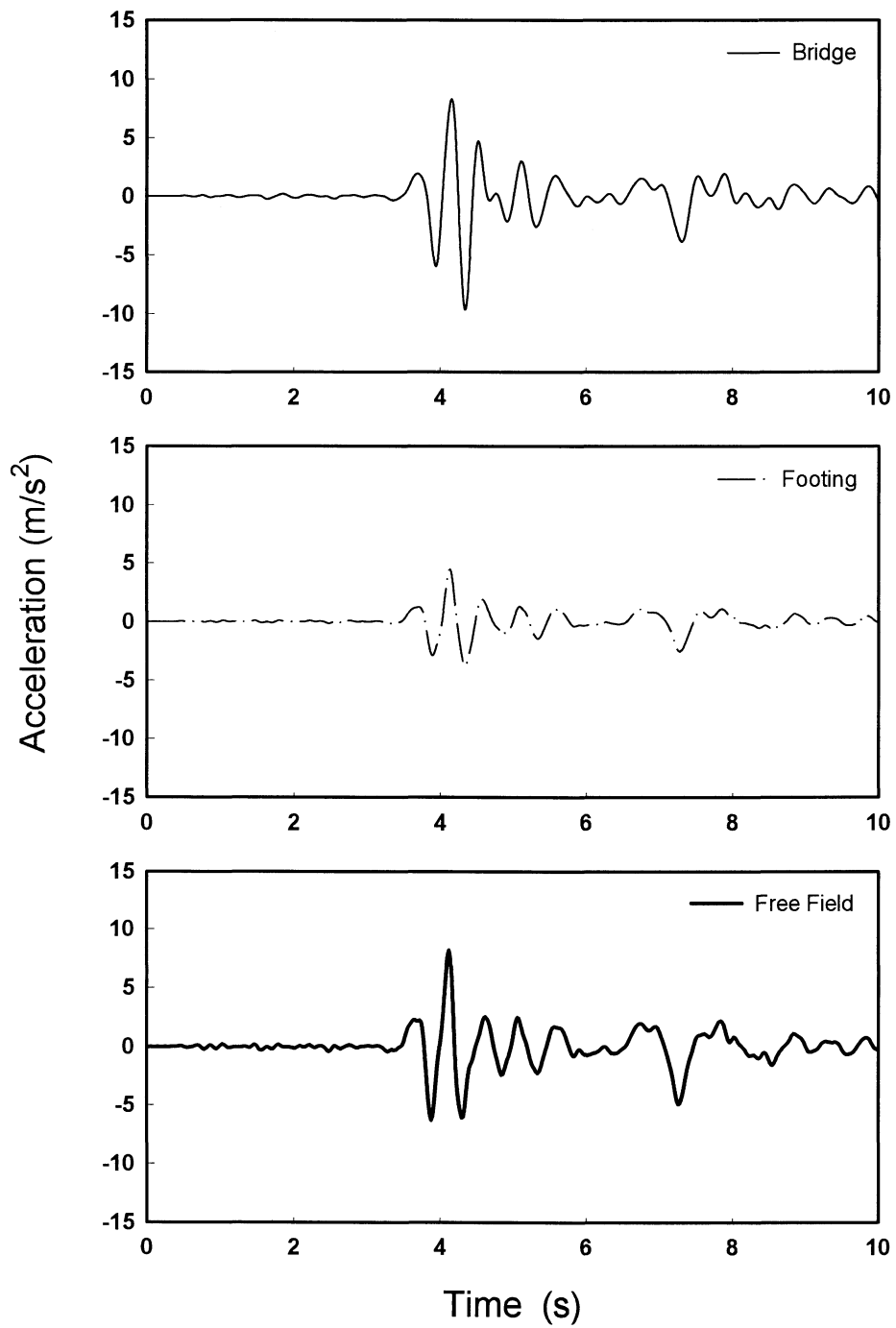
FIGURE A-51 Case A443: Acceleration histories for Pacoima, Northridge (1994) rock motion
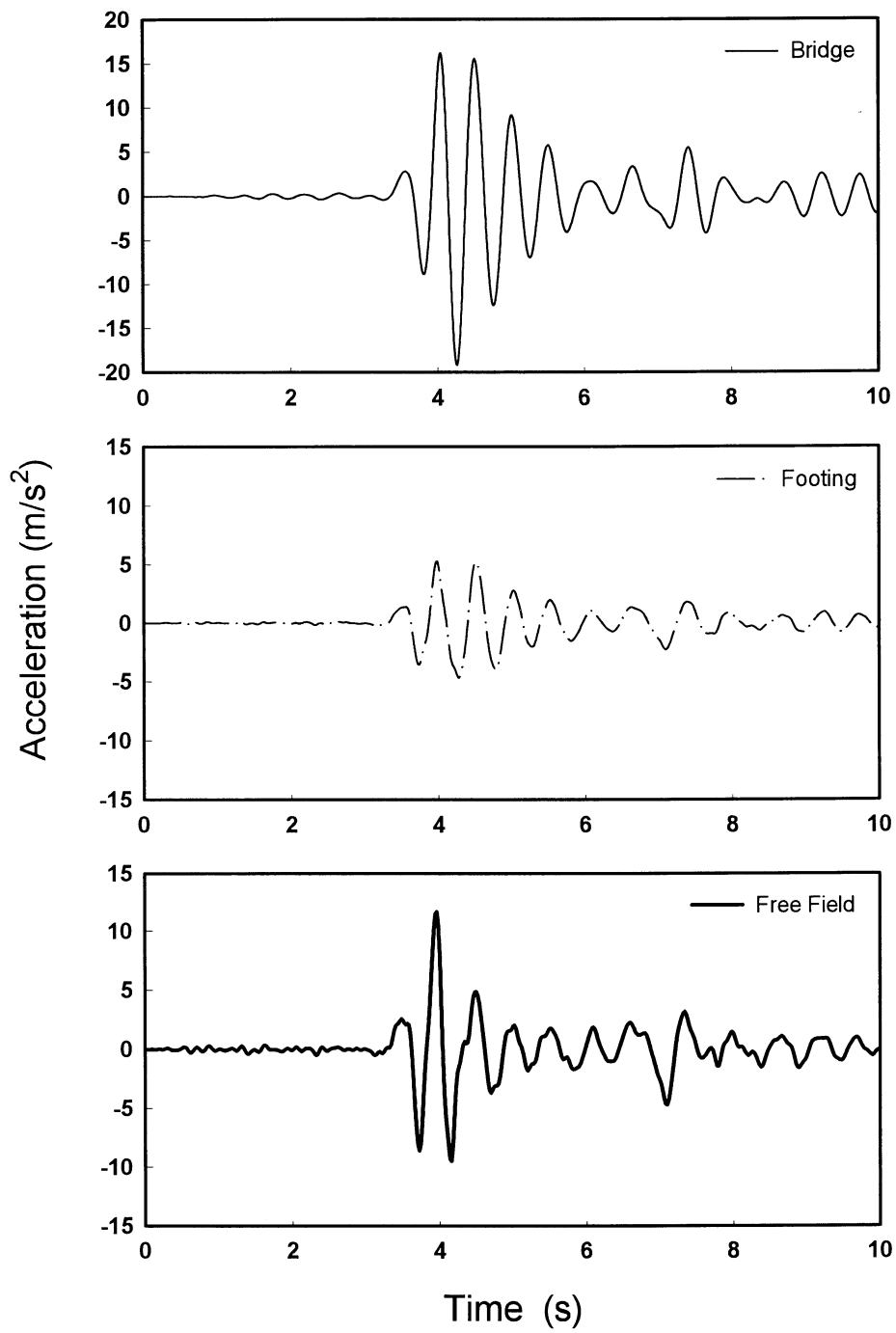
FIGURE A-52 Case B441: Acceleration histories for Pacoima, Northridge (1994) rock motion
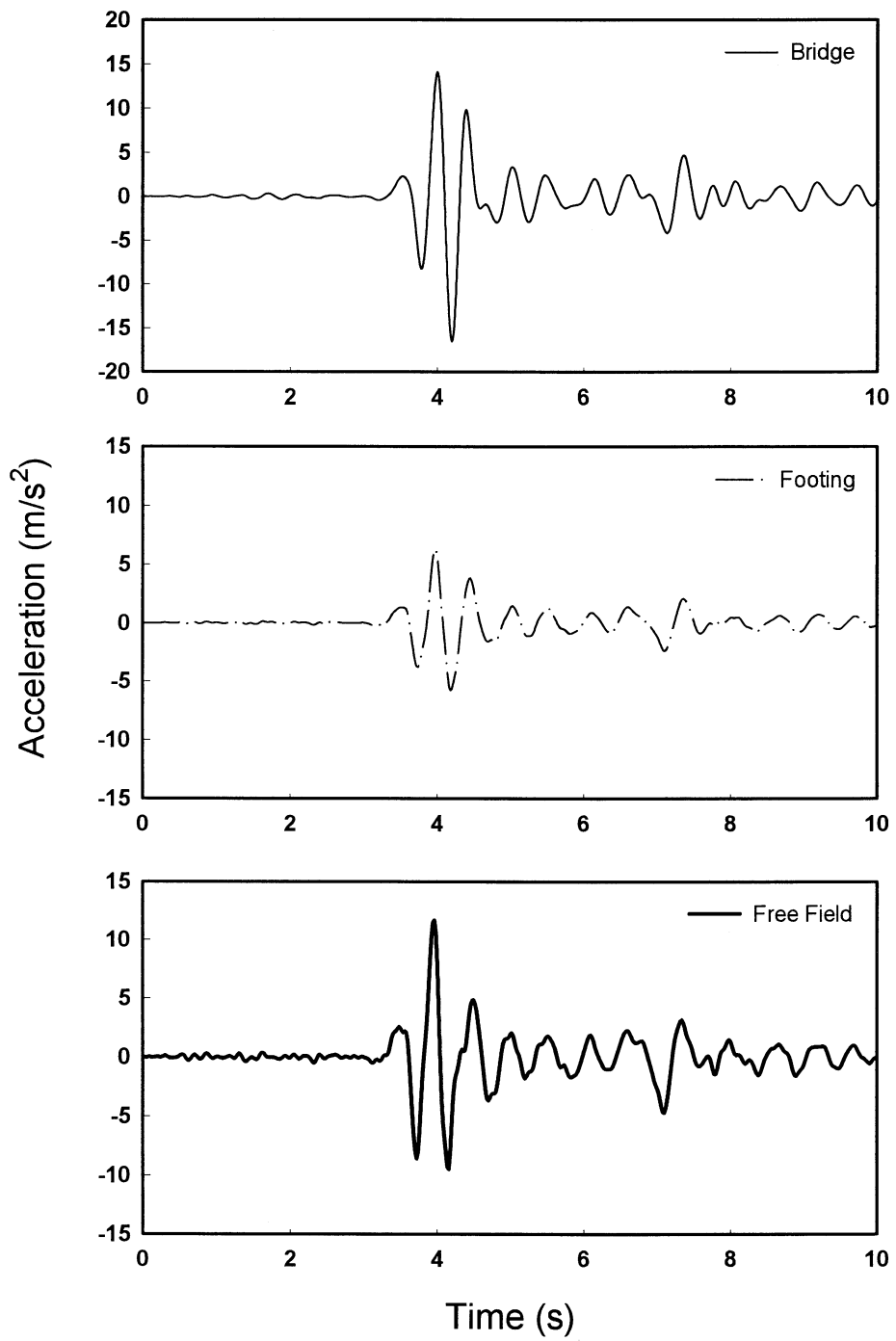
FIGURE A-53 Case B442: Acceleration histories for Pacoima, Northridge (1994) rock motion
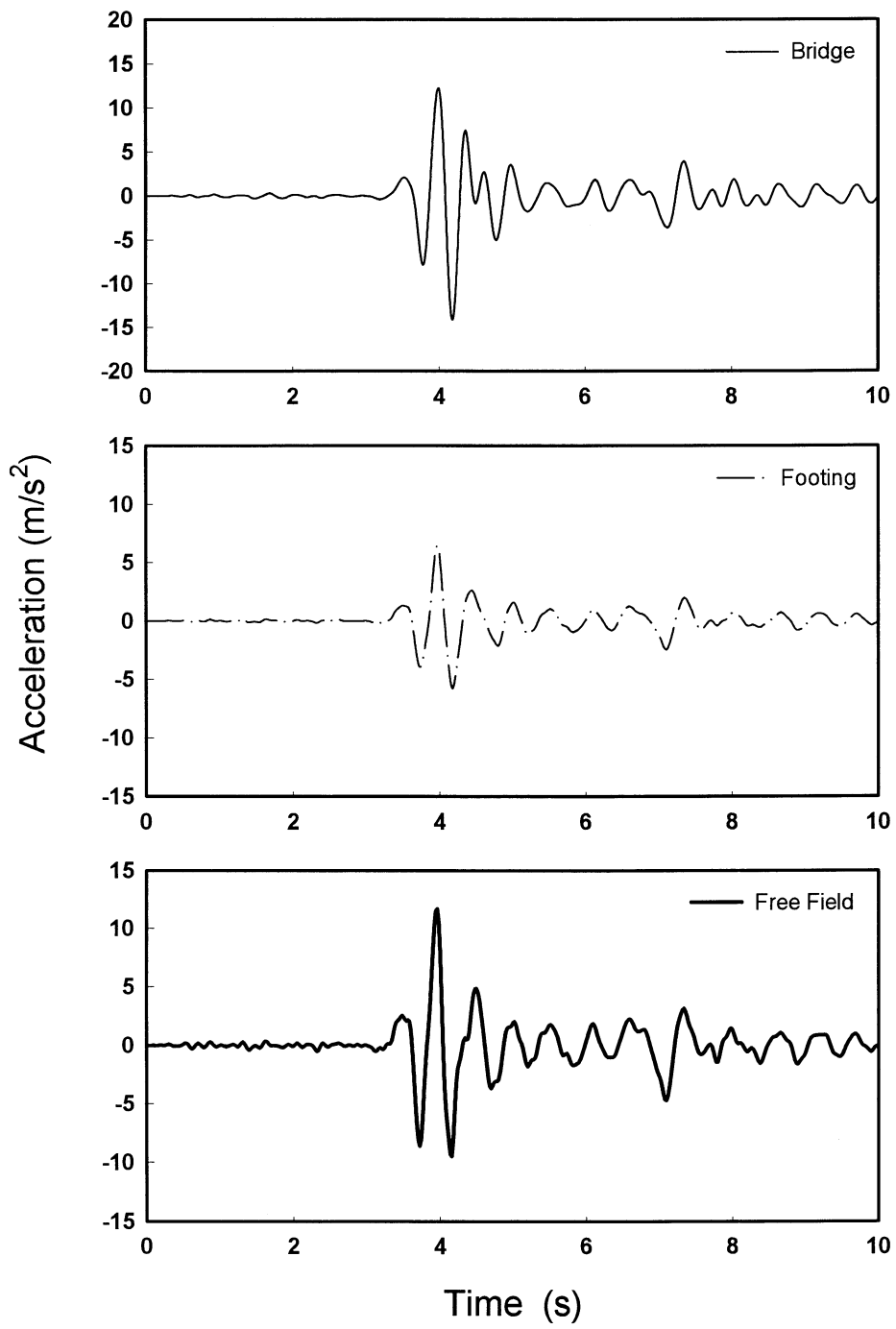
FIGURE A-54 Case B443: Acceleration histories for Pacoima, Northridge (1994) rock motion
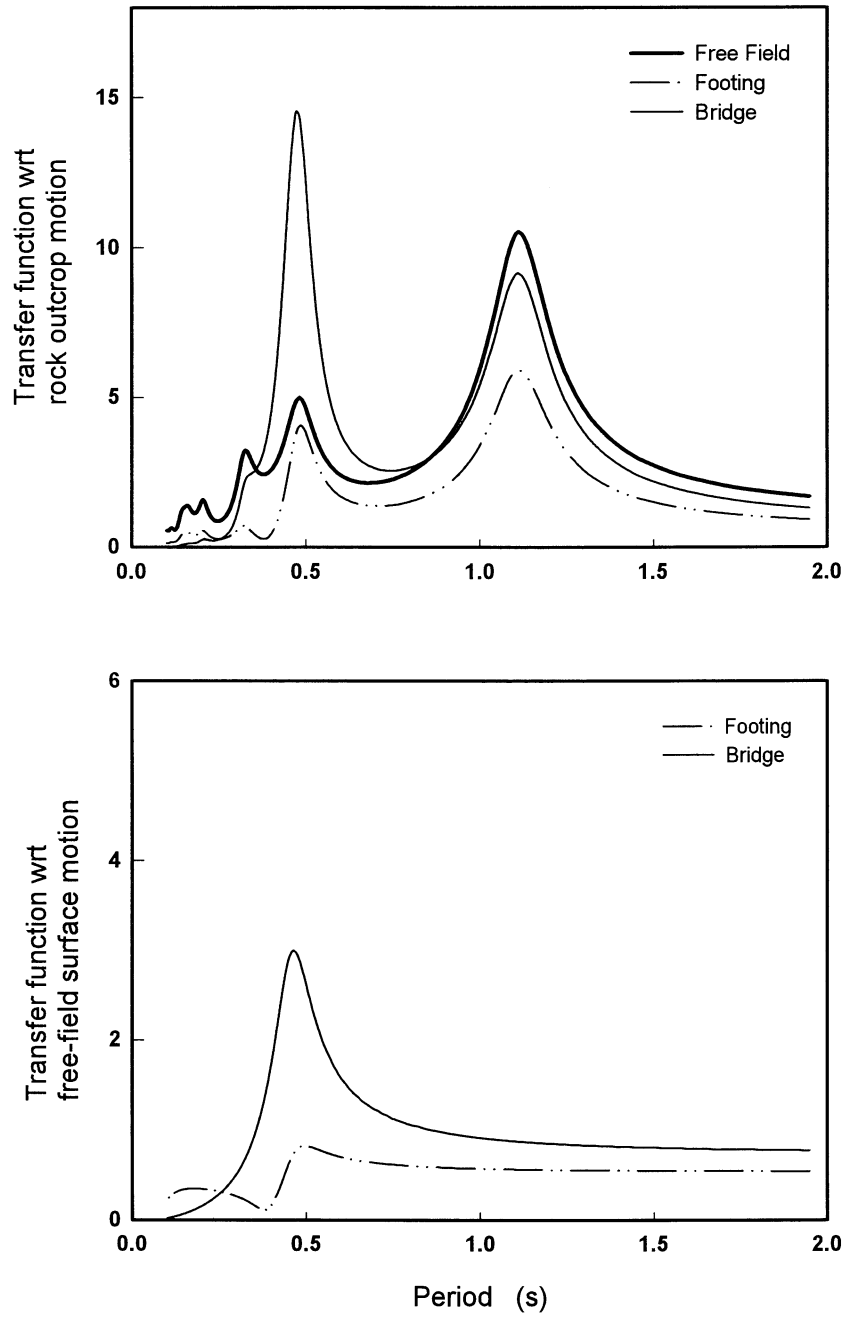
Deep Profile
H = 93 m
V_{S1} = 80 m/s
Rigid Rock
I_R = Infinite

Footing
D = 1.5 m
d = 1.5 m
R = 1.5 m

Column
H_c = 6 m
d_c = 1.3 m
E_c = 25 GPa
β = 5%
m_s = 350 Mg
No rotation at
column top

FIGURE A-55 Case A441: Harmonic Steady-State Transfer Functions
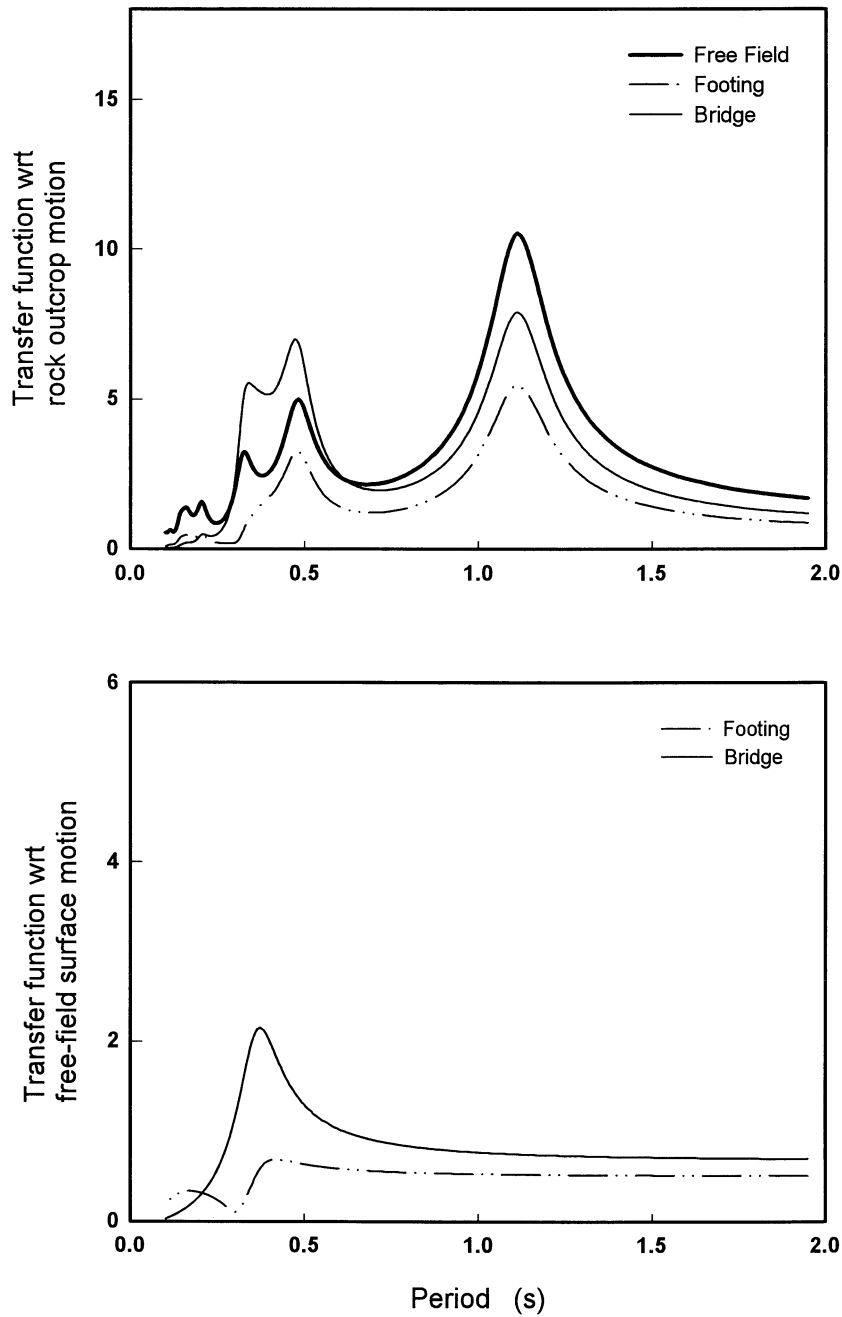
154

Deep Profile
H = 93 m
V_{S1} = 80 m/s
Rigid Rock
I_R = Infinite

Footing
D = 1.5 m
d = 1.5 m
R = 3 m

Column
H_c = 6 m
d_c = 1.3 m
E_c = 25 GPa
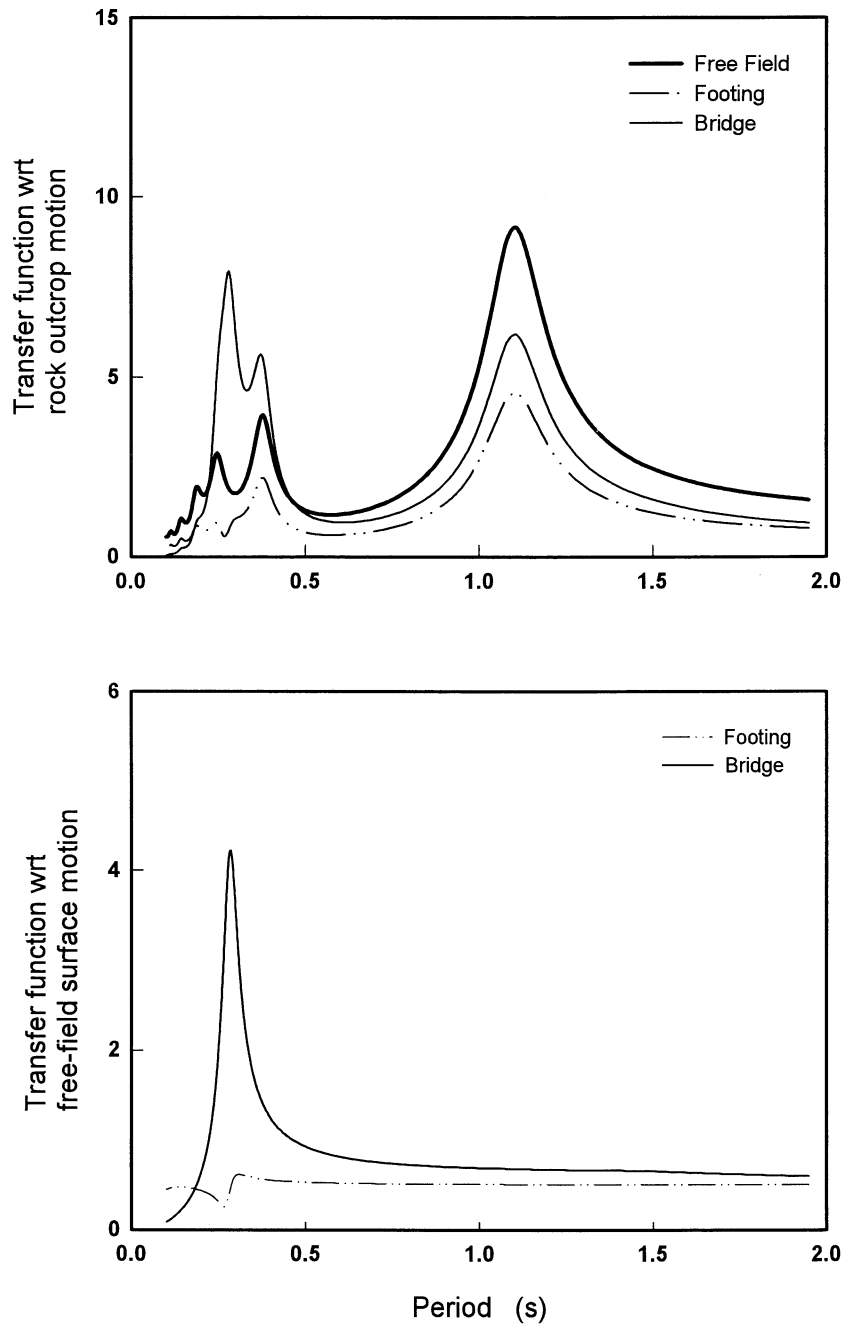β = 5%
m_s = 350 Mg
No rotation at column top

FIGURE A-56 Case A442: Harmonic Steady-State Transfer Functions
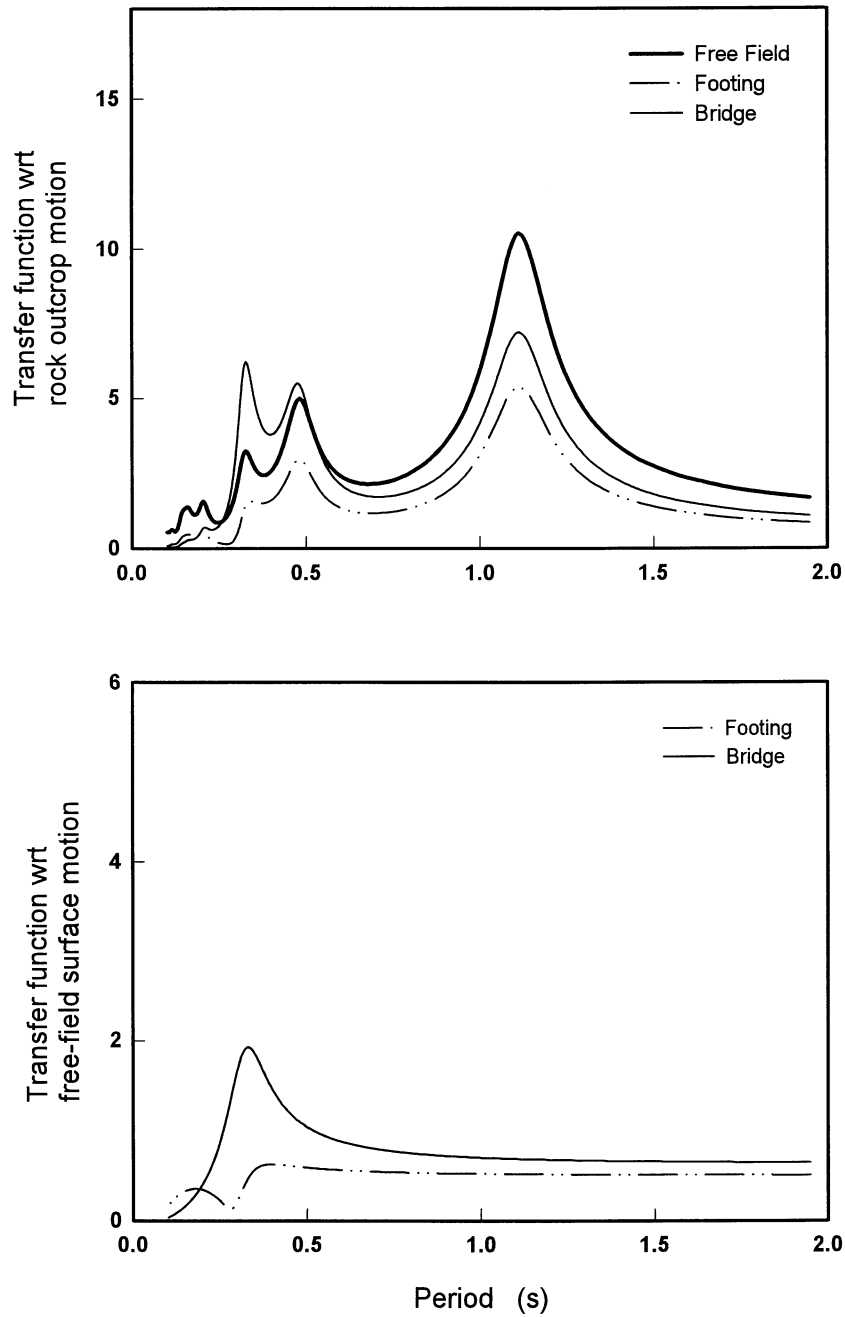
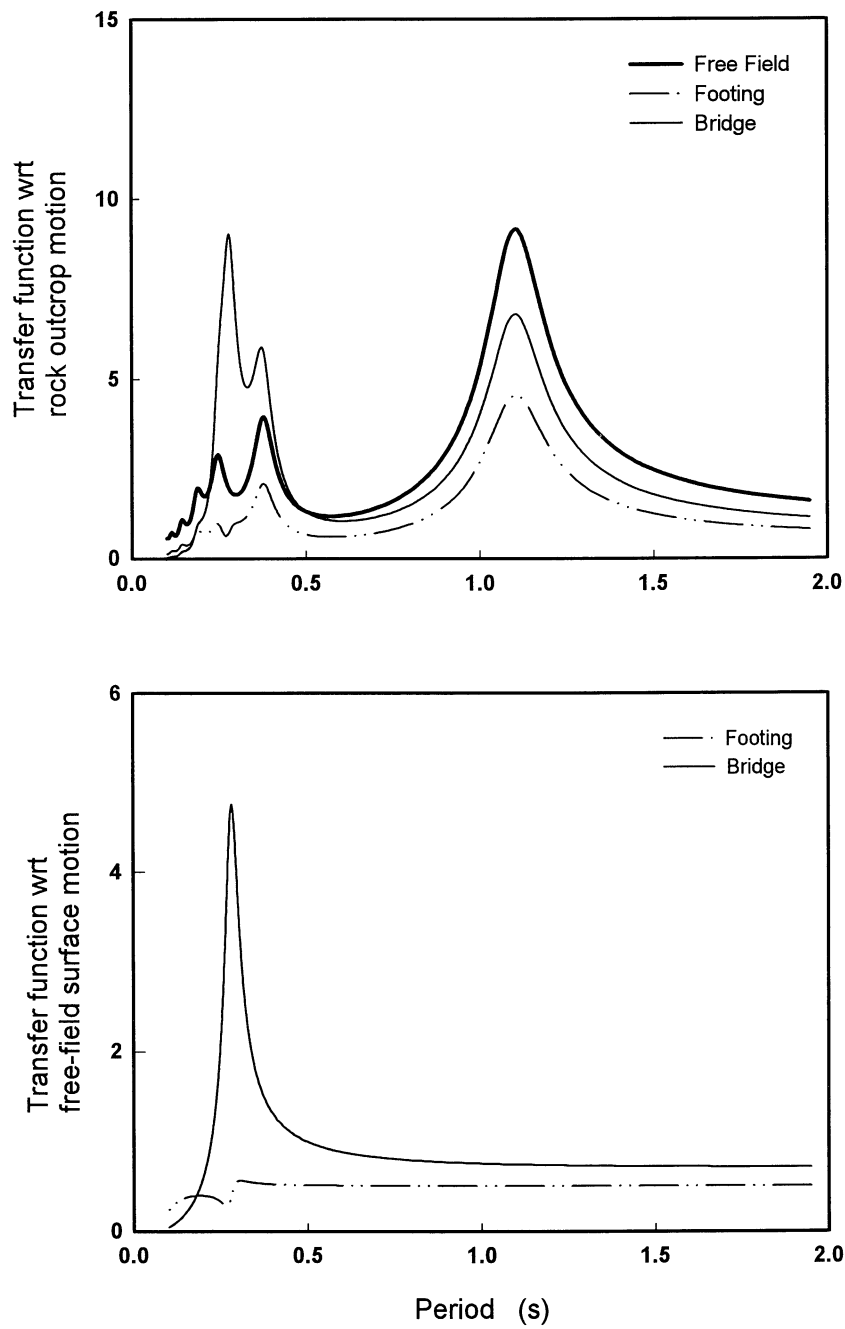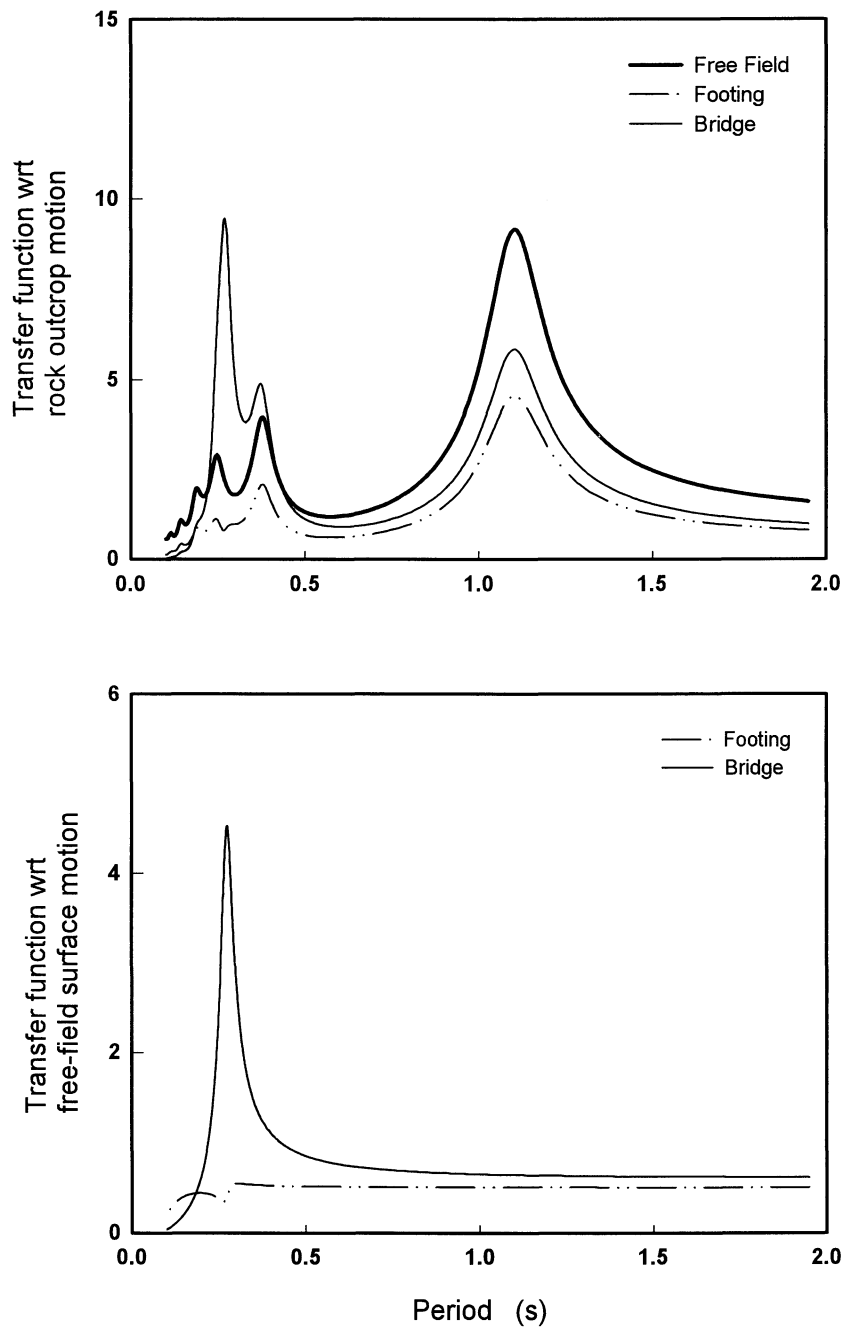**FIGURE A-57 Case A443: Harmonic Steady-State Transfer Functions**

Deep Profile
H = 93 m
V_{S1} = 80 m/s
Rigid Rock
I_R = Infinite

Footing
D = 3 m
d = 3 m
R = 3 m

Column
H_c = 6 m
d_c = 1.3 m
E_c = 25 GPa
β = 5%
m_s = 350 Mg
No rotation at column top
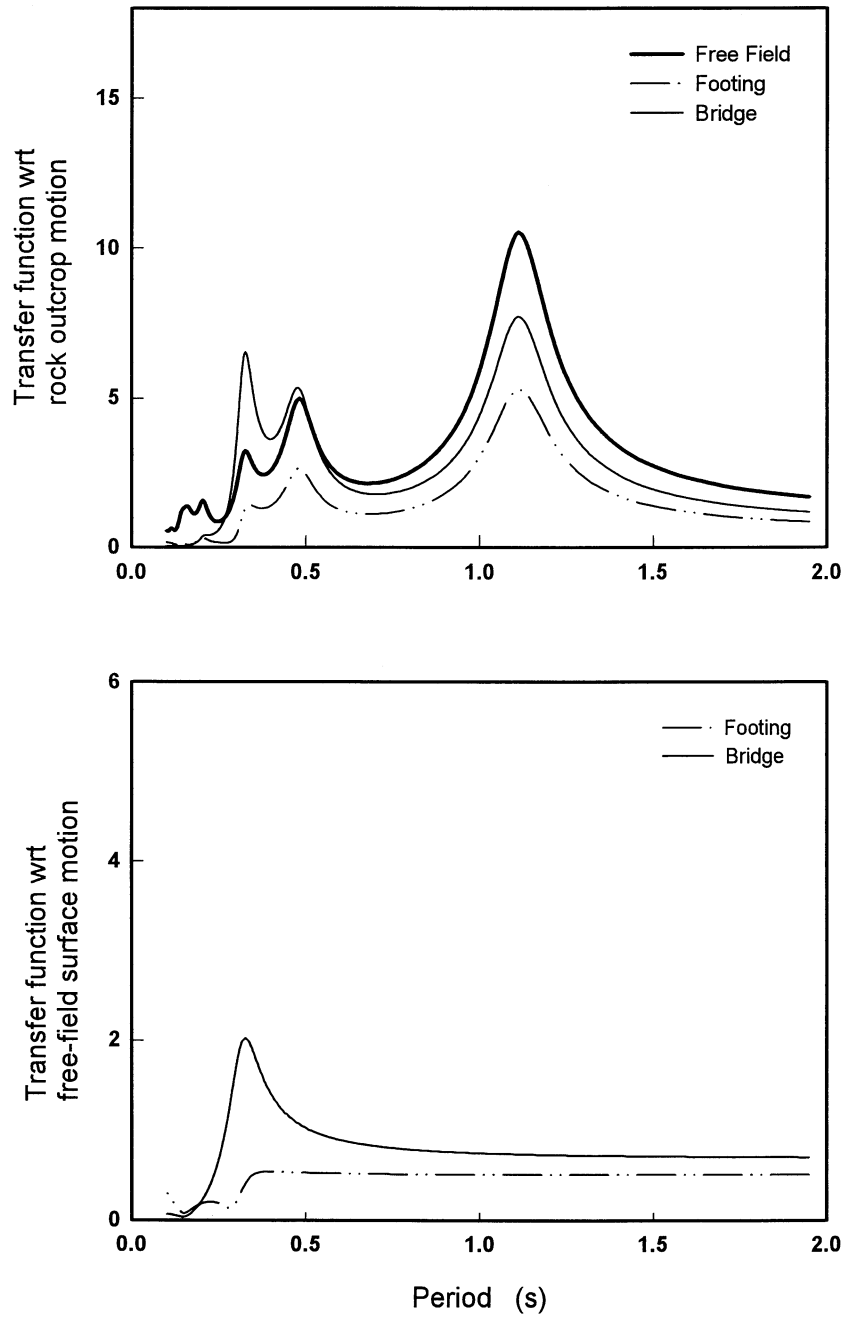
FIGURE A-58 Case A421: Harmonic Steady-State Transfer Functions

The figure contains two plots and a text box on the right side.

Top plot:
- Y-axis: Transfer function wrt rock outcrop motion (0 to 15)
- X-axis: 0.0 to 2.0
- Legend: Free Field, Footing, Bridge

Bottom plot:
- Y-axis: Transfer function wrt free-field surface motion (0 to 6)
- X-axis: Period (s), 0.0 to 2.0
- Legend: Footing, Bridge

Text box:

Deep Profile
H = 93 m
V_{S1} = 80 m/s
Rigid Rock
I_R = Infinite

Footing
D = 3 m
d = 3 m
R = 6 m

Column
H_c = 6 m
d_c = 1.3 m
E_c = 25 GPa
β = 5%
m_s = 350 Mg
No rotation at column top

FIGURE A-59 Case A422: Harmonic Steady-State Transfer Functions

Deep Profile
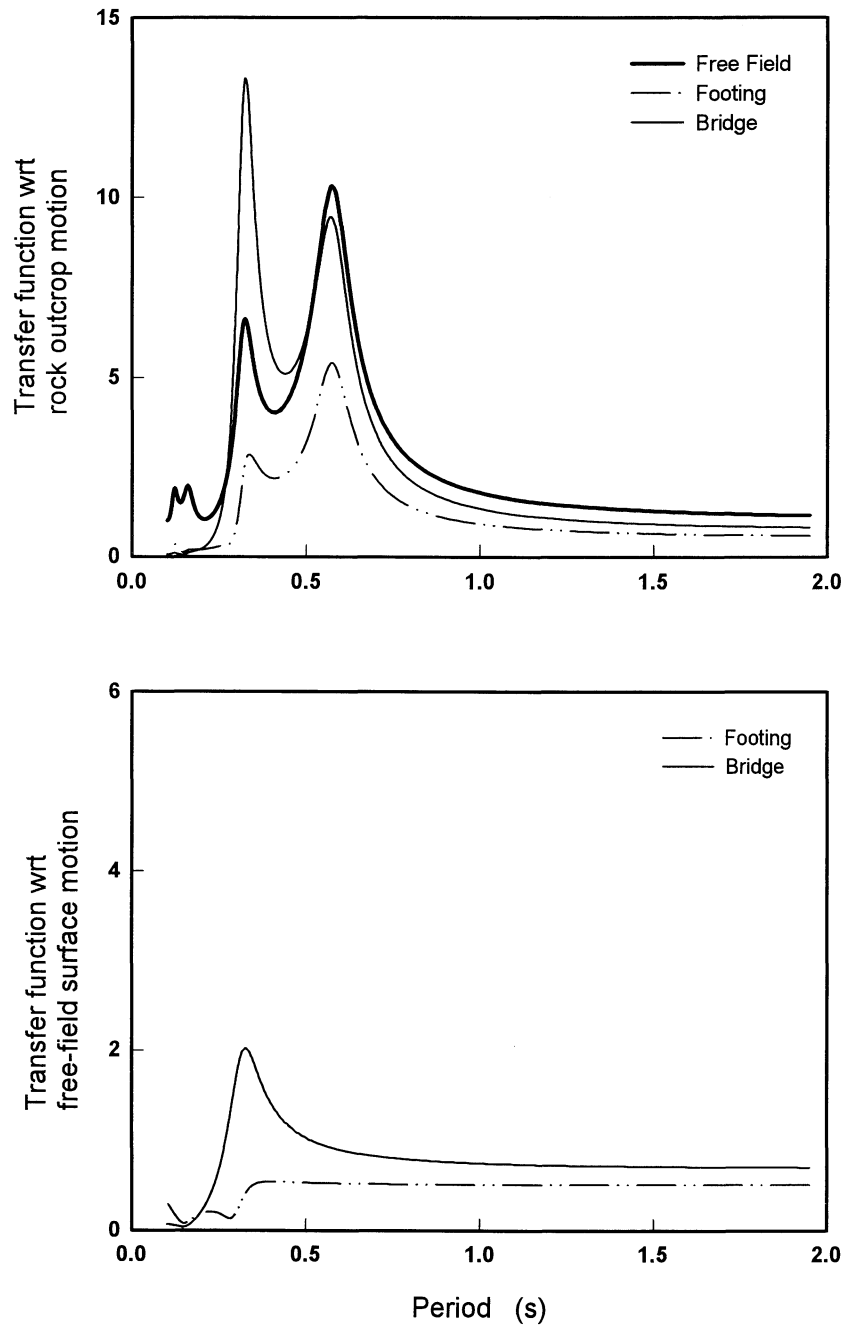H = 93 m
V_{S1} = 80 m/s
Rigid Rock
I_R = Infinite

Footing

D = 3 m
d = 3 m
R = 9 m

Column

H_c = 6 m
d_c = 1.3 m
E_c = 25 GPa
β = 5%
m_s = 350 Mg
No rotation at
column top
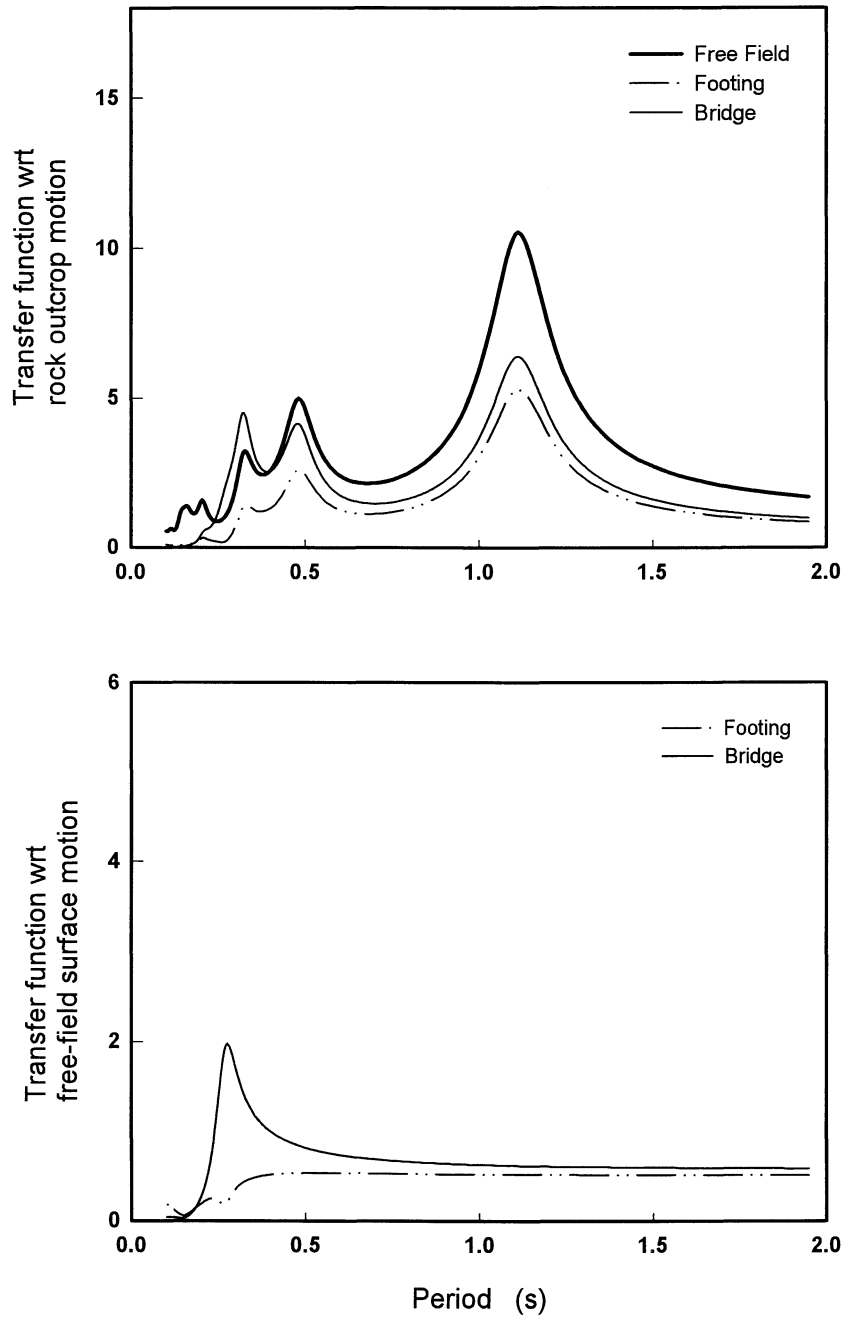
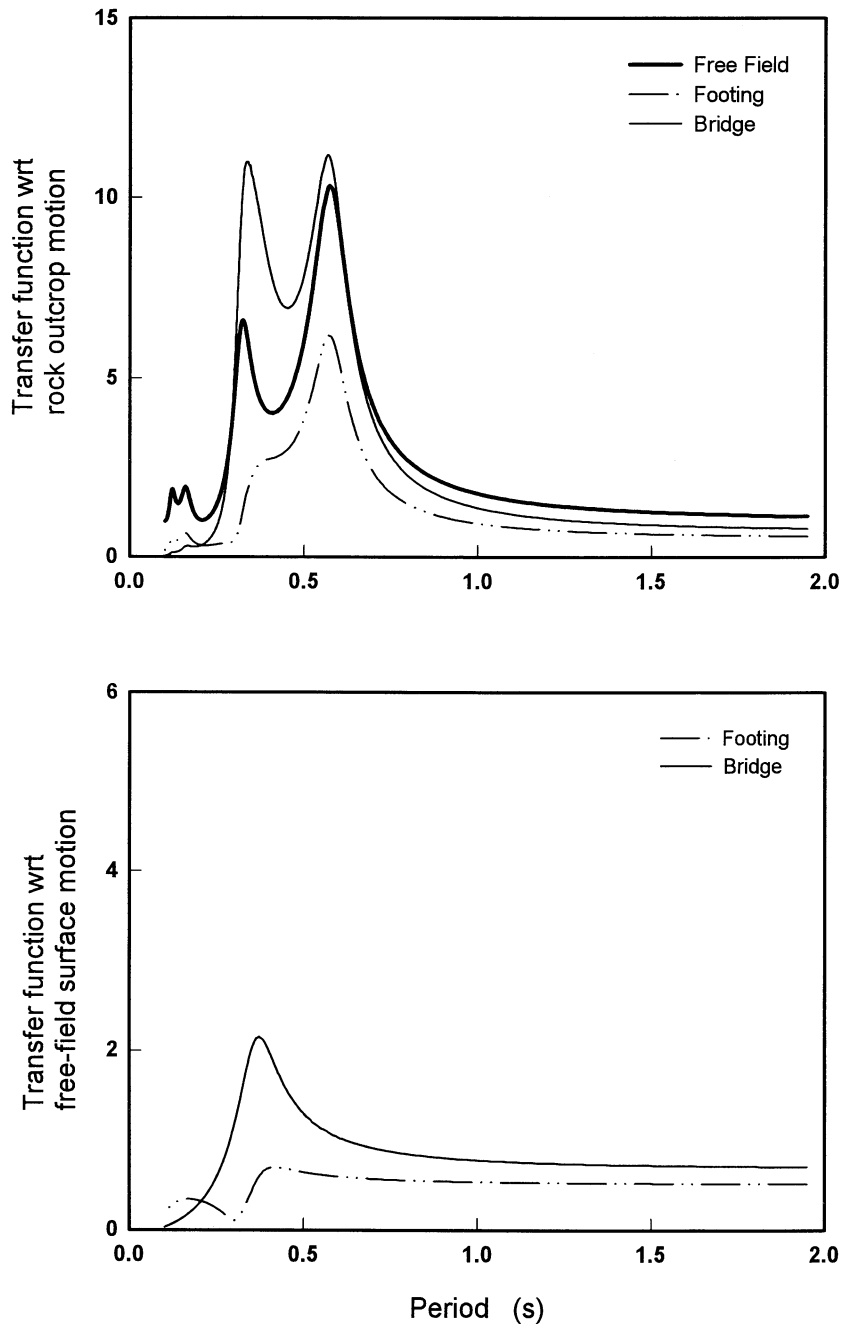**FIGURE A-60 Case A423: Harmonic Steady-State Transfer Functions**

159

The chart contains the following data and labels:

Upper plot (Transfer function wrt rock outcrop motion):
- Legend: Free Field, Footing, Bridge
- Y-axis: 0, 5, 10, 15
- X-axis: 0.0, 0.5, 1.0, 1.5, 2.0

Lower plot (Transfer function wrt free-field surface motion):
- Legend: Footing, Bridge
- Y-axis: 0, 2, 4, 6
- X-axis: 0.0, 0.5, 1.0, 1.5, 2.0
- X-axis label: Period (s)

Side panel:

Deep Profile
H = 93 m
V_{S1} = 160 m/s
Rigid Rock
I_R = Infinite

Footing
D = 1.5 m
d = 1.5 m
R = 1.5 m

Column
H_c = 6 m
d_c = 1.3 m
E_c = 25 GPa
β = 5%
m_s = 350 Mg
No rotation at column top

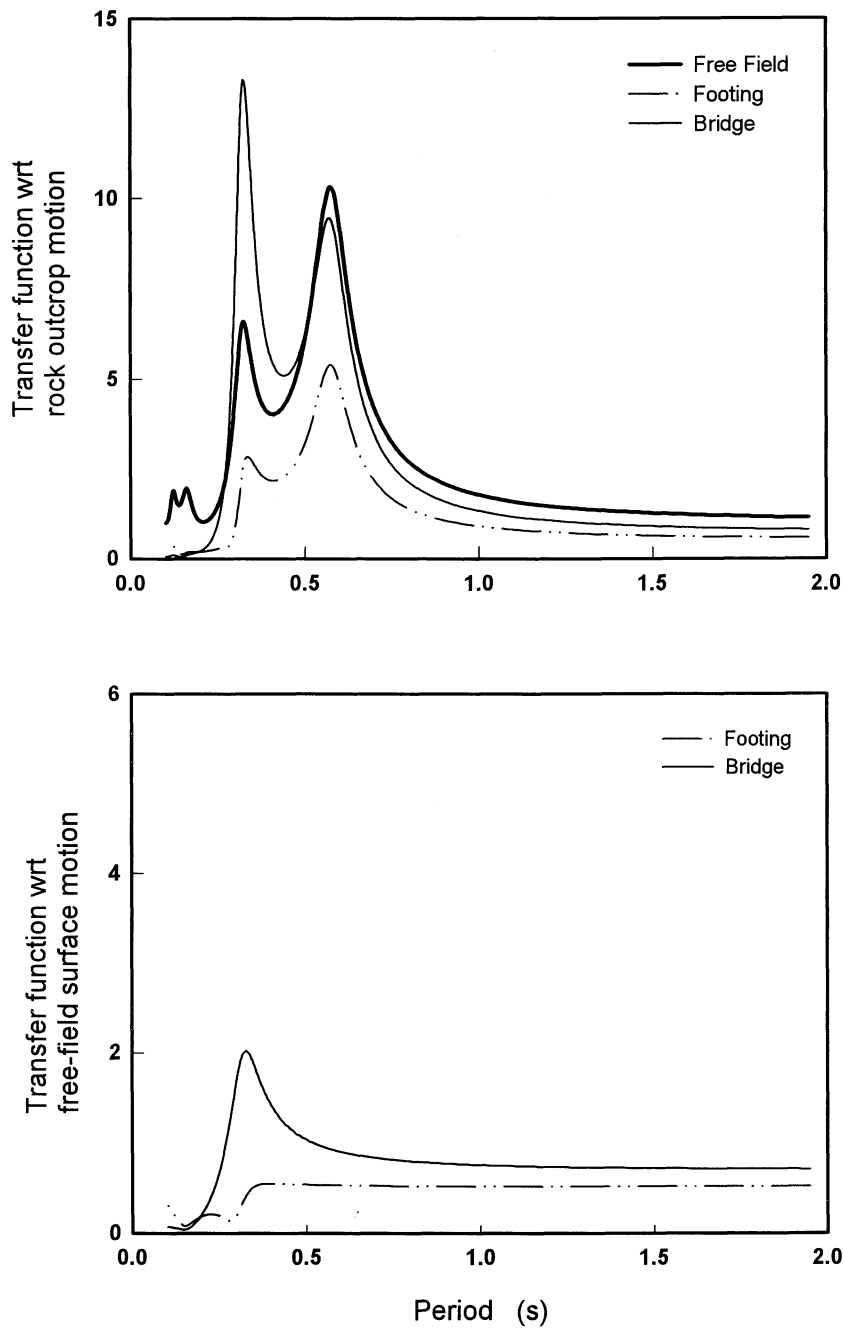**FIGURE A-61 Case A241: Harmonic Steady-State Transfer Functions**
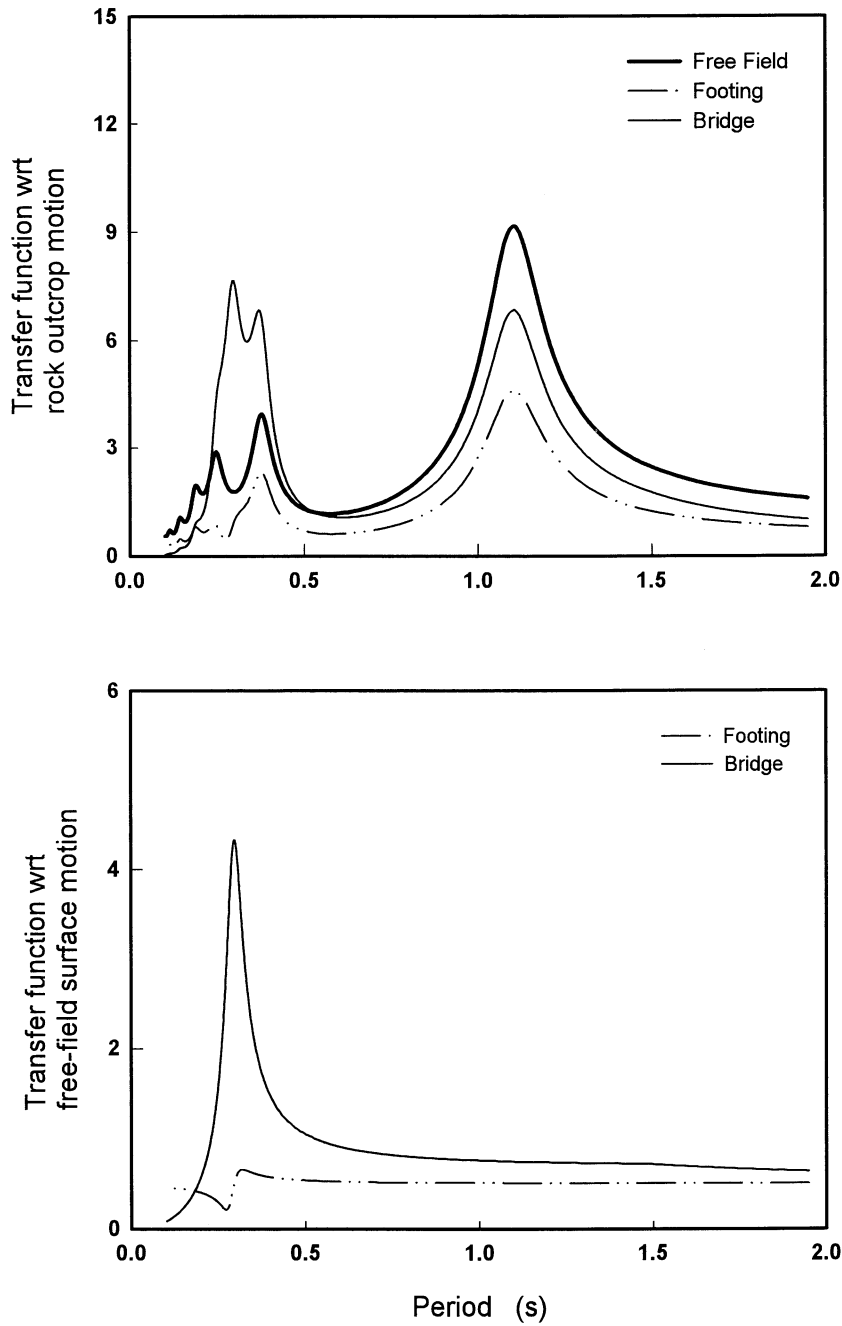
160

The chart contains two graphs with the following data:

Top graph:
- Y-axis: Transfer function wrt rock outcrop motion (0 to 15)
- X-axis: Period (0.0 to 2.0)
- Legend: Free Field, Footing, Bridge

Bottom graph:
- Y-axis: Transfer function wrt free-field surface motion (0 to 6)
- X-axis: Period (s) (0.0 to 2.0)
- Legend: Footing, Bridge

Side box:

Deep Profile
H = 93 m
V_{S1} = 160 m/s
Rigid Rock
I_R = Infinity

Footing
D = 1.5 m
d = 1.5 m
R = 3 m

Column
Hc = 6 m
dc = 1.3 m
Ec = 25 GPa
β = 5%
m_s = 350 Mg
No rotation at column top

FIGURE A-62 Case A242: Harmonic Steady-State Transfer Functions

Deep Profile
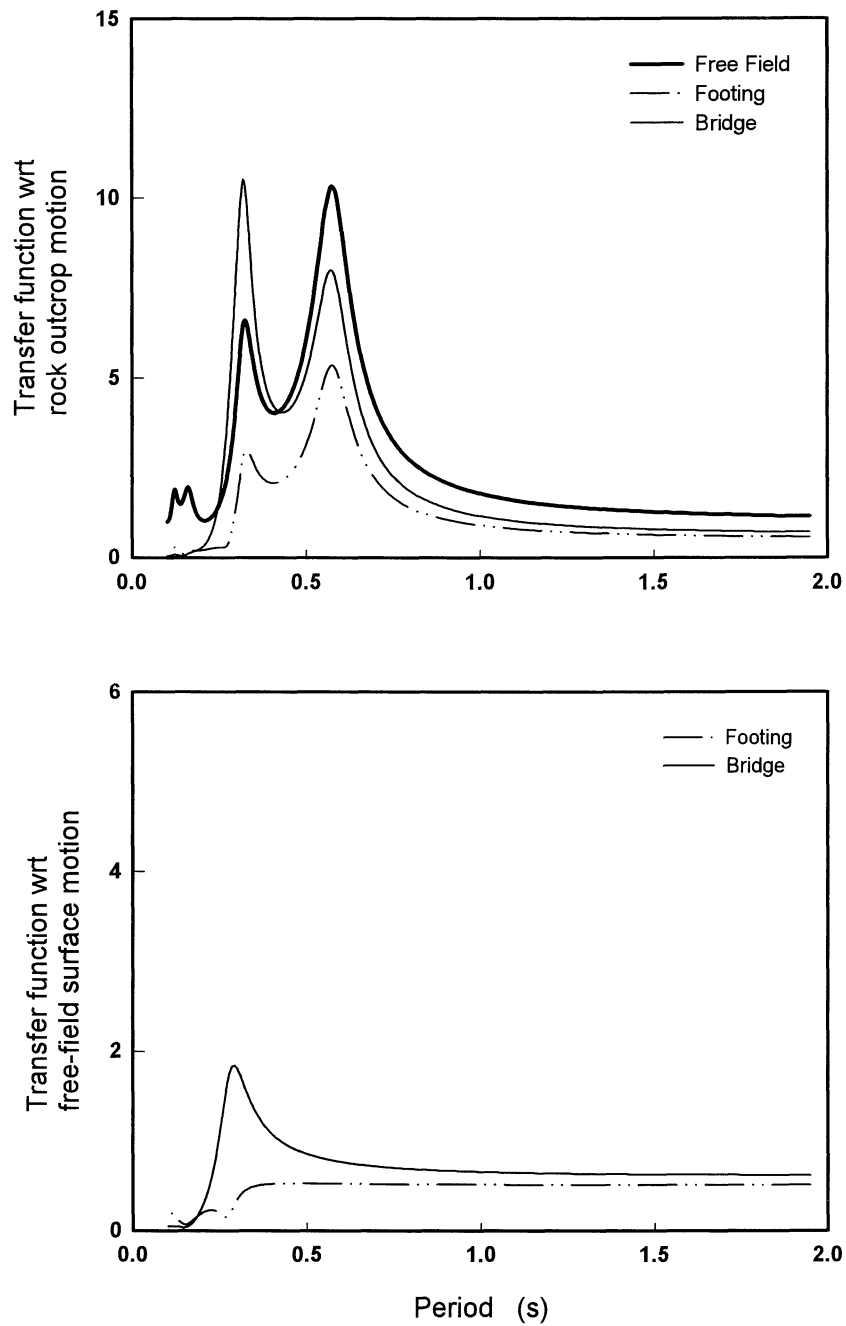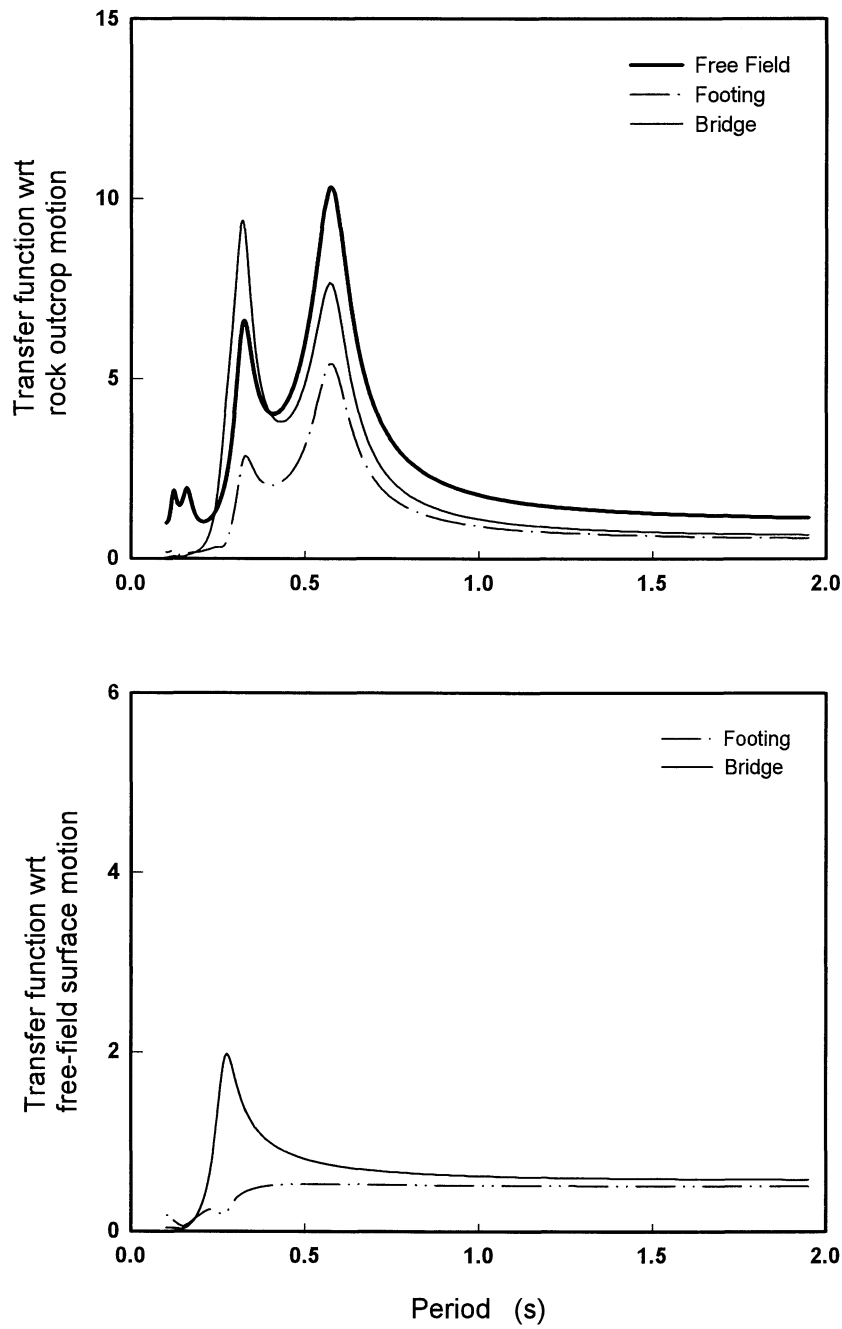H = 93 m
V_{S1} = 160 m/s
Rigid Rock
I_R = Infinite

Footing

D = 1.5 m
d = 1.5 m
R = 4.5 m

Column

H_c = 6 m
d_c = 1.3 m
E_c = 25 GPa
β = 5%
m_s = 350 Mg
No rotation at
column top

FIGURE A-63 Case A243: Harmonic Steady-State Transfer Functions

Upper plot legend:
- Free Field
- Footing
- Bridge

Y-axis: Transfer function wrt rock outcrop motion

Lower plot legend:
- Footing
- Bridge

Y-axis: Transfer function wrt free-field surface motion

X-axis: Period (s)

Side panel:

Deep Profile
H = 83.5 m
V_{S1} = 160 m/s
Rigid Rock
I_R = Infinite

Footing
D = 3 m
d = 3 m
R = 3 m

Column
H_c = 6 m
d_c = 1.3 m
E_c = 25 GPa
β = 5%
m_s = 350 Mg
No rotation at
column top

FIGURE A-64 Case A221: Harmonic Steady-State Transfer Functions

163

Deep Profile
H = 93 m
V_{S1} = 160 m/s
Rigid Rock
I_R = Infinity

Footing
D = 3 m
d = 3 m
R = 6 m

Column
H_c = 6 m
d_c = 1.3 m
E_c = 25 GPa
β = 5%
m_s = 350 Mg
No rotation at column top

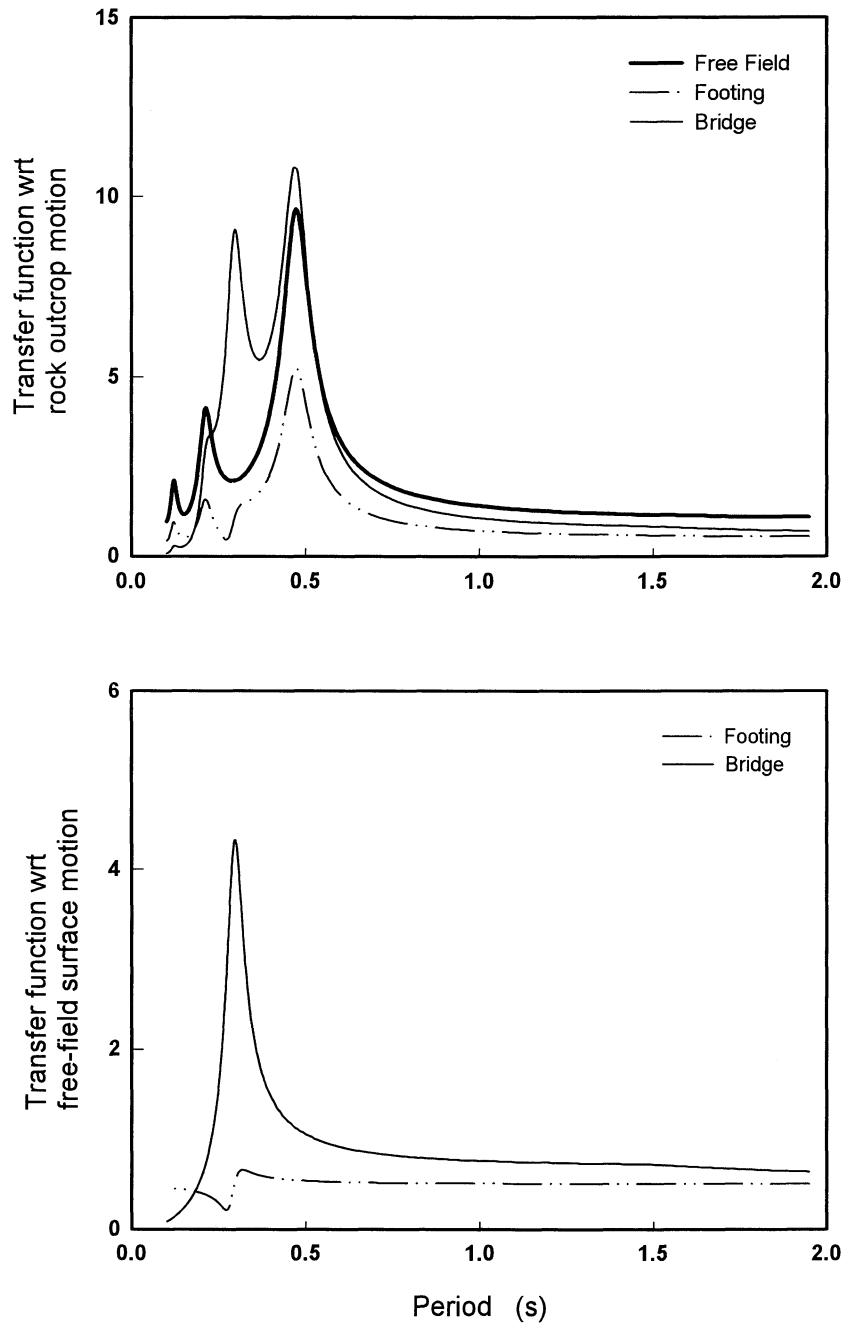**FIGURE A-65 Case A222: Harmonic Steady-State Transfer Functions**
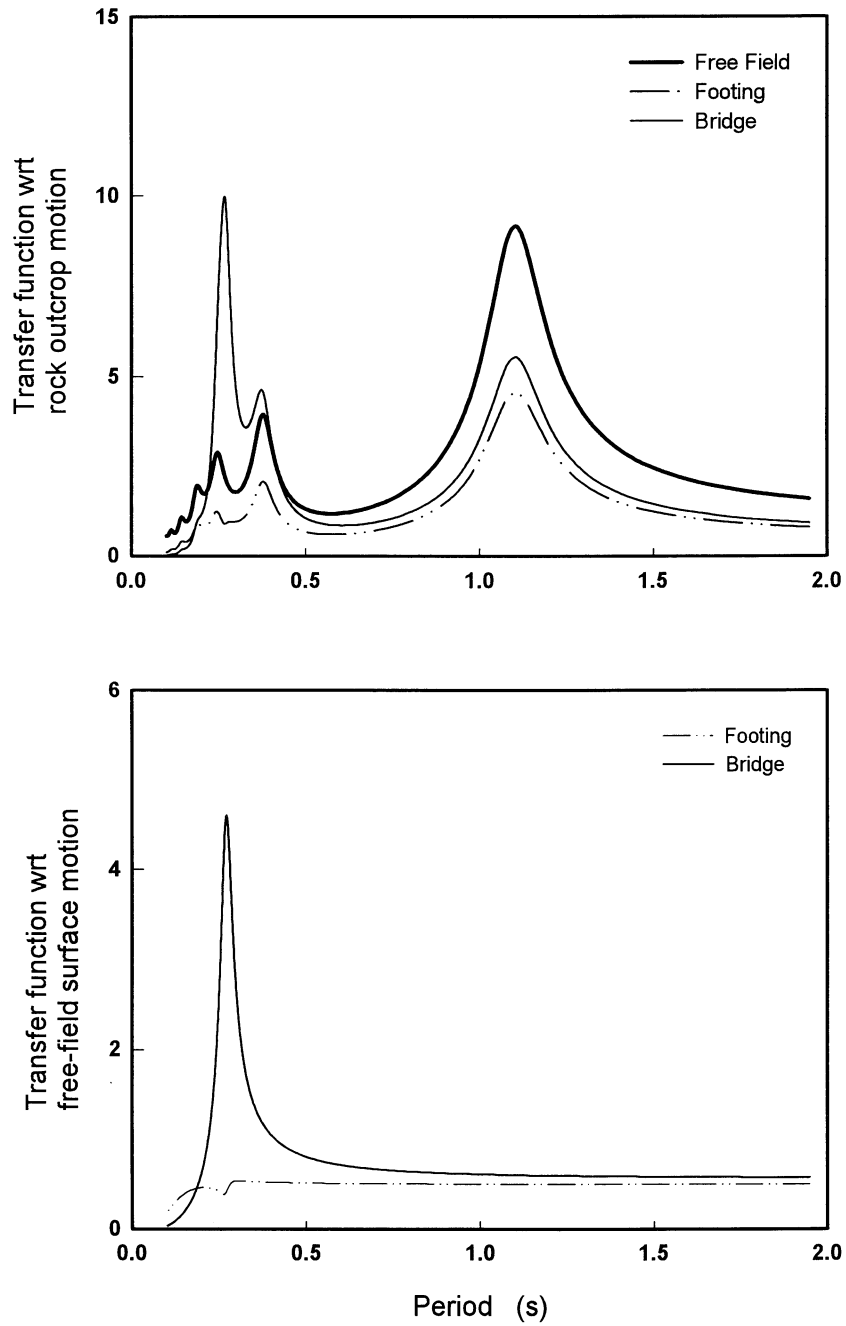
Deep Profile

H = 93 m
V_{S1} = 160 m/s
Rigid Rock
I_R = Infinite

Footing

D = 3 m
d = 3 m
R = 9 m

Column

H_c = 6 m
d_c = 1.3 m
E_c = 25 GPa
β = 5%
m_s = 350 Mg
No rotation at
column top

FIGURE A-66 Case A223: Harmonic Steady-State Transfer Functions

Shallow Profile
H = 39.5 m
V_{S1} = 80 m/s
Rigid Rock
I_R = Infinite

Footing
D = 1.5 m
d = 1.5 m
R = 1.5 m

Column
H_c = 6 m
d_c = 1.3 m
E_c = 25 GPa
β = 5%
m_s = 350 Mg
No rotation at
column top

FIGURE A-67 Case B441: Harmonic Steady-State Transfer Functions

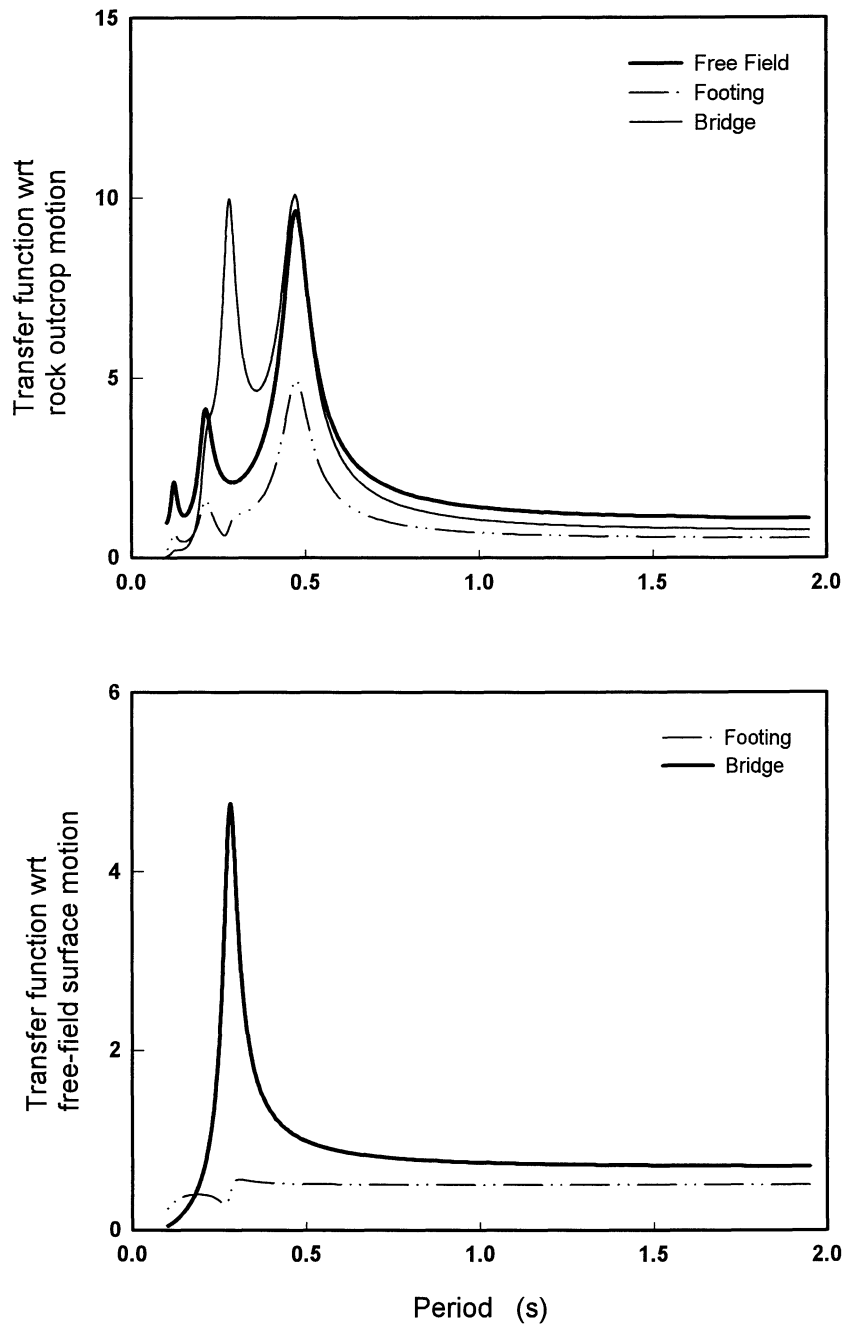**FIGURE A-68 Case B442: Harmonic Steady-State Transfer Functions**
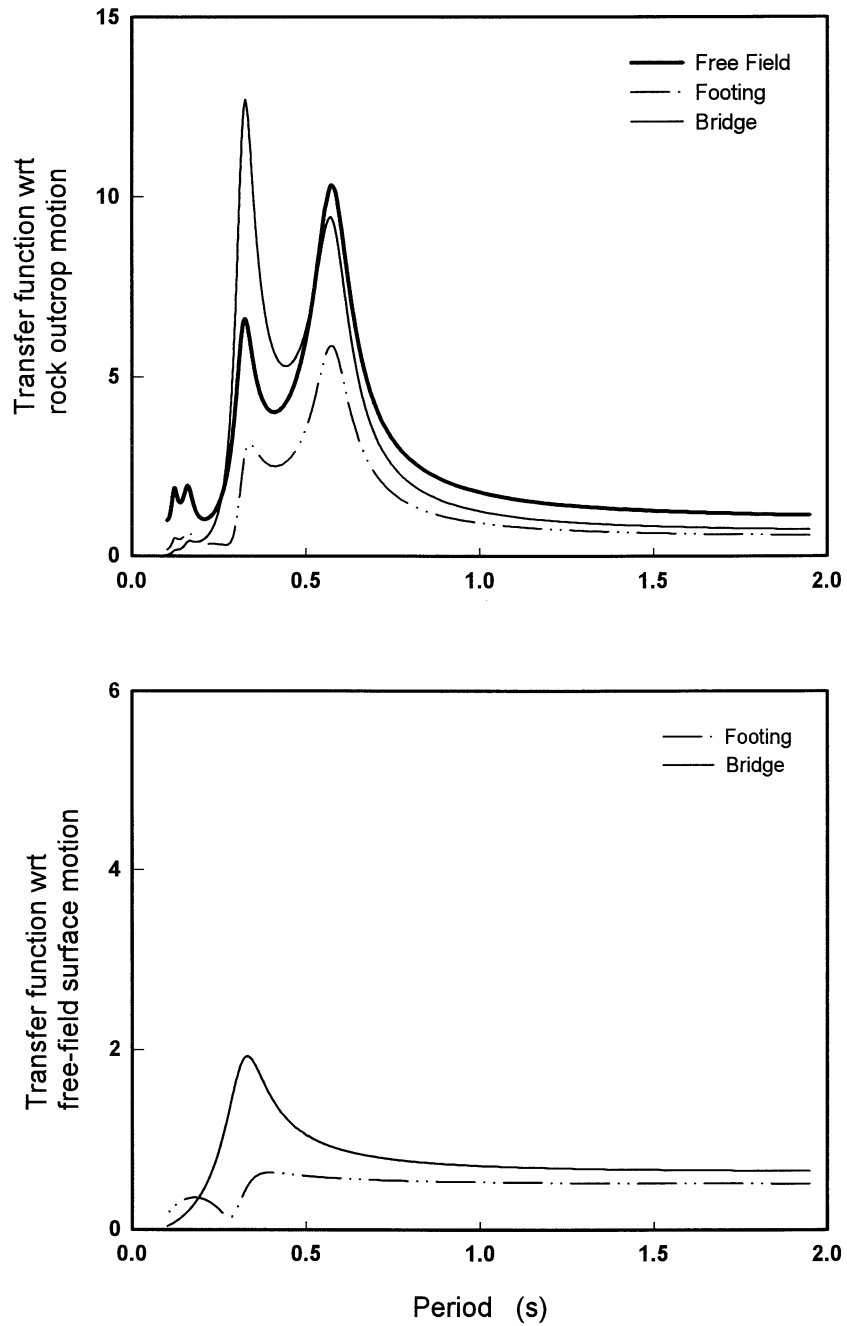
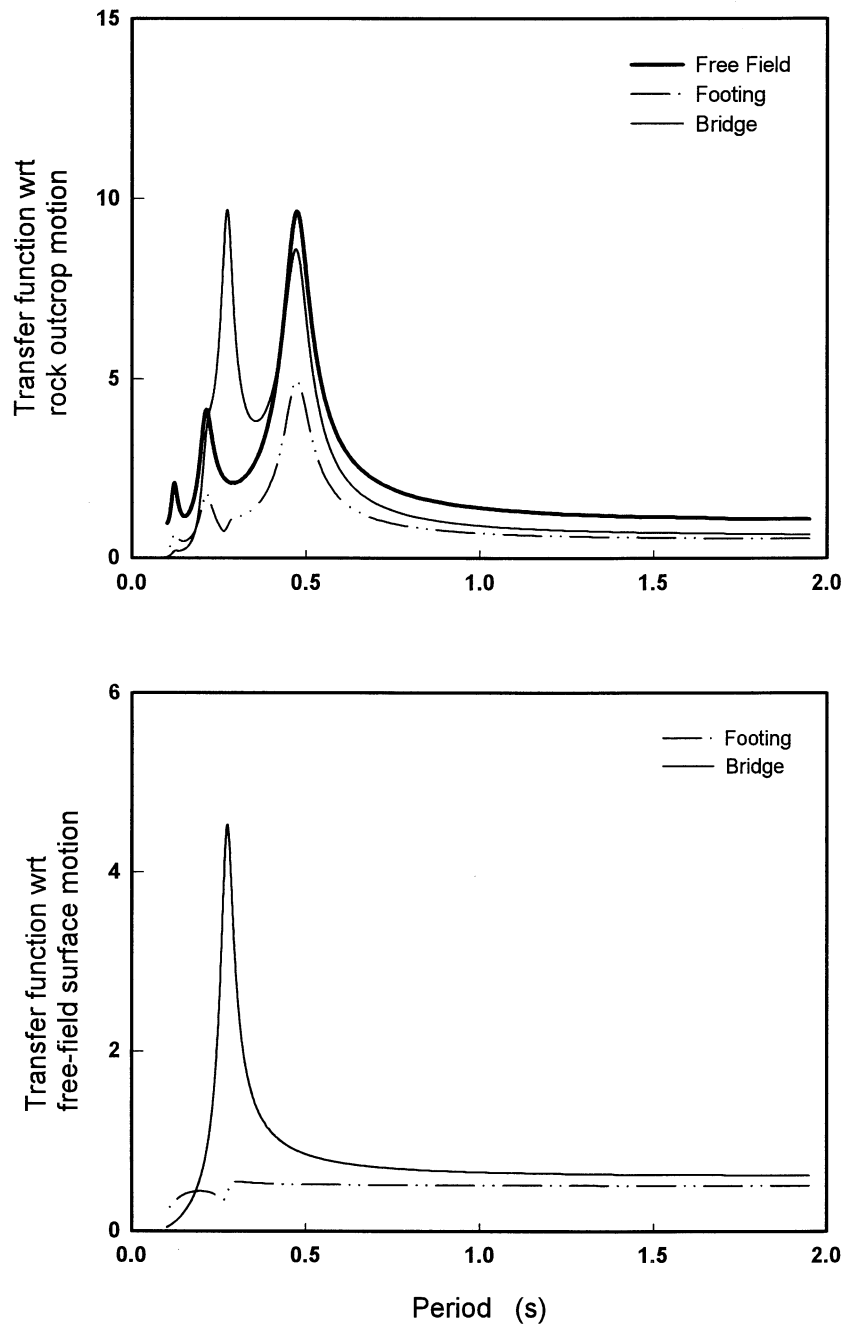**Shallow Profile**
H = 39.5 m
V_{S1} = 80 m/s
Rigid Rock
I_R = Infinite

Footing
D = 1.5 m
d = 1.5 m
R = 4.5 m

Column
H_c = 6 m
d_c = 1.3 m
E_c = 25 GPa
β = 5%
m_s = 350 Mg
No rotation at column top

FIGURE A-69 Case B443: Harmonic Steady-State Transfer Functions

Shallow Profile
H = 39.5 m
V_{S1} = 80 m/s
Rigid Rock
I_R = Infinite

Footing
D = 3 m
d = 3 m
R = 3 m

Column
H_c = 6 m
d_c = 1.3 m
E_c = 25 GPa
β = 5%
m_s = 350 Mg
No Rotation at
column top

FIGURE A-70 Case B421: Harmonic Steady-State Transfer Functions

Shallow Profile
H = 39.5 m
V_{S1} = 80 m/s
Rigid Rock
I_R = Infinite

Footing
D = 3 m
d = 3 m
R = 6 m

Column
H_c = 6 m
d_c = 1.3 m
E_c = 25 GPa
β = 5%
m_s = 350 Mg
No rotation at column top

FIGURE A-71 Case B422: Harmonic Steady-State Transfer Functions

FIGURE A-72 Case B423: Harmonic Steady-State Transfer Functions
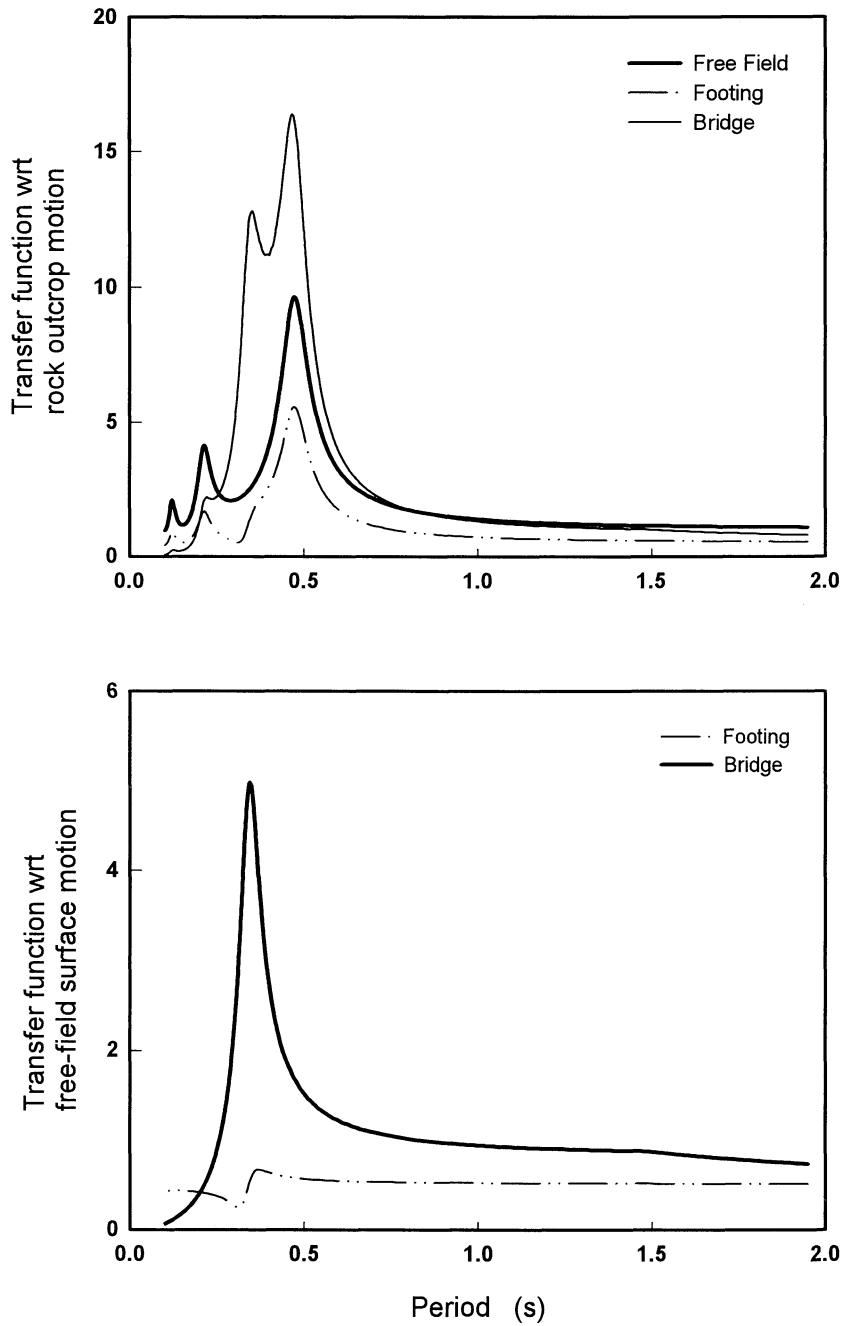
Shallow Profile
H = 39.5 m
V_{S1} = 160 m/s
Rigid Rock
I_R = Infinite

Footing
D = 1.5 m
d = 1.5 m
R = 1.5 m

Column
H_c = 6 m
d_c = 1.3 m
E_c = 25 GPa
β = 5%
m_s = 350 Mg
No rotation at
column top

FIGURE A-73 Case B241: Harmonic Steady-State Transfer Functions

FIGURE A-74 Case B242: Harmonic Steady-State Transfer Functions

173

Shallow Profile
H = 39.5 m
V_{S1} = 160 m/s
Rigid Rock
I_R = Infinite

Footing
D = 1.5 m
d = 1.5 m
R = 4.5 m

Column
H_c = 6 m
d_c = 1.3 m
E_c = 25 GPa
β = 5%
m_s = 350 Mg
No rotation at
column top
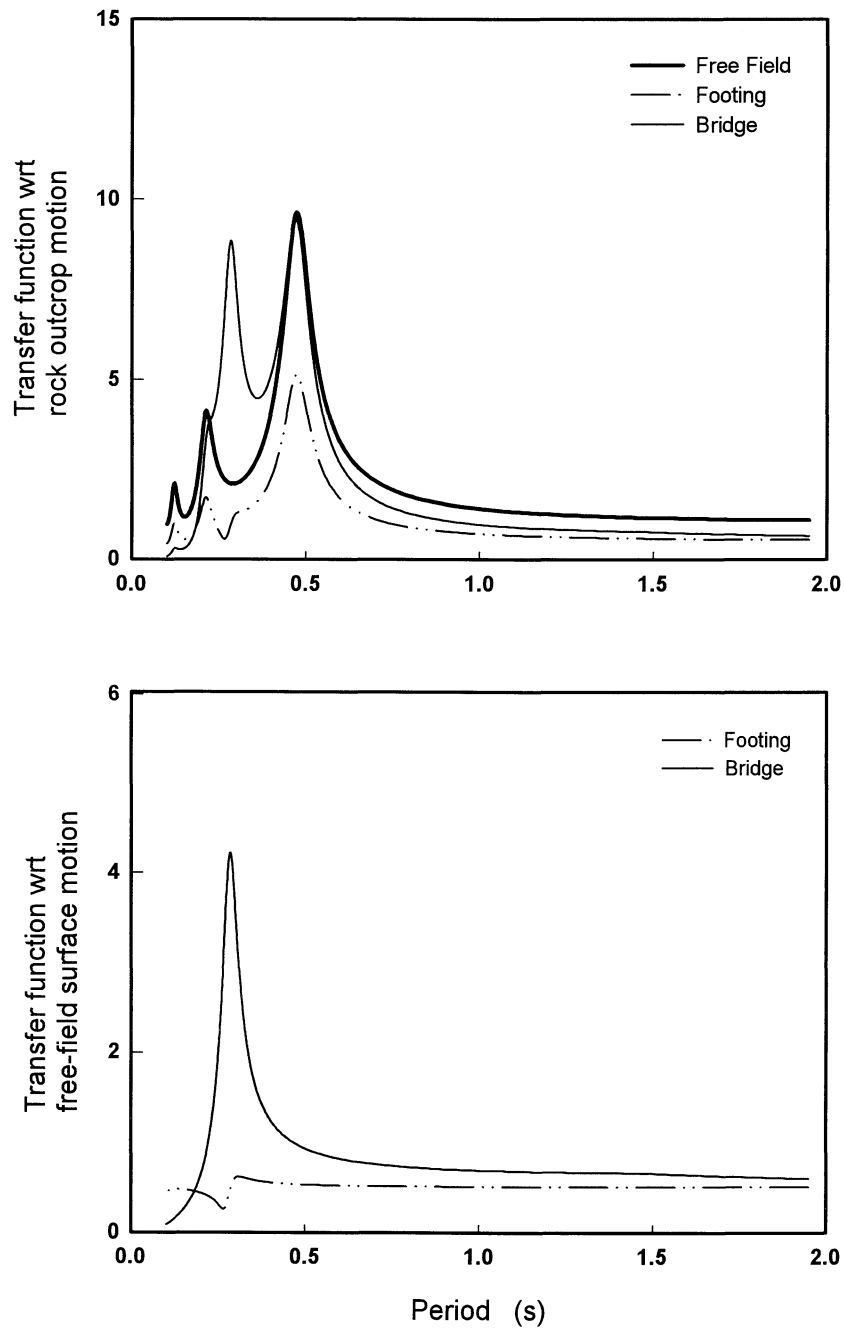
FIGURE A-75 Case B243: Harmonic Steady-State Transfer Functions

Transfer function wrt rock outcrop motion

15

10

5

0

Free Field
Footing
Bridge

0.0   0.5   1.0   1.5   2.0

Transfer function wrt free-field surface motion

6

4

2

0

Footing
Bridge

0.0   0.5   1.0   1.5   2.0

Period (s)

Shallow Profile
H = 39.5 m
V_{S1} = 160 m/s
Rigid Rock
I_R = Infinite

Footing
D = 3 m
d = 3 m
R = 3 m

Column
H_c = 6 m
d_c = 1.3 m
E_c = 25 GPa
β = 5%
m_s = 350 Mg
No rotation at column top

FIGURE A-76 Case B221: Harmonic Steady-State Transfer Functions

Shallow Profile

H = 39.5 m

V_{S1} = 160 m/s

Rigid Rock

I_R = Infinite

Footing

D = 3 m

d = 3 m

R = 6 m

Column

H_c = 6 m

d_c = 1.3 m

E_c = 25 GPa

β = 5%

m_s = 350 Mg

No Rotation at column top

FIGURE A-77 Case B222: Harmonic Steady-State Transfer Functions

Shallow Profile
H = 39.5 m
V_{S1} = 160 m/s
Rigid Rock
I_R = Infinite

Footing

D = 3 m
d = 3 m
R = 9 m

Column

H_c = 6 m
d_c = 1.3 m
E_c = 25 GPa
β = 5%
m_s = 350 Mg
No rotation at
column top
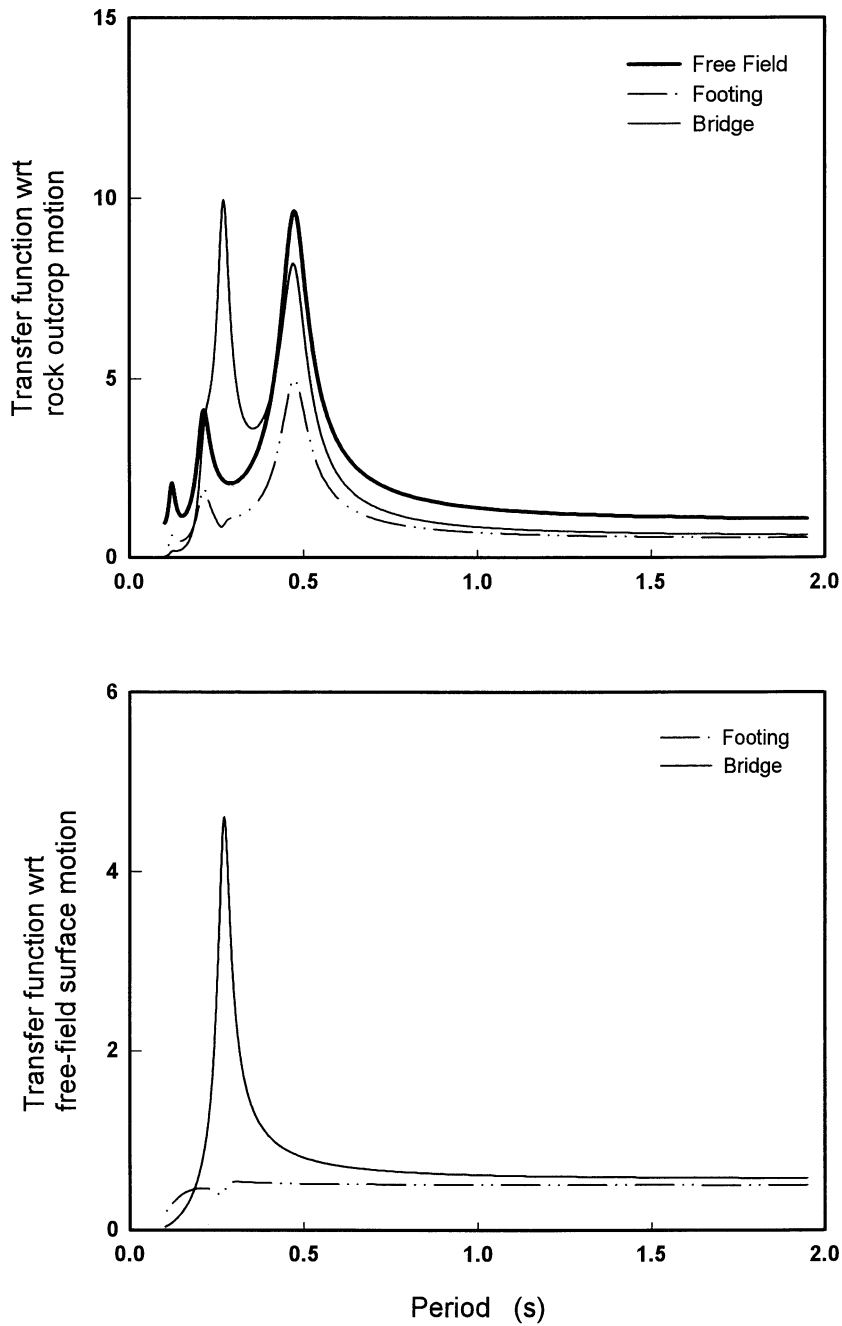
**FIGURE A-78 Case B223: Harmonic Steady-State Transfer Functions**
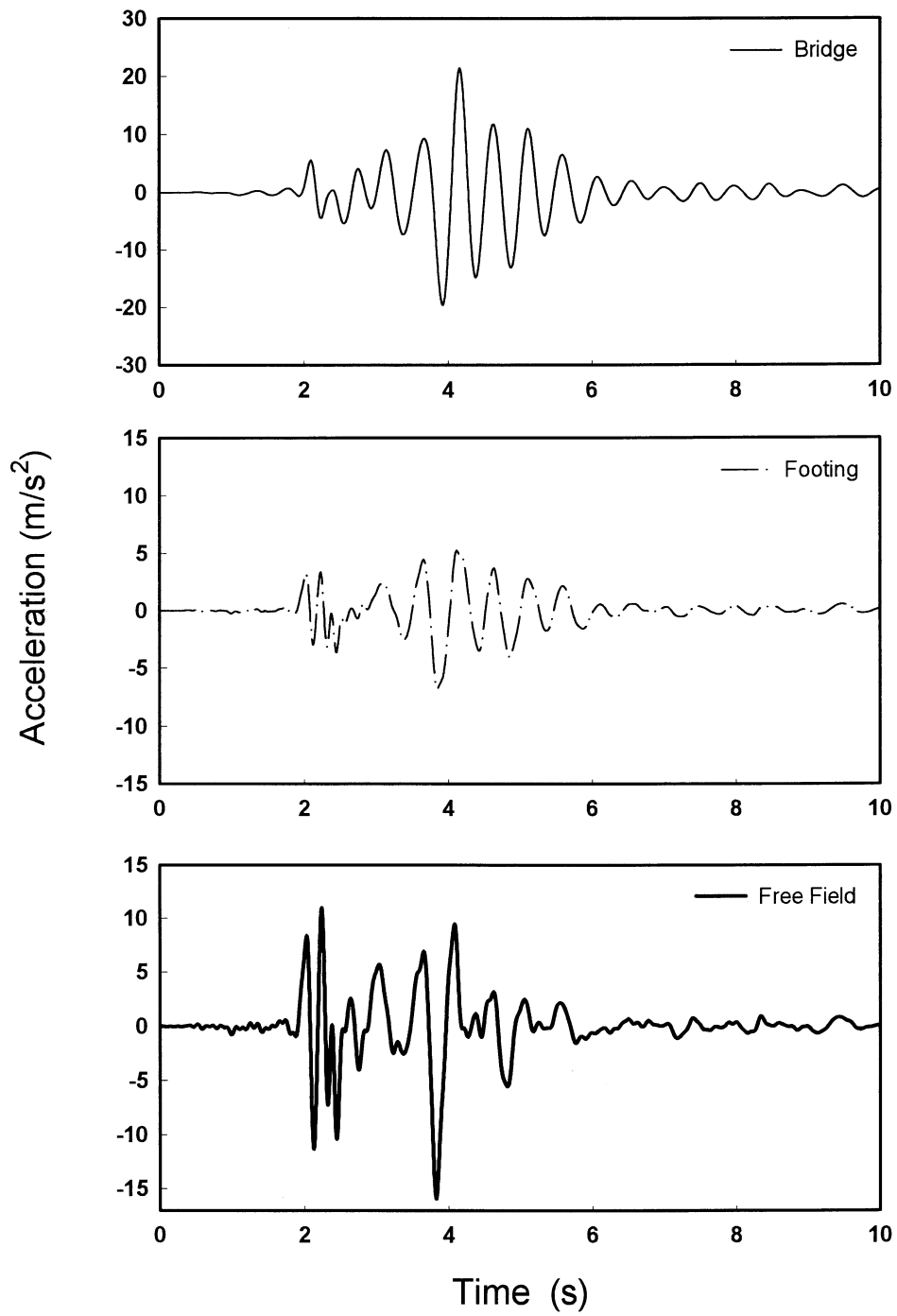
FIGURE A-79 Case A441: Acceleration histories for 0.4g artificial excitation rock motion
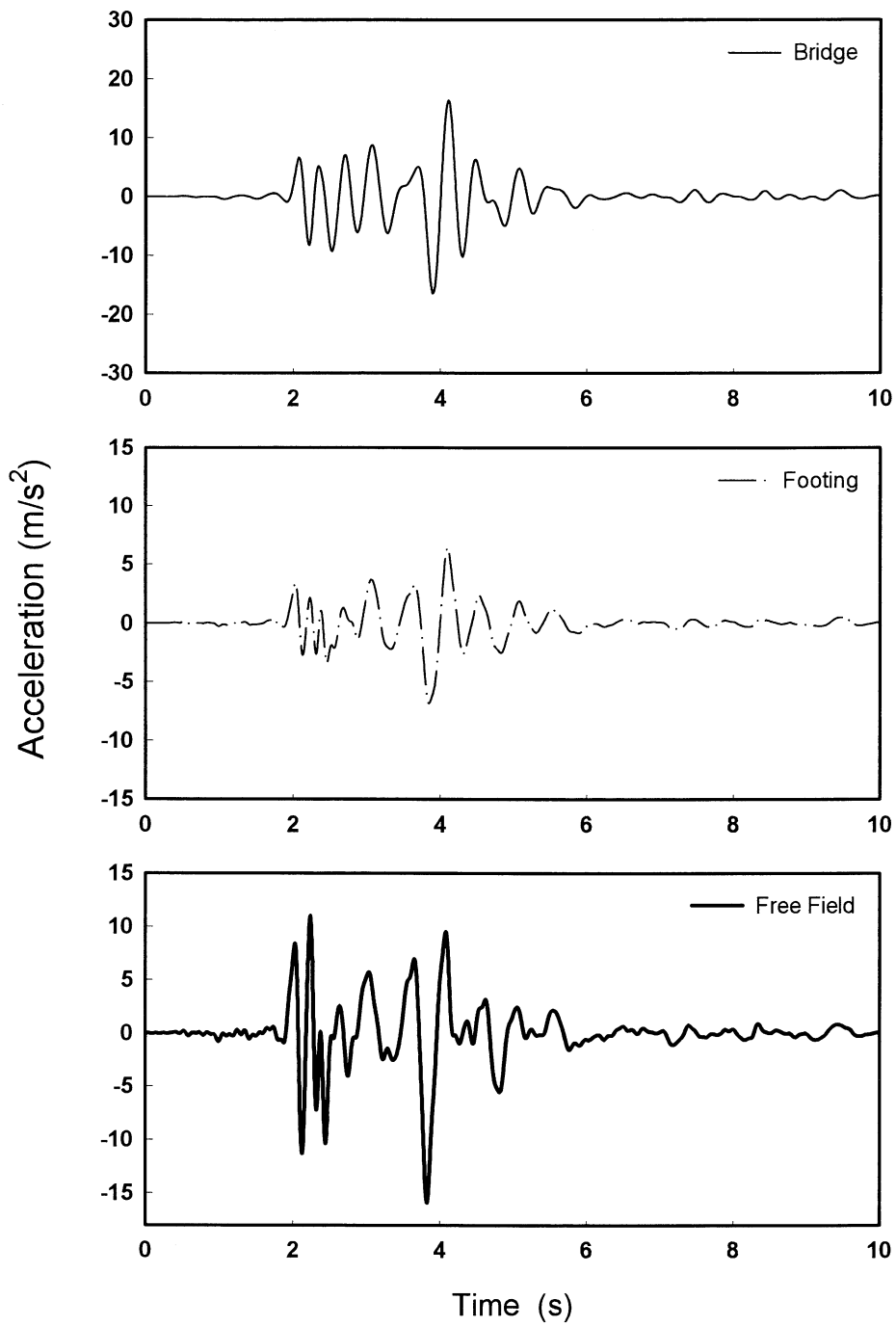
FIGURE A-80 Case A442: Acceleration histories for 0.4g artificial excitation rock motion
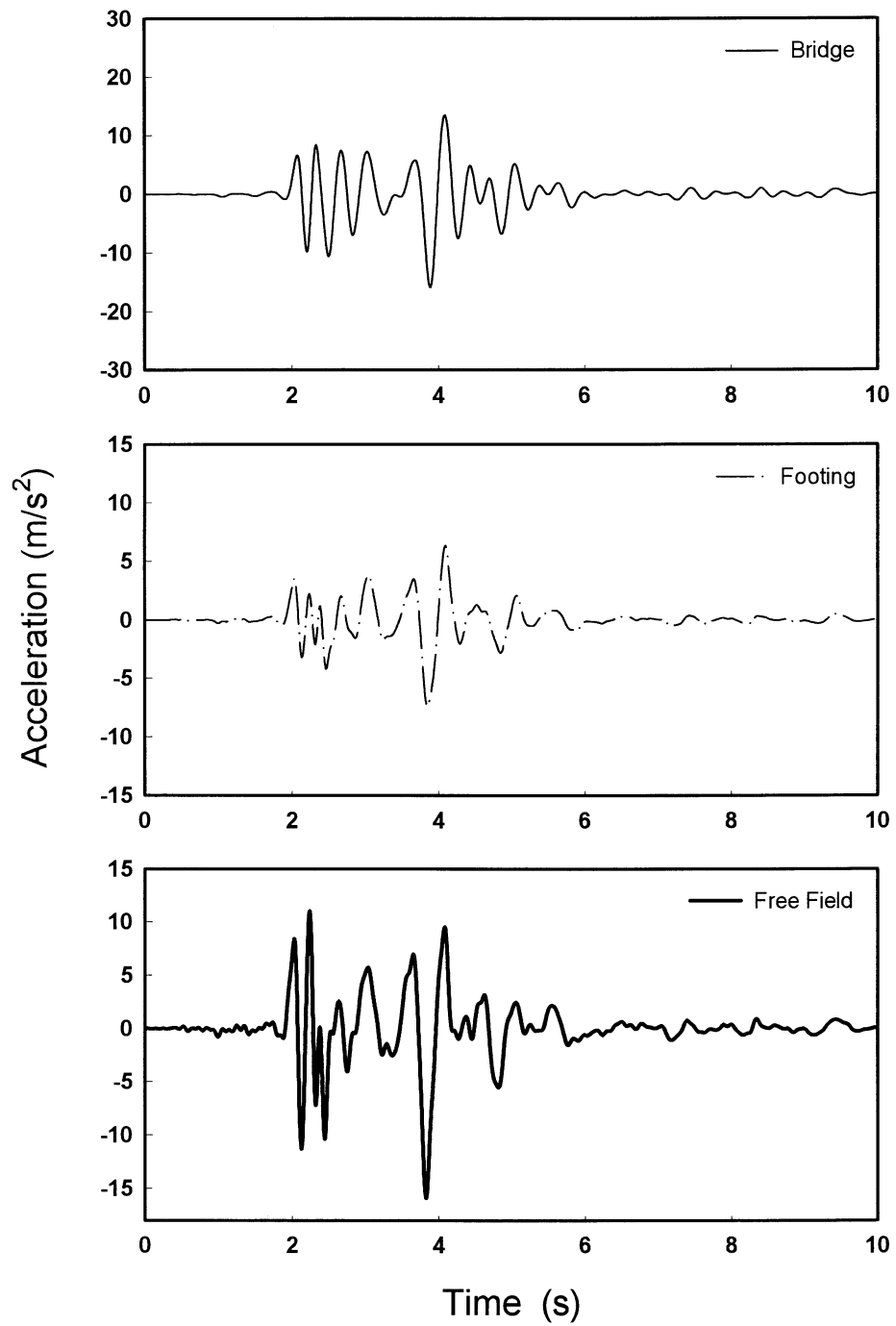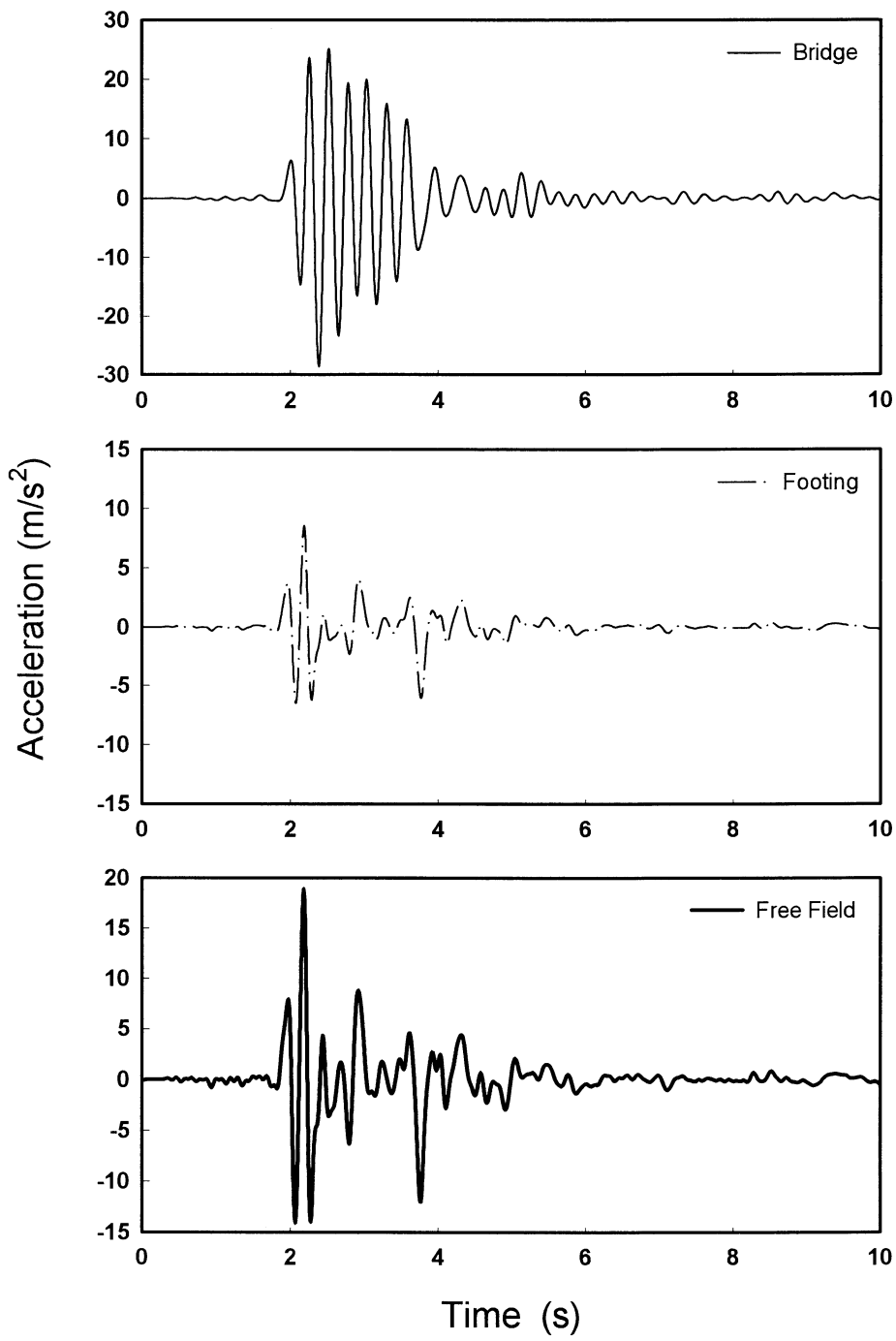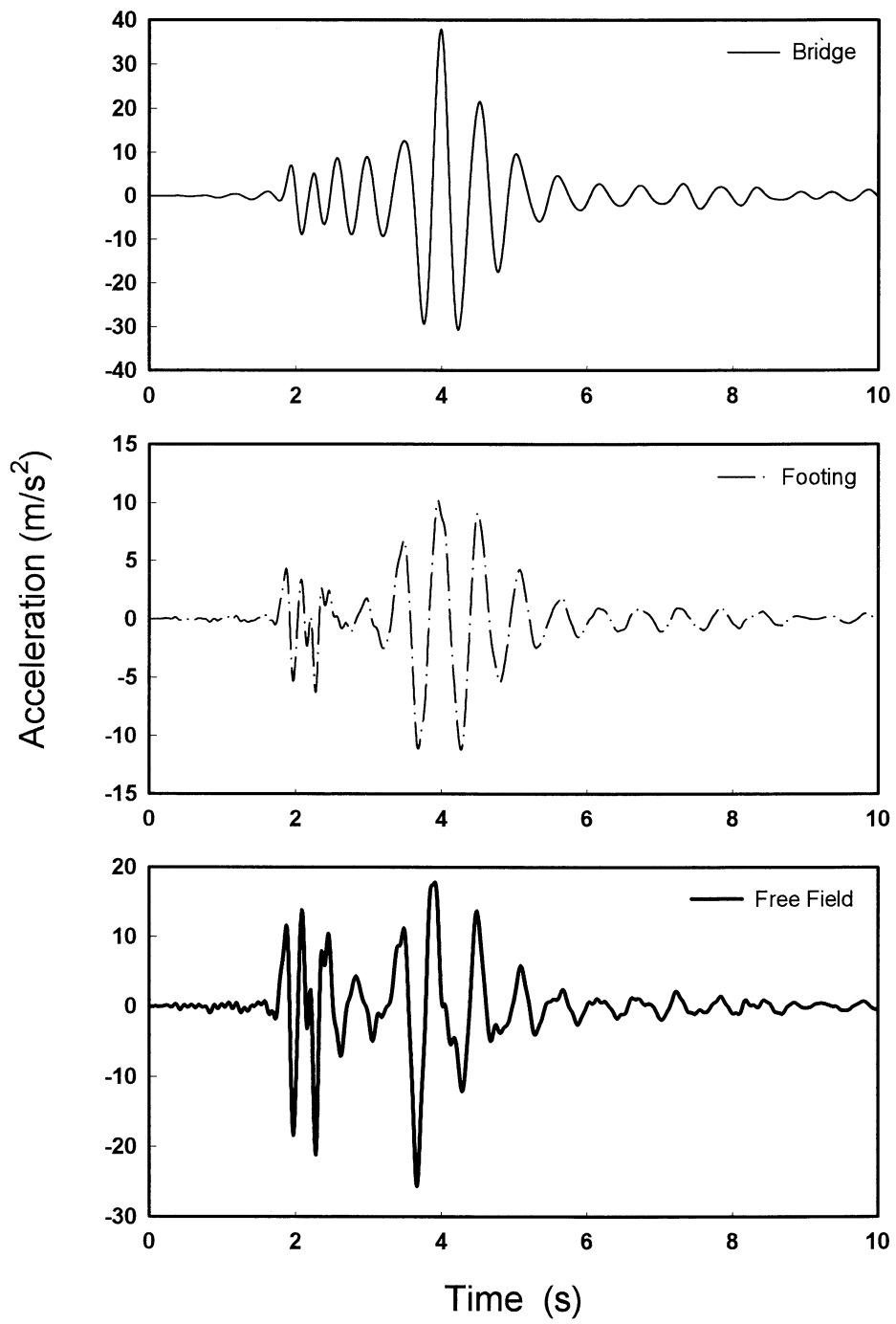
FIGURE A-81 Case A443: Acceleration histories for 0.4g artificial excitation rock motion
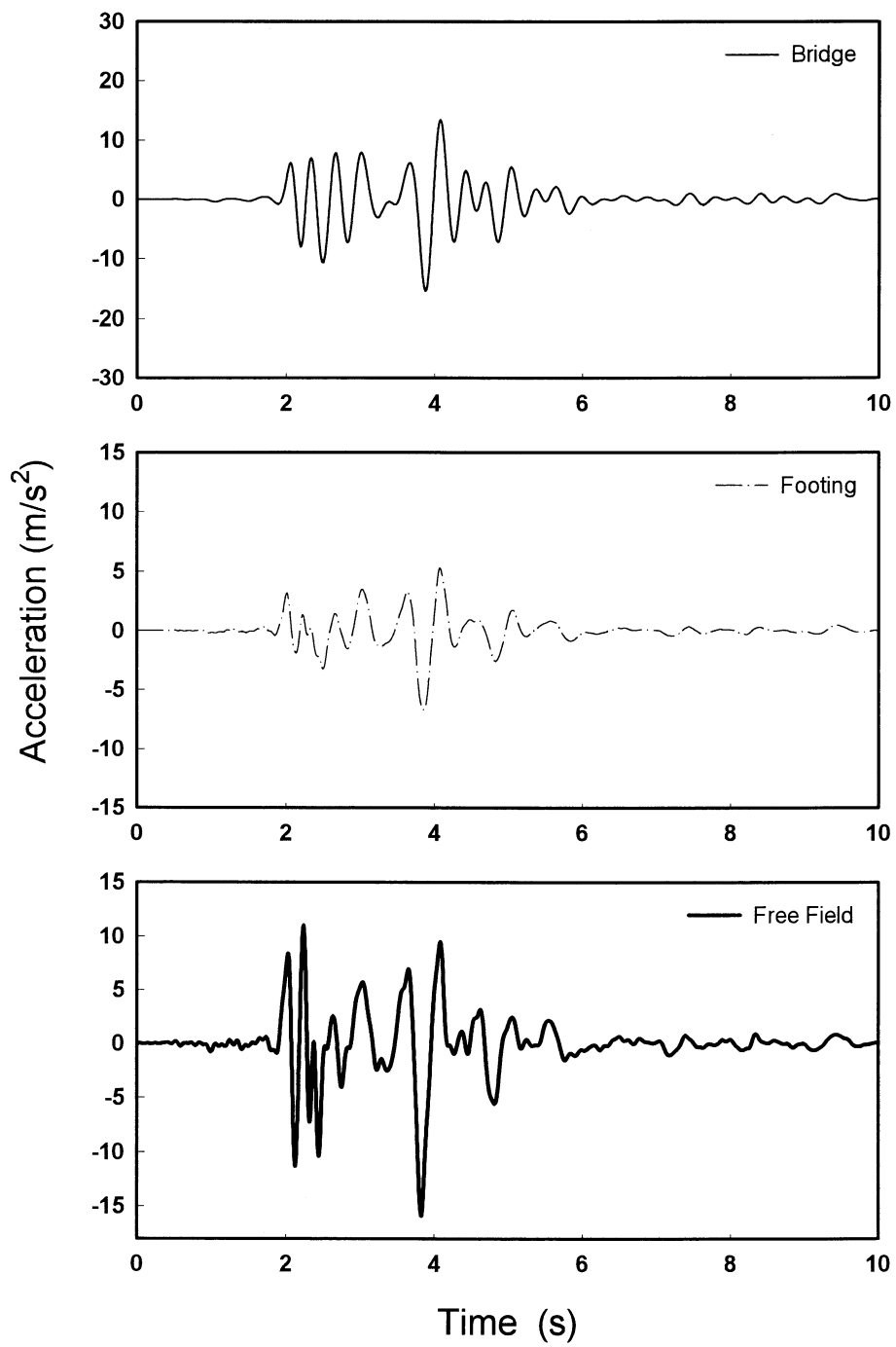
FIGURE A-82 Case A421: Acceleration histories for 0.4g artificial excitation rock motion
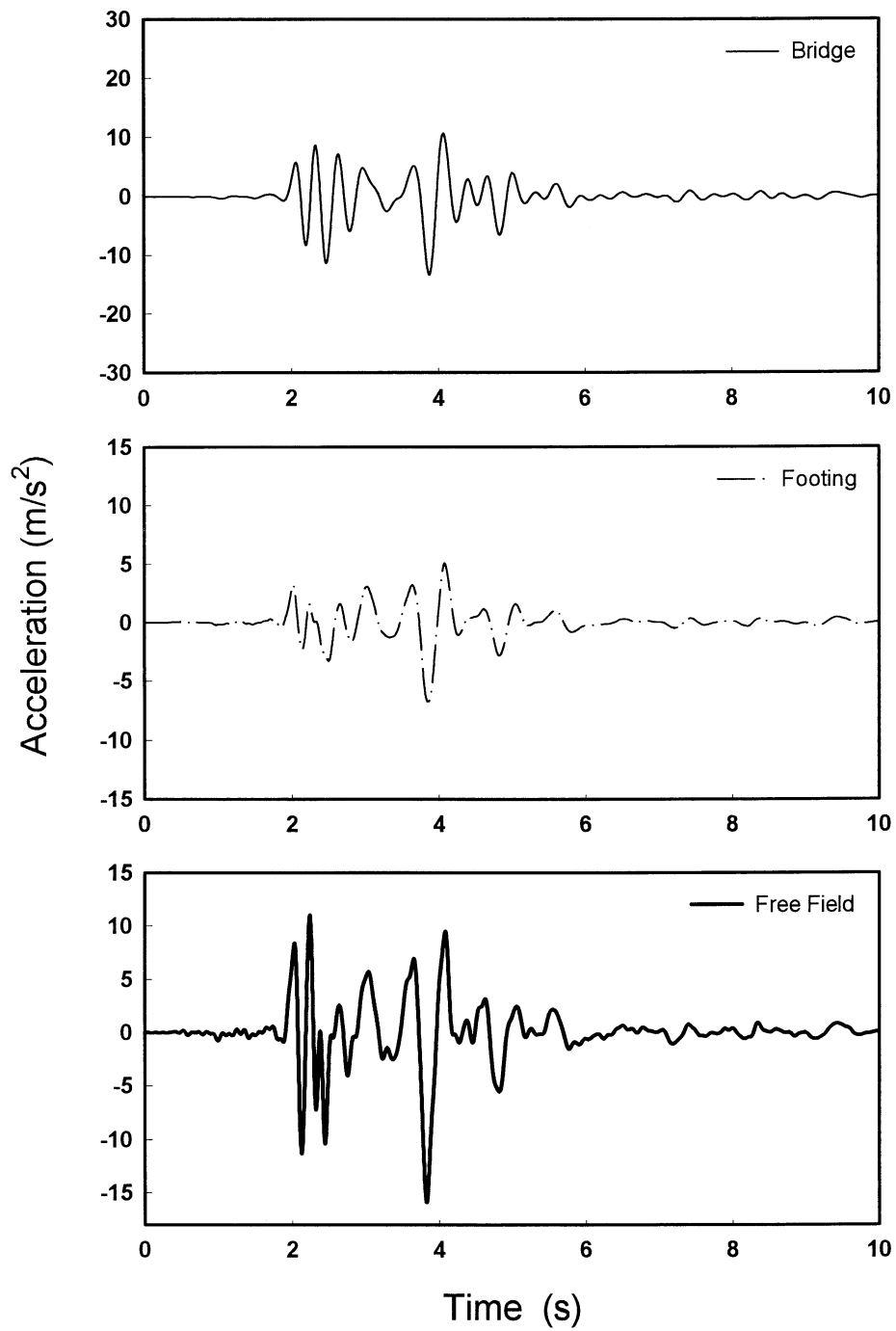
FIGURE A-83 Case A422: Acceleration histories for 0.4g artificial excitation rock motion
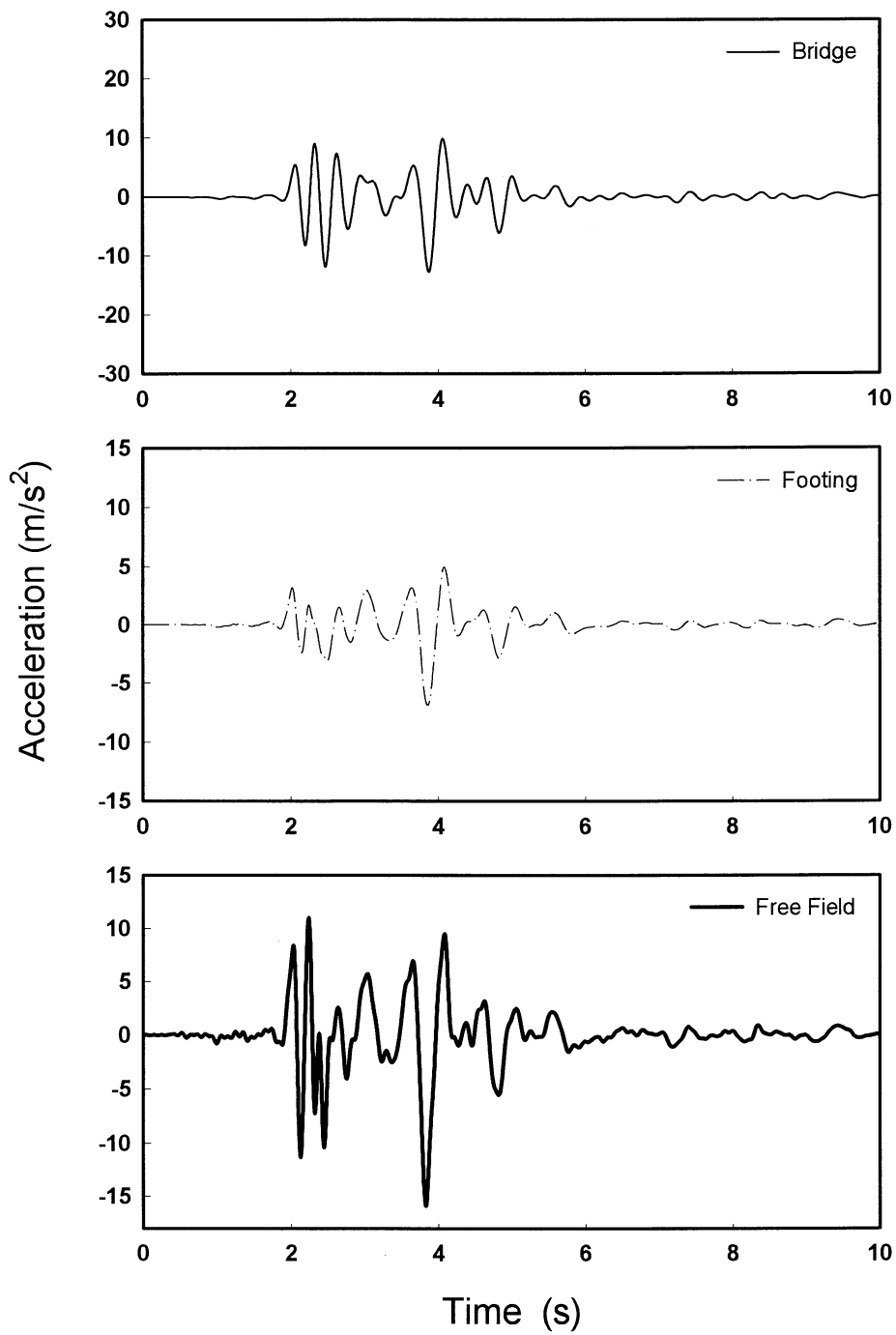
FIGURE A-84 Case A423: Acceleration histories for 0.4g artificial excitation rock motion
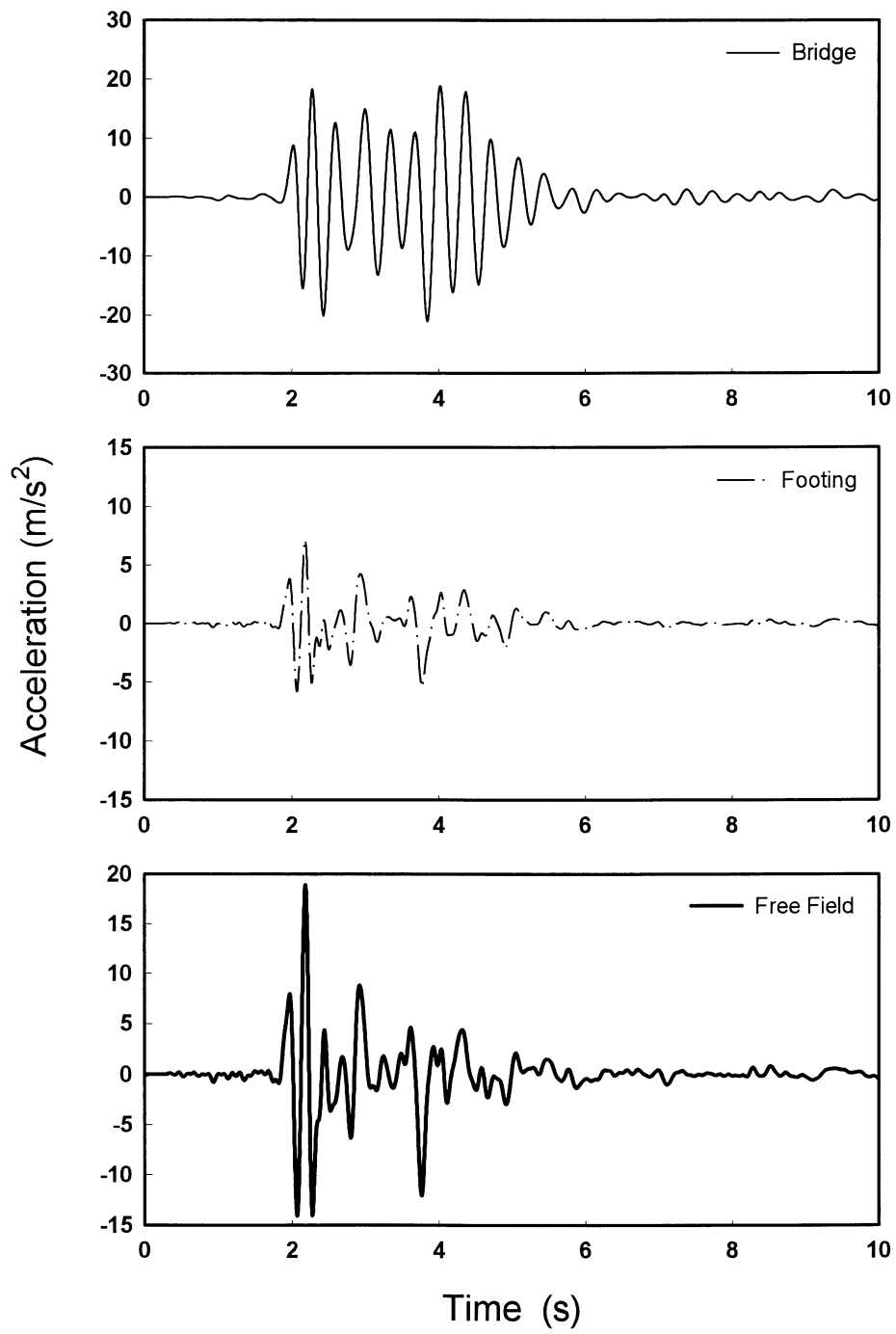
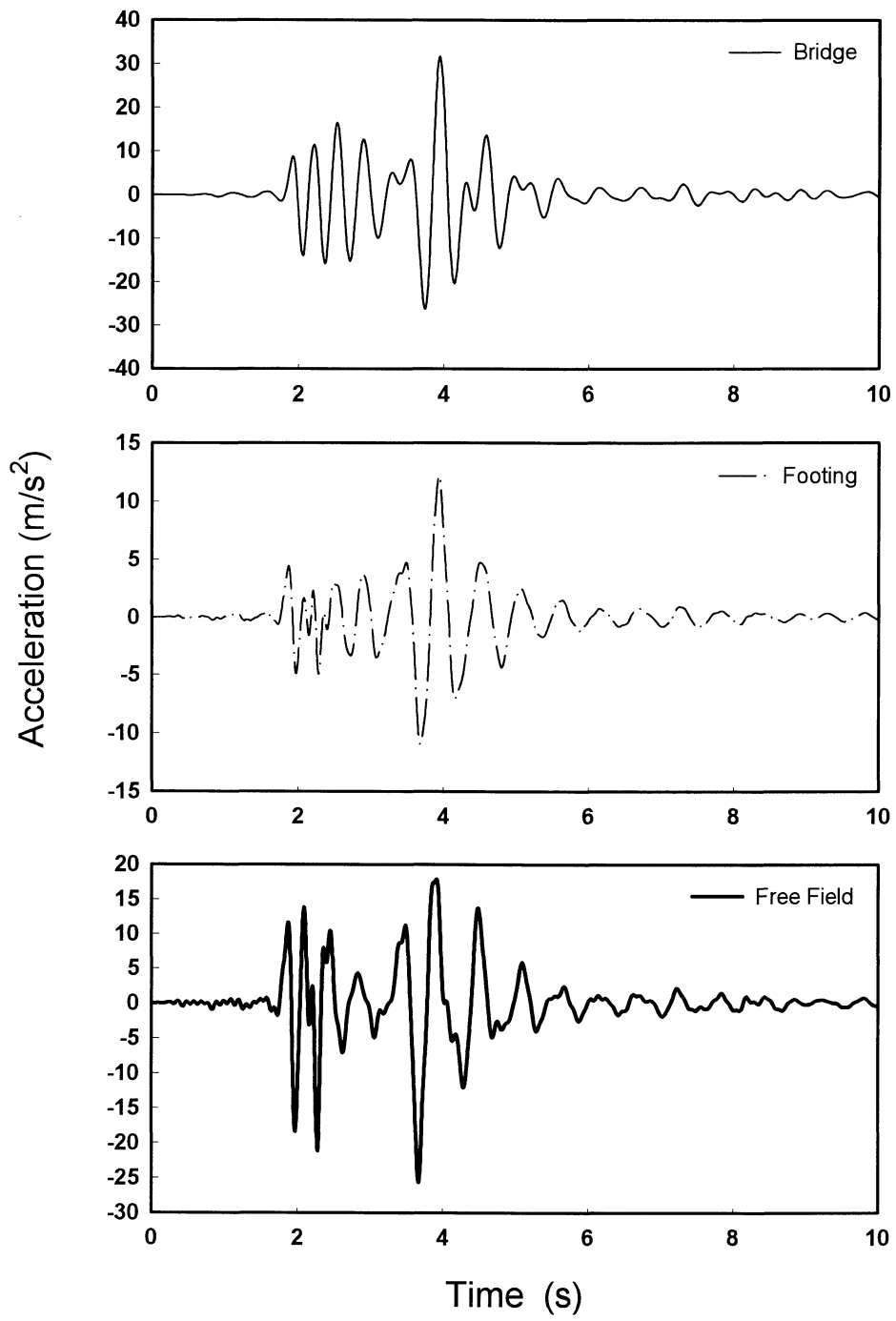**FIGURE A-85 Case A241: Acceleration histories for 0.4g artificial excitation rock motion**
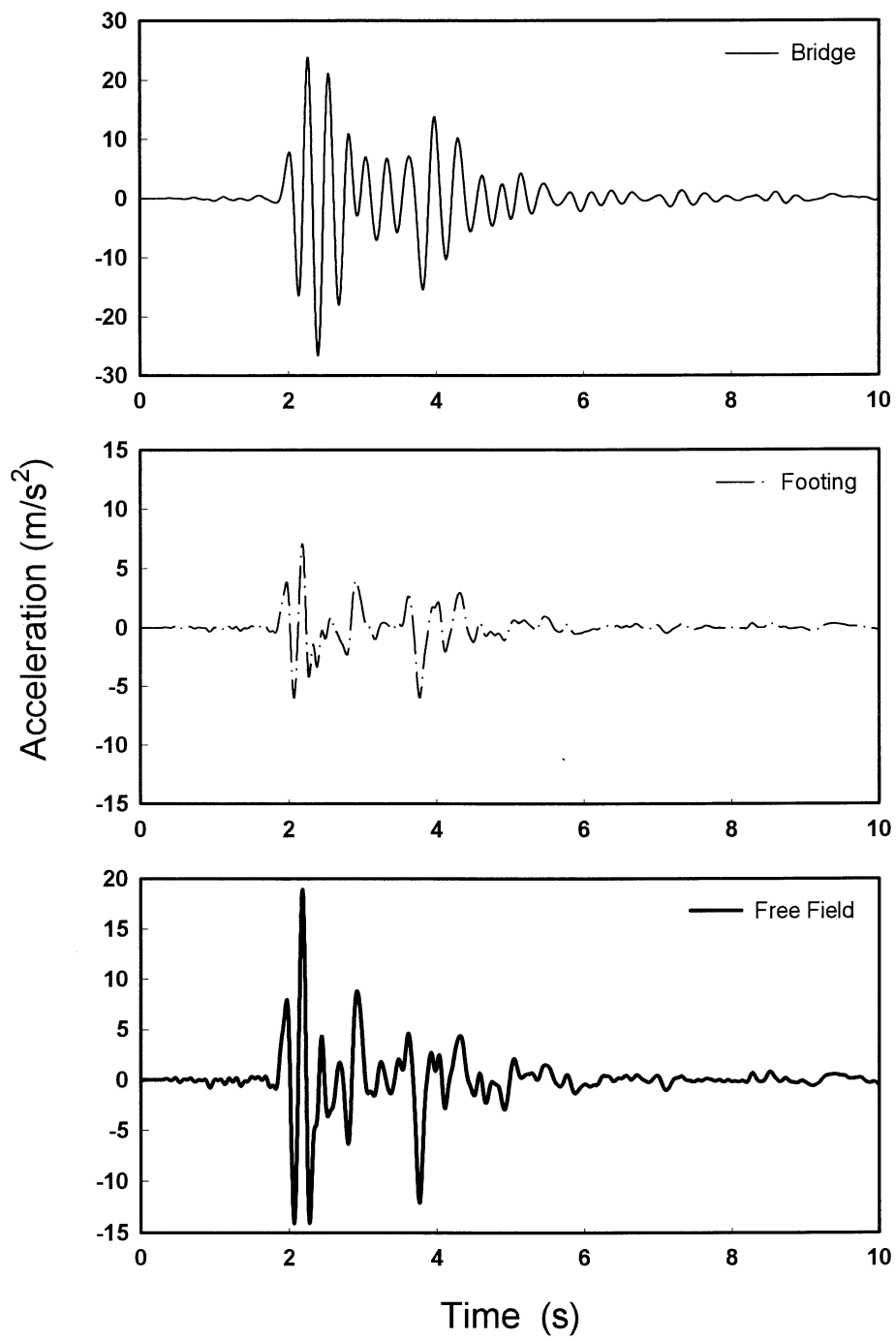
FIGURE A-86 Case A242: Acceleration histories for 0.4g artificial excitation rock motion
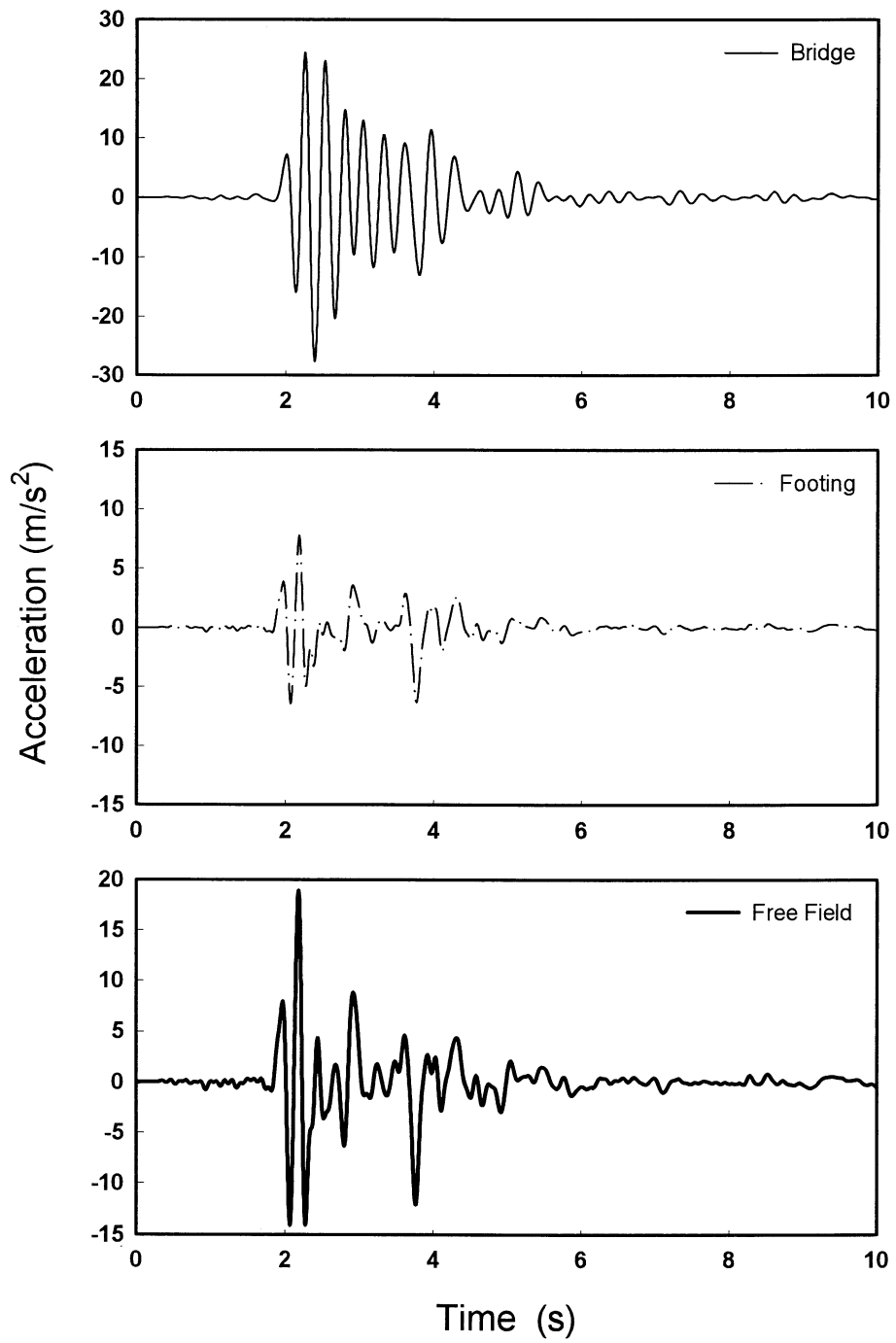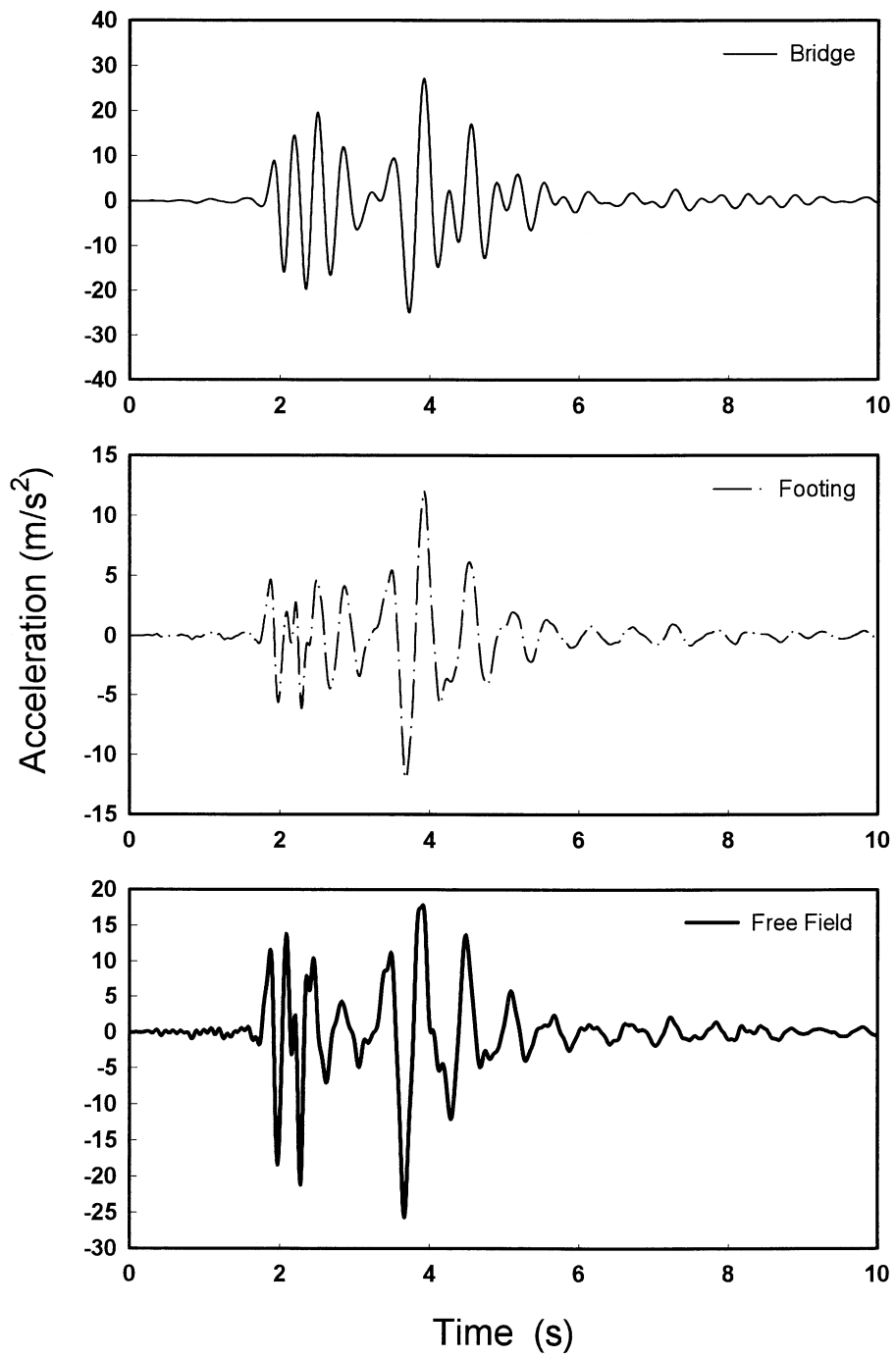
FIGURE A-87 Case A243: Acceleration histories for 0.4g artificial excitation rock motion
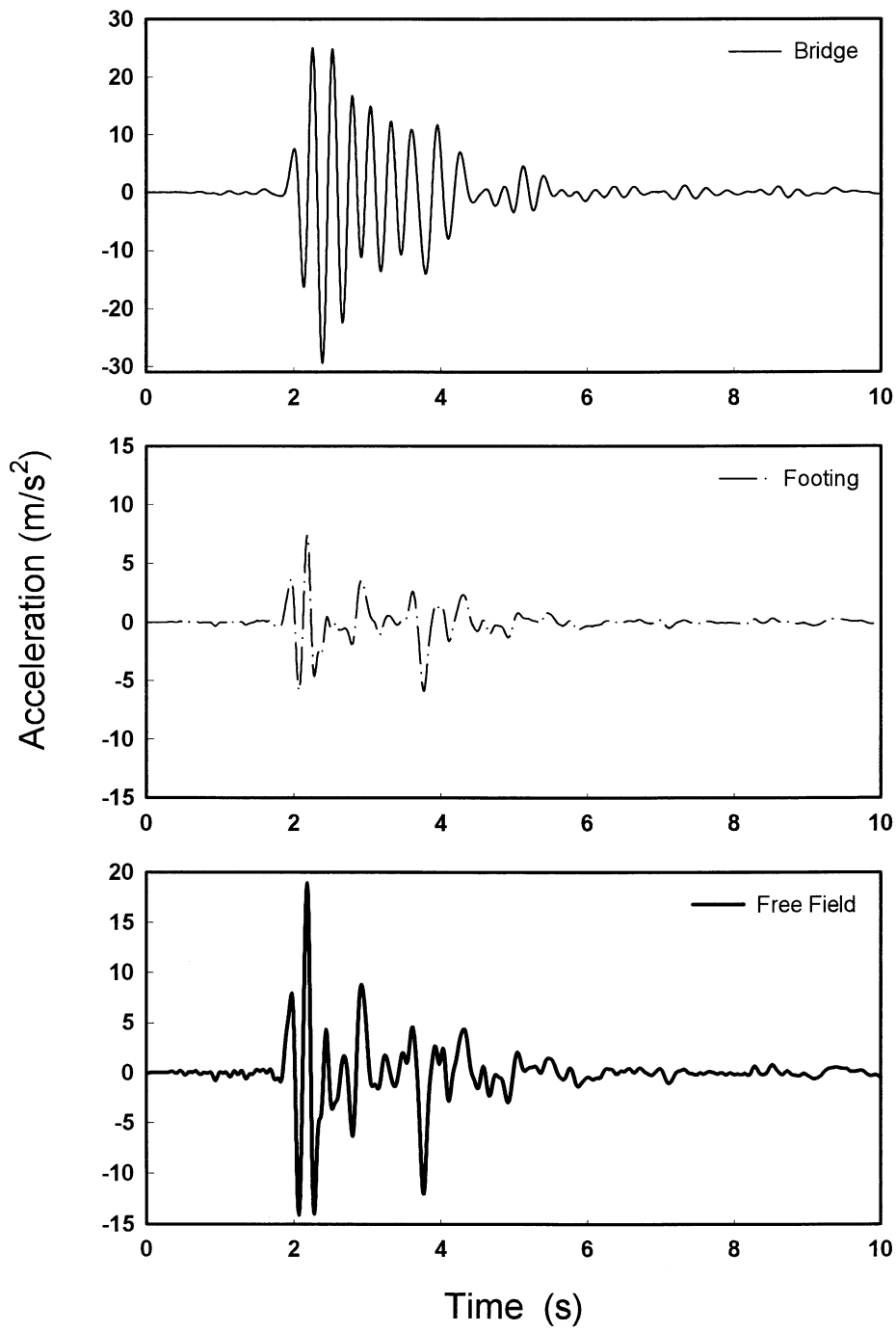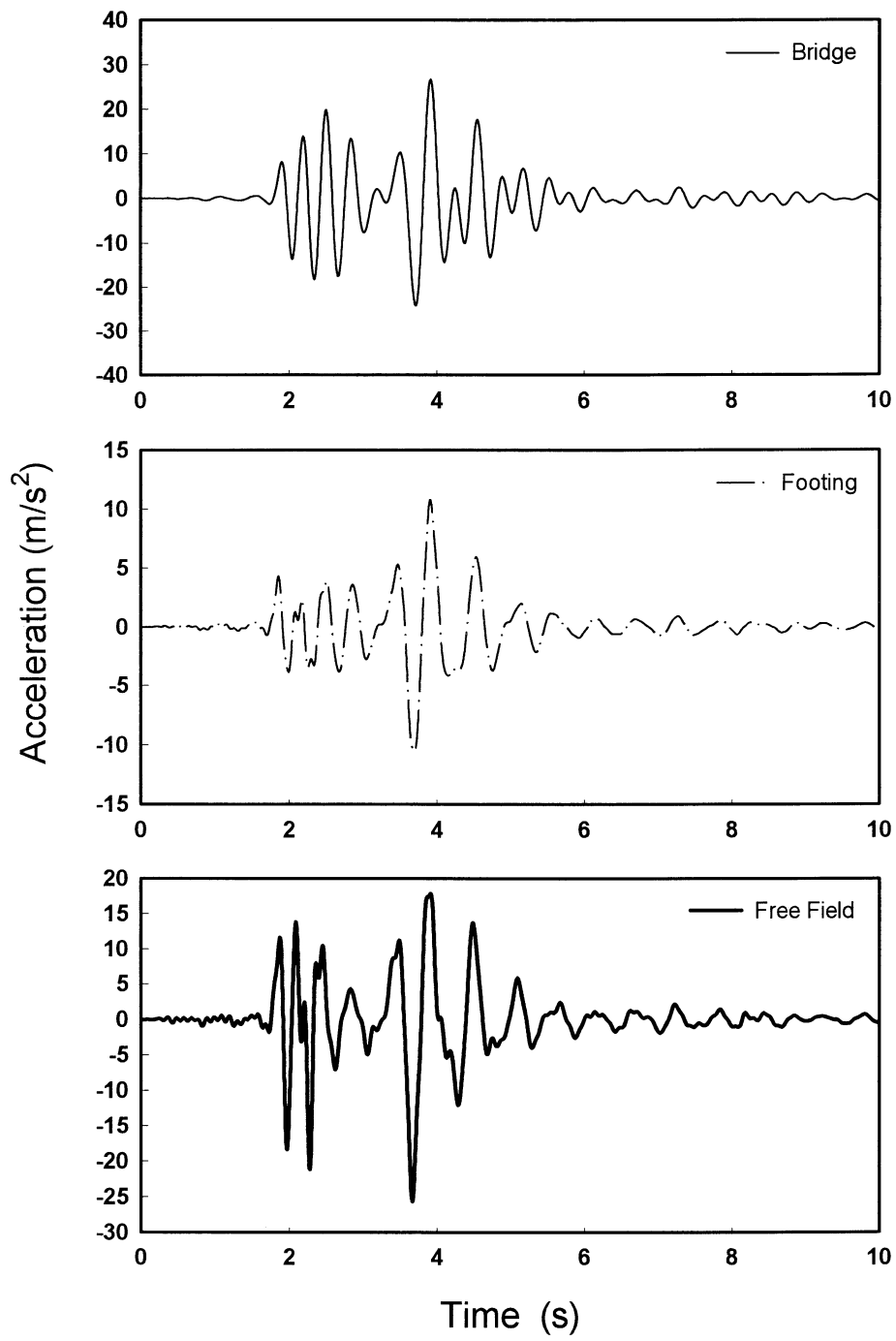
FIGURE A-88 Case A221: Acceleration histories for 0.4g artificial excitation rock motion
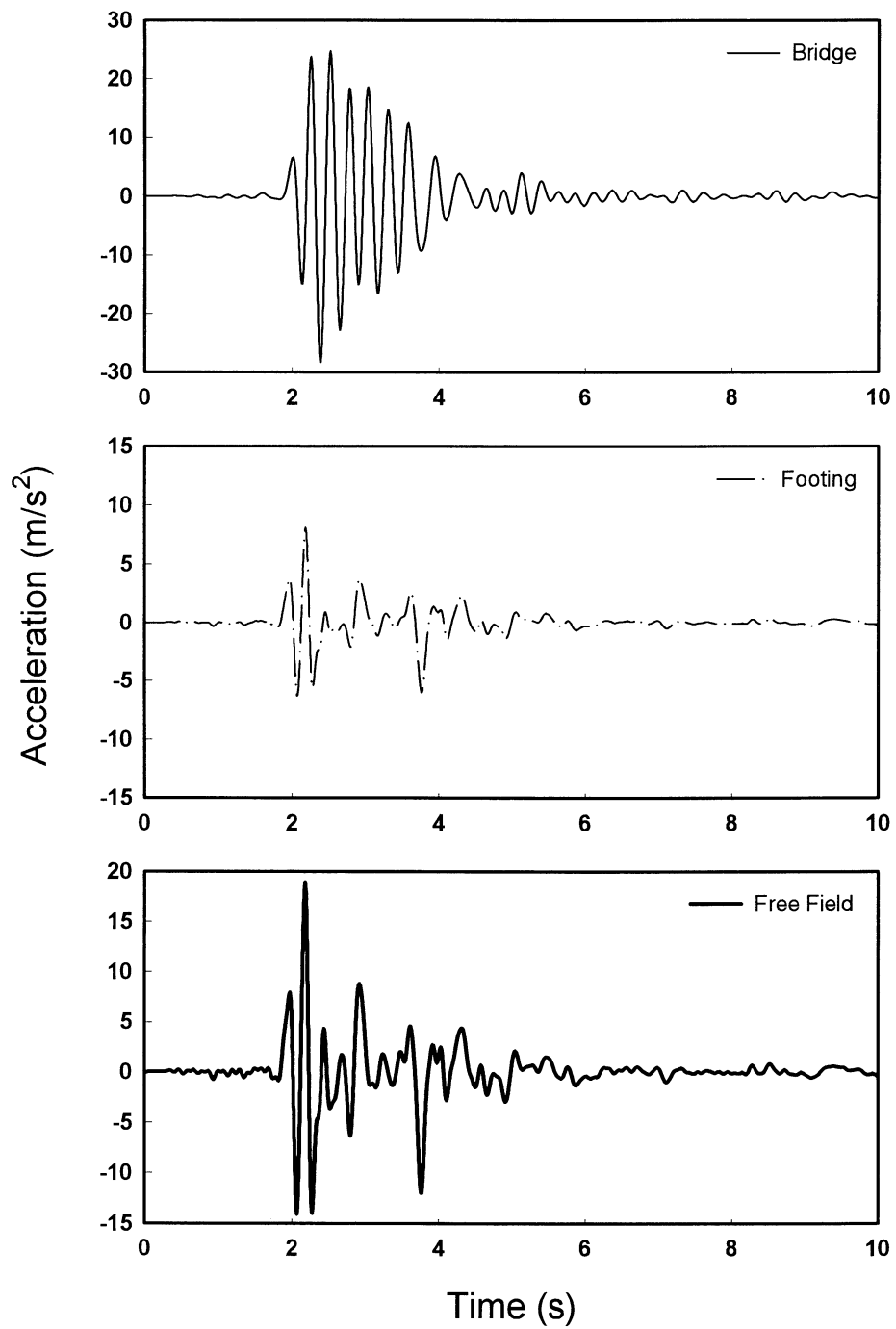
FIGURE A-89 Case A222: Acceleration histories for 0.4g artificial excitation rock motion

FIGURE A-90 Case A223: Acceleration histories for 0.4g artificial excitation rock motion

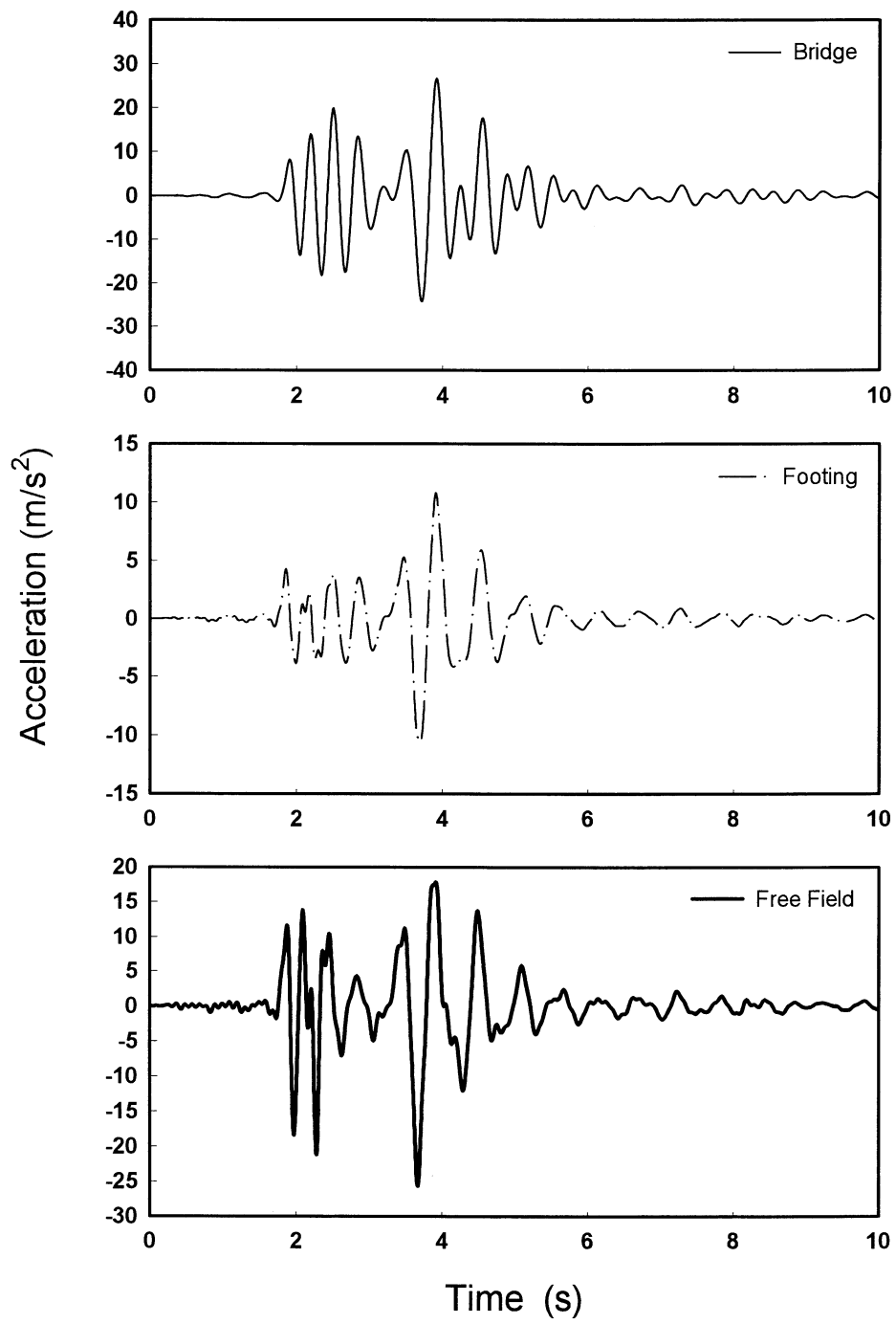**FIGURE A-91 Case B441: Acceleration histories for 0.4g artificial excitation rock motion**

FIGURE A-92 Case B442: Acceleration histories for 0.4g artificial excitation rock motion
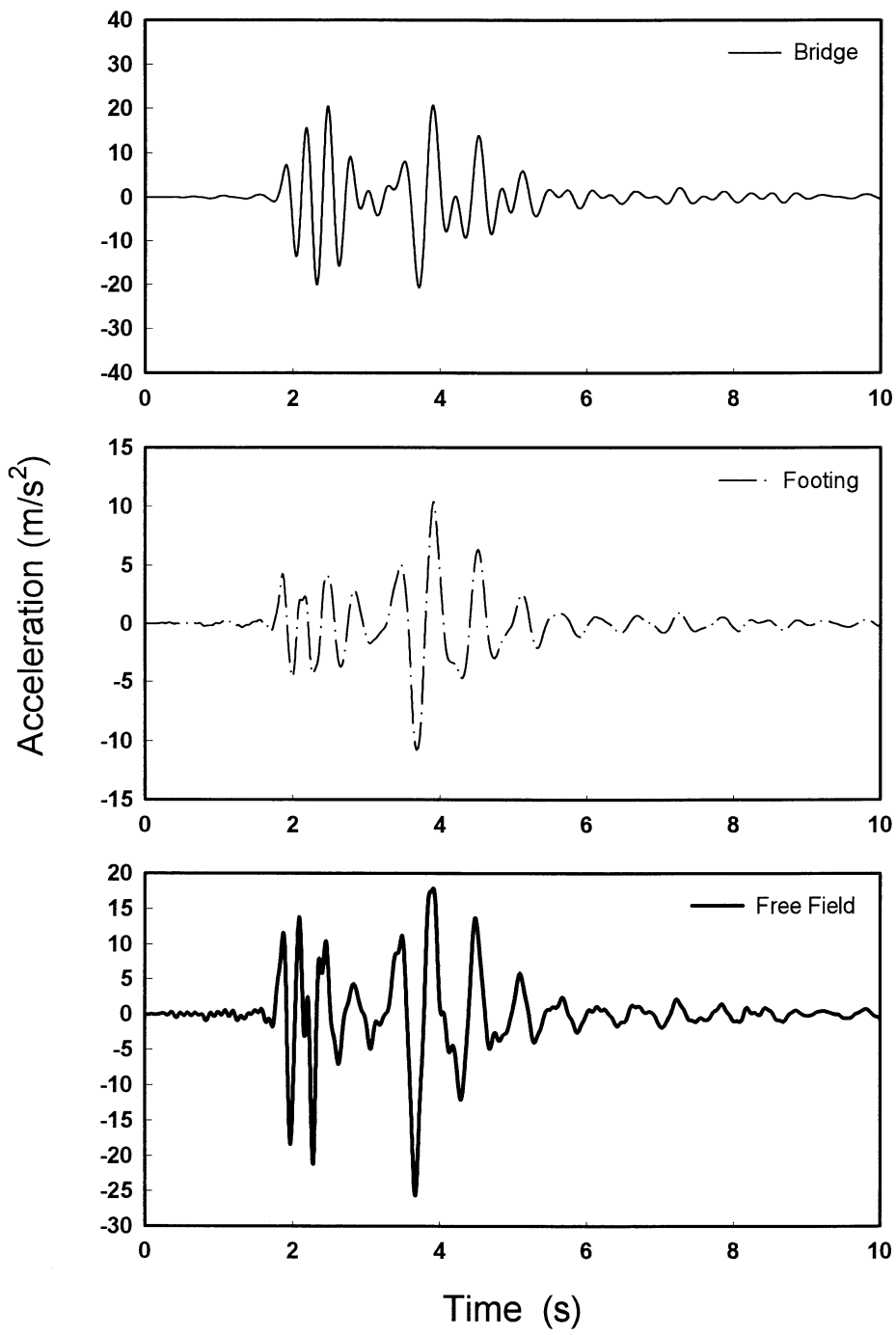
FIGURE A-93 Case B443: Acceleration histories for 0.4g artificial excitation rock motion

FIGURE A-94 Case B421: Acceleration histories for 0.4g artificial excitation rock motion

FIGURE A-95 Case B422: Acceleration histories for 0.4g artificial excitation rock motion

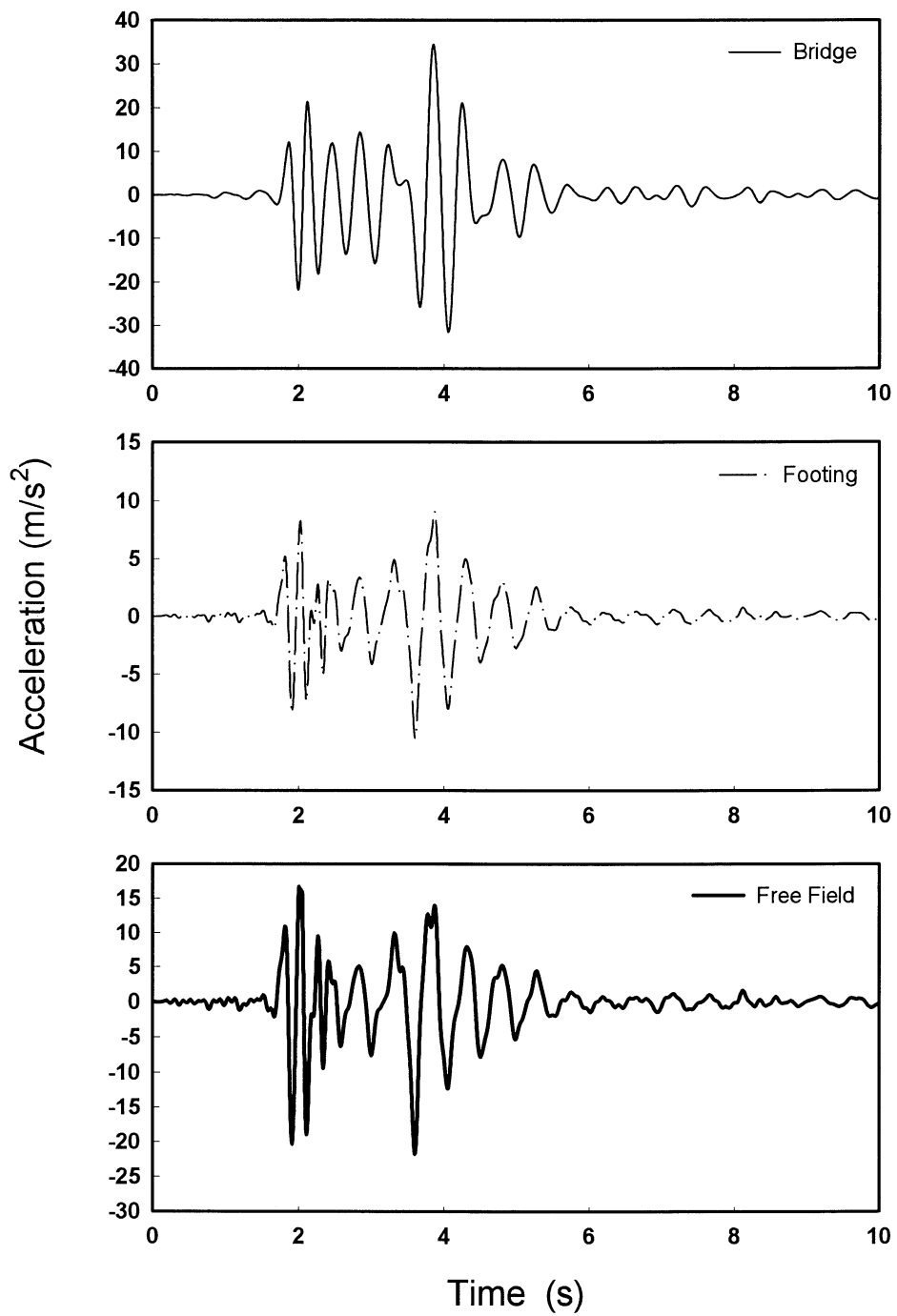**FIGURE A-96 Case B423: Acceleration histories for 0.4g artificial excitation rock motion**

FIGURE A-97 Case B241: Acceleration histories for 0.4g artificial excitation rock motion
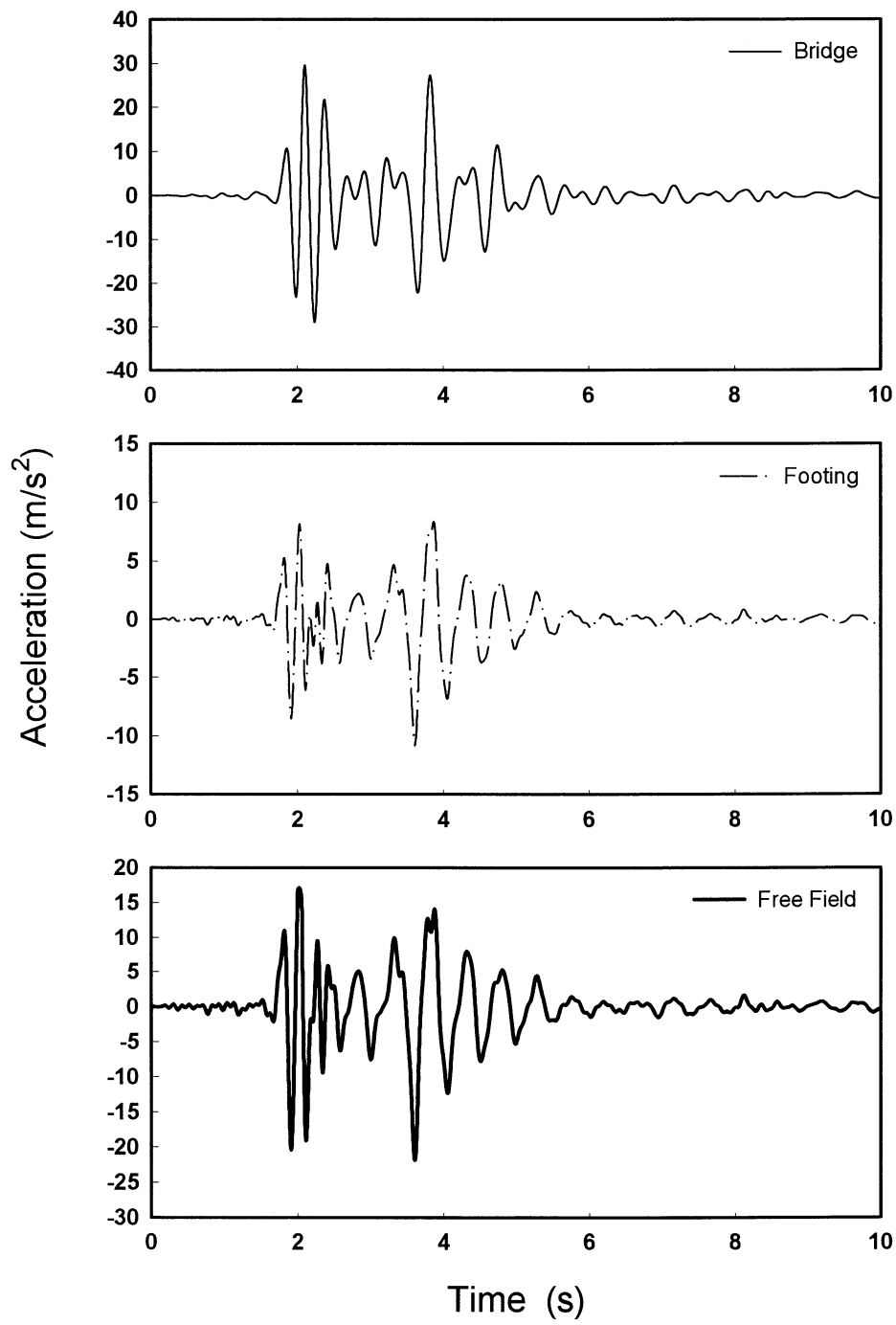
FIGURE A-98 Case B242: Acceleration histories for 0.4g artificial excitation rock motion
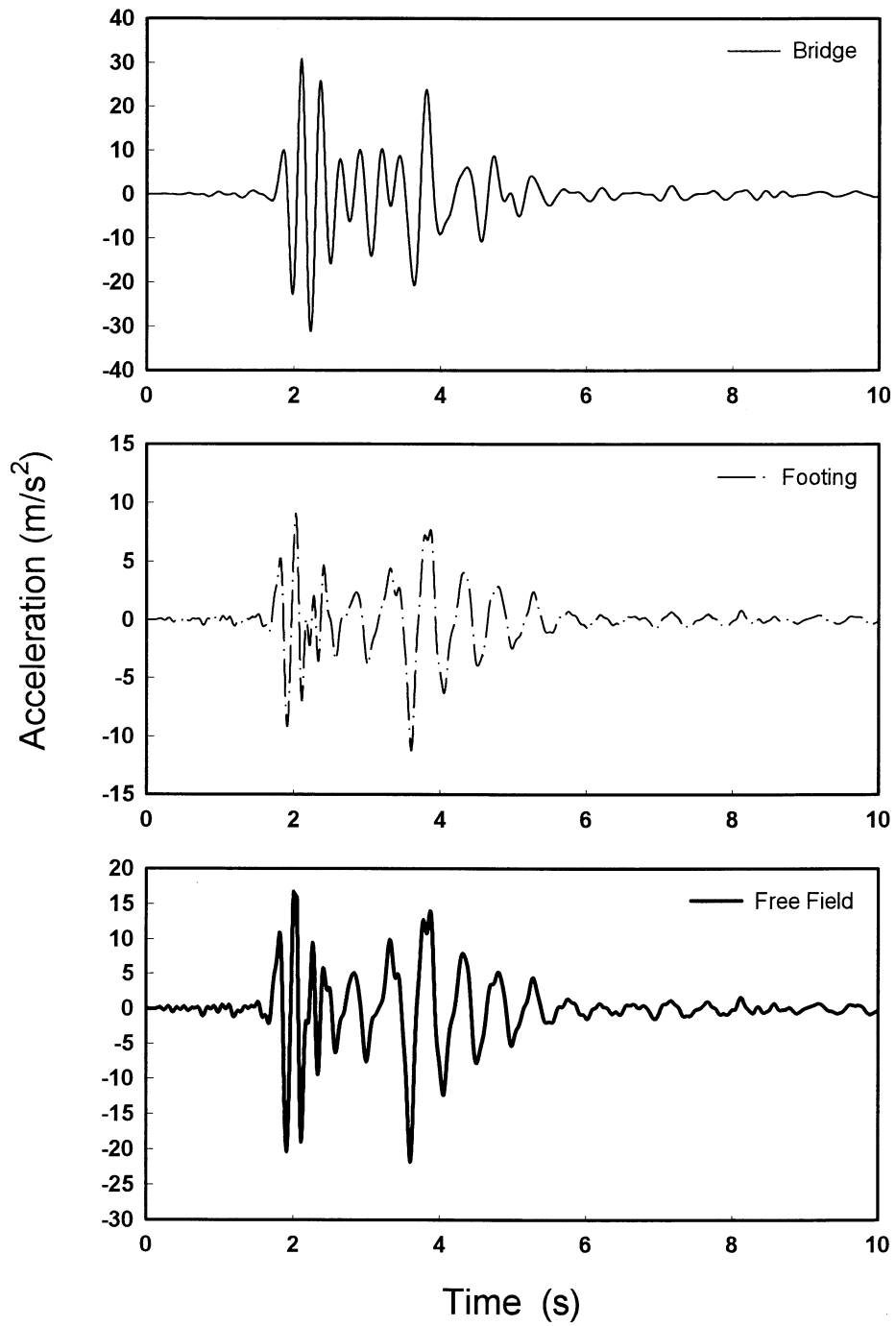
FIGURE A-99 Case B243: Acceleration histories for 0.4g artificial excitation rock motion
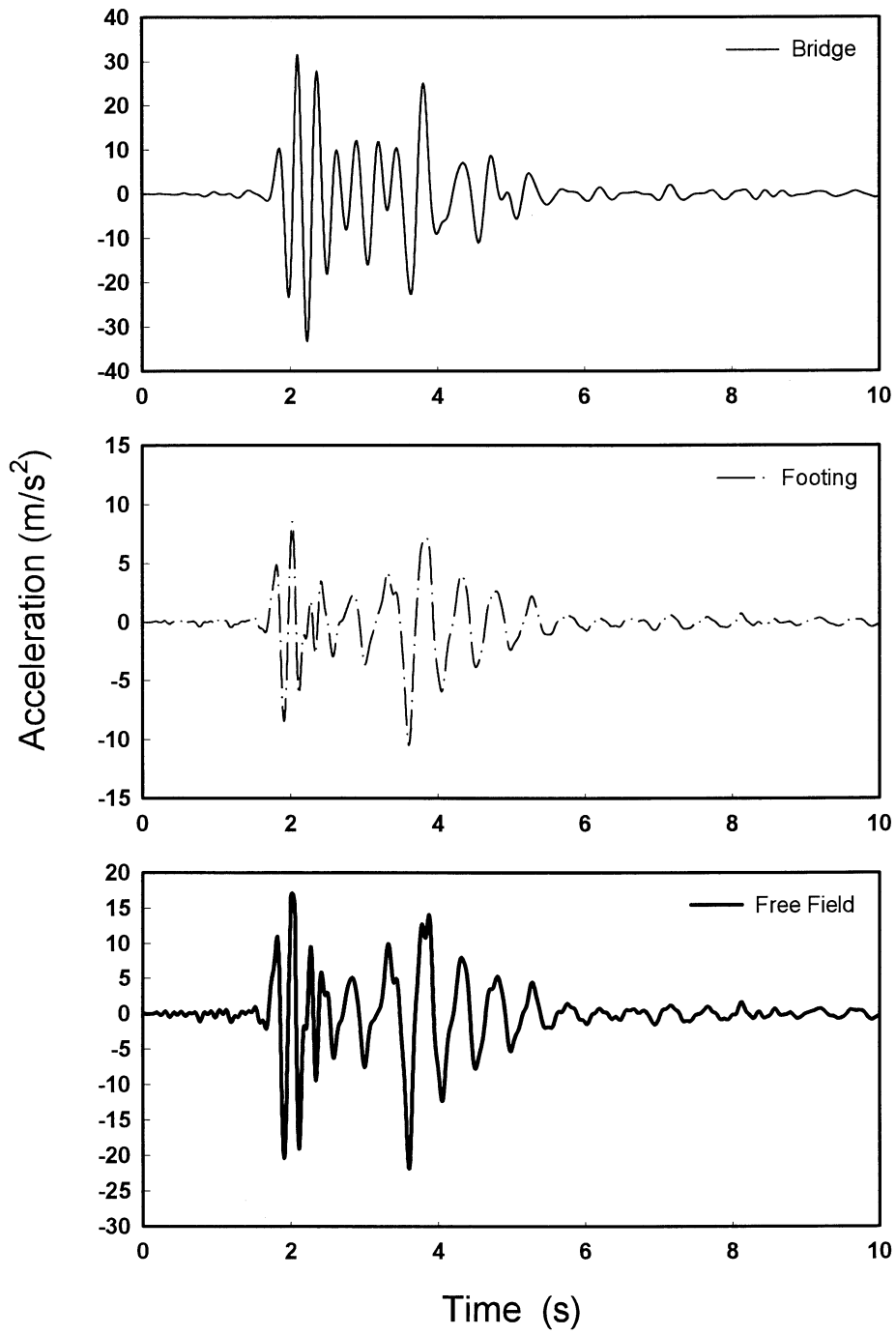
FIGURE A-100 Case B221: Acceleration histories for 0.4g artificial excitation rock motion
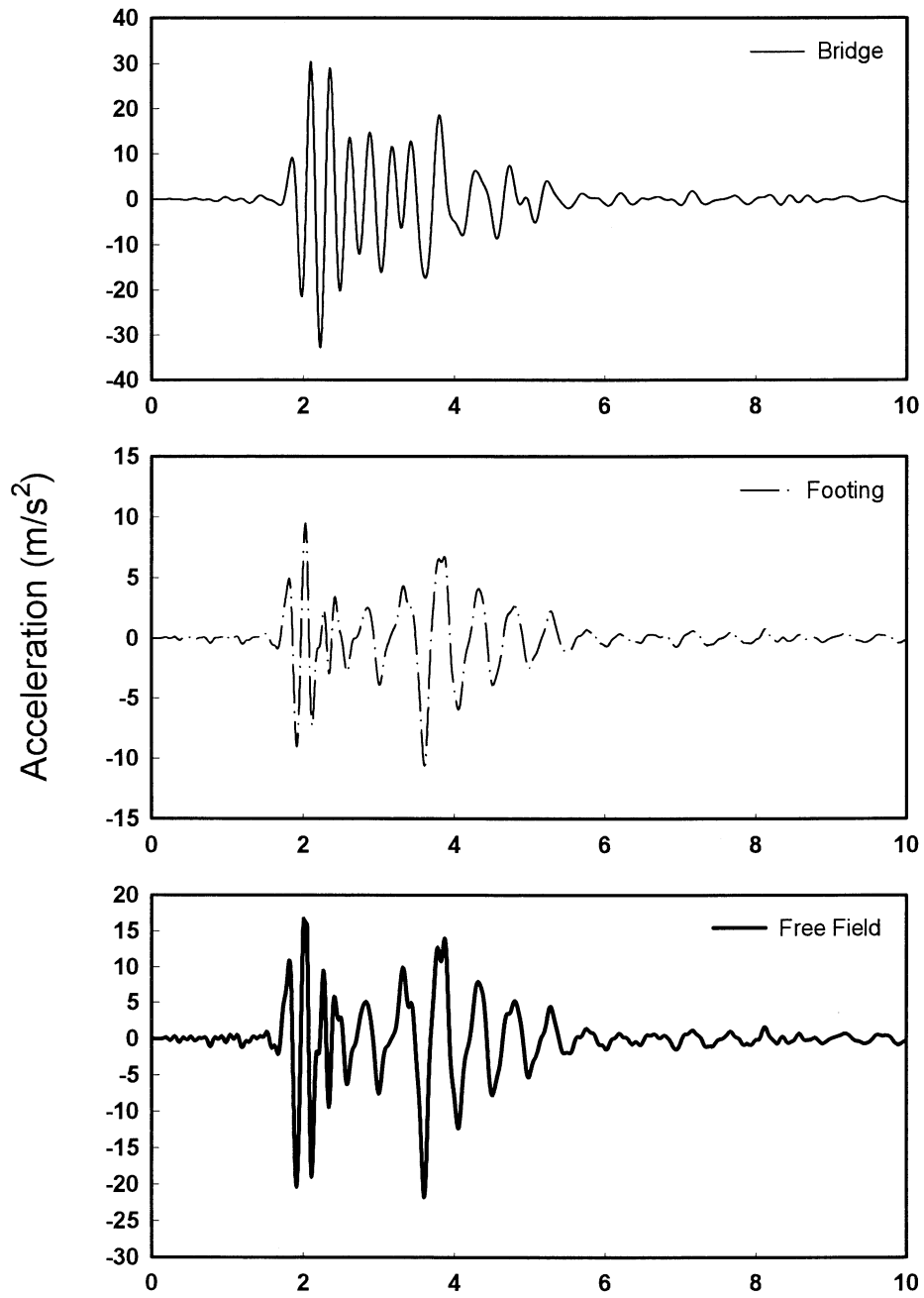
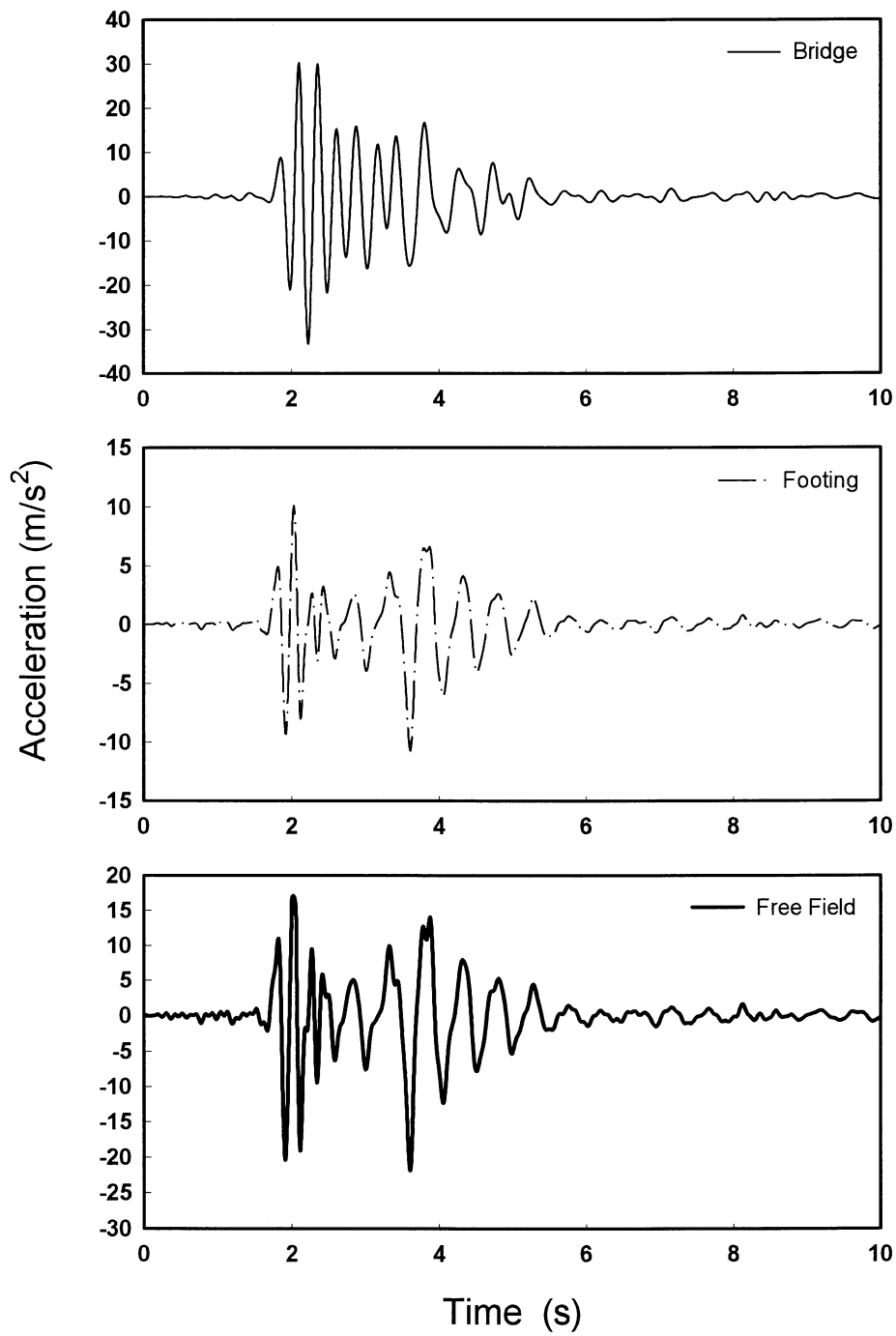**FIGURE A-101 Case B222: Acceleration histories for 0.4g artificial excitation rock motion**

FIGURE A-102 Case B223: Acceleration histories for 0.4g artificial excitation rock motion

FIGURE A-103 Case A441: Acceleration histories for Pacoima, Northridge (1994) rock motion

FIGURE A-104 Case A442: Acceleration histories for Pacoima, Northridge (1994) rock motion
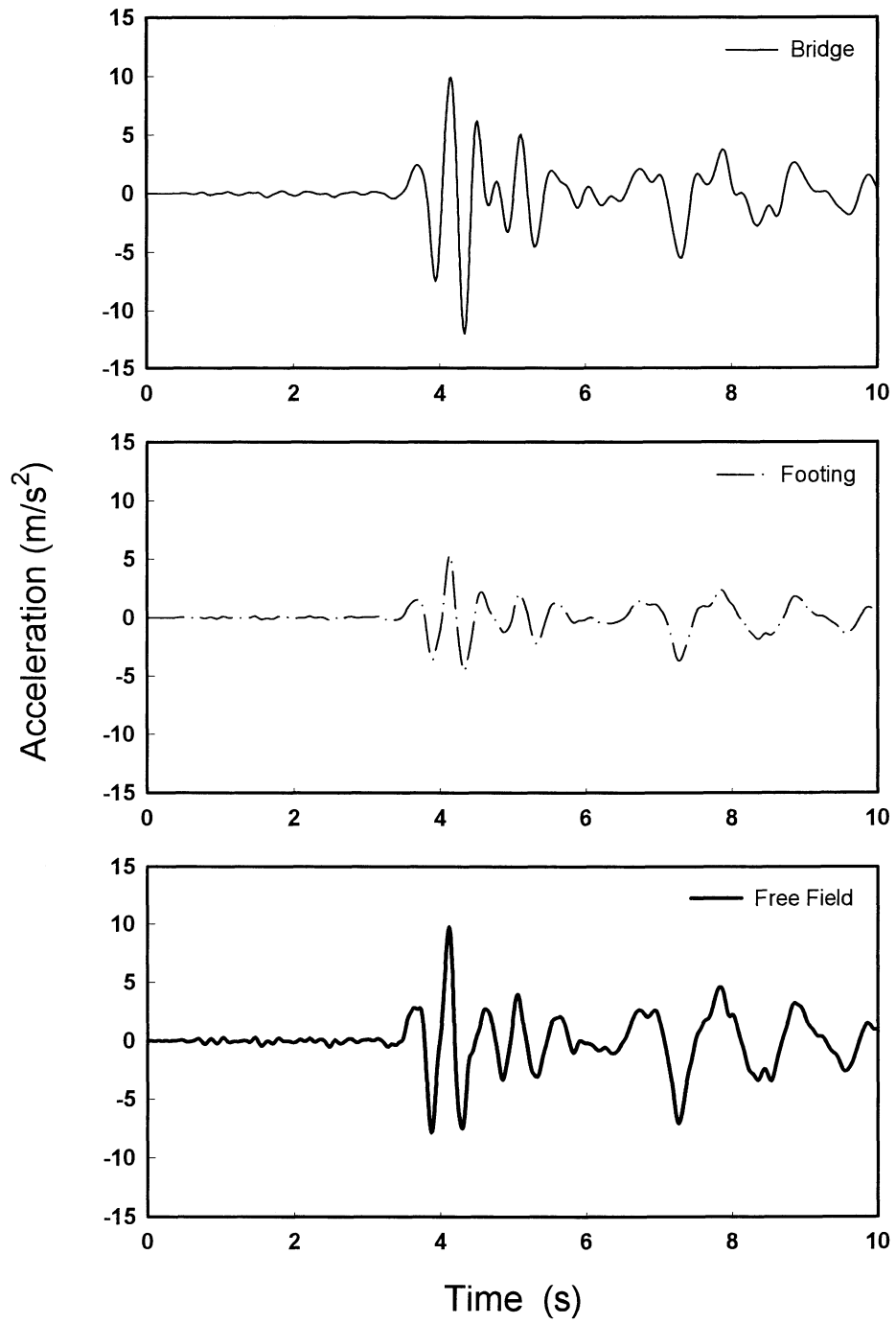
FIGURE A-105 Case A443: Acceleration histories for Pacoima, Northridge (1994) rock motion
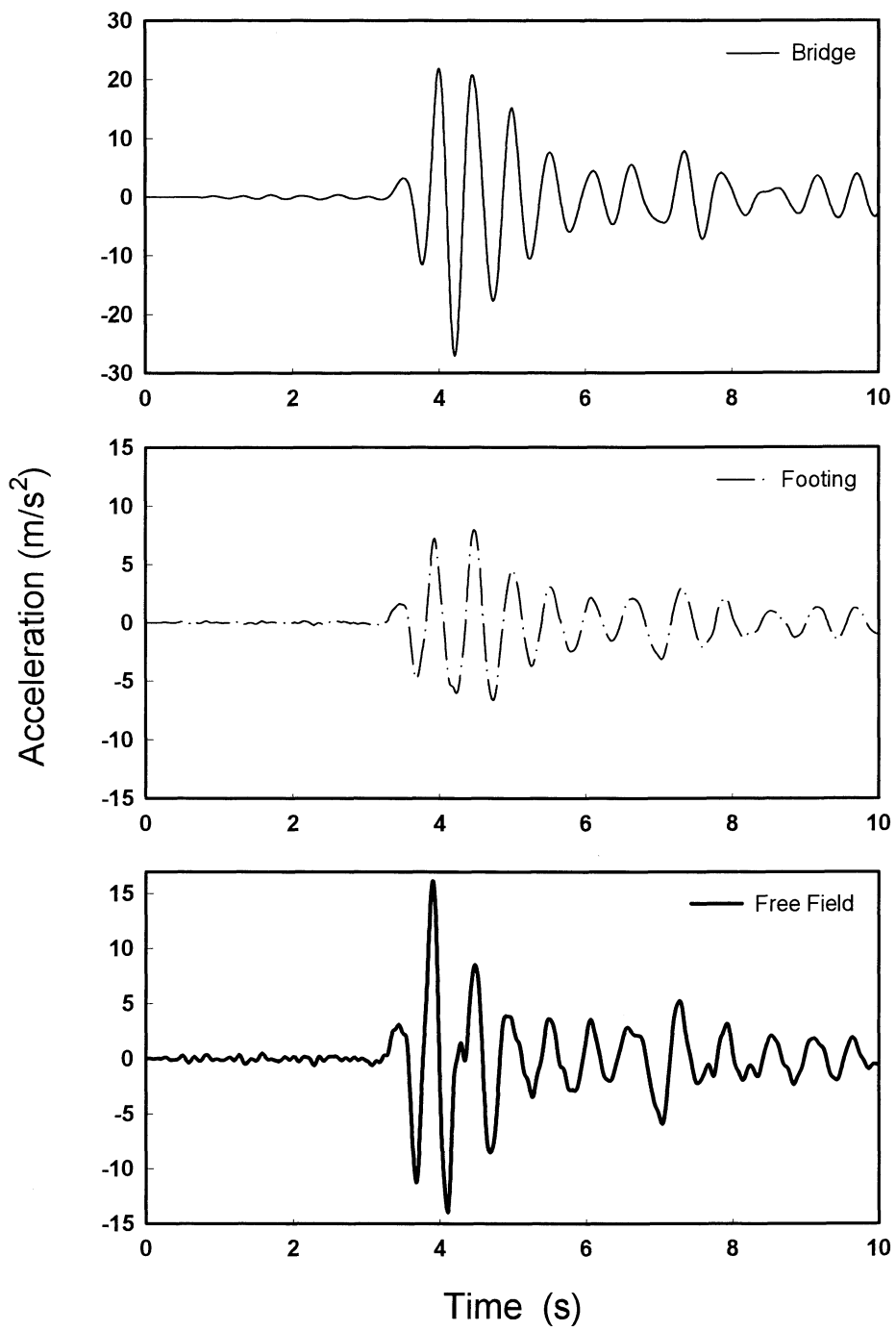
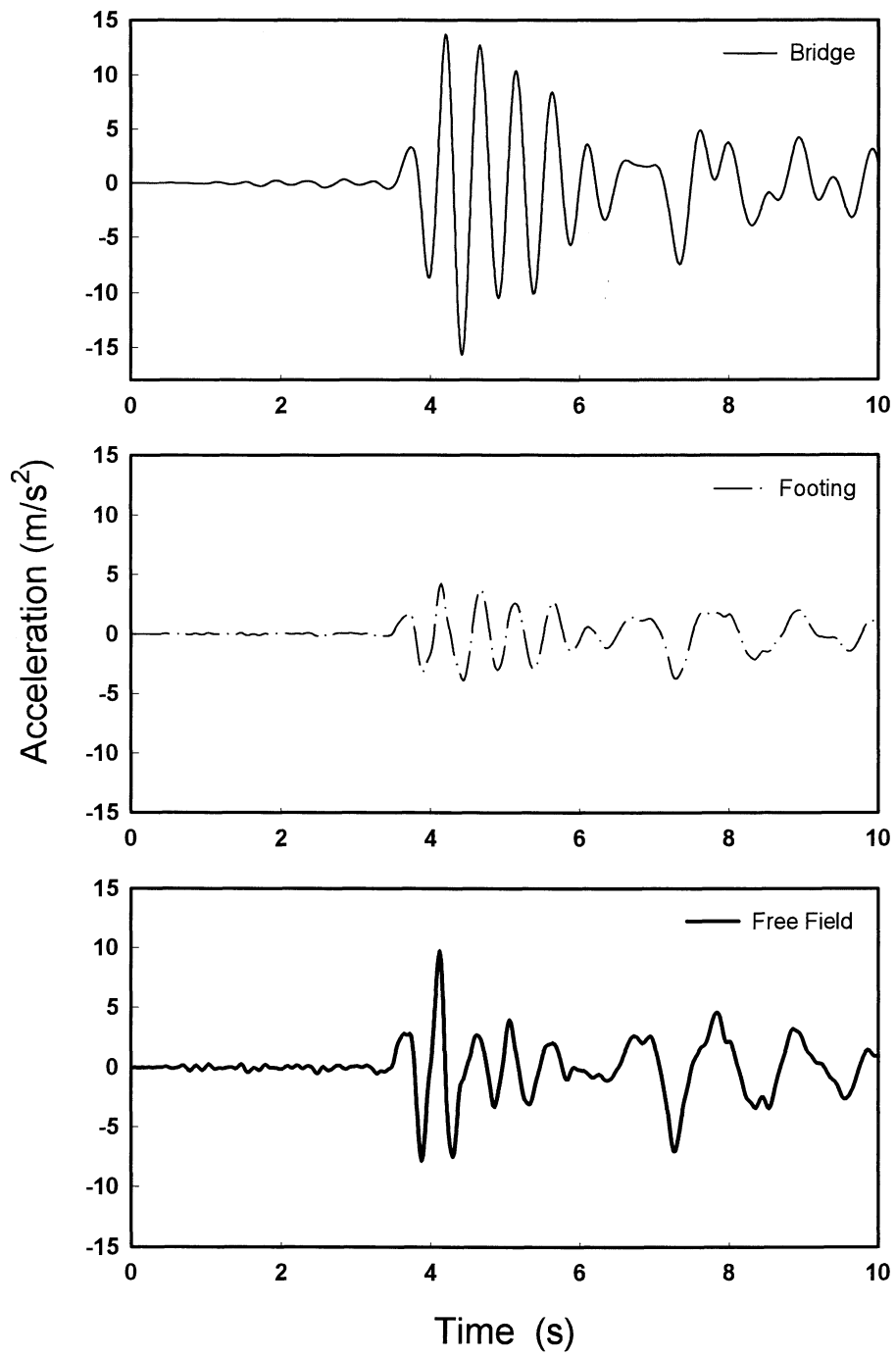**FIGURE A-106 Case B441: Acceleration histories for Pacoima, Northridge (1994) rock motion**
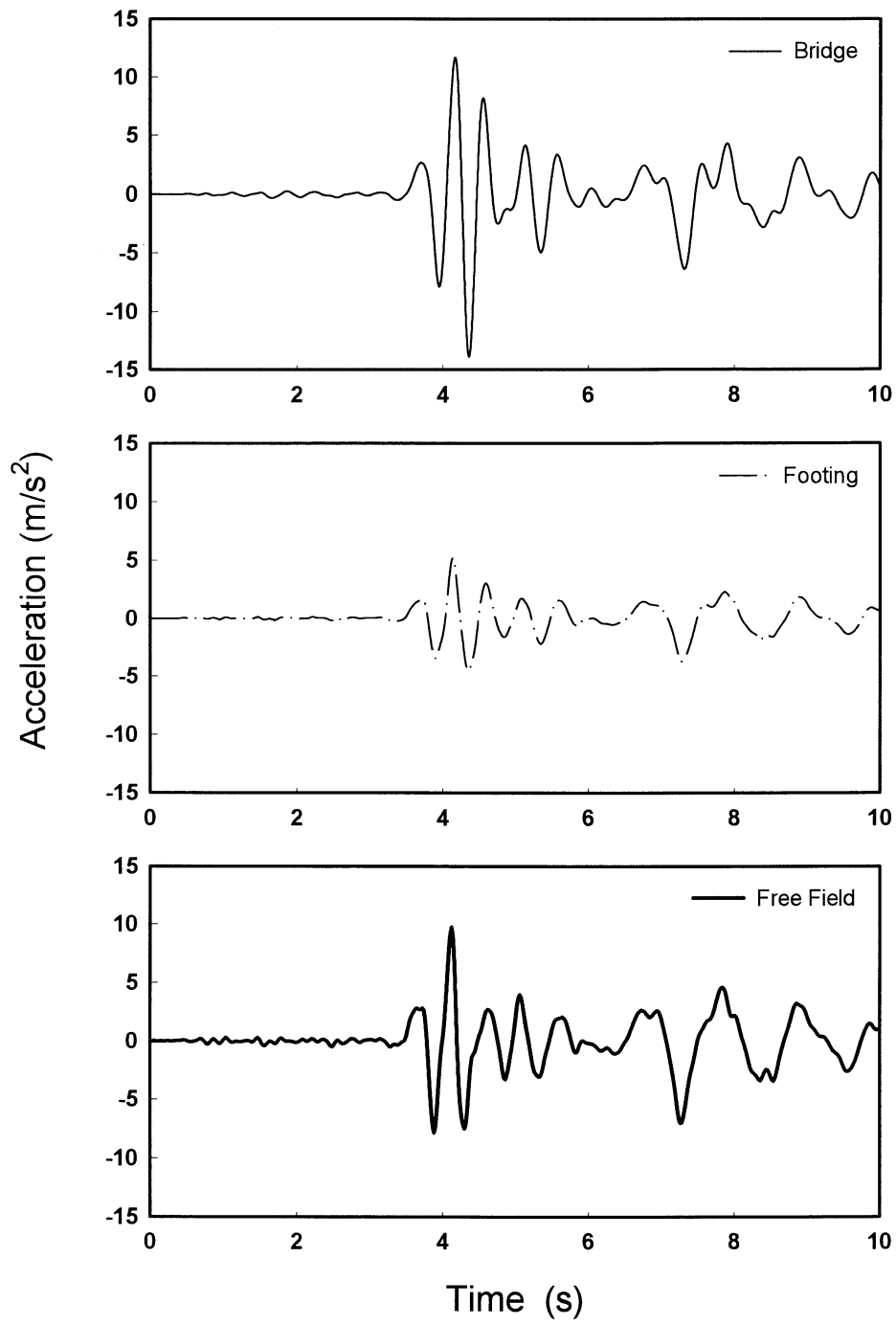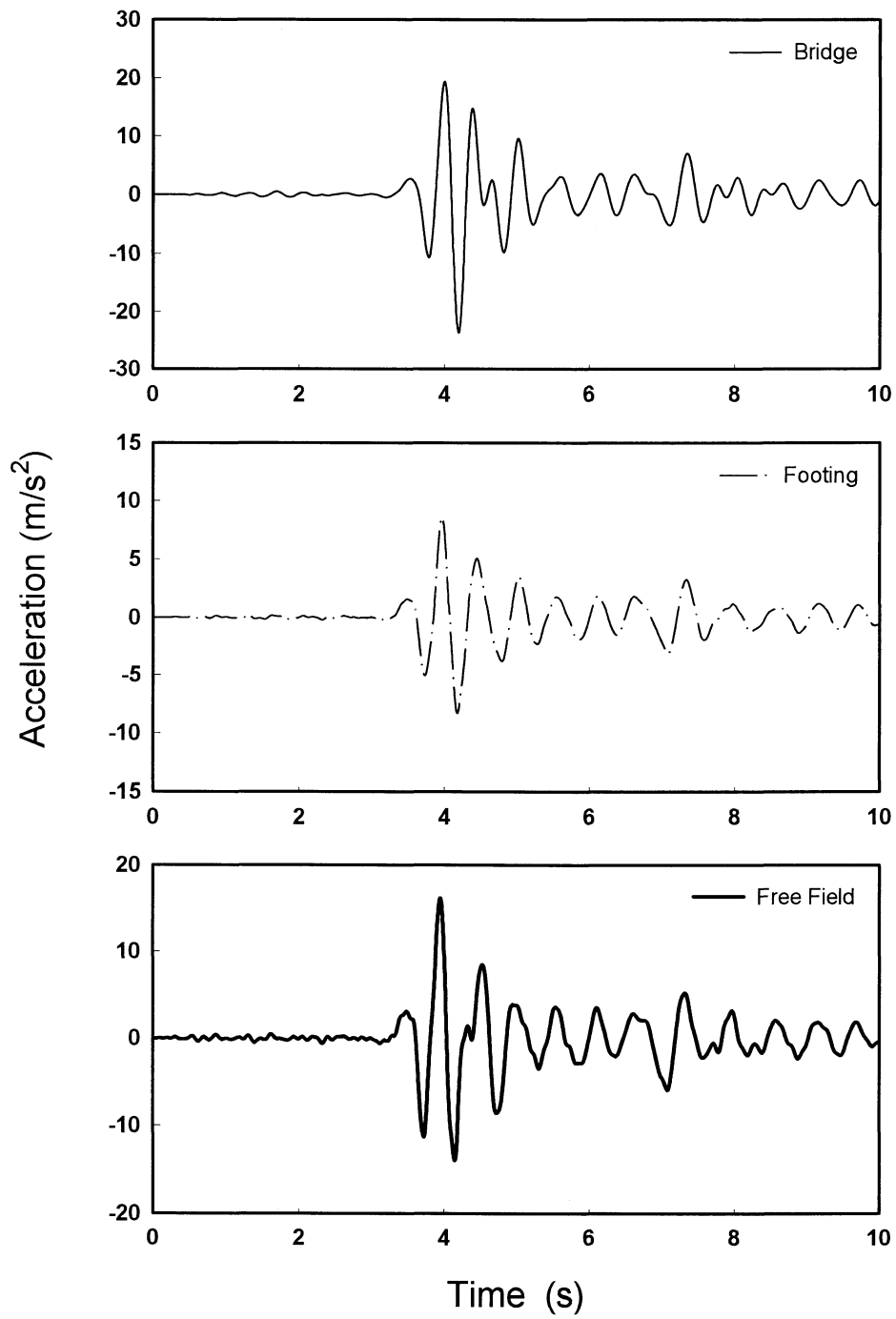
FIGURE A-107 Case B442: Acceleration histories for Pacoima, Northridge (1994) rock motion
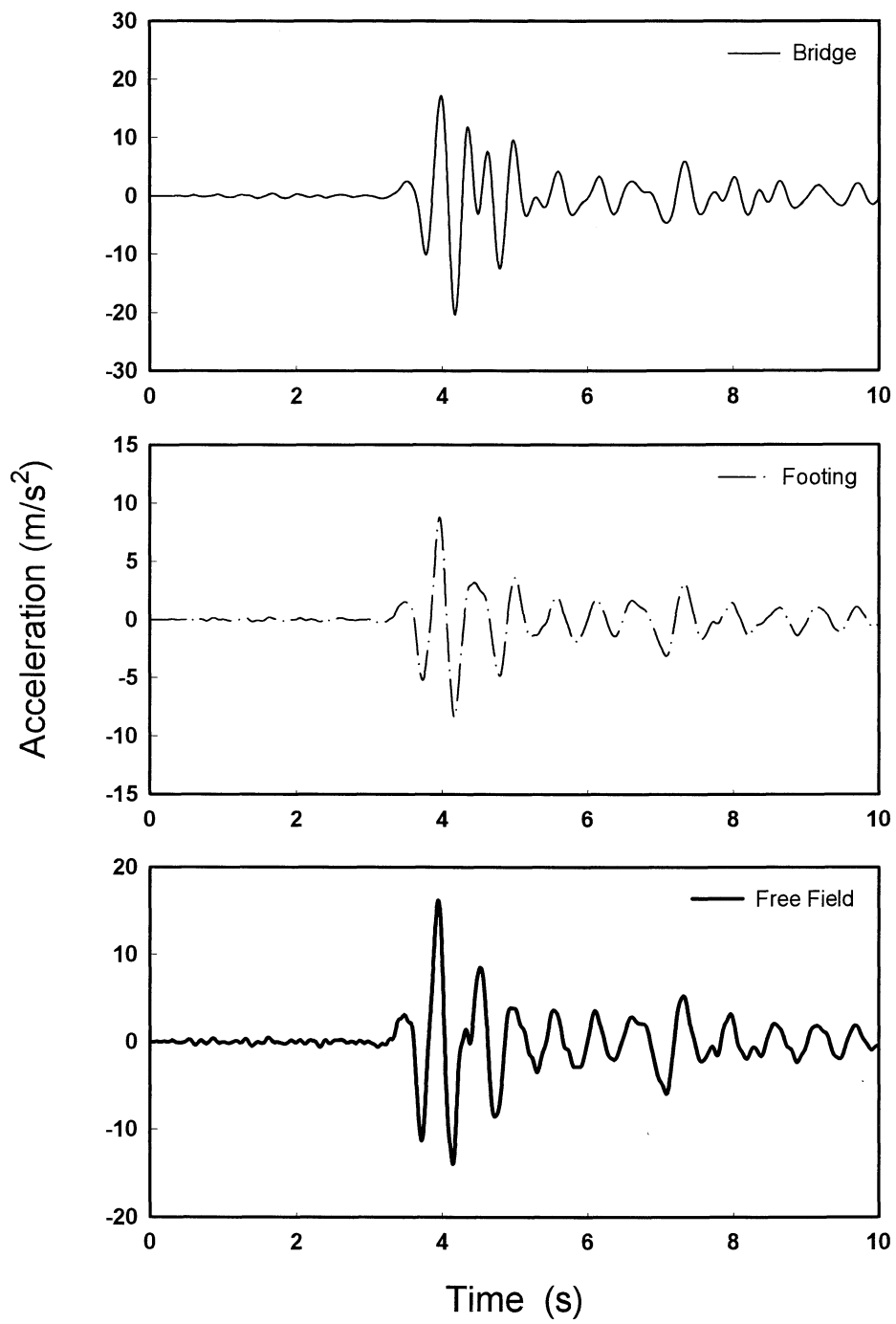
FIGURE A-108 Case B443: Acceleration histories for Pacoima, Northridge (1994) rock motion

Deep Profile
H = 93 m
V_{S1} = 80 m/s
Rigid Rock
I_R = Infinite

Footing

D = 1.5 m
d = 1.5 m
R = 1.5 m

Column

H_c = 6 m
d_c = 1.3 m
E_c = 25 GPa.
β = 5%
m_s = 350 Mgr.
Column top
free to rotate
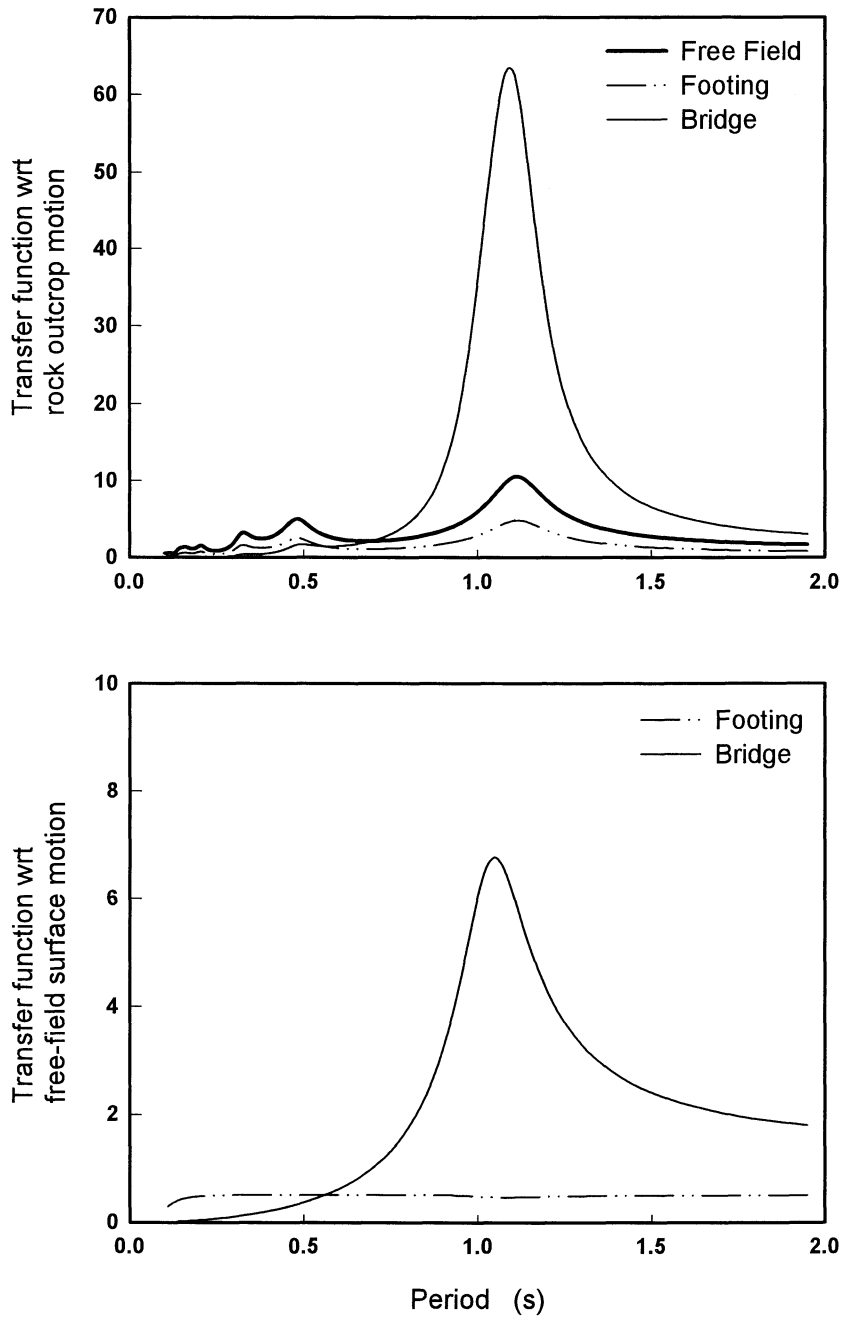
FIGURE A-109 Case A441F: Harmonic Steady-State Transfer Functions

Deep Profile
H = 93 m
V_{S1} = 80 m/s
Rigid Rock
I_R = Infinite

Footing
D = 1.5 m
d = 1.5 m
R = 3.0 m

Column
H_c = 6 m
d_c = 1.3 m
E_c = 25 GPa
β = 5%
m_s = 350 Mg
Column top
free to rotate
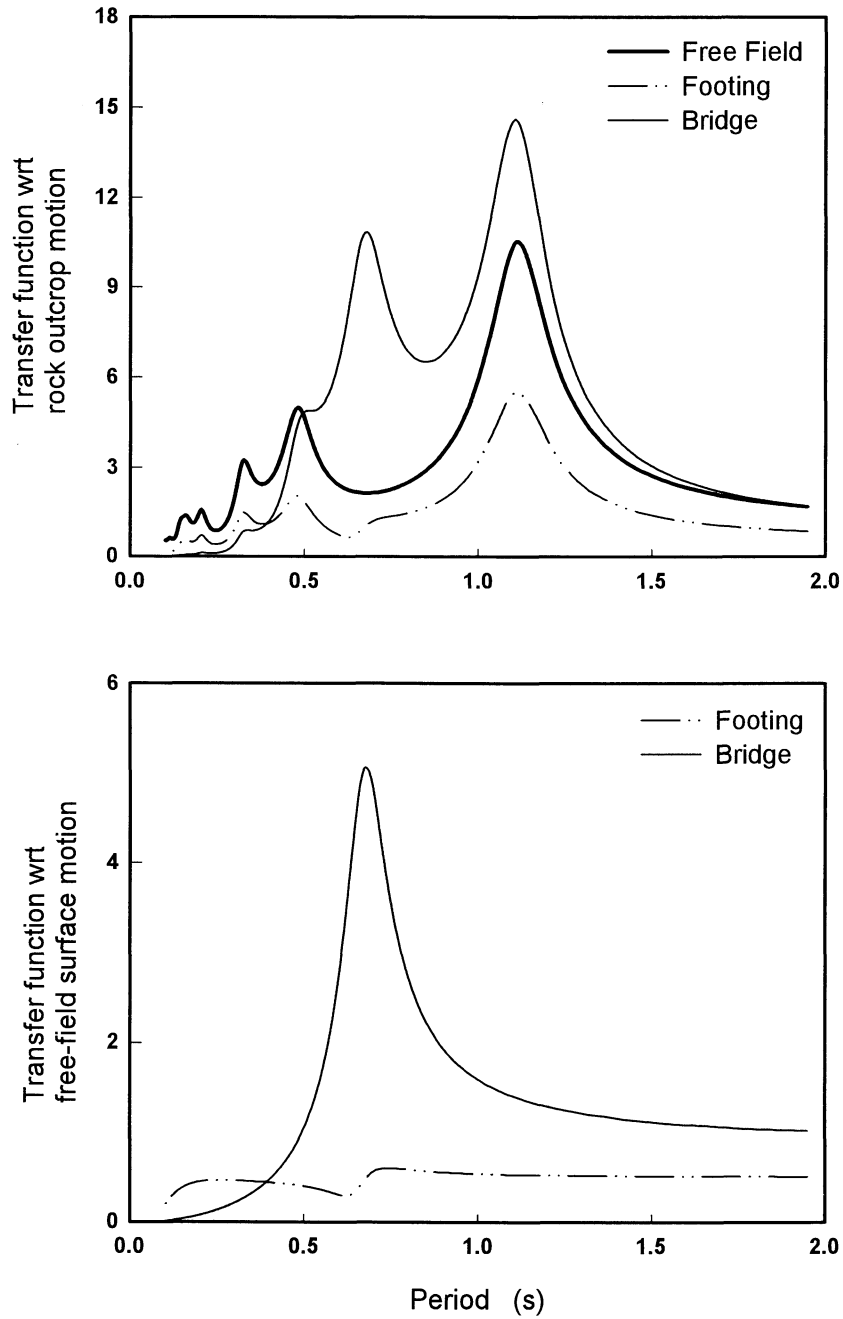
FIGURE A-110 Case A442F: Harmonic Steady-State Transfer Functions

Deep Profile
H = 93 m
V_{S1} = 80 m/s
Rigid Rock
I_R = Infinite

Footing
D = 1.5 m
d = 1.5 m
R = 4.5 m

Column
H_c = 6 m
d_c = 1.3 m
E_c = 25 GPa
β = 5%
m_s = 350 Mg
Column top
free to rotate
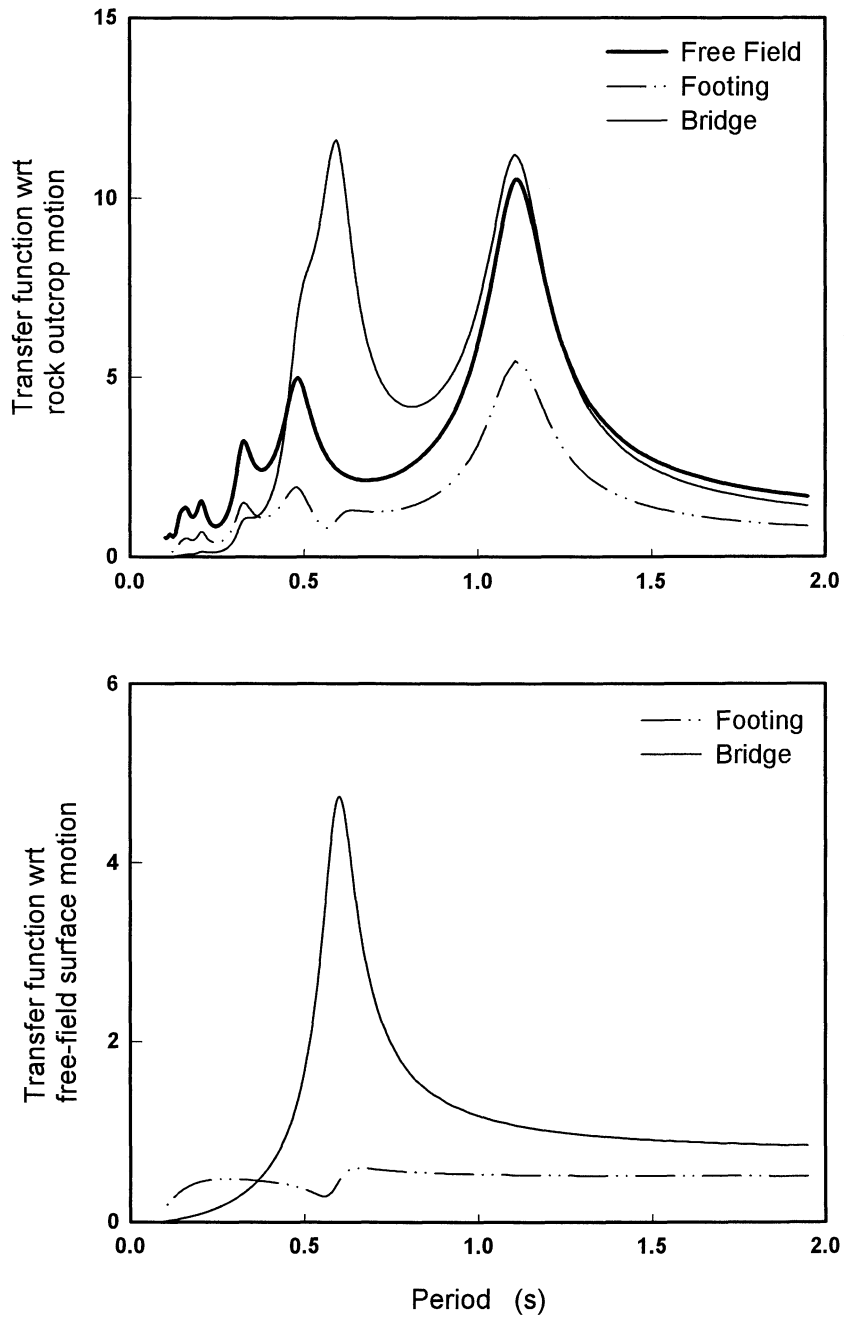
FIGURE A-111 Case A443F: Harmonic Steady-State Transfer Functions

Free Field
Footing
Bridge

Shallow Profile
H = 39.5 m
V_{S1} = 80 m/s
Rigid Rock
I_R = Infinite

Footing
D = 1.5 m
d = 1.5 m
R = 1.5 m

Column
H_c = 6 m
d_c = 1.3 m
E_c = 25 GPa
β = 5%
m_s = 350 Mg
Column top
free to rotate
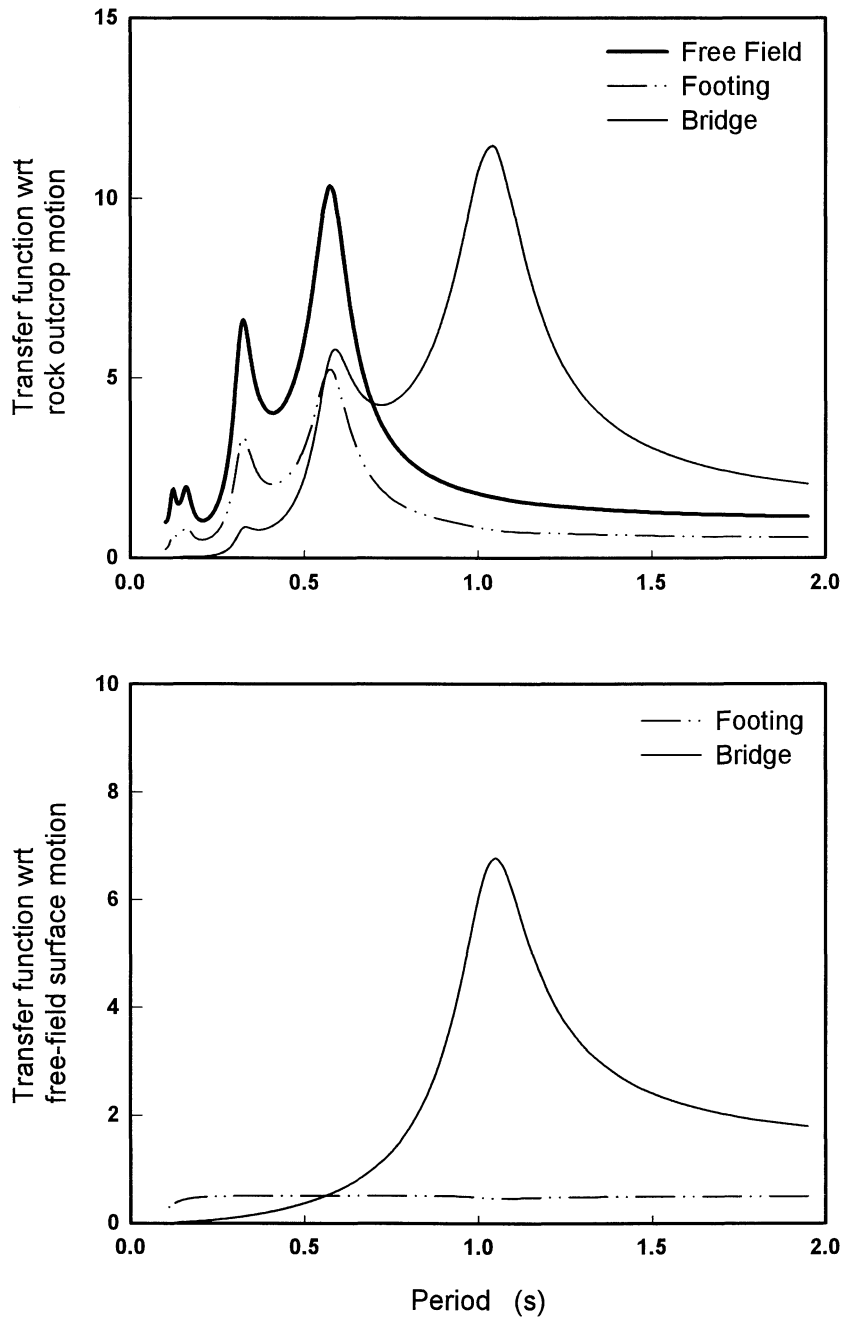
Footing
Bridge

FIGURE A-112 Case B441F: Harmonic Steady-State Transfer Functions

211

Shallow Profile
H = 39.5 m
V_{S1} = 80 m/s
Rigid Rock
I_R = Infinity

Footing
D = 1.5 m
d = 1.5 m
R = 3.0 m

Column
H_c = 6 m
d_c = 1.3 m
E_c = 25 GPa
β = 5%
m_s = 350 Mg
Column top
free to rotate
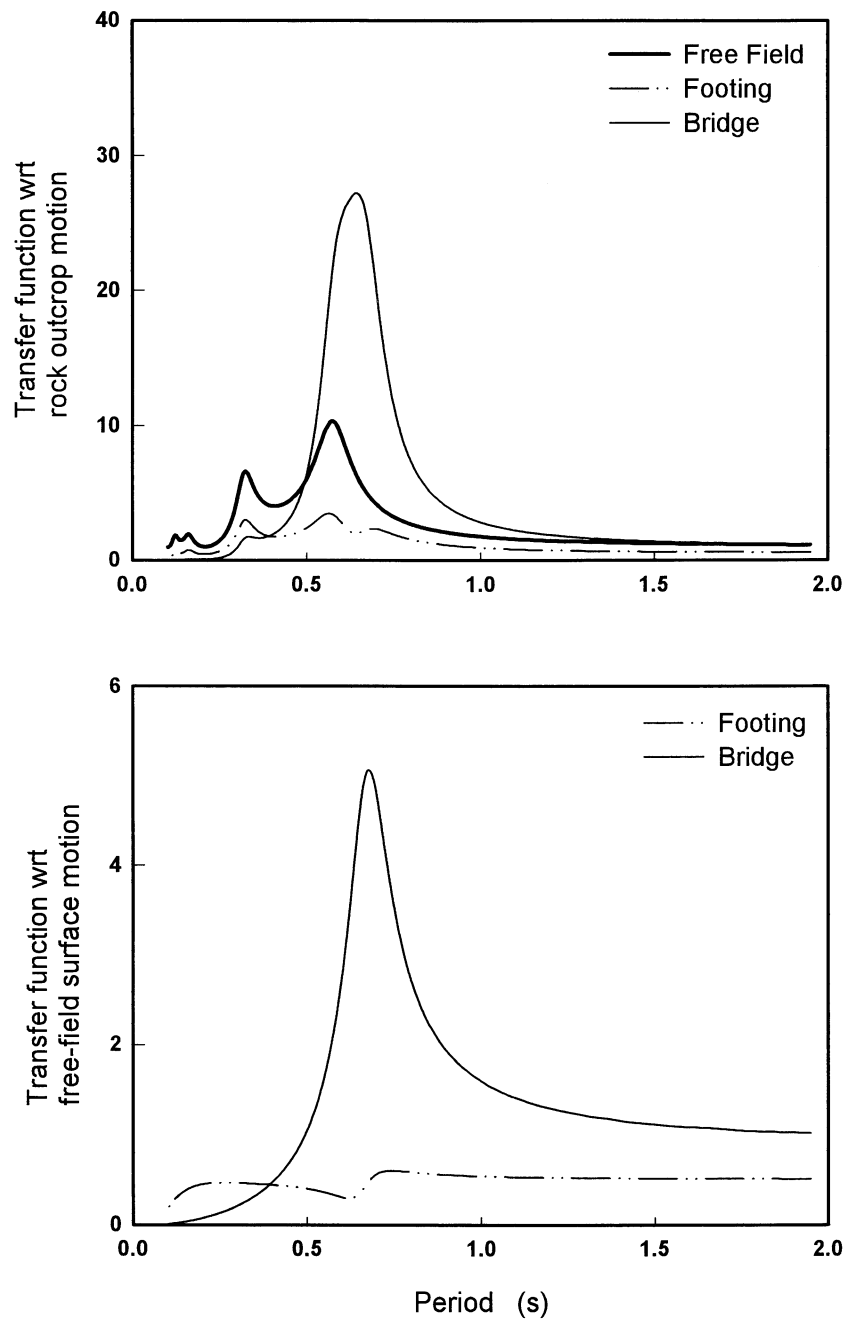
FIGURE A-113 Case B442F: Harmonic Steady-State Transfer Functions
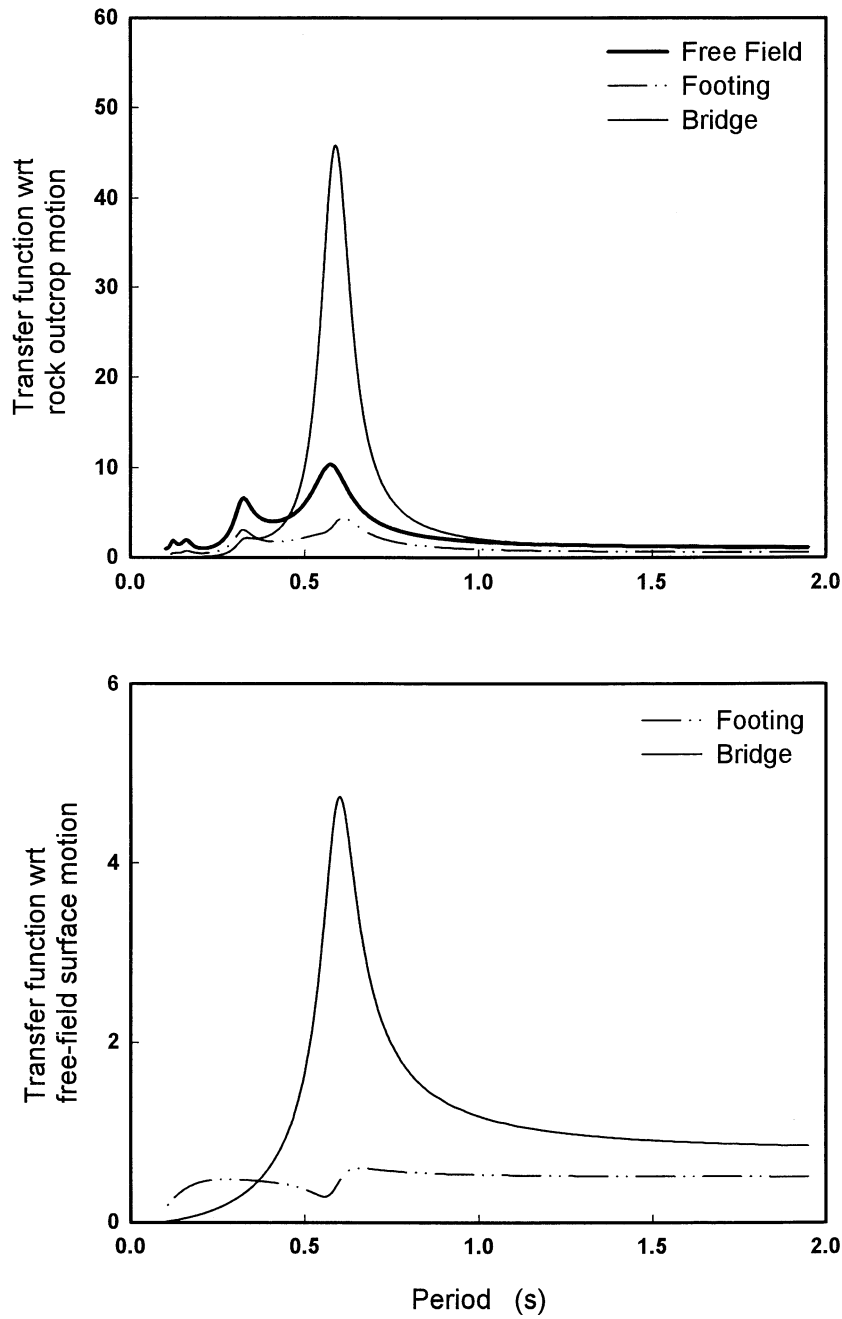
Shallow Profile
H = 39.5 m
V_{S1} = 80 m/s
Rigid Rock
I_R = Infinite

Footing
D = 1.5 m
d = 1.5 m
R = 4.5 m

Column
H_c = 6 m
d_c = 1.3 m
E_c = 25 GPa.
β = 5%
m_s = 350 Mgr.
Column top
free to rotate

FIGURE A-114 Case B443F: Harmonic Steady-State Transfer Functions

FIGURE A-115 Case A441F : Acceleration histories for 0.4g artificial excitation

FIGURE A-116 Case A442F : Acceleration histories for 0.4g artificial excitation

FIGURE A-117 Case A443F : Acceleration histories for 0.4g artificial excitation

FIGURE A-118 Case B441F: Acceleration histories for 0.4g artificial excitation

217

FIGURE A-119 Case B442F: Acceleration histories for 0.4g artificial excitation
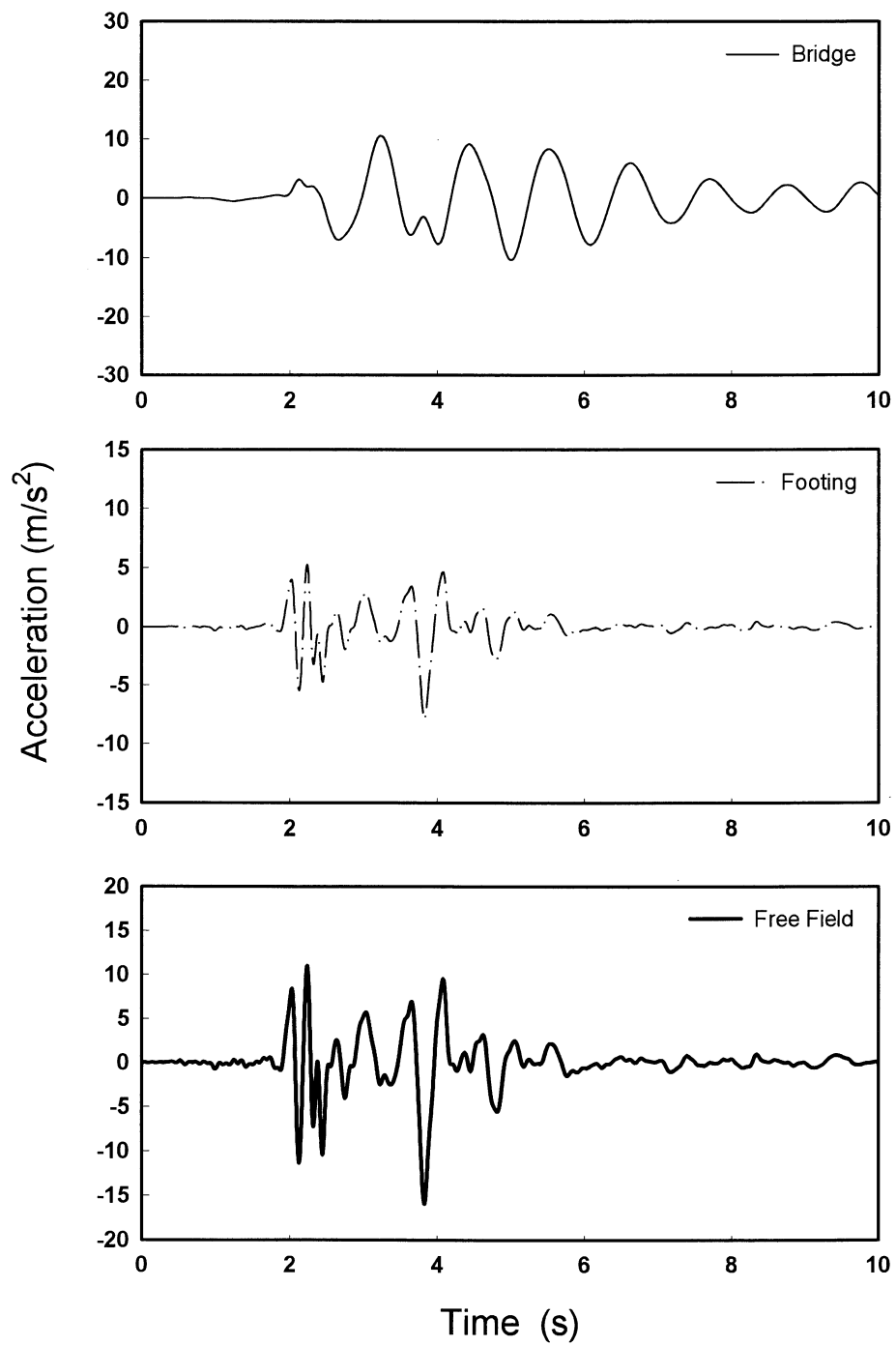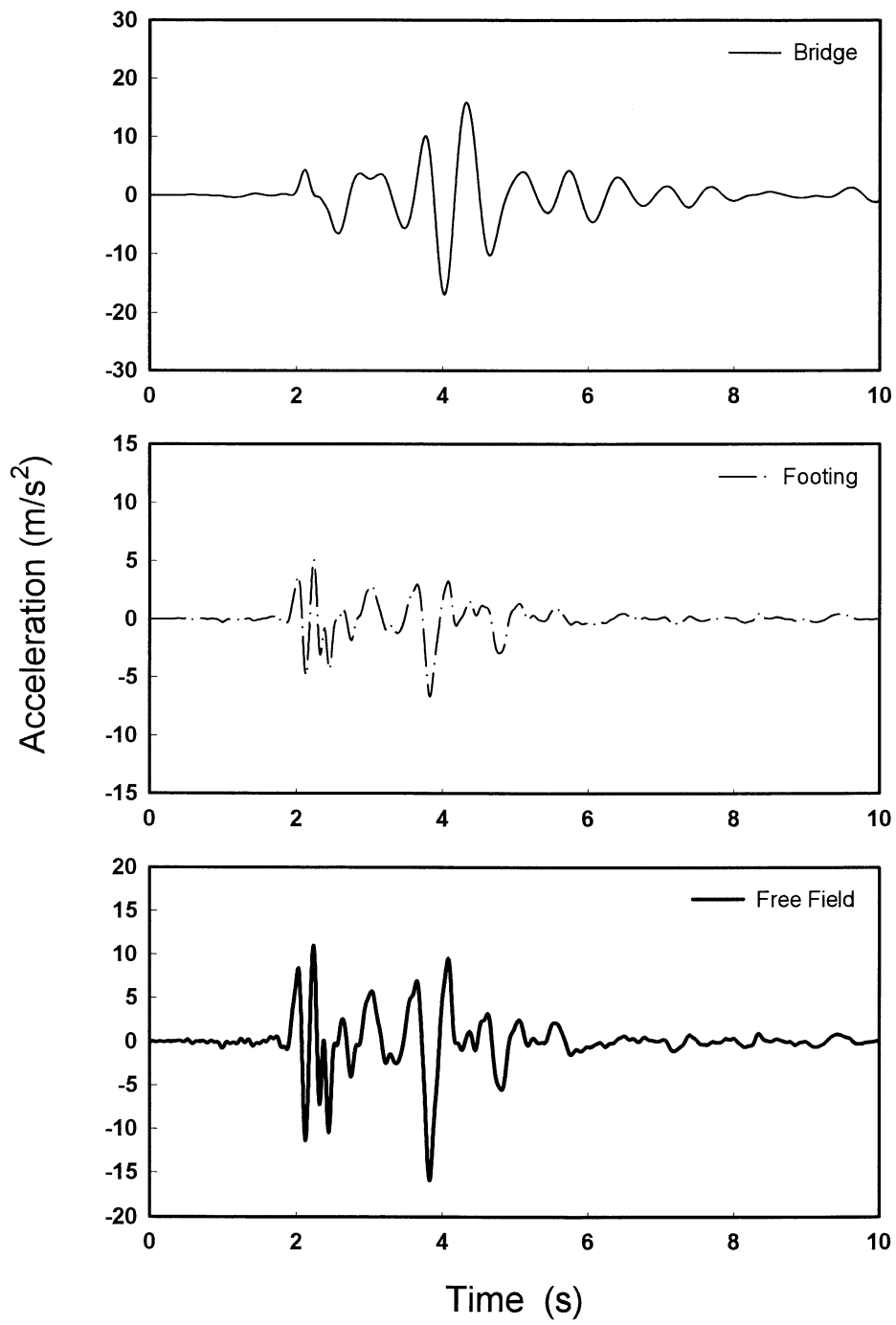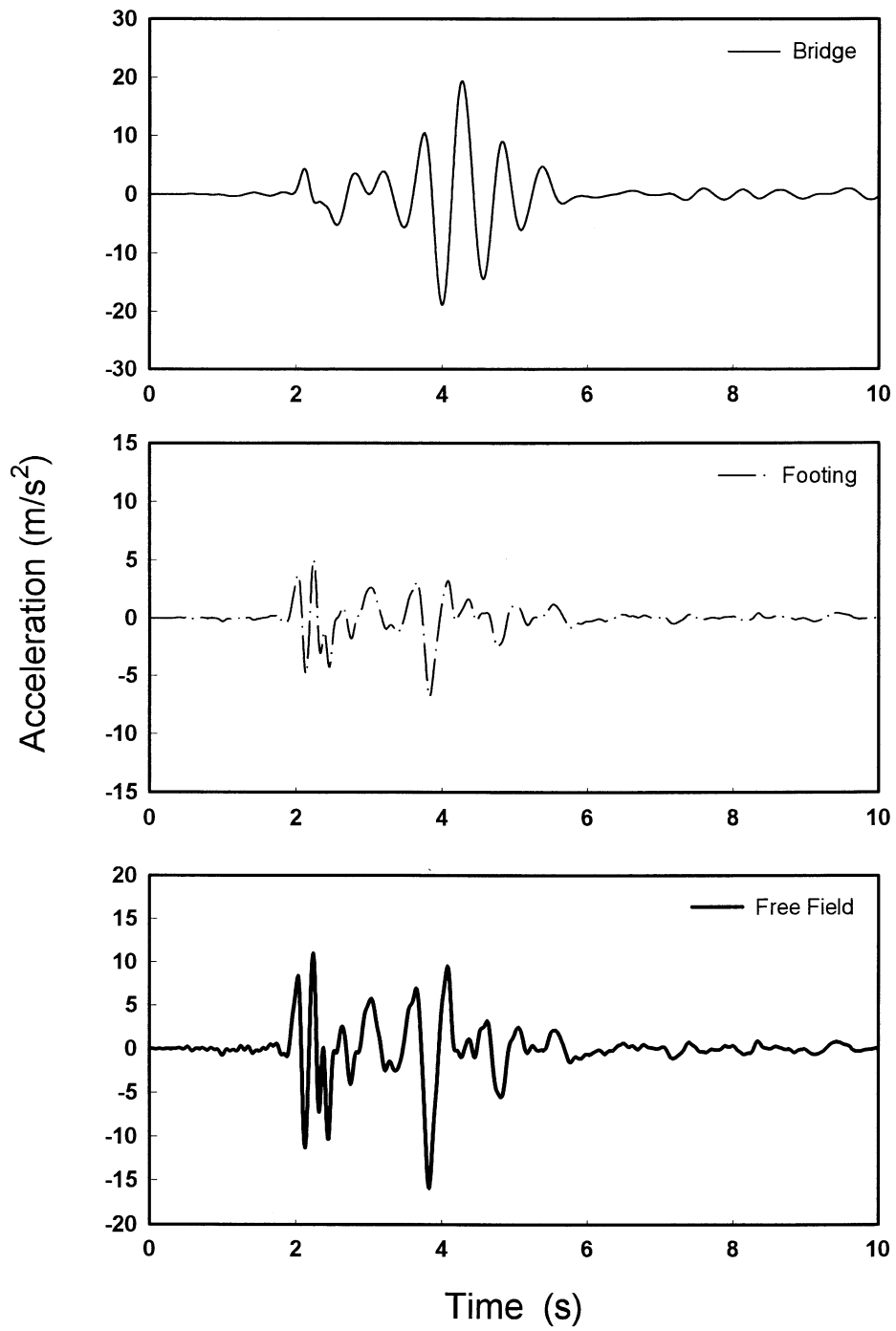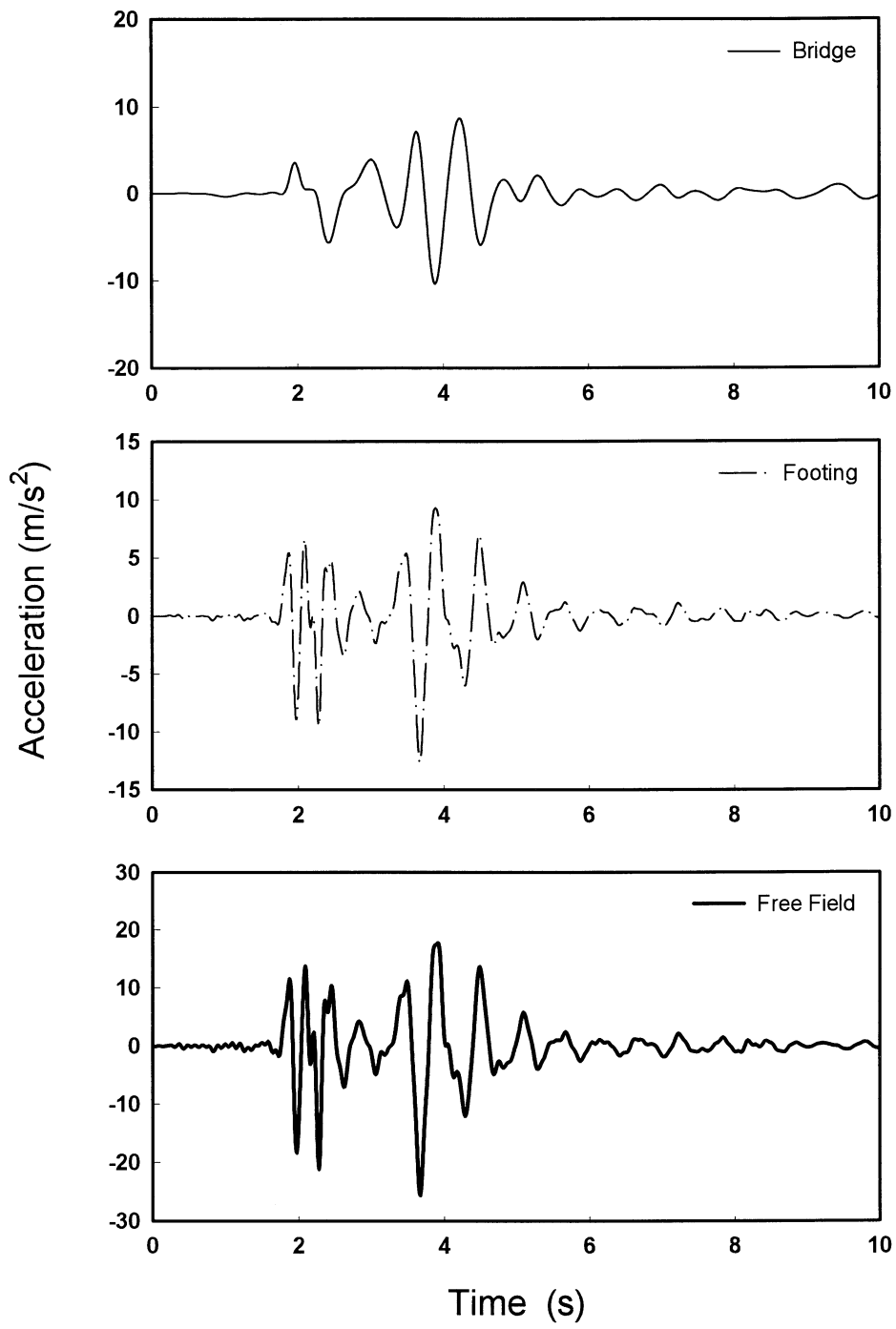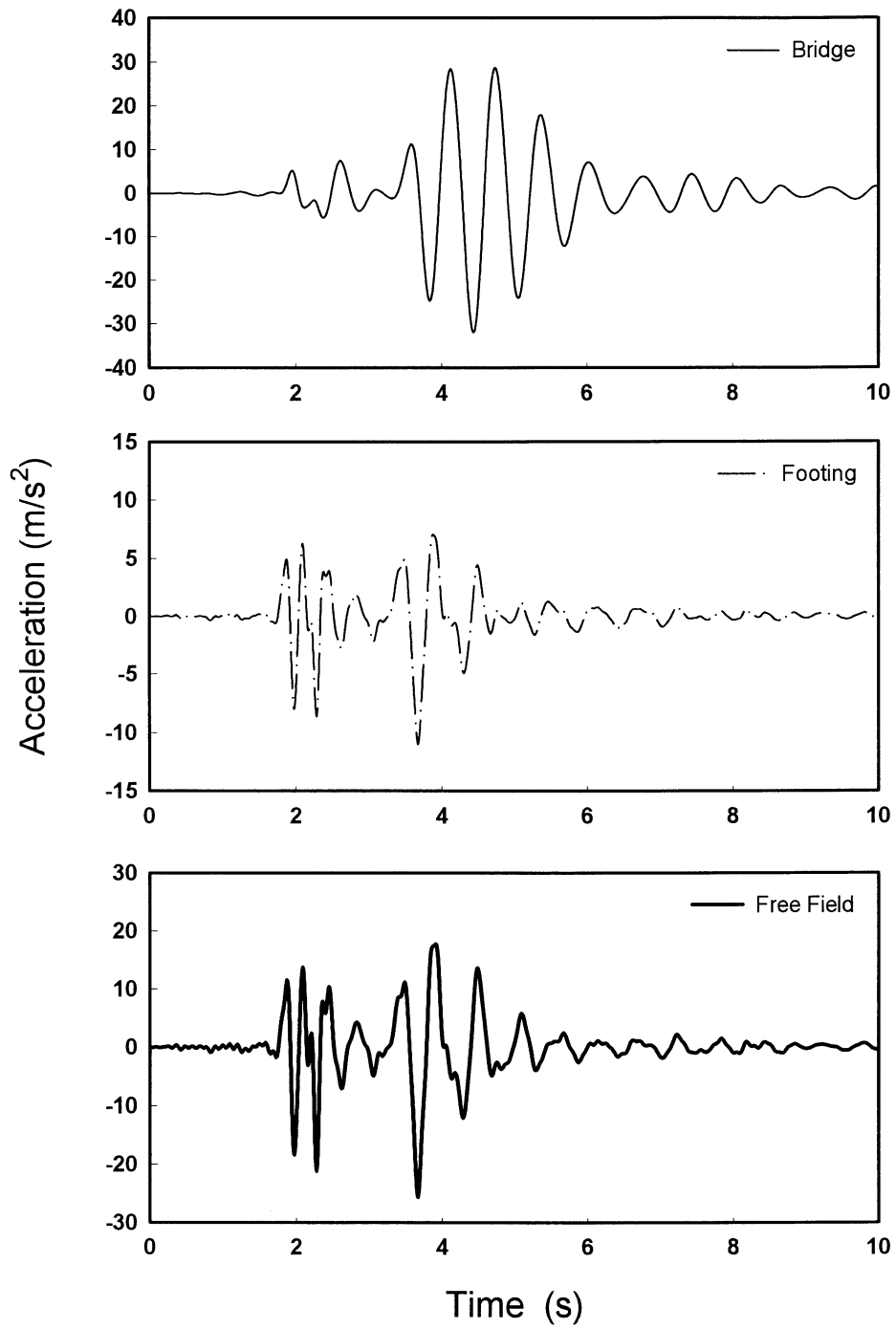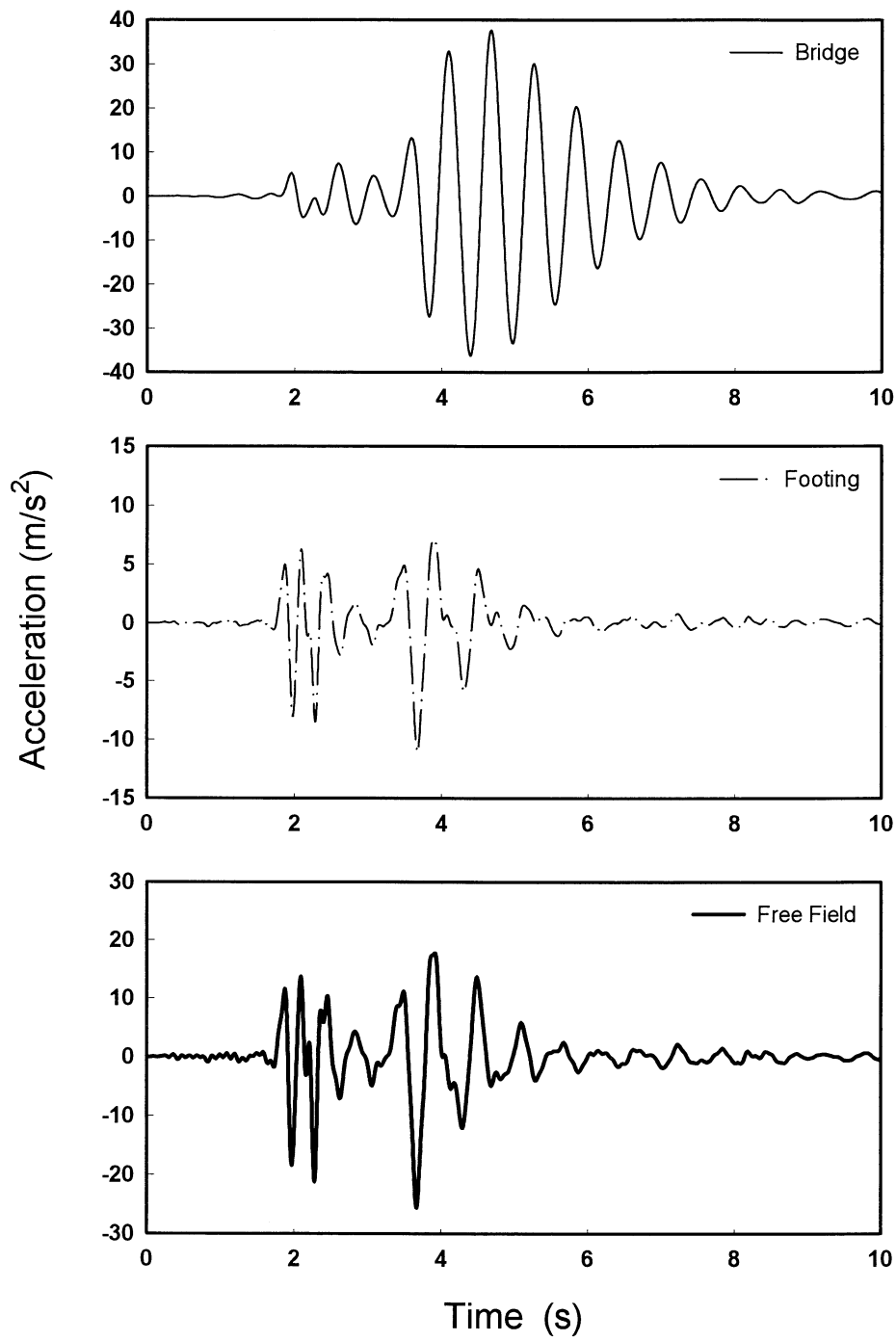
FIGURE A-120 Case B443F : Acceleration histories for 0.4g artificial excitation

APPENDIX B

LIST OF SYMBOLS

SYMBOL	EXPLANATION
A	soil amplification function
a	Ramberg-Osgood parameter
A_b	foundation basemat-soil contact area
α_c	critical value of horizontal acceleration to cause bearing capacity settlement in an earthquake
α_h	horizontal soil surface acceleration, critical horizontal acceleration value
$a_k(t)$	Kinematic Acceleration
A_w	total area of the actual sidewall-soil contact surface
A_{wce}	sum of projections of all sidewall area in directions perpendicular to loading
A_{ws}	sum of projections of all sidewall area in directions parallel to loading
β	linear hysteretic damping factor, parameter equal to the ratio of ϕ^c_{max} over ϕ_{cr}
B	foundation halfwidth or "equivalent" radius in the direction examined, or of circumscribed rectangle
C	"dashpot" modulus of a footing
$C, C(\omega)$	radiation damping ("dashpot") coefficient
C_1, C_2, C_3	parameters for pore pressure computation
C_{rad}	radiation damping
d	total height of the actual sidewall-soil contact surface
D	embedment depth of footing
δ	permanent vertical displacement due to a_c
Δ	displacement computed according to Newmark (1965) / Franklin-Chang (1977) / Richards-Elms (1979)
d_1, d_2, d_3	parameters for pore pressure computation

d_c	diameter of bridge pier
e	eccentricity
E_s	soil modulus of elasticity
ε_v	permanent vertical strain
Φ	free-field pseudo-rotation
f	frequency in Hz of the harmonic seismic wave
ϕ	phase angle
$F(U_A)$	Fourier Amplitude Spectrum of the design motion at the free-field ground surface
Φ_B	rotation about out-of-plane horizontal axis through the center of foundation base
f_c	fundamental natural frequency of the soil deposit in compression-extension
ϕ_{cr}	critical angle at which lift-off happens in the absence of vertical oscillations
f_D	natural frequency in shear of a hypothetical soil stratum of thickness D
FIM	Foundation Input Motion
ϕ_{max}^c	maximum angle of rotation which would occur if uplift were not allowed
ϕ_p	peak friction angle
f_s	fundamental natural frequency of the soil deposit in shear
G	shear modulus
g	acceleration of gravity
γ	soil unit weight
γ_c	cyclic shear strain amplitude in percent
G_o	maximum low-strain soil shear modulus
γ_p	plastic threshold strain
γ_y	characteristic shear strain
h	distance of the (effective) sidewall centroid from the ground surface
H_c	height of bridge pier
H_ε	horizontal force amplitude due to inertia on the masses of the superstructure
i	imaginary unity

I.I.	Inertial Interaction
I_1	mass moment of inertia of the superstructure
I_b	polar moment of inertia about z of soil foundation contact surface
I_{bx}	moment of inertia about x of soil foundation contact surface
I_{by}	moment of inertia about y of soil foundation contact surface
I_Φ	rotational kinematic interaction factors
I_o	mass moment of inertia of the foundation
I_R	impedance contrast between soil and rock
I_U	translational kinematic interaction factors
$\overline{K} = \overline{K}(\omega)$	dynamic stiffness ("spring")
k	complex wavenumber of S waves
K	static stiffness
$k, k(\omega)$	dynamic stiffness coefficient :
K.I.	Kinematic Interaction
$\overline{K}_{emb}$, C_{emb}	dynamic stiffnesses and dashpot coefficients of an embedded foundation
$\mathscr{K}_{rx}'$	rocking impedance (moment-rotation ratio), for rotational motion about the long axis of the foundation basemat
$\mathscr{K}_{ry}'$	the rocking impedance (moment-rotation ratio), for rotational motion about the short axis of the foundation
K_{str}	dynamic structural impedance of the superstructure
$\overline{K}_{sur}$, C_{sur}	dynamic stiffnesses and dashpot coefficients of a surface foundation
$\mathscr{K}_t'$	torsional impedance (moment-rotation ratio), for rotational oscillation about the vertical axis
$\mathscr{K}_{x\text{-}ry}'$, $\mathscr{K}_{y\text{-}rx}'$	cross-coupling horizontal-rocking impedances
$\mathscr{K}_y'$	longitudinal (swaying) impedance (force-displacement ratio), for horizontal motion in the long direction
L	semi length of footing (or of circumscribed rectangle)
λ_R	wave length of the Rayleigh wave

m_1	mass of the superstructure
M_ε	overturning moment amplitude due to inertia on the masses of the superstructure
m_0	mass of the foundation
N	vertical load on the footing, number of cycles with uniform shear strain
ν,	Poisson's ratio
N_{cs} to N_{ce}	cohesion-related bearing capacity factors
N_γ, N_q, N_c	Terzaghi bearing capacity factors
$N_{\gamma e}$ and N_{qe}.	
P	axial gravity load carried by the bridge system
PGA, pga	Peak Ground Acceleration
$P_z(t)$	vertical force
r	Ramberg-Osgood parameter
R	radius of bridge footing
ρ_r	elastic rock mass density
ρ_s	soil mass density
SA	spectral acceleration
SDOF	Single Degree of Freedom system
SH	horizontally polarized S waves
SSI	soil-structure interaction
st	static components of forces and moments
S_u	undrained shear strength
SV	vertically polarized S waves
σ_z	vertical normal stress
$\tilde{T}$	effective period
T	period
t	time
T_1	fundamental period of the interacting system when lift-off is not allowed
u_h	peak value of horizontal ground velocity.

u_r	residual pore pressures
$u_z(t)$	vertical displacement of foundation
V_a	apparent wave propagation velocity along the surface
V_ε	vertical force amplitude due to inertia on the masses of the superstructure
V_{La}	"Lysmer's analog" wave velocity
V_r	average shear wave velocity, shear wave velocity of elastic rock
V_s	propagation velocity of shear waves in the soil
V_s	soil shear wave velocity
ω	cyclic frequency
$\tilde{\xi}$	effective damping of the system
ψ	angle of incidence of an S wave along the horizontal axis
z	depth from soil surface
z_v, z_h, z_t, z_t	depths of influence in vertical, horizontal, rocking, and torsional vibration